



Universidad de Concepción  
Dirección de Postgrado  
Facultad de Ciencias Físicas y Matemáticas  
Programa de Doctorado en Ciencias Aplicadas  
con Mención en Ingeniería Matemática

**SISTEMAS SHALLOW WATER MULTICAPA PARA SEDIMENTACIÓN  
POLIDISPERSA**

**ON MULTILAYER SHALLOW WATER SYSTEMS FOR POLYDISPERSE  
SEDIMENTATION**

Tesis para optar al grado de Doctor en Ciencias  
Aplicadas con mención en Ingeniería Matemática

VÍCTOR ANDRÉS OSORES ESCALONA  
CONCEPCIÓN-CHILE  
2019

Profesor Guía: Raimund Bürger  
CI<sup>2</sup>MA y Departamento de Ingeniería Matemática  
Universidad de Concepción, Chile

Cotutor: Enrique D. Fernández-Nieto  
Departamento de Matemática Aplicada I, ETS Arquitectura  
Universidad de Sevilla, España

# **On multilayer shallow water systems for polydisperse sedimentation**

Víctor Andrés Osores Escalona

**Director de Tesis:** Prof. Raimund Bürger, Universidad de Concepción, Chile.

**Codirector de Tesis:** Prof. Enrique D. Fernández-Nieto, Universidad de Sevilla, España.

**Director de Programa:** Prof. Rodolfo Rodríguez, Universidad de Concepción, Chile.

## **COMISIÓN EVALUADORA**

Prof. Stefan Diehl, Lund University, Suecia.

Prof. Tomás Morales de Luna, Universidad de Córdoba, España.

Prof. Yuri Dumaresq Sobral, Universidade de Brasilia, Brasil.

Prof. Yohan Penel, Sorbonne Université ,Francia

## **COMISIÓN EXAMINADORA**

Firma: \_\_\_\_\_

Prof. Raimund Bürger, Universidad de Concepción, Chile.

Firma: \_\_\_\_\_

Prof. Fernando Betancourt, Universidad de Concepción, Chile.

Firma: \_\_\_\_\_

Prof. Enrique D. Fernández-Nieto, Universidad de Sevilla, España.

Firma: \_\_\_\_\_

Prof. Christian F. Ihle, Universidad de Chile, Chile.

Firma: \_\_\_\_\_

Prof. Oscar Link, Universidad de Concepción, Chile.

Calificación: \_\_\_\_\_

Concepción, 19 de Noviembre de 2019

---

## Agradecimientos

---

En primer lugar, agradecer a mis padres María y Juan por todo lo que han entregado y que entregan incansablemente y en todo momento a sus hijos, Romina, Jonnathan y a quien escribe. Gracias por los valores que nos han entregado y por siempre inculcar en nosotros el camino del bien, del esfuerzo y del respeto a los demás. A mi tía Cecilia por el cariño que siempre me entregó, quien luchó hasta el final con todas sus fuerzas contra el cáncer.

A mi señora Francisca por la paciencia, por el apoyo incondicional, por estar a mi lado en las buenas y en las no tan buenas y por todos los momentos que hemos vivido juntos. A mi hermoso hijo quien ha logrado poco a poco salir adelante luego de su accidente cerebrovascular, ya son 5 años viendo su esfuerzo y sus ganas de superar dificultades. Hijo eres un ganador, gracias por tu ejemplo de superación y perdón por los momentos que no he estado a tu lado.

A la Sra. Ximena, por ayudarnos con el cuidado de nuestro hijo cuando ambos padres estamos en la Universidad.

A mi director de tesis, el profesor Raimund Bürgger por su tiempo, por su disposición, por su voluntad, por su apoyo en las diferentes situaciones que han acontecido, por guiar mi trabajo y por estar dispuesto a formar parte de mi crecimiento como profesional. A Enrique Fernández-Nieto mi co-director de tesis quien desde el primer momento estuvo dispuesto a trabajar conmigo, quien me recibió amablemente en mis pasantías en Sevilla. Enrique muchas gracias por tus consejos, por guiar este trabajo y por permitirme compartir con su familia y con sus pares académicos.

A mis amigos Diego, Patrick (Patrih), Felipe, Camilo, Sebastian y Rodrigo unos mas cerca que otros (en  $\|\cdot\|$ ), por los buenos momentos que hemos compartido, por estar en el momento preciso, por el consejo sincero y por su apoyo. A mis compañeros del CI<sup>2</sup>MA (con  $\hat{\{2\}}$ ) por las conversaciones de sobre mesa, por la buena convivencia y por el intercambio de ideas. Al Señor Gabriel N. Gatica en su calidad de Director del Centro de Investigación en Ingeniería Matemática (CI<sup>2</sup>MA) por brindar la posibilidad de ser parte de este centro, así como también por los espacios de trabajo, oficinas equipadas, limpia y siempre con todo lo necesario para que como estudiantes del programa estemos en condiciones óptimas. Se agradece y se valora la gestión y el inmenso trabajo que hay detrás para que este centro funcione de la mejor manera posible.

Finalmente, agradecer a las siguientes instituciones por financiar este proyecto de investigación. Al Centro de Recursos Hídricos para la agricultura y la minería (CRHIAM) a través del proyecto CONICYT/FONDAP/15130015 por financiar parcialmente los inicios de este proyecto, a CONICYT/PIA/Concurso Apoyo a Centros Científicos y Tecnológicos de Excelencia con Financiamiento Basal AFB170001. Y a CONICYT beca de doctorado nacional.

Víctor Andrés Osores Escalona.

---

## Resumen

---

El propósito de este trabajo es presentar un modelo matemático y, posteriormente, un método numérico que permita simular el proceso de sedimentación polidispersa, para ello, primero se acopla un modelo multicapa de aguas poco profundas con el modelo 1D existente para sedimentación polidispersa, obteniendo de esta manera, un modelo matemático que no solo captura el movimiento vertical de las partículas sólidas si no que también el movimiento horizontal de estas.

Posteriormente, introducimos el enfoque multicapa para la descripción aproximada del proceso de sedimentación polidispersa y transporte de sedimentos en un fluido viscoso. Suponemos aquí que el fluido transporta partículas finas, esféricas y sólidas dispersas en él pertenecientes a un número finito de especies ( $N$ ), las cuales difieren en densidad y tamaño. Estas especies segregan y forman áreas de diferente composición. Además, el asentamiento de las partículas influye en el movimiento del fluido. Una característica distintiva de este enfoque es la definición de la velocidad promedio de la mezcla. Esta tiene en cuenta las densidades de las partículas sólidas ( $\rho_j$ , para  $j = 1, \dots, N$ ) y la densidad total de la mezcla ( $\rho$ ) y nos permite recuperar la ley de conservación de masa y la ley de balance del momento lineal global de la mezcla. Esta definición motiva naturalmente una modificación de las MLB-velocities (Masliyah-Lockett-Bassoon), velocidades de sedimentación de cada una de las especies involucradas.

Luego, introducimos términos que modelan la compresibilidad del sedimento y la viscosidad de la mezcla. Como consecuencia de hacer un análisis dimensional sobre las ecuaciones de conservación de masa y las ecuaciones de momento lineal, las componentes horizontales de los términos de compresión y de la viscosidad son descartados. Esto da como resultado final un modelo que es verticalmente consistente con modelos de sedimentación clásicos.

Además, derivamos un modelo multicapa para sedimentación polidispersa con una extensión a presión no hidrostática. Esta presión no hidrostática se introduce en el modelo como una desviación de la presión hidrostática. Algunas ecuaciones adicionales son necesarias para cerrar el modelo resultante, así como una suposición adicional sobre el campo de velocidad de la mezcla. El propósito de esta extensión es obtener un modelo potencialmente más realista.

Los modelos resultantes se escriben en forma de modelos multicapa con densidad variable, cuyas incógnitas son las velocidades y concentraciones de cada especie en cada capa  $\Omega_\alpha$ , los términos de transferencia a través de la interfaz y la masa total de la mezcla. Bajo la suposición de presión no hidrostática, los términos de presión no hidrostática en cada interfaz aparecen como nuevas incógnitas del modelo.

Una fórmula explícita de los términos de transferencia conducen a una forma reducida de este sistema.

Cotas para los valores propios mínimo y máximo de la matriz de transporte del sistema son utilizados para diseñar un método numérico path conservativo del tipo Harten-Lax-van Leer (HLL).

Finalmente, se presentan algunas simulaciones numéricas uno-dimensional, dos-dimensional y tres-dimensional para diferentes tiempos, las cuales ilustran el proceso sedimentación polidispersa acoplado a un flujo horizontal en varios escenarios, entre ellos, sedimentación sobre fondos similares a las que se suelen utilizar en la industria minera, así como también, en topografías complejas que dan lugar a recirculaciones del fluido. Para cerrar, mostramos algunas simulaciones numéricas que permiten analizar el comportamiento de la mezcla cuando activamos y/o desactivamos la compresibilidad del sedimento y la viscosidad de la mezcla.

---

## Abstract

---

The purpose of this work is to present a mathematical model and subsequently a numerical method that allows to simulate polydisperse sedimentation processes, to this end, we couple a multilayer shallow water model with existing one-dimensional polydisperse sedimentation models to obtain a mathematical model that captures not only vertical movement of the solid particles but, also the horizontal flow of the mixture.

Later, we introduce a multilayer shallow water approach for the approximate description of polydisperse sedimentation and sediment transport in a viscous fluid. The fluid is assumed to carry finely dispersed solid spherical particles that belong to a finite number of species ( $N$ ) that differ in density and size. These species segregate and form areas of different composition. In addition, the settling of particles influences the motion of the ambient fluid. A distinct feature of the new approach is the particular definition of the average velocity of the mixture. It takes into account the densities of the solid particles ( $\rho_j$ , for  $j = 1, \dots, N$ ) and the mixture density ( $\rho$ ) and allows us to recover the global mass conservation and linear momentum balance laws of the mixture. This definition motivates a modification of the Masliyah-Lockett-Bassoon (MLB) settling velocities of each species.

Then, we incorporate sediment compressibility and mixture viscosity through a viscous stress tensor. As a consequence of a dimensional analysis applied to the global mass conservation and linear momentum balance equations, the horizontal components of the compression term and the horizontal terms of the viscous stress tensor may be neglected. This results in a final model that is vertically consistent with the classical one-dimensional vertical model.

Furthermore, we derive an extended multilayer model for polydisperse sedimentation with non-hydrostatic pressure. This pressure is introduced to the model as a deviation of the hydrostatic pressure. Some equations to close the resulting model are needed, as well as an additional assumption on velocity field of the mixture. The purpose of this extension is to create a potentially more realistic model.

The resulting models can then be written as a multilayer model with variable density where the unknowns are the average velocities and concentrations in each layer  $\Omega_\alpha$ , the transfer terms across each interface and the total mass. Under the assumption of non-hydrostatic pressure, the non-hydrostatic pressure at each interface appears as a new unknown of the model.

An explicit formula of the transfer terms leads to a reduced form of the system. Bounds of the minimum and maximum eigenvalues of the transport matrix of the system are utilized to design a Harten-Lax-van Leer (HLL)-type path-conservative numerical method.

Finally, we show some one-dimensional, two-dimensional and three-dimensional plus time numerical

simulations, that illustrate the coupled polydisperse sedimentation and flow fields in various scenarios, including sedimentation process in a type of basin that is used in practice in mining industry and in a basin whose bottom topography gives rise to recirculations of the fluid. To close we show some numerical simulations to see the behavior of the mixture when we activate and deactivate the compressibility of the sediment and mixture viscosity.

---

## Contents

---

<b>Agradecimientos</b>	iii
<b>Resumen</b>	v
<b>Abstract</b>	vii
<b>Contents</b>	ix
<b>List of Figures</b>	xiii
<b>List of Tables</b>	xv
<b>Introduction</b>	1
<b>Introducción</b>	6
<b>Preliminaries: some notation</b>	11
0.1 Layers, interfaces, and boundaries . . . . .	11
0.2 Notation . . . . .	11
<b>1 A dynamic multilayer shallow water model for polydisperse sedimentation</b>	14
1.1 Introduction . . . . .	14
1.2 Governing equations . . . . .	15
1.2.1 Continuity equations . . . . .	15
1.2.2 Linear momentum balances . . . . .	16
1.2.3 Explicit formula for the slip velocities without effective solid stress . . . . .	17
1.2.4 Final form of the model equations . . . . .	19
1.3 A multilayer approach . . . . .	19

1.3.1	Weak solution with discontinuities . . . . .	19
1.3.2	Mass conservation jump conditions . . . . .	21
1.3.3	Momentum conservation jump conditions . . . . .	22
1.3.4	Vertical velocity of the solid particles . . . . .	23
1.3.5	Vertical velocity of the mixture . . . . .	24
1.4	A particular weak solution with hydrostatic pressure . . . . .	25
1.5	Closure and reformulation of the model . . . . .	27
1.5.1	Closure of the model in one horizontal space dimension . . . . .	27
1.5.2	Recovery of primitive variables . . . . .	29
1.6	Numerical schemes . . . . .	29
1.6.1	First-order system of balance equations . . . . .	29
1.6.2	Path-conservative method . . . . .	30
1.7	Numerical tests . . . . .	33
1.7.1	Preliminaries . . . . .	33
1.7.2	Test 1.1: one-dimensional vertical sedimentation . . . . .	34
1.7.3	Test 1.2: sedimentation with imposed velocity . . . . .	35
1.7.4	Test 1.3: sedimentation in a domain with a bump . . . . .	41
1.7.5	Test 1.4: sedimentation in a 3D domain . . . . .	44
<b>2</b>	<b>A multilayer shallow water model for polydisperse sedimentation with sediment compressibility and mixture viscosity</b>	<b>49</b>
2.1	Introduction . . . . .	49
2.2	Governing equations . . . . .	50
2.2.1	Continuity equations and linear momentum balances . . . . .	50
2.2.2	Explicit formula for the slip velocities with effective solid stress . . . . .	51
2.2.3	Final form of the model equations . . . . .	53
2.3	Dimensional analysis . . . . .	53
2.4	A multilayer approach . . . . .	55
2.4.1	Weak solution with discontinuities . . . . .	55
2.4.2	Mass and momentum conservation jump conditions . . . . .	56
2.4.3	Vertical velocity of the mixture . . . . .	58
2.5	Closure of multilayer approach . . . . .	59

2.5.1	Multilayer version of hydrostatic pressure . . . . .	60
2.5.2	Weak formulation . . . . .	60
2.5.3	Multilayer model in original variables . . . . .	61
2.5.4	Closure of the model . . . . .	63
2.6	Numerical scheme . . . . .	65
2.7	Numerical tests . . . . .	72
2.7.1	Test 2.1: bidisperse sedimentation in a domain with a bump . . . . .	72
2.7.2	Test 2.2: cylindrical dam break . . . . .	74
2.7.3	Test 2.3: bidisperse sedimentation process in real bathymetry for different gel point. . . . .	77
2.7.4	Test 2.4: bidisperse sedimentation process in real bathymetry with different $\sigma_0$	79
<b>3</b>	<b>Multilayer shallow water model for polydisperse sedimentation with non-hydrostatic pressure</b>	<b>82</b>
3.1	Introduction . . . . .	82
3.2	Mathematical model . . . . .	83
3.2.1	Mass and linear balance equations . . . . .	83
3.2.2	Final form of the model . . . . .	84
3.3	Multilayer model with non-hydrostatic pressure . . . . .	85
3.3.1	Mass and linear momentum jump conditions . . . . .	85
3.3.2	Integration of the mass balance equation . . . . .	87
3.3.3	Integration of the momentum conservation equation . . . . .	87
3.4	Closure of the multilayer model . . . . .	92
3.4.1	Mass conservation inside each layer . . . . .	92
3.4.2	Closure of the multilayer model with non-hydrostatic pressure . . . . .	93
3.4.3	Final form of the multilayer system with non-hydrostatic pressure . . . . .	94
<b>Conclusions and future work</b>	<b>96</b>	
<b>Conclusiones y trabajos futuros</b>	<b>98</b>	
<b>A Appendix</b>	<b>100</b>	
A.1	Explicit formula of the total interlayer mass fluxes . . . . .	100
A.2	A bound of the characteristic velocities . . . . .	101

A.3 A particular weak solution with hydrostatic pressure: deduction of equations . . . . .	102
A.4 Miscellaneous technical results . . . . .	105
A.4.1 Proof of 1.5.1 . . . . .	105
A.4.2 Proof of 1.3.12 . . . . .	105
<b>Bibliography</b>	<b>110</b>

---

## List of Figures

---

1	Sketch with some notations . . . . .	12
1.1	Sketch of the multilayer approach . . . . .	20
1.2	Sketch of the procedure to calculate the vertical velocity. . . . .	24
1.3	Test 1.1: Concentrations of the solid species with respect the normalized height at times $t = 0, 10, 50, 150, 500$ , and $1000$ s. . . . .	34
1.4	Test 1.2: Concentration of solid species $\phi_1, \phi_2$ by layer. . . . .	36
1.5	Test 1.2: Concentration of solid species $\phi_1, \phi_2$ by colors, $\eta(x) = z_B(x) + h(x)$ m. . . . .	37
1.6	Test 1.2: Magnitude of the velocity field $\vec{u}$ and free surface, $\eta(x) = z_B(x) + h(x)$ m. . .	38
1.7	Test 1.2: Concentration for different constant velocities imposed in the left boundary in $t = 100$ s. . . . .	39
1.8	Test 1.3: Concentration of $\phi_1$ and $\phi_2$ by color in a domain with a bump, $\eta(x) = z_B(x) + h(x)$ m. . . . .	40
1.9	Test 1.3: Concentration by color by $\phi_T = \phi_1 + \phi_2$ , $\eta(x) = z_B(x) + h(x)$ m. . . . .	41
1.10	Test 1.3: Velocity field $\vec{u}$ over concentration $\phi_1$ , $\eta(x) = z_B(x) + h(x)$ . . . . .	42
1.11	Test 1.3: Magnitude of the velocity field $\vec{u}$ , $\eta(x) = z_B(x) + h(x)$ . . . . .	43
1.12	Test 1.4: Concentration of $\phi_1$ by color in a 3D domain, $\eta(\mathbf{x}) = z_B(\mathbf{x}) + h(\mathbf{x})$ m. . . . .	45
1.13	Test 1.4: Concentration of $\phi_2$ by color in a 3D domain, $\eta(\mathbf{x}) = z_B(\mathbf{x}) + h(\mathbf{x})$ m. . . . .	46
1.14	Test 1.4: Concentration by color by $\phi_T = \phi_1 + \phi_2$ , $\eta(\mathbf{x}) = z_B(\mathbf{x}) + h(\mathbf{x})$ m. . . . .	47
1.15	Test 1.4: Concentration by color by $\phi_T = \phi_1 + \phi_2$ , $\eta(\mathbf{x}) = z_B(\mathbf{x}) + h(\mathbf{x})$ m. . . . .	48
2.1	Sketch of the multilayer approach . . . . .	55
2.2	Test 2.1: Concentration of species 1 ( $\phi_1$ ) by color in a domain with a bump. . . . .	69
2.3	Test 2.1: Concentration of species 2 ( $\phi_2$ ) by color in a domain with a bump. . . . .	70
2.4	Test 2.1: Total concentration of solid particles, $\phi_T = \phi_1 + \phi_2$ by color in a domain with a bump. . . . .	71
2.5	Test 2.1: Velocity field of the mixture over magnitude of the velocity. . . . .	72

2.6 Test 2.2: Concentration of species 1 ( $\phi_1$ ) by color in a 3D domain with compression and viscous stress tensor deactivated (left) versus concentration of species 1 with stress tensor and compression terms activated (right). . . . .	73
2.7 Test 2.2: Concentration of species 2 ( $\phi_2$ ) by color in a 3D domain with compression and viscous stress tensor deactivated (left) versus concentration of species 2 with stress tensor and compression terms activated (right). . . . .	74
2.8 Test 2.2: Total concentration of solid particles $\phi_T = \phi_1 + \phi_2$ by color in a 3D domain with compression and viscous stress tensor deactivated (left) versus total concentration of solid particles with stress tensor and compression terms activated (right). . . . .	75
2.9 Test 2.2: Velocity field of mixture over her magnitud by color. Comparison between a a mixture with compression and viscous stress tensor deactivated (left) versus a mixture with stress tensor and compression terms activated (right). . . . .	76
2.10 Test 2.4: Concentration of species 1 ( $\phi_1$ ) by color with gel point $\phi_c = 0.08$ (left) versus concentration of species 1 with gel point $\phi_c = 0.15$ (right). . . . .	77
2.11 Test 2.4: Total concentration of solid species $\phi_T$ with gel point $\phi_c = 0.08$ (left) versus total concentration of solid species with gel point $\phi_c = 0.15$ (right). . . . .	78
2.12 Test 2.4: Velocity field of the mixture with gel point $\phi_c = 0.15$ . . . . .	79
2.13 Test 2.4: Concentration of species 1 ( $\phi_1$ ) by color with $\sigma_0 = 0.22$ (left) versus $\sigma_0 = 0.88$ (right) with a fixed gel point $\phi_c = 0.1$ . . . . .	80
2.14 Test 2.4: Total concentration of solid species $\phi_T = \phi_1 + \phi_2$ by color with $\sigma_0 = 0.22$ (left) versus $\sigma_0 = 0.88$ (right) with a fixed gel point $\phi_c = 0.1$ . . . . .	81

## List of Tables



---

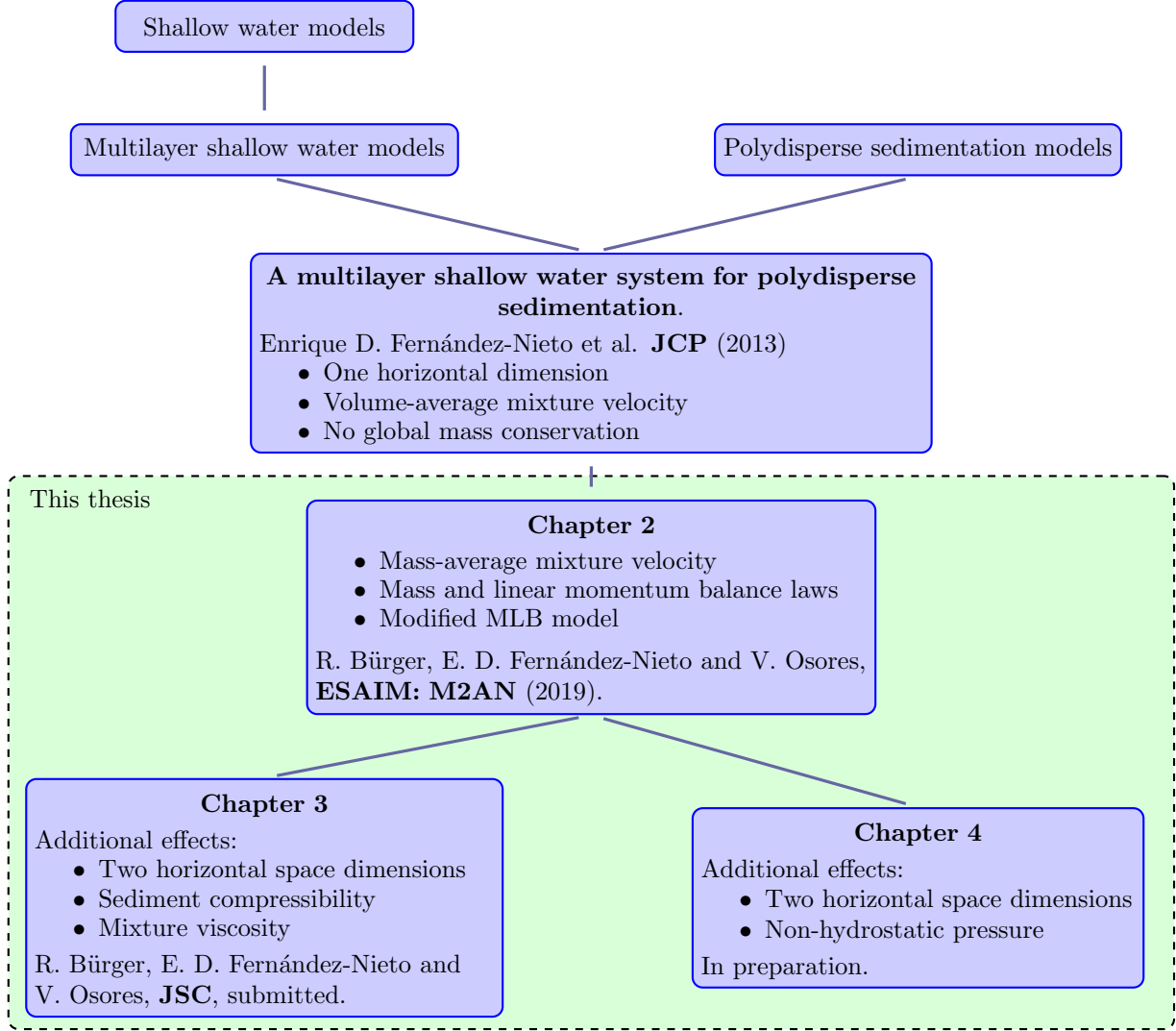
## Introduction

---

The process of sedimentation of small particles suspended in a viscous fluid, water or air combined with the flow of the solid-fluid mixture arises in numerous geophysical situations such as settling and convective sediment transport in rivers and estuaries, gravity currents and debris flows, as well as in clarification tanks, wastewater treatment plants, thickeners in the mining industry and in other fields [6, 10, 32, 49, 57]. It is frequently assumed that the volume fractions (concentrations) of the solid species are constant in each horizontal cross section, wall effects are neglected, and all field variables are assumed to depend on the vertical coordinate and time only. These assumptions lead to a one-dimensional vertical model that is aligned with the gravity body force (mostly gravity) [15, 16, 19], which is adequate for models of unit operations in industrial applications.

We are here interested in flows that involve a significant horizontal bulk flow of the mixtures in addition to vertical segregation, and where typically the horizontal dimensions of the domain are much larger than the vertical. In these situations, instead of solving a fully three-dimensional model (such as the three-dimensional Navier-Stokes equations for an incompressible fluid), one prefers a so-called shallow water or Saint-Venant approach that is based on a vertically integrated version of the underlying model. In the presence of large friction coefficients, considerable water depth, wind, and other effects, however, the standard single-layer shallow water approach is considered invalid since the horizontal velocity can hardly be approximated by a vertically constant velocity. In this case so-called multilayer shallow water models are preferred [1, 2, 58]. The multilayer approach consists in subdividing the computational domain into  $M$  layers in vertical direction, which leads to a system of Saint-Venant equations (one version of the Saint-Venant system for each layer). If a hydrostatic pressure is assumed then the unknowns commonly are a horizontal velocity for each layer and point of the horizontal computational grid plus the total mass of the mixture at that position, along with the solids concentrations in each layer at that position. The vertical velocity components can be calculated by post-processing of data using the horizontal velocity components (no partial differential equations need to be solved).

General references to models of polydisperse sedimentation are included in [7, 47]. Models of polydisperse sedimentation in one space dimension similar to the MLB model (Masliyah-Lockett-Bassoon [46, 48]), and which give rise to strongly coupled systems of nonlinear conservation laws or possibly degenerate convection-diffusion equations were thoroughly studied in recent years including analyses of hyperbolicity [17, 33], extensions to flocculated suspensions forming compressible sediments [9], construction of entropy solutions [8, 34], development of efficient numerical schemes [11, 14, 18], and applications in geophysics [35], water resource recovery [16], and others (see also references in the cited works). Theoretical and experimental works on polydisperse gravity currents, with which our



numerical results could in principle be compared, include [10, 30, 44].

On the other hand, in [24, 55] the authors have included terms accounting for sediment compressibility to one-dimensional sedimentation models. A theory of polydisperse sedimentation with compressibility terms was developed in [9] for a three-dimensional setting, but numerical results were presented for one space dimension only. Efficient implicit-explicit (IMEX) numerical techniques to solve the one-dimensional sedimentation model with compressibility terms and related strongly degenerate parabolic-hyperbolic equations are presented in [11, 12, 22].

Bristeau et al. [13] derived a non-hydrostatic shallow water model in order to approximate incompressible Euler and Navier-Stokes systems with free surface. They compare their results with the well-known Green-Naghdi model for the description of dispersive water waves [42, 43]. A numerical method to solve the Green-Naghdi model is proposed in [51]. In recent works [25, 36] the authors introduce alternative techniques to solve numerically a non-hydrostatic system derived by Yamazaki et al. in [62]. Multilayer models incorporating non-hydrostatic effects to approximate the Euler equations are derived by Penel et al. in [41]. They use a rigorous derivation process based on a Galerkin-type

approximation along the vertical axis.

To put this thesis further into the proper perspective, we mention that suspended sediment transport in shallow regimes by using a Saint-Venant or shallow water model combined with passive transport equations for the different species is a well-known approach [27, 37, 40, 45, 50, 61]. These models are obtained by averaging the original three-dimensional equations along the height of the fluid and allow one to simulate sediment transport with a relative small computational cost. The drawback of these models is that they only take into account the mean depth-average concentration of solid particles in suspension. The vertical distribution and settling of the particles suspended within the fluid is not described, which is achieved by the present multilayer Saint-Venant approach [1, 2, 3, 4, 58]. In fact, numerical simulations by using a multilayer approach allow one to recover interesting properties that are not observed when using just a hydrostatic shallow water model [4]. Moreover, in that paper it is shown that the multilayer approach provides an alternative to the solution of the free-surface Navier-Stokes system, leading to a precise description of the vertical profile of the horizontal velocity while preserving the robustness and the computational efficiency of the usual Saint-Venant system. Similar conclusions have been obtained by applying the multilayer technique to density-stratified flows [5].

## Outline of the thesis

The outlined of this thesis is organized as follows.

- In **Preliminaries**, Section 0.1, layers, interfaces, and boundaries arising in the multilayer approach are summarized, followed by definition of some notations in Section 0.2.
- In **Chapter 1**, we introduce the partial differential equations (PDEs) governing polydisperse sedimentation, starting with the continuity equations (Section 1.2.1) and the linear momentum balances (Section 1.2.2) for the solids and fluid phases and the mixture. The definition of the slip velocity, or solid-fluid relative velocity, for each of the solids phases in terms of the modified form of the MLB model is outlined in Section 1.2.3. We summarize in Section 1.2.4 the governing PDEs to which the multilayer approach is subsequently applied in Section 1.3.

The general concept of weak solutions of the governing PDEs in the multilayer setting, based on the appropriate jump conditions across the interface between adjacent layers, is introduced in Section 1.3.1. From the jump conditions of the mass conservation and linear momentum balance equations of Section 1.2.4, we obtain an expression for the mass transfer fluxes across the interlayer interfaces and we deduce a relation of jump between the extra (or viscous) stress tensors and the velocity field, see Sections 1.3.2 and 1.3.3, respectively.

In Section 1.3.4 we show how the vertical velocities for each solids species are defined for each layer. The corresponding vertical velocities of the mixture are derived in Section 1.3.5. Then, in Section 1.4 we introduce the assumption of a hydrostatic pressure. The closure of the model is described in Section 1.5, and the final form of the equations that will actually be solved is developed. In particular, in Section 1.5.1 the treatment is limited to one horizontal space dimension and fixed proportionalities of each layer with respect to the total height of the mixture are introduced. The assumptions stated so far lead to the interlayer mass fluxes in closed form and reduce the model to  $M(N + 1) + 1$  scalar PDEs, where  $M$  and  $N$  are number of layers

and number of solid species in the mixture. From the conservative variables one may recover the primitive variables, namely, total height of the mixture, solids concentrations and horizontal velocity components in each layer Section 1.5.2. The expression for the total interlayer mass flux is deduced in Appendix A.1. In Section 1.6 we present a numerical scheme to solve and simulate numerically the polydisperse sedimentation process. Specifically, we demonstrate in Section 1.6.1 that the final model takes the form of a first-order system of balance equations. In Section 1.6.2, an HLL-path-conservative method is proposed to the numerical approximation of the system of PDEs.

Section 1.7 is devoted to the presentation of four numerical examples, namely for bidisperse sedimentation in solely one vertical space dimension (Test 1.1), bidisperse sedimentation in a horizontal channel with an inclined bottom (Test 1.2), sedimentation in a domain whose bottom has a “bump” (Test 1.3), and cylindrical dam break involving bidisperse sedimentation over a 3D paraboloid bottom (Test 1.4) (see Sections 1.7.2 to 1.7.5).

The contents of **Chapter 1** has been published in the following article:

- [20] R. BÜRGER, E. D. FERNÁNDEZ-NIETO, AND V. OSORES, *A dynamic multilayer shallow water model for polydisperse sedimentation*. ESAIM: Math. Model. Numer. Anal., vol. 53, 4, pp. 1391–1432, (2019).

- In **Chapter 2**, Section 2.2 as in **Chapter 1** is devoted to show the partial differential equations (PDEs) governing polydisperse sedimentation coupled with the shallow water approach including sediment compressibility and mixture viscosity. In Section 2.2.2 we define the solid-fluid relative velocity for each solid phase. These velocities include in his definition the effective solid stress (discarded in **Chapter 1**) and the modified form of the Masliyah-Lockett-Bassoon (MLB; [46, 48]) model introduced in **Chapter 1**. In **Chapter 1** we have only used a simplified model for MLB-velocities, see equation (1.2.14). From equation (2.2.5) we see as the effective solid stress is only active during consolidation process, that is wherever the local total solids volume fraction  $\phi$  exceeds a critical concentration or gel point  $\phi_c$ . The final form of the multilayer approach with sediment compressibility and mixture viscosity is summarized in Section 2.2.3.

In Section 2.3 we perform a thorough dimensional analysis applied to mass and linear momentum balance equations in order to attain a simplified system of governing partial differential equations.

The notion of a weak solution to the governing multilayer PDEs, based on appropriate jump conditions across each interface between adjacent layers, is introduced in Section 2.4.1. Mass and linear momentum jump conditions across the interlayer interfaces and the approximation of viscous stress tensors at the interfaces are computed in Section 2.4.2 with dimensionless variables. In Section 2.4.3 we recover vertical velocities of the mixture in each layer by post-processing of data.

The multilayer model is derived in Section 2.5. To this end we introduce in Section 2.5.1 the assumption of a hydrostatic pressure. Then we recall that the multilayer approach arises from a variational formulation of the balance equations, and notice that the multilayer model is a particular weak solution of these variational identities. The corresponding weak formulation is introduced in Section 2.5.2.

In Section 2.5.3 we use the dimensional analysis done in Section 2.3 to compute the final form of the multilayer model (returning to the original variables). And we close the model in Section 2.5.4 by establishing that the thickness of each layer is a fixed fraction of the total height of the fluid, and the final form of the equations that will actually be solved is developed.

In Section 2.6 we formulate a 2D numerical scheme to solve this model using the rotational invariance property of the system to solve and simulate polydisperse sedimentation process over different scenarios. Four numerical examples and some interpretations of the results can be find in Section 2.7. First, in Section 2.7.1 we simulate a bi-bidisperse sedimentation process in two horizontal space dimensions over a domain with a bump (Test 2.1), where the compressibility of the sediment and viscosity mixture terms are deactivated, this simulation is the 3D version of (Test 1.3) of the **Chapter 1**. In Section 2.7.2 we simulate a cylindrical dam break bidisperse sedimentation process over paraboloid bottom and we compare the behavior of the mixture where the sediment compressibility and mixture viscosity terms are activated and deactivated respectively. In Section 2.7.3 we simulate a bidisperse sedimentation process over a real bathymetry with compression and mixture viscosity terms activated. Here, we compare the behavior of the mixture for different values of the gel point  $\phi_c$ . Finally, in Section 2.7.4 we simulate the same mixture for different  $\sigma_0$ , keeping constant the gel point at  $\phi_c = 0.1$ .

The contents of **Chapter 2** has been submitted for publication:

R. BÜRGER, E. D. FERNÁNDEZ-NIETO, AND V. OSORES, *A multilayer shallow water approach for polydisperse sedimentation with sediment compressibility and mixture viscosity.* CI<sup>2</sup>MA preprint 2019-29, submitted to J. Sci. Comput.

- In **Chapter 3** we present ongoing work, in which we extend the results of **Chapter 1** to non-hydrostatic effects. In Section 3.2 we present a mathematical model with non-hydrostatic pressure, which is included as a deviation of the hydrostatic pressure. Sediment compressibility and mixture viscosity have been discarded in this model. Section 3.3 is devoted to the formulation of the multilayer model for polydisperse sedimentation with non-hydrostatic pressure, starting with the derivation of the mass and linear momentum jump conditions across each interface in Section 3.2.1, and followed by the deduction of the multilayer version of the mass and linear momentum balance equations (Sections 3.3.2 and 3.3.3, respectively). In Section 3.4 we derive an additional equation to close the multilayer system obtained in previous sections. The final form of the multilayer model for polydisperse sedimentation with non-hydrostatic effect is summarized in Section 3.4.3. The definition of a suitable numerical scheme, as well as the computation of numerical examples, are in preparation.
- In Appendix A.2, we introduce a bound for the characteristic velocities of the proposed multilayer model formulated in Section 1.5. In Appendix A.3 we provide details of some of the calculations that lead to the final system of Section 1.4.

---

## Introducción

---

El proceso de sedimentación de pequeñas partículas suspendidas en un fluido viscoso, agua o aire, combinado con el flujo de una mezcla sólido-fluido surge en numerosas situaciones geofísicas, como la sedimentación y el transporte de sedimentos en ríos y estuarios, corrientes y flujos de escombros, así como también en tanques de relave, plantas de tratamiento de aguas servidas, espesadores en la industria minera y en otros campos [6, 10, 32, 49, 57]. Con frecuencia se supone que las fracciones volumétricas (concentraciones) de las especies sólidas son constantes en cada sección transversal horizontal, que los efectos de la pared pueden ser descartados y además se supone que todas las variables dependen solo de la coordenada vertical y el tiempo. Estos supuestos conducen a un modelo unidimensional vertical alineado con la fuerza de cuerpo (gravedad) [15, 16, 19], los cuáles son adecuados para modelos de operación en aplicaciones industriales.

Estamos interesados en flujos que involucran movimiento horizontal significativo de mezclas además de la segregación vertical de partículas en estas, y en donde las dimensiones horizontales del dominio típicamente son mucho mas grande que la dimensión vertical. En este caso, en vez de resolver modelos tres-dimensionales (tales como las ecuaciones 3-dimensional de Navier-Stokes para fluidos incompresibles), preferimos las aproximaciones shallow water o Saint-Venant los cuáles están basados en una versión verticalmente integrada del modelo subyacente. En presencia de coeficientes de fricción grandes, profundidad considerable, vientos, y otros efectos, sin embargo, aproximaciones estandares de una capa de los modelos shallow water son consideradas en cierto sentido, inválidas ya que la velocidad horizontal difícilmente puede ser aproximada verticalmente constante. En estos casos, los modelos shallow water multicapa son preferidos [1, 2, 58]. Las aproximaciones multicapa consisten en subdividir el dominio computacional en  $M$  capas en la dirección vertical, lo cuál lleva a un sistema de ecuaciones Saint-Venant (una versión de un sistema Saint-Venant, pero para cada capa). Si se supone presión hidrostática comúnmente las incógnitas involucradas son la velocidad horizontal en cada capa y en cada punto del mallado horizontal, la masa total de la mezcla en cada punto del mallado, la concentración en cada capa y punto del mallado para cada una de las especies sólidas. La componente vertical del campo de velocidades en cada capa puede ser calculada por post-procesamiento de datos, usando las componentes horizontales del campo de velocidad (no es necesario resolver una ecuación diferencial parcial).

Algunas referencias generales para modelos de sedimentación polidispersa se pueden encontrar en [7, 47]. Modelos de sedimentación polidispersa en una dimensión espacial similares al modelo MLB (Masliyah-Lockett-Bassoon [46, 48]), los cuales dan lugar a sistemas fuertemente acoplados de leyes de conservación no lineales o posiblemente ecuaciones de convección-difusión degeneradas se han estudiado exhaustivamente en los últimos años, incluyendo un respectivo análisis de hiperbolidad [17, 33],

extensiones a suspensiones con floculantes, las cuales forman sedimentos compresibles [9], construcción de soluciones de entropía [8, 34], desarrollo de esquemas numéricos eficientes [11, 14, 18], y aplicaciones en geofísica [35], como en la recuperación de recursos hídricos [16], entre otros (ver también referencias en los trabajos citados). Por otro lado, algunos trabajos teóricos y experimentales sobre corrientes con material polidisperso, con las cuales en principio, nuestros resultados podrían compararse, se incluyen en [10, 30, 44].

Por otro lado, en [24, 55] los autores han incluido en los modelos de sedimentación unidimensionales términos que modelan el proceso compresión del sedimento. Se ha desarrollado teoría de sedimentación polidispersa con términos de compresibilidad en problemas tridimensionales [9], pero los resultados presentados son unidimensionales (vertical). En [11, 12, 22] se presentan técnicas numéricas eficientes (IMEX) para resolver un modelo de sedimentación unidimensional con términos de compresibilidad de sedimento, los cuales dan lugar a ecuaciones del tipo parabólicas-hiperbólicas fuertemente degeneradas. Bristeau et al. han derivado un modelo de aguas poco profundas con presión no hidrostática con el propósito de aproximar las ecuaciones de Euler y Navier-Stokes incompresibles con superficie libre. Ellos comparan sus resultados con el bien conocido modelo de Green-Naghdi, el cual a sido presentado como un modelo para la descripción ondas de agua dispersivas [42, 43]. Un método numérico para resolver el modelo de Green-Naghdi es propuesto en [51]. En trabajos recientes [25, 36] los autores presentan técnicas alternativas para resolver numéricamente el sistema de EDPs con presión no hidrostática desarrollado por Yamazaki et al. en [62]. Modelos multicapa que incorporan efectos de presión no hidrostática para aproximar las ecuaciones de Euler han sido derivados por Penel et al. en [41]. Ellos presentan una derivación rigurosa basada en una aproximación de tipo Galerkin a lo largo de el eje vertical.

Para poner en perspectiva esta tesis, mencionamos que el transporte de sedimentos suspendidos en regímenes poco profundos usando modelos Saint-Venant o shallow water combinados con ecuaciones de transporte para las diferentes especies dispersas es un enfoque bien conocido [27, 37, 40, 45, 50, 61]. Estos modelos pueden ser obtenidos definiendo promedios de las ecuaciones tridimensionales originales en la dirección vertical (altura del fluido) y permiten simular el transporte de sedimentos con costos computacionales relativamente bajos. Un inconveniente de estos modelos (una capa) es que solo tienen en cuenta la concentración promedio de las partículas sólidas en suspensión. No se describe una distribución vertical de concentraciones, ni el proceso de sedimentación de las partículas suspendidas en el fluido. Lo cual si se logra mediante el enfoque multi capas [1, 2, 3, 4, 58]. De hecho, las simulaciones numéricas producidas por modelos multicapa permiten recuperar propiedades interesantes que no se observan cuando se usan modelos shallow water [4]. En esta tesis se muestra que el enfoque multicapa proporciona una alternativa a la solución a las ecuaciones de Navier-Stokes de superficie libre, lo que lleva a una descripción precisa del perfil vertical de la velocidad horizontal preservando la robustez y la eficiencia computacional de los sistemas Saint-Venant clásicos. Se han obtenido conclusiones similares mediante la aplicación de modelos multicapa a flujos con densidad estratificada [5].

## Organización de la tesis

Esta tesis se organiza como sigue.

- En **Preliminares**, Sección 0.1, se define la frontera, las capas, las interfaces entre capas que

aparecen posterior a la approximación multicapa del dominio. En la Sección 0.2 se presentan algunas notaciones a ser usadas en capítulos posteriores.

- En el **Capítulo 1**, introducimos las ecuaciones en derivadas parciales que gobiernan el proceso de sedimentación polidispersa. Comenzamos con la ecuación de continuidad (Sección 1.2.1) y de balance de momento lineal (Sección 1.2.2) para las fases sólidas, para el fluido y para la mezcla. La definición para la velocidad relativa sólido-fluido o slip-velocity, para cada una de las fases incluyendo la modificación que hemos propuesto para el modelo MLB es detallada en la Sección 1.2.3. Un resumen de las ecuaciones que modelan el proceso de sedimentación polidispersa se puede consultar en la Sección 1.2.4. Y para este modelo matemático resultante, presentamos una aproximación multicapa en la Sección 1.3.

El concepto de soluciones débiles para ecuaciones en derivadas parciales en el marco multicapa, basadas en condiciones de salto apropiadas a través de las interfaces entre capas adyacentes, es introducido en la Sección 1.3.1. De las condiciones de salto para las ecuaciones de conservación de masa y de balance momento lineal Sección 1.2.4, obtenemos una expresión para los flujos de transferencia de masa a través de cada interface y además, se deduce una relación de salto entre el tensor de estrés viscoso y el campo de velocidades, ver Sección 1.3.2 y 1.3.3, respectivamente.

En la Sección 1.3.4 mostramos como recuperar la velocidad vertical de cada una de las especies sólidas dispersas en el fluido. Análogamente en la Section 1.3.5, se muestra el procedimiento para obtener la velocidad vertical de la mezcla. Luego, en la Sección 1.4 introducimos la suposición de presión hidrostática. En la Sección 1.5 se describe como cerrar el modelo, y se presenta modelo multicapa en su forma final, modelo sobre el cual diseñaremos un método numérico. En particular, en la Sección 1.5.1 nuestro tratamiento se limita a una dimensión espacial horizontal (mas una vertical) y se fija el ancho de cada capa proporcional a la altura total de la mezcla. Los supuestos establecidos hasta ahora conducen a obtener términos de transferencia de masa entre capas en forma cerrada y reducen el modelo multicapa a  $M(N + 1) + 1$  PDEs escalares, donde  $M$  y  $N$  representan el número de capas (división en la dirección vertical) y el número de especies sólidas en la mezcla, respectivamente. A partir de las variables conservadas, se puede recuperar variables primitivas de interés, a saber, la altura total de la mezcla, las concentraciones de sólidos y la velocidad horizontal de la mezcla en cada capa Sección 1.5.2. La expresión para el término de transferencia de masa total entre capas se deduce en el Anexo A.1. En la Sección 1.6 proponemos un esquema numérico para resolver y simular numéricamente el proceso de sedimentación polidispersa. Específicamente, mostramos en la Sección 1.6.1 que el modelo final toma la forma de un sistema de ecuaciones de primer orden. En la Sección 1.6.2, se propone un método HLL-path conservativo para la aproximación numérica del sistema de ecuaciones diferenciales parciales resultantes.

La sección 1.7 está dedicada a presentar cuatro ejemplos numéricos. Proceso de sedimentación bidispersa unidimensional (vertical) (Test 1.1), proceso de sedimentación bidispersa sobre un canal horizontal inclinado (Test 1.2), sedimentación bidispersa sobre un dominio con un montículo (Test 1.3), y finalmente simulamos un rotura de presa cilíndrica sobre un fondo parabólico (Test 1.4) (ver Secciones 1.7.2 a 1.7.5).

El contenido del **Capítulo 1** ha sido publicado en el siguiente artículo:

[20] R. BÜRGER, E. D. FERNÁNDEZ-NIETO, AND V. OSORES, *A dynamic multilayer shallow water model for polydisperse sedimentation.* ESAIM: Math. Model. Numer. Anal., vol. 53, 4, pp. 1391–1432, (2019).

- En el **Capítulo 2**, Sección 2.2, tal como en el **Capítulo 1**, está dedicado a presentar las ecuaciones diferenciales en derivadas parciales que modelan el proceso de sedimentación polidispersa acopladas con el modelo de aguas poco profundas en donde, a diferencia del capítulo anterior, se incluyen el efecto de compresibilidad de sedimento y viscosidad de la mezcla. En la Sección 2.2.2, definimos la velocidad relativa sólido-fluido para cada fase sólida. Estas velocidades incluyen en su definición, el estrés efectivo de sólidos (el cual no ha sido considerado en el **Capítulo 1**) y la forma modificada del modelo MLB (Masliyah-Lockett-Bassoon), la cual fue deducida en el **Capítulo 1**. En **Chapter 1** solo hemos usado un modelo MLB simplificado (ver ecuación (1.2.14)). De la ecuación (2.2.5), se puede observar que el estrés efectivo de sólidos solo se activa durante el proceso de consolidación de las partículas, esto ocurre, cuando la fracción volumétrica total  $\phi$  excede una concentración crítica o mas bien conocida como gel point  $\phi_c$ . La forma final del modelo multicapa con compresibilidad de sedimento y viscosidad de la mezcla se resume en la Sección 2.2.3.

En la Sección 2.3, hacemos un análisis dimensional sobre las ecuaciones de balance de masa de cada una de las especies sólidas y sobre la ecuación de balance de momento lineal de la mezcla, para obtener un sistema de EDPs con algunas simplificaciones.

La noción de solución débil para modelos multicapa (como en el capítulo anterior), la cual se basa en condiciones de salto apropiadas a través de cada una de las interfaces entre capas adyacentes, es presentada en la Sección 2.4.1. La condición de salto de masa y de momento lineal a través de cada interface resultantes, y la aproximación del tensor de estrés viscoso en cada interface, son calculados en la Sección 2.4.2 para variables adimensionales. Como en el capítulo anterior, en la Sección 2.4.3, recuperamos la velocidad vertical de la mezcla en cada una de las capas a través de un post-procesamiento de datos.

El modelo multicapa resultante es obtenido en la Sección 2.5. Para este propósito, hemos introducido, al igual que en el capítulo anterior, el supuesto de presión hidrostática Sección 2.5.1. Comentar, que el modelo multicapa surge tras considerar una formulación débil de las ecuaciones de balance de masa y de momento lineal. Luego de un tratamiento matemático de estas ecuaciones se deduce el modelo multicapa como una solución particular de estas identidades variacionales. Esta formulación es introducida en la Sección 2.5.2.

En la Sección 2.5.3, hacemos uso del análisis dimensional hecho en la Sección 2.3, para obtener el modelo multicapa en las variables originales. Cerramos el modelo en la Sección 2.5.4, tras establecer que el grosor de cada capa es una fracción fija de la altura total del fluido.

En la Sección 2.6 proponemos un esquema numérico en 2-dimensiones horizontales, en donde hemos utilizado la propiedad de invariancia a través de rotaciones del sistema multicapa resultante, el cual nos permite simular el proceso de sedimentación polidispersa en diferentes escenarios. Se presentan algunos ejemplos numéricos e impresiones de los resultados obtenidos en la Sección 2.7. En la Sección 2.7.1 simulamos un proceso de sedimentación bidispersa en dos dimensiones horizontales (más la vertical) sobre un dominio con un monte al centro (Test 2.1) (fondo no plano), donde en primera instancia hemos desactivado los términos que tienen relación

con la compresibilidad del sedimento y con la viscosidad de la mezcla. Esta simulación es la versión 3D del Test 1.3 presentado en el **Capítulo 1**. En la Sección 2.7.2 se simula un proceso de sedimentación bidispersa tras una ruptura de presa cilíndrica sobre un fondo paraboloide y comparamos el comportamiento de la mezcla cuando se tiene términos de compresibilidad del sedimento y viscosidad activados versus cuando estos están desactivados. En la Sección 2.7.3 simulamos un proceso de sedimentación bidispersa sobre una batimetría real, con términos de compresión de sedimentos y de viscosidad de la mezcla activados. Aquí, se compara el comportamiento de la mezcla para diferentes valores del gel-point  $\phi_c$ . Finalmente, en la Sección 2.7.4 se simula la misma mezcla anterior, y comparamos su comportamiento respecto de diferentes valores para el parámetro  $\sigma_0$ , manteniendo constante  $\phi_c = 0.1$ .

El contenido del **Capítulo 2** a sido sometido para su publicación:

R. BÜRGER, E. D. FERNÁNDEZ-NIETO, AND V. OSORES, *A multilayer shallow water approach for polydisperse sedimentation with sediment compressibility and mixture viscosity.* CI<sup>2</sup>MA pre-print and submitted to JCP, (2019).

- El **Capítulo 3** está dedicado a presentar un trabajo en proceso, en el cual extendemos los resultados obtenidos en el **Capítulo 1** a efectos de presión no hidrostática. En la Sección 3.2 se presenta un modelo matemático, donde hemos incluido la presión no hidrostática, la cual es incluida una desviación de la presión hidrostática. Efectos de compresibilidad de sedimento y viscosidad de la mezcla han sido descartados en este modelo. La Sección 3.3 está dedicada a la formulación del modelo multicapa para sedimentación polidispersa con presión no hidrostática, donde comenzamos con la obtención de los respectivos saltos de masa y de momento lineal a través de cada interface, en la Sección 3.2.1, seguido de la deducción de la versión multicapa de las ecuaciones de balance de masa y de momento lineal (Sección 3.3.2 y Sección 3.3.3, respectivamente). En la Sección 3.4, obtenemos una ecuación adicional para cerrar el sistema multicapa obtenido en secciones previas. La forma final del modelo multicapa para sedimentación polidispersa con efectos no hidrostáticos se resume en la Sección 3.4.3. La diseño de un esquemas numéricicos adecuados, así como también, ejemplos de simulaciones numéricas, están en preparación.
- En el Anexo A.2, se presentan cotas para las velocidades características del modelo multicapa propuesto en Sección 1.5. Y en el Anexo A.3 se muestran detalles que permiten obtener el sistema resultante en la Sección 1.4.

---

## Preliminaries: some notation

---

### 0.1 Layers, interfaces, and boundaries

We shall consider a  $d$ -dimensional space ( $d = 2, 3$ ). For a given final time  $T > 0$  and each time  $t \in [0, T]$  we denote by  $\Omega_F(t)$  the fluid domain and by  $I_F(t)$  its projection onto the horizontal plane. In order to introduce a multilayer system, the fluid domain is divided along the vertical direction into  $M \in \mathbb{N}^*$  pre-set layers of thickness  $h_\alpha(t, \mathbf{x})$  with  $M + 1$  interfaces

$$\Gamma_{\alpha+1/2}(t) = \{(\mathbf{x}, z) \in \mathbb{R}^d : z = z_{\alpha+1/2}(t, \mathbf{x}), \mathbf{x} \in I_F(t)\}, \quad \alpha = 0, 1, \dots, M \quad (0.1.1)$$

(see Figure 1). We assume that the interfaces  $\Gamma_{\alpha+1/2}(t)$  are smooth, concretely at least of class  $C^1$  in time and space. We denote by  $z_B = z_{1/2}$  and  $z_S = z_{M+1/2}$  the equations of the bottom and the free surface interfaces  $\Gamma_B(t)$  and  $\Gamma_S(t)$ , respectively. The thickness of layer  $\alpha$  at time  $t$  and horizontal position  $\mathbf{x}$  is

$$h_\alpha = h_\alpha(t, \mathbf{x}) = z_{\alpha+1/2}(t, \mathbf{x}) - z_{\alpha-1/2}(t, \mathbf{x}), \quad \alpha = 1, \dots, M,$$

such that

$$z_{\alpha+1/2} = z_B + h_1 + \dots + h_\alpha, \quad \text{for } \alpha = 1, \dots, M.$$

Then the height of the fluid is  $h := z_S - z_B = h_1 + \dots + h_M$ .

The boundary  $\partial\Omega_F(t)$  of  $\Omega_F(t)$  can be represented as  $\partial\Omega_F(t) = \Gamma_B(t) \cup \Gamma_S(t) \cup \Theta(t)$ , where  $\Theta(t)$  is the inflow/outflow boundary which we assume here to be vertical. The fluid domain is split as  $\overline{\Omega_F(t)} = \cup_{\alpha=1}^M \overline{\Omega_\alpha(t)}$ , where we define the layers and their boundaries as

$$\Omega_\alpha(t) := \{(\mathbf{x}, z) : \mathbf{x} \in I_F(t) \text{ and } z_{\alpha-1/2} < z < z_{\alpha+1/2}\}, \quad (0.1.2)$$

such that

$$\partial\Omega_\alpha(t) := \Gamma_{\alpha-1/2}(t) \cup \Gamma_{\alpha+1/2}(t) \cup \Theta_\alpha(t), \quad \Theta_\alpha(t) := \{(\mathbf{x}, z) : \mathbf{x} \in \partial I_F(t) \text{ and } z_{\alpha-1/2} < z < z_{\alpha+1/2}\}.$$

Hence the inflow/outflow boundary is split as  $\overline{\Theta(t)} = \cup_{\alpha=1}^M \overline{\Theta_\alpha(t)}$ .

### 0.2 Notation

Based in part on the definition of layers above, we introduce the following notation:

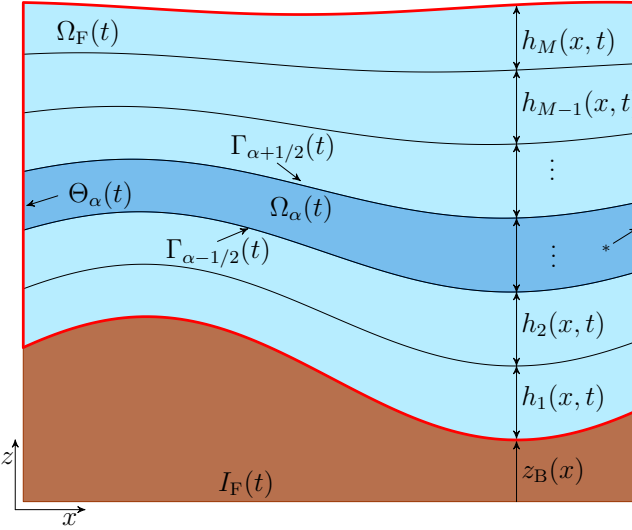


Figure 1: Sketch with some notations

- (i) For two tensors  $\mathbf{a}$  and  $\mathbf{b}$  of sizes  $(n, m)$  and  $(n, p)$  respectively, we shall denote by  $(\mathbf{a}; \mathbf{b})$  the tensor of size  $(n, m + p)$  which is the concatenation of  $\mathbf{a}$  and  $\mathbf{b}$  in this order.
- (ii) For  $\mathbf{x} = (x_1, \dots, x_{d-1})$  and the differential operator  $\nabla = (\partial_{x_1}, \dots, \partial_{x_{d-1}}, \partial_z)$ , we define

$$\bar{\nabla} := (\partial_t; \nabla) = (\partial_t, \partial_{x_1}, \dots, \partial_{x_{d-1}}, \partial_z), \quad \nabla_{\mathbf{x}} := (\partial_{x_1}, \dots, \partial_{x_{d-1}}).$$

- (iii) For  $\alpha = 0, 1, \dots, M$  and for a function  $f$ , we set

$$f_{\alpha+1/2}^- := (f|_{\Omega_\alpha(t)})|_{\Gamma_{\alpha+1/2}(t)}, \quad f_{\alpha+1/2}^+ := (f|_{\Omega_{\alpha+1}(t)})|_{\Gamma_{\alpha+1/2}(t)}.$$

If  $f$  is continuous across  $\Gamma_{\alpha+1/2}(t)$ , we simply set  $f_{\alpha+1/2} := f|_{\Gamma_{\alpha+1/2}(t)}$ . We shall also use the notation

$$\tilde{f}_{\alpha+1/2} := \frac{1}{2}(f_{\alpha+1/2}^+ + f_{\alpha+1/2}^-).$$

- (iv) We denote by  $\boldsymbol{\eta}_{\alpha+1/2}$  the spatial unit normal vector to the interface  $\Gamma_{\alpha+1/2}(t)$  outward to the layer  $\Omega_\alpha(t)$  for a given time  $t$ , that is

$$\boldsymbol{\eta}_{\alpha+1/2} := \frac{1}{\sqrt{1 + |\nabla_{\mathbf{x}} z_{\alpha+1/2}|^2}} (\nabla_{\mathbf{x}} z_{\alpha+1/2}, -1)^T, \quad \alpha = 0, \dots, M.$$

Furthermore,  $\mathbf{n}_{t,\alpha+1/2}$  denotes the (space-time) unit normal vector  $\Gamma_{\alpha+1/2}(t)$  pointing to  $\Omega_{\alpha+1}(t)$ , i.e.,

$$\mathbf{n}_{t,\alpha+1/2} := \frac{1}{\sqrt{1 + |\nabla_{\mathbf{x}} z_{\alpha+1/2}|^2 + (\partial_t z_{\alpha+1/2})^2}} (\partial_t z_{\alpha+1/2}, \nabla_{\mathbf{x}} z_{\alpha+1/2}, -1)^T, \quad \alpha = 0, \dots, M.$$

- (v) Let  $\alpha \in \{1, \dots, M-1\}$ , and assume that  $y$  is a scalar, vectorial, or tensorial quantity defined in  $\Omega_\alpha(t)$  and  $\Omega_{\alpha+1}(t)$ , such that the one-sided limits of  $y$  on either side of  $\Gamma_{\alpha+1/2}(t)$ , that is

$$y_{t,\alpha+1/2}^+ := \lim_{\substack{z \rightarrow z_{\alpha+1/2} \\ z > z_{\alpha+1/2}}} y(\mathbf{x}, z, t), \quad y_{t,\alpha+1/2}^- := \lim_{\substack{z \rightarrow z_{\alpha+1/2} \\ z < z_{\alpha+1/2}}} y(\mathbf{x}, z, t),$$

are well defined. Then we denote by  $\llbracket y \rrbracket_{t,\alpha+1/2}$  the jump of  $y$  across  $\Gamma_{\alpha+1/2}(t)$ , that is,

$$\llbracket y \rrbracket_{t,\alpha+1/2} = y_{t,\alpha+1/2}^+ - y_{t,\alpha+1/2}^-.$$

If  $y$  does not depend on  $z$  within each of the layers  $\Omega_\alpha(t)$  and  $\Omega_{\alpha+1}(t)$ , then this implies

$$\llbracket y \rrbracket_{t,\alpha+1/2} = (y|_{\Omega_{\alpha+1}(t)} - y|_{\Omega_\alpha(t)})|_{\Gamma_{\alpha+1/2}(t)}. \quad (0.2.1)$$

**Remark 0.2.1.** *If we add the time variable as one more dimension, then the corresponding domain  $\Omega_T$  is actually given by  $\Omega_T = \{(t, \mathbf{x}, z) : t \in (0, T], (\mathbf{x}, z) \in \Omega_F(t)\}$  with  $\partial\Omega_T = \Lambda_T \cup \Lambda_1 \cup \Lambda_2$ , where  $\Lambda_T = \{(t, \mathbf{x}, z) : t \in (0, T), (\mathbf{x}, z) \in \partial\Omega_F(t)\}$ ,  $\Lambda_1 = \{0\} \times \Omega_F(0)$ , and  $\Lambda_2 = \{T\} \times \Omega_F(T)$ . Since we integrate over  $\Omega_F(t)$ , we retain here the boundary  $\Lambda_T$  for the computations even if it means cancelling the tests functions over the boundaries  $\Lambda_1$  and  $\Lambda_2$ .*

# CHAPTER 1

---

## A dynamic multilayer shallow water model for polydisperse sedimentation

---

### 1.1 Introduction

The purpose of **Chapter 1** is to develop a multilayer shallow water model framework of polydisperse sedimentation such that allows to recover global mass and linear momentum balance laws of the mixture, along with a method for the numerical solution in the case of one horizontal space dimension. Important phenomena such that sediment compressibility and mixture viscosity will be analysed in **Chapter 2**, as also, the two horizontal dimensions extension of the model.

Here polydispersivity means that the solid particles belong to a finite number  $N$  of species that differ in size or density, and where particles of different species segregate and form areas of different composition. Theory of mixture allow us to consider that the  $N + 1$  solid species plus the fluid are described as a superimposed continuous phases.

The main novelty is the choice of the mass average of the velocities of the  $N + 1$  phases to describe the movement of the mixture, in contrast to a previous work [39] where the velocity was defined as a volume average of phase velocities. The advantage of the present approach is that the mass and linear momentum balance of the mixture are recovered, and therefore consistency with a single-phase flow model is recovered. In [39] the vertical settling velocities of the  $N$  solids phases as nonlinear functions of the local composition are determined by the well-known Masliyah-Lockett-Bassoon (MLB) model [46, 48]. This model is also utilized herein but in a modified form.

The final model that is eventually solved can be stated as a system of balance laws of the type

$$\partial_t \mathbf{w} + \partial_x \mathcal{F}(\mathbf{w}) = \mathcal{S}(\mathbf{w}, \partial_x \mathbf{w}) + \mathcal{G}(\mathbf{w}, \partial_x \mathbf{w}), \quad (1.1.1)$$

where  $t$  is time,  $x$  is the horizontal space coordinate, the unknown  $\mathbf{w} = \mathbf{w}(t, x)$  is a vector of  $(N + 1)M + 1$  scalar unknown functions that represent the total mass of the mixture, the horizontal velocity component in each of the  $M$  layers, and the  $N$  solids concentrations in each of the  $M$  layers. The flux vector  $\mathcal{F}(\mathbf{w})$  and the source terms  $\mathcal{S}(\mathbf{w}, \partial_x \mathbf{w})$  and  $\mathcal{G}(\mathbf{w}, \partial_x \mathbf{w})$  arise from reduced versions of the balance equations, as well as from jump conditions across the interfaces between the layers. These ingredients will be specified in later parts of **Chapter 1**. The particular form (1.1.1) is suitable for the application of specialized methods for first-order hyperbolic systems with non-conservative terms.

The numerical solution of the resulting multilayer model (1.1.1) is based on recently developed specialized methods for first-order hyperbolic systems with non-conservative products. In [31] the authors propose a formal definition for such products and provide a notion of weak solution. Numerical schemes to solve systems of partial differential equation in non-conservative form are proposed in [28, 53, 54, 60] (this list is not complete). In [26] the authors introduce new first-order finite volume solvers, so-called PVM (polynomial viscosity matrix) methods, to solve Cauchy problems for hyperbolic systems of conservation laws with source terms and/or non-conservative products. This method allows one to compute an approximation of the viscosity matrix by a polynomial evaluation of a Roe matrix, which avoids the necessity to compute the complete characteristic decomposition of this matrix.

To calculate the complete velocity field of the mixture within the approach developed herein, we will use the mass balance equation of the mixture and the mass jump condition in the interfaces between layers to compute the vertical velocity of the mixture. As we will see later, this vertical velocity is linear by layer and it has possibly a jump between adjacent layers given by the jump condition. In [38] the authors introduced this idea for an incompressible fluid. Here in the mixture each species has a constant density but the mixture itself is compressible. The mixture is consistent with a single phase flow satisfying laws of conservation of mass and momentum.

## 1.2 Governing equations

### 1.2.1 Continuity equations

Let us consider  $N \in \mathbb{N}$  species of spherical solid particles dispersed in a viscous fluid. For each solid species  $j$ ,  $j = 1, \dots, N$ , we denote by  $\phi_j$ ,  $\rho_j$ , and  $d_j$  its volumetric concentration, density, and particle diameter, respectively, where we assume that  $d_1 \geq d_2 \geq \dots \geq d_N$ . Furthermore, in  $d = 3$  space dimensions we denote by  $\mathbf{v}_j = (u_j, v_j, w_j)^T \in \mathbb{R}^3$  its phase velocity with the horizontal component  $(u_j, v_j) \in \mathbb{R}^2$ , while in  $d = 2$  space dimensions (one horizontal, one vertical) the velocity is  $(u_j, w_j) \in \mathbb{R}^2$  with the scalar horizontal component  $u_j$ . In both cases,  $w_j$  is the vertical velocity component. The same notation is used for the fluid indexed by  $j = 0$ . The model is based on the continuity and linear momentum balance equations for the  $N$  solid species and the fluid. The continuity equations are given by

$$\partial_t(\rho_j \phi_j) + \nabla \cdot (\rho_j \phi_j \mathbf{v}_j) = 0, \quad j = 0, \dots, N. \quad (1.2.1)$$

Since all densities  $\rho_j$  are constant, we may divide the  $j$ -th equation in (1.2.1) by  $\rho_j$ , obtaining

$$\partial_t \phi_j + \nabla \cdot (\phi_j \mathbf{v}_j) = 0, \quad j = 0, \dots, N.$$

(Here and in the remaining of the paper, partial derivatives of indexed quantities are always understood in the sense  $\partial_t \phi_j = \partial_t(\phi_j)$ , etc.) Let  $\Phi := (\phi_0, \dots, \phi_N)^T$ . We define the density of the mixture

$$\rho := \rho(\Phi) := \rho_0 \phi_0 + \rho_1 \phi_1 + \dots + \rho_N \phi_N.$$

(Notice that while the individual phase densities  $\rho_0, \rho_1, \dots, \rho_N$  are constants,  $\rho = \rho(\Phi)$  is variable and depends on the local composition  $\Phi$  of the mixture. Since the components of  $\Phi$  are dimensionless

volume fractions, the dimension of  $\rho$  is again a density). Then summing all equations in (1.2.1) yields that the mass average velocity of the mixture

$$\mathbf{v} := (u, v, w)^T := \frac{1}{\rho} \sum_{m=0}^N \rho_m \phi_m \mathbf{v}_m = \frac{1}{\rho} \left[ \left( \rho - \sum_{j=1}^N \rho_j \phi_j \right) \mathbf{v}_0 + \sum_{k=1}^N \rho_k \phi_k \mathbf{v}_k \right] \quad (1.2.2)$$

satisfies the global mass balance of the mixture

$$\partial_t \rho + \nabla \cdot (\rho \mathbf{v}) = 0, \quad (1.2.3)$$

where we observe that (1.2.3) has the same form as the continuity equation of a single-phase fluid with variable density  $\rho$  and velocity  $\mathbf{v}$ ; in fact, the mass average velocity  $\mathbf{v}$  is introduced precisely for the purpose of achieving this form. Defining the slip velocities  $\mathbf{u}_i := \mathbf{v}_i - \mathbf{v}_0$  ( $\mathbf{u}_0 = 0$ ) and  $\lambda_i := \rho_i \phi_i / \rho$  for  $i = 1, \dots, N$ , we now derive the identity

$$\rho_j \phi_j \mathbf{v}_j = \rho_j \phi_j (\mathbf{u}_j + \mathbf{v} - (\lambda_1 \mathbf{u}_1 + \dots + \lambda_N \mathbf{u}_N)), \quad j = 1, \dots, N; \quad (1.2.4)$$

hence the solids mass balance equations from (1.2.1) can be rewritten in terms of  $\mathbf{v}$  and  $\mathbf{u}_1, \dots, \mathbf{u}_N$  as

$$\partial_t (\rho_j \phi_j) + \nabla \cdot (\rho_j \phi_j (\mathbf{u}_j + \mathbf{v} - (\lambda_1 \mathbf{u}_1 + \dots + \lambda_N \mathbf{u}_N))) = 0, \quad j = 1, \dots, N.$$

Summing all these equations plus that of the fluid, we recover, again, the mass balance of the mixture.

**Remark 1.2.1.** *The main difference between the model that we present here and the one introduced in [38] comes from the definition of the average velocity  $\mathbf{v}$  (equation (1.2.2)). In [38] authors consider a multilayer approach of a polydisperse sedimentation model with the classical MLB settling velocity and average velocity*

$$\mathbf{v} := \sum_{m=0}^N \phi_m \mathbf{v}_m. \quad (1.2.5)$$

*The usual definition of the average velocity only consider the concentrations of the species and the fluid. The definition of mass average velocity of the mixture (1.2.2) considers densities and concentrations of each one of the solids species and of the fluid in which the particles are dispersed. This fact gives a superior behavior to the proposed mass average velocity because it allows us to recover global mass and linear momentum balance laws of the mixture. Moreover, using this definition we also propose a modification of the classical MLB model, which now consider the total density of the mixture too (see Section 1.2.3).*

## 1.2.2 Linear momentum balances

The respective momentum balance equations for the  $N$  solids species and the fluid are given by

$$\partial_t (\rho_j \phi_j \mathbf{v}_j) + \nabla \cdot (\rho_j \phi_j \mathbf{v}_j \otimes \mathbf{v}_j) = \nabla \cdot \mathbf{T}_j + \rho_j \phi_j \mathbf{b} + \mathbf{m}_j^f + \mathbf{m}_j^s, \quad j = 1, \dots, N, \quad (1.2.6)$$

$$\partial_t (\rho_0 \phi_0 \mathbf{v}_0) + \nabla \cdot (\rho_0 \phi_0 \mathbf{v}_0 \otimes \mathbf{v}_0) = \nabla \cdot \mathbf{T}_0 + \rho_0 \phi_0 \mathbf{b} - (\mathbf{m}_1^f + \dots + \mathbf{m}_N^f). \quad (1.2.7)$$

Here  $\mathbf{T}_j$  denotes the stress tensor of the particle species  $j$ ,  $j = 1, \dots, N$ ,  $\mathbf{T}_0$  that of the fluid,  $\mathbf{b}$  is the body force,  $\mathbf{m}_j^f$  and  $\mathbf{m}_j^s$  are the interaction forces per unit volume between solid species  $j$  and the fluid

and between the solid species  $j$  and  $i$ , respectively, and  $\mathbf{m}_j^s = \mathbf{m}_{j1}^s + \cdots + \mathbf{m}_{jN}^s$  is the particle-particle interaction terms of species  $j$ . In light of considerable experimental and theoretical justification [9], the quantities  $\mathbf{m}_{ji}^s$  are neglected at the very low Reynolds numbers considered here.

Summing all equations in (1.2.6) plus (1.2.7) and setting  $\mathbf{T} = \sum_{j=0}^N \mathbf{T}_j$  yields

$$\partial_t \left( \sum_{j=0}^N \rho_j \phi_j \mathbf{v}_j \right) + \nabla \cdot \left( \sum_{j=0}^N \rho_j \phi_j \mathbf{v}_j \otimes \mathbf{v}_j \right) = \nabla \cdot \mathbf{T} + \rho \mathbf{b}.$$

Defining the diffusion velocities  $\mathbf{u}_j^d := \mathbf{v}_j - \mathbf{v}$  for  $j = 0, \dots, N$ , we may rewrite the above expression as

$$\partial_t(\rho \mathbf{v}) + \nabla \cdot (\rho \mathbf{v} \otimes \mathbf{v}) = \nabla \cdot \left( \mathbf{T} - \sum_{j=0}^N \rho_j \phi_j \mathbf{u}_j^d \otimes \mathbf{u}_j^d \right) + \rho \mathbf{b}.$$

Finally, the linear momentum balance equation for the mixture is given by

$$\partial_t(\rho \mathbf{v}) + \nabla \cdot (\rho \mathbf{v} \otimes \mathbf{v}) = \nabla \cdot \boldsymbol{\Sigma} + \rho \mathbf{b},$$

where  $\boldsymbol{\Sigma} := \mathbf{T} - \sum_{j=0}^N \rho_j \phi_j \mathbf{u}_j^d \otimes \mathbf{u}_j^d$  denotes the stress tensor of the mixture. (This reduces to  $\boldsymbol{\Sigma} = \mathbf{T}$  if the fluid and solid velocities are the same.)

We assume here that the stress tensors of the solid and fluid phases can be written as  $\mathbf{T}_j = -p_j \mathbf{I} + \mathbf{T}_j^E$  for  $j = 1, \dots, N$  and  $\mathbf{T}_0 = -p_0 \mathbf{I} + \mathbf{T}_0^E$ , respectively, where  $p_j = (\phi_j/\phi)(\phi p + \sigma_e(\phi))$  denotes the phase pressure of particle species  $j$ ,  $p_0 = (1-\phi)p$  that of the fluid. The total concentration of particles is  $\phi = \phi_1 + \cdots + \phi_N = 1 - \phi_0$ .  $\mathbf{T}_0^E$  and  $\mathbf{T}_j^E$  are the viscous stress tensors of the fluid and solid phases respectively, and  $\sigma_e$  is the effective solid stress.

The interaction solid-fluid force per unit volume is given by

$$\mathbf{m}_j^f = \alpha_j(\Phi) \mathbf{u}_j + \beta_j(\Phi) \nabla \phi_j, \quad (1.2.8)$$

where  $\alpha_j$  is the resistance coefficient for the transfer of momentum between the fluid and solid phase species  $j$ . Following the argument of [9], namely inserting (1.2.8) into the linear momentum balances, considering the mixture at equilibrium in a settling column so that all slip velocities and the fluid velocity vanish and  $\nabla p = -\rho_0 g \mathbf{k}$ , where  $\mathbf{k}$  is the upward-pointing unit vector, we obtain that  $\beta_1(\Phi) = \cdots = \beta_N(\Phi) = p$ . Introducing the continuity equation (1.2.1) in the momentum equations (1.2.6) and assuming that gravity is the only body force, i.e.,  $\mathbf{b} = g \mathbf{k}$  where  $\mathbf{k}$  is the downward-pointing unit vector, we obtain the linear momentum balances in the following form:

$$\rho_j \phi_j D_t \mathbf{v}_j = \nabla \cdot \mathbf{T}_j^E - \phi_j \nabla p - \rho_j \phi_j g \mathbf{k} + \alpha_j(\Phi) \mathbf{u}_j + \mathbf{m}_j^s - \nabla \left( \frac{\phi_j}{\phi} \sigma_e(\phi) \right), \quad j = 1, \dots, N, \quad (1.2.9)$$

$$\rho_0 D_t \mathbf{v}_0 = -\nabla p + \frac{1}{1-\phi} \nabla \cdot \mathbf{T}_0^E - \rho_0 g \mathbf{k} - (\alpha_1 \mathbf{u}_1 + \cdots + \alpha_N \mathbf{u}_N), \quad (1.2.10)$$

where we use the standard notation  $D_t \mathbf{v} = \partial_t \mathbf{v} + (\mathbf{v} \cdot \nabla) \mathbf{v}$ .

### 1.2.3 Explicit formula for the slip velocities without effective solid stress

An explicit expression for the slip velocities  $\mathbf{u}_j$  is derived in [9] by a dimensional analysis applied to the linear momentum equations for the solid species and the fluid, (1.2.9) and (1.2.10), respectively.

This procedure yields the explicit form

$$\mathbf{u}_j = g \frac{\phi_j}{\alpha_j(\Phi)} \left( (\bar{\rho}_j - \bar{\rho}^T \Phi) \mathbf{k} + \frac{\sigma_e(\phi)}{g\phi_j} \nabla \left( \frac{\phi_j}{\phi} \right) + \frac{1-\phi}{g\phi} \nabla \sigma_e(\phi) \right), \quad j = 1, \dots, N, \quad (1.2.11)$$

where we introduce the reduced densities  $\bar{\rho}_j := \rho_j - \rho_0$ ,  $j = 1, \dots, N$  and the vector  $\bar{\rho} := (\bar{\rho}_1, \dots, \bar{\rho}_N)^T$ . Following [9, 46, 48] we choose  $\phi_j/\alpha_j(\Phi) = -d_j^2 V(\phi)/18\mu_0$ , where  $\mu_0$  is the viscosity of the fluid, and the function  $V(\phi)$ , known as hindered settling factor, that is supposed to satisfy  $V(\phi) > 0$  and  $V'(\phi) < 0$  for  $0 < \phi < \phi_{\max}$ . A common choice of this function is the Richardson-Zaki [56] expression

$$V(\phi) = \begin{cases} (1-\phi)^{n_{RZ}-2} & \text{for } \phi \leq 1, \\ 0 & \text{for } \phi > 1, \end{cases} \quad n_{RZ} > 2. \quad (1.2.12)$$

Since we are interested in modelling only the sedimentation process we will not consider effects of sediment compressibility, so we assume that the effective solid stress  $\sigma_e$  is equal to 0. Therefore the final form of the slip velocities is given by

$$\mathbf{u}_j = \mu \delta_j V(\phi) (\bar{\rho}_j - \bar{\rho}^T \Phi) \mathbf{k}, \quad j = 1, \dots, N, \quad (1.2.13)$$

where we introduce the parameters  $\mu := -gd_1^2/(18\mu_0)$  and  $\delta_j := d_j^2/d_1^2$ ,  $j = 1, \dots, N$ , where we recall that  $d_1$  is the largest particle diameter.

Inserting (1.2.13) into (1.2.4) we get

$$\rho_j \phi_j \mathbf{v}_j = \rho_j \phi_j \mathbf{v} + \rho_j f_j^M(\Phi) \mathbf{k} \quad \text{for } j = 1, \dots, N. \quad (1.2.14)$$

Note that we use the mass average velocity (1.2.2) instead of the classical definition given by the volume average velocity (1.2.5). Then we obtain a modification of MLB model, defined by

$$f_j^M(\Phi) := \phi_j v_j^{\text{MLB}} = \phi_j \mu V(\phi) \left( \delta_j (\bar{\rho}_j - \bar{\rho}^T \Phi) - \sum_{k=1}^N \lambda_k \delta_k (\bar{\rho}_k - \bar{\rho}^T \Phi) \right), \quad j = 1, \dots, N. \quad (1.2.15)$$

Finally, the continuity and momentum equations for the solids can be written as

$$\begin{aligned} \partial_t \phi_j + \nabla \cdot (\phi_j \mathbf{v} + f_j^M(\Phi) \mathbf{k}) &= 0, \quad j = 1, \dots, N, \\ \rho_j (\partial_t (\phi_j \mathbf{v}_j) + \nabla \cdot (\phi_j \mathbf{v}_j \otimes \mathbf{v}_j)) &= \nabla \cdot \mathbf{T}_j^E - \phi_j \nabla p - \rho_j \phi_j g \mathbf{k} + \alpha_j(\Phi) \mathbf{u}_j, \quad j = 1, \dots, N. \end{aligned} \quad (1.2.16)$$

We remark here that the vertical velocities of particles expressed as combination of the vertical average velocity of the mixture  $w = \lambda_0 w_0 + \dots + \lambda_N w_N$  and the fluxes  $f_j^M(\Phi)$  satisfy

$$\rho_j \phi_j w_j = \rho_j \phi_j w + \rho_j f_j^M(\Phi), \quad (1.2.17)$$

moreover we have the identity

$$\sum_{j=1}^N \lambda_j w_j = (1 - \lambda_0)w + \frac{1}{\rho} \sum_{j=1}^N \rho_j f_j^M$$

that can be rearranged as

$$\lambda_0 w_0 = \lambda_0 w - \frac{1}{\rho} \sum_{j=1}^N \rho_j f_j^M.$$

From the above equation we may define a similar relation as (1.2.14) for the velocity of the fluid

$$\rho_0 \phi_0 \mathbf{v}_0 := \rho_0 \phi_0 \mathbf{v} + \rho_0 f_0^M(\Phi) \mathbf{k} = \rho_0 \phi_0 \mathbf{v} - \sum_{j=1}^N \rho_j f_j^M(\Phi) \mathbf{k}. \quad (1.2.18)$$

### 1.2.4 Final form of the model equations

The final form of the model is given by the mass conservation and linear momentum balance equations for the solids species after introducing (1.2.11) into (1.2.16) and the fluid, it can be written as

$$\partial_t(\rho_j \phi_j) + \nabla \cdot (\rho_j \phi_j \mathbf{v}_j) = 0, \quad j = 0, \dots, N, \quad (1.2.19)$$

$$\rho_j (\partial_t(\phi_j \mathbf{v}_j) + \nabla \cdot (\phi_j \mathbf{v}_j \otimes \mathbf{v}_j)) = \nabla \cdot \mathbf{T}_j^E - \phi_j \nabla p - \phi_j \rho g \mathbf{k}, \quad j = 0, \dots, N, \quad (1.2.20)$$

and where the quantities  $\rho_j \phi_j \mathbf{v}_j$  are given by (1.2.14). If we sum up from 0 to  $N$  the equations (1.2.20), then we have

$$\partial_t \left( \sum_{j=0}^N \rho_j \phi_j \mathbf{v}_j \right) + \nabla \cdot \left( \sum_{j=0}^N \rho_j \phi_j \mathbf{v}_j \otimes \mathbf{v}_j \right) = \nabla \cdot \mathbf{T} - \rho g \mathbf{k}, \quad (1.2.21)$$

with  $\mathbf{T} = \sum_{j=0}^N T_j = -p \mathbf{I} + \mathbf{T}^E$ .

## 1.3 A multilayer approach

### 1.3.1 Weak solution with discontinuities

Let us recall the conditions to be satisfied by a piecewise smooth weak solution  $(\mathbf{v}_0, \dots, \mathbf{v}_N, \phi_0, \dots, \phi_N, p)$  of (1.2.19)–(1.2.21), where  $\mathbf{v}_0, \mathbf{v}_j$  are defined by (1.2.14) and (1.2.18) respectively.

**Definition 1.3.1.** Assume that the velocities  $\mathbf{v}_0, \mathbf{v}_1, \dots, \mathbf{v}_N$ , the pressure  $p$  and the volume fractions  $\phi_0, \phi_1, \dots, \phi_N$  are smooth in each  $\Omega_\alpha(t)$ , but possibly discontinuous across the predetermined hyper-surfaces  $\Gamma_{\alpha+1/2}(t)$  for  $\alpha = 1, \dots, M-1$ . Then

$$\mathbf{y} := (\mathbf{v}_0, \dots, \mathbf{v}_N, \phi_0, \dots, \phi_N, p) : \Omega_T \ni (t, \mathbf{x}, z) \mapsto \mathbf{y}(t, \mathbf{x}, z) \in \mathbb{R}^{N+1} \times \mathbb{R}^{N+1} \times \mathbb{R}$$

is a weak solution of (1.2.19)–(1.2.21) if the following conditions hold:

- (i) The function  $\mathbf{y}$  is a standard weak solution of (1.2.19)–(1.2.21) in each layer  $\Omega_\alpha(t)$ ,  $\alpha = 1, \dots, M$ .

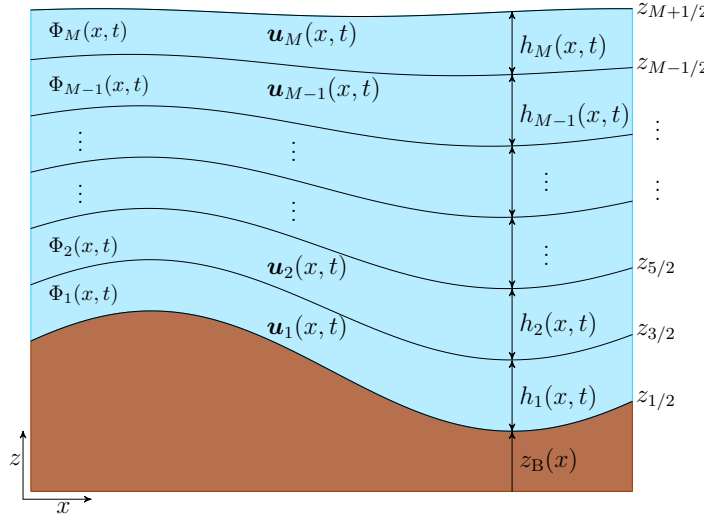


Figure 1.1: Sketch of the multilayer approach

(ii) For each  $\alpha = 1, \dots, M - 1$  and  $t \in (0, T]$ , the following normal flux jump conditions across the interface  $\Gamma_{\alpha+1/2}(t)$  are satisfied: for the conservation of mass equations (1.2.19),

$$[(\rho_j \phi_j; \rho_j \phi_j \mathbf{v}_j)]_{t, \alpha+1/2} \cdot \mathbf{n}_{t, \alpha+1/2} = 0 \quad \text{for all } j = 0, \dots, N, \quad (1.3.1)$$

and for the momentum conservation law corresponding to equation (1.2.21),

$$\left[ \left( \sum_{m=0}^N \rho_m \phi_m \mathbf{v}_m; \sum_{m=0}^N \rho_m \phi_m \mathbf{v}_m \otimes \mathbf{v}_m - \mathbf{T} \right) \right]_{t, \alpha+1/2} \mathbf{n}_{t, \alpha+1/2} = 0, \quad (1.3.2)$$

where

$$\mathbf{T} = -p \mathbf{I} + \mathbf{T}^E \quad (1.3.3)$$

is the stress tensor of the mixture.

In order to develop the multilayer model, we assume the layers thicknesses small enough to neglect the dependence of the horizontal velocities and the concentrations on the vertical variable inside each layer. Moreover, we assume that the vertical velocity is piecewise linear in  $z$ , and possibly discontinuous. Concretely, for all  $\alpha = 1, \dots, M$  and  $j = 0, \dots, N$  we denote  $\mathbf{v}_j|_{\Omega_\alpha(t)} := \mathbf{v}_{j,\alpha} := (\mathbf{u}_\alpha, w_{j,\alpha})^T$ ,  $\phi_{j,\alpha} := \phi_j|_{\Omega_\alpha(t)}$ , and for all  $\alpha = 1, \dots, M$ ,  $p_\alpha := p|_{\Omega_\alpha(t)}$ , where  $\mathbf{u}_\alpha, \phi_{j,\alpha} w_{j,\alpha} = \phi_{j,\alpha} w_\alpha + f_{j,\alpha}^M$ , and  $\phi_{j,\alpha}$ , respectively, stand for the horizontal and vertical velocities and volumetric concentration of species  $j$  in layer  $\alpha$ . Let us also denote the average velocity of each layer by

$$\mathbf{v}^\alpha := \frac{1}{\bar{\rho}_\alpha} \sum_{j=0}^N \rho_j \phi_{j,\alpha} \mathbf{v}_{j,\alpha} = (\mathbf{u}_\alpha, w_\alpha), \quad \alpha = 1, \dots, M,$$

(where we choose an upper index for  $\alpha$  to avoid confusion with the lower index  $j$ ), and assume that

$$\partial_z \mathbf{u}_\alpha = 0, \quad \partial_z \phi_{j,\alpha} = 0, \quad \partial_z w_{j,\alpha} = d_{j,\alpha}(t, \mathbf{x}), \quad \partial_z p_\alpha(t, \mathbf{x}) = g_\alpha(t, \mathbf{x}), \quad (1.3.4)$$

for some smooth functions  $d_{j,\alpha}(t, \mathbf{x})$  and  $g_\alpha(t, \mathbf{x})$ . That is, we suppose that the horizontal velocity  $\mathbf{u}_\alpha$  and the concentration of each of the species  $\phi_{j,\alpha}$  do not depend on  $z$  inside each layer, and that  $w_{j,\alpha}$  and  $p_\alpha$  are linear in  $z$  inside each layer.

There is no hope for such a particular set  $((\mathbf{u}_\alpha, w_{1,\alpha})^T, \dots, (\mathbf{u}_\alpha, w_{N,\alpha})^T, \phi_{1,\alpha}, \dots, \phi_{N,\alpha}, p_\alpha)$  to be a solution of the complete equations in the layer  $\Omega_\alpha(t)$ . Instead, we shall consider a reduced weak formulation with particular test functions, that we describe in the following sections. Let us also denote  $\Phi_\alpha = (\phi_{0,\alpha}, \phi_{1,\alpha}, \dots, \phi_{N,\alpha})^T$  and

$$\bar{\rho}_\alpha := \rho_0 \phi_{0,\alpha} + \rho_1 \phi_{1,\alpha} + \dots + \rho_N \phi_{N,\alpha}. \quad (1.3.5)$$

### 1.3.2 Mass conservation jump conditions

In what follows we analyze the jump conditions (1.3.1) and (1.3.2), where we recall that (1.3.4) implies that

$$\mathbf{u}_{\alpha-1/2}^+(t, \mathbf{x}) = \mathbf{u}_{\alpha+1/2}^-(t, \mathbf{x}) = \mathbf{u}_\alpha(t, \mathbf{x}), \quad \text{and} \quad \phi_{j,\alpha-1/2}^+(t, \mathbf{x}) = \phi_{j,\alpha+1/2}^-(t, \mathbf{x}) = \phi_{j,\alpha}(t, \mathbf{x}),$$

so that the jumps  $[\![\mathbf{u}]\!]_{t,\alpha+1/2}$  and  $[\![\phi_j]\!]_{t,\alpha+1/2}$ ,  $j = 0, \dots, N$ , are indeed given by (0.2.1). The mass conservation jump conditions (1.3.1) are then satisfied provided that

$$G_{j,\alpha+1/2} := G_{j,\alpha+1/2}^- = G_{j,\alpha+1/2}^+, \quad j = 0, 1, \dots, N, \quad (1.3.6)$$

where we define for  $j = 0, 1, \dots, N$

$$\begin{aligned} G_{j,\alpha+1/2}^+ &:= \rho_j \phi_{j,\alpha+1} (\partial_t z_{\alpha+1/2} + \mathbf{u}_{\alpha+1} \cdot \nabla_{\mathbf{x}} z_{\alpha+1/2} - w_{j,\alpha+1/2}^+), \\ G_{j,\alpha+1/2}^- &:= \rho_j \phi_{j,\alpha} (\partial_t z_{\alpha+1/2} + \mathbf{u}_\alpha \cdot \nabla_{\mathbf{x}} z_{\alpha+1/2} - w_{j,\alpha+1/2}^-). \end{aligned} \quad (1.3.7)$$

(We remark that  $G_{j,\alpha+1/2}$  is the normal mass flux for species  $j$  at the interface  $\Gamma_{\alpha+1/2}(t)$ .) Taking into account the structure of the vertical velocity, let us denote

$$w_{j,\alpha+1/2}^\pm = w_{\alpha+1/2}^\pm + f_{j,\alpha+1/2}^\pm / \phi_{j,\alpha+1/2}^\pm. \quad (1.3.8)$$

where  $f_{j,\alpha+1/2}^\pm$  must satisfy

$$\sum_{j=0}^N \rho_j f_{j,\alpha+1/2}^+ = \sum_{j=0}^N \rho_j f_{j,\alpha+1/2}^- = 0.$$

If we add up in  $j$ , it becomes clear that  $G_{\alpha+1/2} = G_{\alpha+1/2}^- = G_{\alpha+1/2}^+$ , where

$$G_{\alpha+1/2} := \sum_{j=0}^N G_{j,\alpha+1/2}$$

and

$$\begin{aligned} G_{\alpha+1/2}^+ &= \bar{\rho}_{\alpha+1} (\partial_t z_{\alpha+1/2} + \mathbf{u}_{\alpha+1} \cdot \nabla_{\mathbf{x}} z_{\alpha+1/2} - w_{\alpha+1/2}^+), \\ G_{\alpha+1/2}^- &= \bar{\rho}_\alpha (\partial_t z_{\alpha+1/2} + \mathbf{u}_\alpha \cdot \nabla_{\mathbf{x}} z_{\alpha+1/2} - w_{\alpha+1/2}^-), \end{aligned} \quad (1.3.9)$$

which corresponds to the jump condition for (1.2.3). (The quantity  $G_{\alpha+1/2}$  will be referred to as total normal mass flux across the interface  $\Gamma_{\alpha+1/2}(t)$ .) Then, from (1.3.7), (1.3.8) and (1.3.9) we obtain

$$G_{j,\alpha+1/2}^+ = \frac{\rho_j \phi_{j,\alpha+1}}{\bar{\rho}_{\alpha+1}} G_{\alpha+1/2} - \rho_j f_{j,\alpha+1/2}^+, \quad G_{j,\alpha+1/2}^- = \frac{\rho_j \phi_{j,\alpha}}{\bar{\rho}_\alpha} G_{\alpha+1/2} - \rho_j f_{j,\alpha+1/2}^-,$$

and these two equations allow us to obtain

$$G_{j,\alpha+1/2} = \tilde{\phi}_{j,\alpha+1/2} G_{\alpha+1/2} - \rho_j \tilde{f}_{j,\alpha+1/2}, \quad (1.3.10)$$

where we define the averages

$$\tilde{\phi}_{j,\alpha+1/2} := \frac{1}{2} \left( \frac{\rho_j \phi_{j,\alpha+1}}{\bar{\rho}_{\alpha+1}} + \frac{\rho_j \phi_{j,\alpha}}{\bar{\rho}_\alpha} \right), \quad \tilde{f}_{j,\alpha+1/2} = \frac{1}{2} (f_{j,\alpha+1/2}^+ + f_{j,\alpha+1/2}^-), \quad j = 0, \dots, N. \quad (1.3.11)$$

Let us also remark that condition (1.3.6) can be written as

$$f_{j,\alpha+1/2}^+ - f_{j,\alpha+1/2}^- = G_{\alpha+1/2} \left( \frac{\phi_{j,\alpha+1}}{\bar{\rho}_{\alpha+1}} - \frac{\phi_{j,\alpha}}{\bar{\rho}_\alpha} \right).$$

Then, from previous equations we obtain

$$f_{j,\alpha+1/2}^\pm = \tilde{f}_{j,\alpha+1/2} \pm \frac{G_{\alpha+1/2}}{2} \left( \frac{\phi_{j,\alpha+1}}{\bar{\rho}_{\alpha+1}} - \frac{\phi_{j,\alpha}}{\bar{\rho}_\alpha} \right).$$

### 1.3.3 Momentum conservation jump conditions

The momentum jump condition (1.3.2) is rewritten as

$$[\![\mathbf{T}]\!]_{t,\alpha+1/2} \cdot (\nabla_{\mathbf{x}} z_{\alpha+1/2}, -1)^T = \sum_{j=0}^N [\![(\rho_j \phi_j \mathbf{v}_j; \rho_j \phi_j \mathbf{v}_j \otimes \mathbf{v}_j)]\!]_{t,\alpha+1/2} \cdot (\partial_t z_{\alpha+1/2}, \nabla_{\mathbf{x}} z_{\alpha+1/2}, -1)^T. \quad (1.3.12)$$

Moreover, using (1.3.6), we have

$$[\![(\rho_j \phi_j \mathbf{v}_j; \rho_j \phi_j \mathbf{v}_j \otimes \mathbf{v}_j)]\!]_{t,\alpha+1/2} \cdot (\partial_t z_{\alpha+1/2}, \nabla_{\mathbf{x}} z_{\alpha+1/2}, -1)^T = G_{j,\alpha+1/2} [\![\mathbf{v}_j]\!]_{t,\alpha+1/2}, \quad j = 0, 1, \dots, N,$$

Inserting this into (1.3.12) we get

$$[\![\mathbf{T}]\!]_{t,\alpha+1/2} \cdot (\nabla_{\mathbf{x}} z_{\alpha+1/2}, -1)^T = \sum_{j=0}^N G_{j,\alpha+1/2} [\![\mathbf{v}_j]\!]_{t,\alpha+1/2}.$$

As a consequence, condition (1.3.2) can be written as

$$[\![\mathbf{T}]\!]_{t,\alpha+1/2} \cdot \boldsymbol{\eta}_{\alpha+1/2} = \frac{1}{\sqrt{1 + |\nabla_{\mathbf{x}} z_{\alpha+1/2}|^2}} \sum_{j=0}^N G_{j,\alpha+1/2} [\![\mathbf{v}_j]\!]_{t,\alpha+1/2}.$$

For  $\alpha = 1, \dots, M-1$ , and consistently with (1.3.3), the total stress is decomposed as

$$\mathbf{T}_{\alpha+1/2}^\pm = -p_{\alpha+1/2} \mathbf{I} + \mathbf{T}_{\alpha+1/2}^{E,\pm}, \quad (1.3.13)$$

where  $p_{\alpha+1/2}$  is the kinematic pressure and  $\mathbf{T}_{\alpha+1/2}^{E,\pm}$  are the limit approximations of  $\mathbf{T}^E$  at  $\Gamma_{\alpha+1/2}$ . This means that  $\mathbf{T}_{\alpha+1/2}^{E,\pm}$  must satisfy

$$\llbracket \mathbf{T}^E \rrbracket_{t,\alpha+1/2} \cdot \boldsymbol{\eta}_{\alpha+1/2} = (\mathbf{T}_{\alpha+1/2}^{E,+} - \mathbf{T}_{\alpha+1/2}^{E,-}) \cdot \boldsymbol{\eta}_{\alpha+1/2} = \frac{1}{\sqrt{1 + |\nabla_{\mathbf{x}} z_{\alpha+1/2}|^2}} \sum_{j=0}^N G_{j,\alpha+1/2} \llbracket \mathbf{v}_j \rrbracket_{t,\alpha+1/2}, \quad (1.3.14)$$

where  $G_{j,\alpha+1/2}$  is defined by (1.3.10). Moreover, by consistency,  $\mathbf{T}_{\alpha+1/2}^{E,\pm}$  should satisfy

$$\frac{1}{2} (\mathbf{T}_{\alpha+1/2}^{E,+} + \mathbf{T}_{\alpha+1/2}^{E,-}) =: \tilde{\mathbf{T}}_{\alpha+1/2}^E = \begin{bmatrix} \tilde{\mathbf{T}}_{h,\alpha+1/2}^E & \tilde{\mathbf{T}}_{xz,\alpha+1/2}^E \\ (\tilde{\mathbf{T}}_{xz,\alpha+1/2}^E)^T & \tilde{\mathbf{T}}_{zz,\alpha+1/2}^E \end{bmatrix}, \quad (1.3.15)$$

where  $\tilde{\mathbf{T}}_{\alpha+1/2}^E$  is an approximation of  $\mathbf{T}^E|_{\Gamma_{\alpha+1/2}}$ , to be defined and  $\tilde{\mathbf{T}}_{h,\alpha+1/2}^E$ ,  $\tilde{\mathbf{T}}_{xz,\alpha+1/2}^E$ , and  $\tilde{\mathbf{T}}_{zz,\alpha+1/2}^E$  denote the horizontal, mixed, and vertical components of  $\tilde{\mathbf{T}}_{\alpha+1/2}^E$ , respectively. Concretely, if we utilize the expression for a viscous-linear fluid,

$$\mathbf{T}^E = \mathbf{T}^E(\mathbf{v}) = \mu \mathbf{D}(\mathbf{v}) = \frac{\mu}{2} (\nabla \mathbf{v} + (\nabla \mathbf{v})^T),$$

where  $\mathbf{D}(\mathbf{v}) = (1/2)(\nabla \mathbf{v} + (\nabla \mathbf{v})^T)$  is the infinitesimal rate of strain, then we define  $\tilde{\mathbf{T}}_{\alpha+1/2}^E = \mu \tilde{\mathbf{D}}_{\alpha+1/2}$ , where  $\tilde{\mathbf{D}}_{\alpha+1/2}$  is an approximation of  $\mathbf{D}(\mathbf{v})$  at the interface  $z_{\alpha+1/2}$ . Finally, we can solve the system defined by (1.3.14) and the equation resulting by multiplying scalarly (1.3.15) by the vector  $\boldsymbol{\eta}_{\alpha+1/2}$ . This way, we obtain the expression of  $\mathbf{T}_{\alpha+1/2}^{E,\pm}$  that satisfies the jump condition and the consistency condition on the interface. We can solve it easily and we obtain

$$\mathbf{T}_{\alpha+1/2}^{E,\pm} \cdot \boldsymbol{\eta}_{\alpha+1/2} = \tilde{\mathbf{T}}_{\alpha+1/2}^E \cdot \boldsymbol{\eta}_{\alpha+1/2} \pm \frac{1}{2} \frac{1}{\sqrt{1 + |\nabla_{\mathbf{x}} z_{\alpha+1/2}|^2}} \sum_{j=0}^N G_{j,\alpha+1/2} \llbracket \mathbf{v}_j \rrbracket_{t,\alpha+1/2}. \quad (1.3.16)$$

### 1.3.4 Vertical velocity of the solid particles

First, we select  $\alpha \in \{1, \dots, M\}$ , and integrate vertically the mass balance equations (1.2.19) over  $(z_{\alpha-1/2}, z)$  for  $z \in (z_{\alpha-1/2}, z_{\alpha+1/2})$ . This yields

$$\int_{z_{\alpha-1/2}}^z (\partial_t(\rho_j \phi_j) + \nabla \cdot (\rho_j \phi_j \mathbf{v}_j)) d\zeta = 0, \quad j = 1, \dots, N.$$

Under the assumptions (1.3.4) and recalling that  $\mathbf{v}_j = \mathbf{v} + f_j^M(\Phi)/\phi_j \mathbf{k} = (\mathbf{u}, w_j)$  and  $w_j = w + f_j^M(\Phi)/\phi_j$ , we obtain

$$\partial_t(\rho_j \phi_j, \alpha)(z - z_{\alpha-1/2}) + \nabla_{\mathbf{x}} \cdot (\rho_j \phi_j, \alpha \mathbf{u}_{\alpha})(z - z_{\alpha-1/2}) + \rho_j \phi_j, \alpha (w_{j,\alpha}(t, \mathbf{x}, z) - w_{j,\alpha-1/2}^+) = 0.$$

This equation implies that the vertical velocity  $w_{j,\alpha}$  is given by

$$w_{j,\alpha}(t, \mathbf{x}, z) = w_{j,\alpha-1/2}^+ - \frac{1}{\rho_j \phi_j, \alpha} (\partial_t(\rho_j \phi_j, \alpha) + \nabla_{\mathbf{x}} \cdot (\rho_j \phi_j, \alpha \mathbf{u}_{\alpha})) (z - z_{\alpha-1/2}), \quad j = 1, \dots, N. \quad (1.3.17)$$

In addition, from the condition (1.3.9) at the interfaces, we obtain the quantities

$$\begin{aligned} w_{j,\alpha-1/2}^+ &= \frac{1}{\rho_j \phi_j, \alpha} ((\rho_j \phi_{j,\alpha} - \rho_j \phi_{j,\alpha-1}) \partial_t z_{\alpha-1/2} \\ &\quad + (\rho_j \phi_{j,\alpha} \mathbf{u}_{\alpha} - \rho_j \phi_{j,\alpha-1} \mathbf{u}_{\alpha-1}) \cdot \nabla_{\mathbf{x}} z_{\alpha-1/2} + \rho_j \phi_{j,\alpha-1} w_{j,\alpha-1}^-), \end{aligned}$$

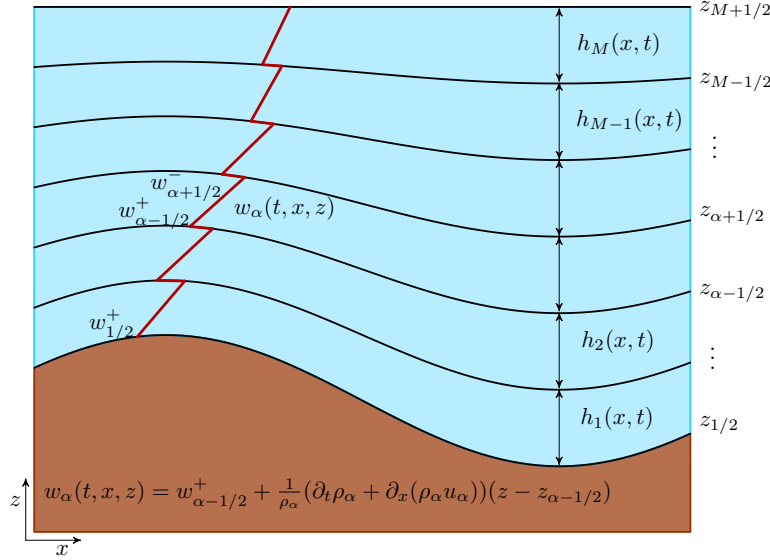


Figure 1.2: Sketch of the procedure to calculate the vertical velocity.

where

$$w_{j,\alpha-1/2}^- = w_{j,\alpha-3/2}^+ - \frac{h_{\alpha-1}}{\rho_j \phi_{j,\alpha-1}} (\partial_t (\rho_j \phi_{j,\alpha-1}) + \nabla_{\mathbf{x}} \cdot (\rho_j \phi_{j,\alpha-1} \mathbf{u}_{\alpha-1})).$$

Using the horizontal velocities specified by the model, the average vertical velocities in the layers are computed successively from below to above as follows. First the quantity  $w_{j,1/2}^+$  is determined from the given mass transfer  $G_{j,1/2}$ , through the bottom condition (1.3.6) at the bottom by

$$w_{j,1/2}^+ = \partial_t z_B + \mathbf{u}_1 \cdot \nabla_{\mathbf{x}} z_B - \frac{G_{1/2}}{\rho_j \phi_{j,1}}.$$

Then, for  $\alpha = 1, \dots, M$  and  $z \in (z_{\alpha-1/2}, z_{\alpha+1/2})$ , we set

$$\begin{aligned} w_{j,\alpha}(t, \mathbf{x}, z) &= w_{j,\alpha-1/2}^+ - \frac{1}{\rho_j \phi_{j,\alpha}} (\partial_t (\rho_j \phi_{j,\alpha}) + \nabla_{\mathbf{x}} \cdot (\rho_j \phi_{j,\alpha} \mathbf{u}_\alpha)) (z - z_{\alpha-1/2}) \\ w_{j,\alpha+1/2}^- &= w_{j,\alpha-1/2}^+ - \frac{h_\alpha}{\rho_j \phi_{j,\alpha}} (\partial_t (\rho_j \phi_{j,\alpha}) + \nabla_{\mathbf{x}} \cdot (\rho_j \phi_{j,\alpha} \mathbf{u}_\alpha)), \\ w_{j,\alpha+1/2}^+ &= \frac{1}{\rho_j \phi_{j,\alpha+1}} ((\rho_j \phi_{j,\alpha+1} - \rho_j \phi_{j,\alpha}) \partial_t z_{\alpha+1/2} \\ &\quad + (\rho_j \phi_{j,\alpha+1} \mathbf{u}_{\alpha+1} - \rho_j \phi_{j,\alpha} \mathbf{u}_\alpha) \cdot \nabla_{\mathbf{x}} z_{\alpha+1/2} + \rho_j \phi_{j,\alpha} w_{j,\alpha+1/2}^-). \end{aligned}$$

### 1.3.5 Vertical velocity of the mixture

The vertical velocity of the mixture inside  $\Omega_\alpha$  is obtained summing from 0 to  $N$  the vertical velocity of the species inside this layer, which is given by (1.3.17). This yields

$$\sum_{j=0}^N \rho_j \phi_{j,\alpha} w_{j,\alpha}(t, \mathbf{x}, z) = \sum_{j=0}^N \left( \rho_j \phi_{j,\alpha} w_{j,\alpha-1/2}^+ - (\partial_t (\rho_j \phi_{j,\alpha}) + \nabla_{\mathbf{x}} \cdot (\rho_j \phi_{j,\alpha} \mathbf{u}_\alpha)) (z - z_{\alpha-1/2}) \right). \quad (1.3.18)$$

This equality implies that

$$w_\alpha(t, \mathbf{x}, z) = w_{\alpha-1/2}^+ - \frac{1}{\bar{\rho}_\alpha} (\partial_t \bar{\rho}_\alpha + \nabla_{\mathbf{x}} \cdot (\bar{\rho}_\alpha \mathbf{u}_\alpha)) (z - z_{\alpha-1/2}), \quad (1.3.19)$$

and using the mass jump condition (1.3.9), we obtain

$$w_{\alpha-1/2}^+ = \frac{1}{\bar{\rho}_\alpha} ((\bar{\rho}_\alpha - \bar{\rho}_{\alpha-1}) \partial_t z_{\alpha-1/2} + (\bar{\rho}_\alpha \mathbf{u}_\alpha - \bar{\rho}_{\alpha-1} \mathbf{u}_{\alpha-1}) \cdot \nabla_{\mathbf{x}} z_{\alpha-1/2} + \bar{\rho}_{\alpha-1} w_{\alpha-1/2}^-),$$

where

$$w_{\alpha-1/2}^- = w_{\alpha-3/2}^+ - \frac{h_{\alpha-1}}{\bar{\rho}_{\alpha-1}} (\partial_t (\bar{\rho}_{\alpha-1}) + \nabla_{\mathbf{x}} \cdot (\bar{\rho}_{\alpha-1} \mathbf{u}_{\alpha-1})).$$

Then the vertical velocities of mixture in the layers can be computed successively from below to above as follows. The quantity  $w_{1/2}^+$  is determined, from the given mass transference  $G_{1/2}$ , through the condition (1.3.6) at the bottom by

$$w_{1/2}^+ = \partial_t z_B + \mathbf{u}_1 \cdot \nabla_{\mathbf{x}} z_B - \frac{G_{1/2}}{\rho_1}.$$

Then, for  $\alpha = 1, \dots, M$  and  $z \in (z_{\alpha-1/2}, z_{\alpha+1/2})$ , we calculate successively

$$\begin{aligned} w_\alpha(t, \mathbf{x}, z) &= w_{\alpha-1/2}^+ - \frac{1}{\bar{\rho}_\alpha} (\partial_t \bar{\rho}_\alpha + \nabla_{\mathbf{x}} \cdot (\bar{\rho}_\alpha \mathbf{u}_\alpha)) (z - z_{\alpha-1/2}), \\ w_{\alpha+1/2}^- &= w_{\alpha-1/2}^+ - \frac{h_\alpha}{\bar{\rho}_\alpha} (\partial_t \bar{\rho}_\alpha + \nabla_{\mathbf{x}} \cdot (\bar{\rho}_\alpha \mathbf{u}_\alpha)), \\ w_{\alpha+1/2}^+ &= \frac{1}{\bar{\rho}_{\alpha+1}} ((\bar{\rho}_{\alpha+1} - \bar{\rho}_\alpha) \partial_t z_{\alpha+1/2} + (\bar{\rho}_{\alpha+1} \mathbf{u}_{\alpha+1} - \bar{\rho}_\alpha \mathbf{u}_\alpha) \cdot \nabla_{\mathbf{x}} z_{\alpha+1/2} + \bar{\rho}_\alpha w_{\alpha+1/2}^-). \end{aligned}$$

The previous procedure is exemplified in Figure 1.2.

## 1.4 A particular weak solution with hydrostatic pressure

This section is devoted to get the multilayer version of the model (1.2.19)-(1.2.21). For this purpose we will use the following assumption for the pressure term.

**Assumption 1.4.1.** *We assume that we have a shallow domain. In this case, the pressure  $p$  can be assumed to be hydrostatic. Then,*

$$p_\alpha(t, \mathbf{x}, z) = p_{\alpha+1/2}(t, \mathbf{x}) + \bar{\rho}_\alpha g(z_{\alpha+1/2} - z), \quad \text{where } p_{\alpha+1/2}(t, \mathbf{x}) = p_S(t, \mathbf{x}) + g \sum_{\beta=\alpha+1}^M \bar{\rho}_\beta h_\beta(t, \mathbf{x}).$$

Here, the component  $p_{\alpha+1/2}$  is the kinematic pressure at  $\Gamma_{\alpha+1/2}(t)$  and  $p_S$  denotes the pressure at the free surface.

Since  $\mathbf{v}_{j,\alpha}$  is a weak solution of (1.2.19)–(1.2.21) in  $\Omega_\alpha(t)$ , where  $\mathbf{v}_j$  defined by (1.2.14), let us begin by considering the weak formulation of this system in  $\Omega_\alpha(t)$  for  $\alpha = 1, \dots, N$ . Assume that  $\mathbf{v}_{j,\alpha} \in L^2(0, T; H^1(\Omega_\alpha(t))^d)$ ,  $\partial_t \mathbf{v}_{j,\alpha} \in L^2(0, T; L^2(\Omega_\alpha(t))^d)$ ,  $\phi_{j,\alpha} \in L^2(0, T; H^1(\Omega_\alpha(t)))$ ,  $\partial_t \phi_{j,\alpha} \in$

$L^2(0, T; L^2(\Omega_\alpha(t)))$  and  $p_\alpha \in L^2(0, T; L^2(\Omega_\alpha(t)))$ . Then a weak solution of the original equations in  $\Omega_\alpha(t)$  should satisfy for all  $\varphi \in L^2(\Omega_\alpha(t))$  and for all  $\boldsymbol{\vartheta} \in H^1(\Omega_\alpha(t))^d$  with  $\boldsymbol{\vartheta}|_{\partial I_F} = 0$  the identities

$$\begin{aligned} & \int_{\Omega_\alpha(t)} (\partial_t \phi_{j,\alpha} + \nabla \cdot (\phi_{j,\alpha} \mathbf{v}_{j,\alpha})) \varphi \, d\Omega = 0, \\ & \int_{\Omega_\alpha(t)} \left( \sum_{j=0}^N \rho_j \partial_t (\phi_{j,\alpha} \mathbf{v}_{j,\alpha}) \right) \cdot \boldsymbol{\vartheta} \, d\Omega + \int_{\Omega_\alpha(t)} \left( \sum_{j=0}^N \rho_j \nabla \cdot (\phi_{j,\alpha} \mathbf{v}_{j,\alpha} \otimes \mathbf{v}_{j,\alpha}) \right) \cdot \boldsymbol{\vartheta} \, d\Omega \\ & + \int_{\Omega_\alpha(t)} \mathbf{T}^E : \nabla \boldsymbol{\vartheta} \, d\Omega - \int_{\Omega_\alpha(t)} p \nabla \cdot \boldsymbol{\vartheta} \, d\Omega + \int_{\Gamma_{\alpha+1/2}(t)} (\mathbf{T}_{\alpha+1/2}^- \boldsymbol{\vartheta}) \cdot \boldsymbol{\eta}_{\alpha+1/2} \, d\Gamma \\ & - \int_{\Gamma_{\alpha-1/2}(t)} (\mathbf{T}_{\alpha-1/2}^+ \boldsymbol{\vartheta}) \cdot \boldsymbol{\eta}_{\alpha-1/2} \, d\Gamma = - \int_{\Omega_\alpha(t)} g \bar{\rho}_\alpha \mathbf{k} \cdot \boldsymbol{\vartheta} \, d\Omega. \end{aligned} \quad (1.4.1)$$

We consider velocity-pressure pairs with the structure given by (1.3.4) that satisfy the previous system with particular weak solutions that satisfy (1.4.1) for test functions such that  $\partial_z \varphi = 0$  and

$$\boldsymbol{\vartheta}(t, \mathbf{x}, z) = (\boldsymbol{\vartheta}_h(t, \mathbf{x}), (z - z_B) \mathcal{V}(t, \mathbf{x}))^\top, \quad (1.4.2)$$

where  $\boldsymbol{\vartheta}_h$  and  $\mathcal{V}$  are smooth functions that do not depend on  $z$ . Now following a similar approach as in [38], after some straightforward calculations (see Appendix B) we get the mass conservation law

$$\partial_t (\rho_j \phi_{j,\alpha} h_\alpha) + \nabla_{\mathbf{x}} \cdot (\rho_j \phi_{j,\alpha} h_\alpha \mathbf{u}_\alpha) = G_{j,\alpha+1/2} - G_{j,\alpha-1/2}, \quad j = 0, 1, \dots, N, \quad \alpha = 1, \dots, M, \quad (1.4.3)$$

where  $G_{j,\alpha+1/2}$  is defined by (1.3.10). We remark that taking into account (1.3.5), we get

$$\partial_t (\bar{\rho}_\alpha h_\alpha) + \nabla_{\mathbf{x}} \cdot (\bar{\rho}_\alpha h_\alpha \mathbf{u}_\alpha) = G_{\alpha+1/2} - G_{\alpha-1/2}, \quad \alpha = 1, \dots, M. \quad (1.4.4)$$

The balance of momentum equations now take the form

$$\begin{aligned} & \partial_t (\bar{\rho}_\alpha h_\alpha \mathbf{u}_\alpha) + \nabla_{\mathbf{x}} \cdot (\bar{\rho}_\alpha h_\alpha \mathbf{u}_\alpha \otimes \mathbf{u}_\alpha) + \int_{z_{\alpha-1/2}}^{z_{\alpha+1/2}} \nabla_{\mathbf{x}} p_\alpha \, dz - \nabla_{\mathbf{x}} \cdot (h_\alpha \mathbf{T}_h^E) \\ & + (\tilde{\mathbf{T}}_{h,\alpha+1/2}^E (\nabla_{\mathbf{x}} z_{\alpha+1/2})^\top - \tilde{\mathbf{T}}_{x,z,\alpha+1/2}^E) - (\tilde{\mathbf{T}}_{h,\alpha-1/2}^E (\nabla_{\mathbf{x}} z_{\alpha-1/2})^\top - \tilde{\mathbf{T}}_{x,z,\alpha-1/2}^E) \\ & = \frac{G_{\alpha+1/2}}{2} (\mathbf{u}_{\alpha+1} + \mathbf{u}_\alpha) - \frac{G_{\alpha-1/2}}{2} (\mathbf{u}_\alpha + \mathbf{u}_{\alpha-1}). \end{aligned} \quad (1.4.5)$$

Introducing the notation

$$\bar{p}_\alpha := p_S + g \sum_{\beta=\alpha+1}^M \bar{\rho}_\beta h_\beta + g \bar{\rho}_\alpha \frac{h_\alpha}{2}, \quad \bar{z}_\alpha := z_B + \sum_{\beta=1}^{\alpha-1} h_\beta + \frac{h_\alpha}{2},$$

we obtain the following system for  $\alpha = 1, \dots, M$ :

$$\begin{aligned} & \partial_t (\rho_j \phi_{j,\alpha} h_\alpha) + \nabla_{\mathbf{x}} \cdot (\rho_j \phi_{j,\alpha} h_\alpha \mathbf{u}_\alpha) = G_{j,\alpha+1/2} - G_{j,\alpha-1/2}, \quad j = 0, \dots, N, \\ & \partial_t (\bar{\rho}_\alpha h_\alpha \mathbf{u}_\alpha) + \nabla_{\mathbf{x}} \cdot (\bar{\rho}_\alpha h_\alpha \mathbf{u}_\alpha \otimes \mathbf{u}_\alpha) + h_\alpha (\nabla_{\mathbf{x}} \bar{p}_\alpha + g \bar{\rho}_\alpha \nabla_{\mathbf{x}} \bar{z}_\alpha) \\ & - \nabla_{\mathbf{x}} \cdot (h_\alpha \mathbf{T}_h^E) + (\tilde{\mathbf{T}}_{h,\alpha+1/2}^E (\nabla_{\mathbf{x}} z_{\alpha+1/2})^\top - \tilde{\mathbf{T}}_{x,z,\alpha+1/2}^E) - (\tilde{\mathbf{T}}_{h,\alpha-1/2}^E (\nabla_{\mathbf{x}} z_{\alpha-1/2})^\top - \tilde{\mathbf{T}}_{x,z,\alpha-1/2}^E) \\ & = \frac{G_{\alpha+1/2}}{2} (\mathbf{u}_{\alpha+1} + \mathbf{u}_\alpha) - \frac{G_{\alpha-1/2}}{2} (\mathbf{u}_\alpha + \mathbf{u}_{\alpha-1}), \end{aligned} \quad (1.4.6)$$

where  $\tilde{\mathbf{T}}_{h,\alpha+1/2}^E$  and  $\tilde{\mathbf{T}}_{x,z,\alpha+1/2}^E$  are defined by (1.3.15).

## 1.5 Closure and reformulation of the model

### 1.5.1 Closure of the model in one horizontal space dimension

For the sake of simplicity, we assume from here so on, that the extra (viscous) stress tensor  $\mathbf{T}^E$  is equal to zero, and we limit the treatment to one horizontal space dimension. In the sequel, we shall denote the horizontal velocities  $\mathbf{u}_\alpha$  merely by  $u_\alpha$ , as well as replace  $\mathbf{x}$  by  $x$ , etc. The following assumption is required to close system (1.4.6).

**Assumption 1.5.1.** *For  $\alpha = 1, \dots, M$ , we assume that the thickness  $h_\alpha$  are proportional to the total height  $h$ , i.e.  $h_\alpha = l_\alpha h$ , with  $l_1, \dots, l_M$  are positive constants satisfying  $l_1 + \dots + l_M = 1$ .*

Furthermore, we define  $r_{j,\alpha} := \rho_j \phi_{j,\alpha} h$  for  $\alpha = 1, \dots, M$  and  $j = 0, \dots, N$ ,  $q_\alpha := \bar{\rho}_\alpha h u_\alpha$  and  $L_\alpha := l_1, \dots, l_\alpha$  for  $\alpha = 1, \dots, M$ . Note that system (1.4.6) consists of  $M(N+2)$  scalar equations for the same number of unknowns, namely  $\{h, \{q_\alpha, \{r_{j,\alpha}\}_{j=1}^N\}_{\alpha=1}^M, \{G_{\alpha+1/2}\}_{\alpha=1}^{M-1}\}$ . Finally, we define

$$m_\alpha := \bar{\rho}_\alpha h = \sum_{j=0}^N r_{j,\alpha} = \rho_0 h + \sum_{j=1}^N \frac{\rho_j - \rho_0}{\rho_j} r_{j,\alpha}. \quad (1.5.1)$$

(The second equality is proved in Section A.4.1 of Appendix A.4.) Then, instead of writing (1.4.6) in terms of  $\{\{r_{j,\alpha}\}_{j=0}^N\}_{\alpha=1}^M$ , we utilize  $\{m_\alpha, \{r_{j,\alpha}\}_{j=1}^N\}_{\alpha=1}^M$ . Moreover, from (1.5.1) we can recover the height of the fluid column as

$$h = \frac{1}{\rho_0} \left( m_\alpha - \sum_{j=1}^N \frac{\rho_j - \rho_0}{\rho_j} r_{j,\alpha} \right). \quad (1.5.2)$$

Consequently, by taking into account the definition (1.3.10) of  $G_{j,\alpha+1/2}$  and Assumption 1.5.1, we can write the system (1.4.6) for  $\alpha = 1, \dots, M$  as follows:

$$\partial_t m_\alpha + \partial_x q_\alpha = \frac{1}{l_\alpha} (G_{\alpha+1/2} - G_{\alpha-1/2}), \quad (1.5.3)$$

$$\begin{aligned} \partial_t r_{j,\alpha} + \partial_x \left( \frac{r_{j,\alpha} q_\alpha}{m_\alpha} \right) &= \frac{1}{l_\alpha} (\tilde{\phi}_{j,\alpha+1/2} G_{\alpha+1/2} - \tilde{\phi}_{j,\alpha-1/2} G_{\alpha-1/2}) \\ &\quad - \frac{\rho_j}{l_\alpha} (\tilde{f}_{j,\alpha+1/2} - \tilde{f}_{j,\alpha-1/2}), \end{aligned} \quad j = 1, \dots, N, \quad (1.5.4)$$

$$\begin{aligned} \partial_t q_\alpha + \partial_x \left( \frac{q_\alpha^2}{m_\alpha} + h \left( p_S + \frac{g}{2} l_\alpha m_\alpha + g \sum_{\beta=\alpha+1}^M l_\beta m_\beta \right) \right) &= \left( p_S + g \sum_{\beta=\alpha+1}^M l_\beta m_\beta \right) \partial_x h \\ &\quad - g m_\alpha \partial_x z_B - g m_\alpha L_{\alpha-1} \partial_x h + \frac{1}{l_\alpha} (\tilde{u}_{\alpha+1/2} G_{\alpha+1/2} - \tilde{u}_{\alpha-1/2} G_{\alpha-1/2}), \end{aligned} \quad (1.5.5)$$

where we define

$$\tilde{u}_{\alpha+1/2} := \frac{1}{2} \left( \frac{q_{\alpha+1}}{m_{\alpha+1}} + \frac{q_\alpha}{m_\alpha} \right)$$

and note that  $\tilde{\phi}_{j,\alpha+1/2}$ , defined by (1.3.11), can be written as

$$\tilde{\phi}_{j,\alpha+1/2} = \frac{1}{2} \left( \frac{r_{j,\alpha+1}}{m_{\alpha+1}} + \frac{r_{j,\alpha}}{m_\alpha} \right). \quad (1.5.6)$$

Finally, we can also compute an explicit expression of the interlayer mass flux  $G_{\alpha+1/2}$ . The deduction of the explicit expression of these terms are presented in Appendix A.1. Moreover, if we introduce the notation

$$R_\beta := q_\beta - \sum_{j=1}^N r_{j\beta} u_\beta \frac{\rho_j - \rho_0}{\rho_j}, \quad \bar{R} := \sum_{\beta=1}^M l_\beta R_\beta,$$

we can compute the following difference for the transfer terms (see equation (A.1.5)), which allows us to define them recursively:

$$\frac{\rho_0(\bar{\rho}_{\alpha+1} + \bar{\rho}_\alpha)}{\bar{\rho}_\alpha \bar{\rho}_{\alpha+1}} G_{\alpha+1/2} - \frac{\rho_0(\bar{\rho}_\alpha + \bar{\rho}_{\alpha-1})}{\bar{\rho}_\alpha \bar{\rho}_{\alpha-1}} G_{\alpha-1/2} = l_\alpha \partial_x (R_\alpha - \bar{R}) + \rho_0 \sum_{j=0}^N (\tilde{f}_{j,\alpha+1/2} - \tilde{f}_{j,\alpha-1/2}). \quad (1.5.7)$$

**Proposition 1.5.1.** *Let assume that  $\phi_{j,\alpha} = 0$  for  $j = 1, \dots, N$  and  $\alpha = 1, \dots, M$ . If  $m_\alpha, q_\alpha, r_{j,\alpha}$  for  $\alpha = 1, \dots, M$  are smooth solution of system (1.5.3)-(1.5.5), we have lake at rest steady state*

$$\begin{aligned} q_\alpha &= 0 \\ h + z_B &= cte \end{aligned}$$

**Proof.** of Prop. 1.5.1 If water is at rest, and using the definition (A.1.5) for  $G_{\alpha+1/2}$  the system (1.5.3)-(1.5.5) is reduced to

$$\partial_x \left( h \left( \frac{g}{2} l_\alpha m_\alpha + g \sum_{\beta=\alpha+1}^M l_\beta m_\beta \right) \right) = \left( g \sum_{\beta=\alpha+1}^M l_\beta m_\beta \right) \partial_x h - g m_\alpha \partial_x z_B - g m_\alpha L_{\alpha-1} \partial_x h, \quad (1.5.8)$$

using in (1.5.8) the fact that  $\rho_\alpha = \rho_0 + \sum_{j=1}^N (\rho_j - \rho_0) \phi_{j,\alpha}$  we get

$$\partial_x \left( g h^2 \left( \frac{1}{2} l_\alpha + \sum_{\beta=\alpha+1}^M l_\beta \right) \right) = g h \left( \sum_{\beta=\alpha+1}^M l_\beta - \sum_{\beta=1}^{\alpha-1} l_\beta \right) \partial_x h - g h \partial_x z_B, \quad (1.5.9)$$

expanding the left hand side of equality (1.5.9) we get

$$g h \partial_x \left( h \left( \frac{1}{2} l_\alpha + \sum_{\beta=\alpha+1}^M l_\beta \right) \right) + g h \left( \frac{1}{2} l_\alpha + \sum_{\beta=\alpha+1}^M l_\beta \right) \partial_x h = g h \left( \sum_{\beta=\alpha+1}^M l_\beta - \sum_{\beta=1}^{\alpha-1} l_\beta \right) \partial_x h - g h \partial_x z_B. \quad (1.5.10)$$

Finally, from (1.5.10) we conclude that

$$\partial_x \left( h \left( l_\alpha + \sum_{\beta=\alpha+1}^M l_\beta \right) + z_B + h \sum_{\beta=1}^{\alpha-1} l_\beta \right) = 0,$$

or equivalently it has that  $h + z_B = cte$ . ■

### 1.5.2 Recovery of primitive variables

Finally, we can deduce the definition of  $G_{\alpha+1/2}$  from previous equations, in terms of the other unknowns of the problem. As a result we obtain a reduced system with  $M(N+1)+1$  equations. The system can be defined by the  $MN$  equations (1.5.4), the  $M$  equations (1.5.5) and the sum of the  $M$  equations (1.5.3). This last equation can be written as

$$\partial_t \bar{m} + \partial_x \left( \sum_{\beta=1}^M l_\beta q_\beta \right) = G_{M+1/2} - G_{1/2}, \quad \text{where } \bar{m} := h \sum_{\beta=1}^M \bar{\rho}_\beta l_\beta = \sum_{\beta=1}^M l_\beta m_\beta. \quad (1.5.11)$$

Then, once the total mass fluxes  $G_{\alpha+1/2}$ ,  $\alpha = 1, \dots, M-1$  are specified (see Section A.1), the unknowns of the system defined by equations (1.5.4), (1.5.5) and (1.5.11) are  $\{\bar{m}, \{q_\alpha, \{r_{j,\alpha}\}_{j=1}^N\}_{\alpha=1}^M\}$ . From these unknowns we can recover primitive variables as follows:

$$\begin{aligned} h &= \frac{1}{\rho_0} \left( \bar{m} - \sum_{\beta=1}^M \sum_{j=1}^N r_{j,\beta} l_\beta \frac{\rho_j - \rho_0}{\rho_j} \right), \\ m_\alpha &= \rho_0 h + \sum_{j=1}^N r_{j,\alpha} \frac{\rho_j - \rho_0}{\rho_j} = \bar{m} + \sum_{\beta=1}^M \sum_{j=1}^N (r_{j,\alpha} - r_{j,\beta}) l_\beta \frac{\rho_j - \rho_0}{\rho_j}, \\ \bar{\rho}_\alpha &= m_\alpha / h, \\ u_\alpha &= q_\alpha / m_\alpha. \end{aligned} \quad (1.5.12)$$

## 1.6 Numerical schemes

### 1.6.1 First-order system of balance equations

In this section we present a numerical scheme to solve the full system composed by (1.5.4), (1.5.5) and (1.5.11). If we denote the vector of unknowns as

$$\mathbf{w} = (\bar{m}, q_1, \dots, q_M, r_{1,1}, \dots, r_{N,1}, \dots, r_{1,\alpha}, \dots, r_{N,\alpha}, \dots, r_{1,M}, \dots, r_{N,M})^T,$$

the system can be written as (1.1.1) in terms of a conservative flux and source terms containing non-conservative products. The flux function  $\mathcal{F}(\mathbf{w})$  and the source terms  $\mathcal{S}(\mathbf{w}, \partial_x \mathbf{w})$  and  $\mathcal{G}(\mathbf{w}, \partial_x \mathbf{w})$  are vectors of dimension  $M(N+1)+1$ , defined respectively as follows:

$$\mathcal{F}(\mathbf{w}) = \begin{pmatrix} \sum_{\beta=1}^M l_\beta \mathcal{F}^{m_\beta} \\ \mathcal{F}^q \\ \mathcal{F}^{r,1} \\ \vdots \\ \mathcal{F}^{r,M} \end{pmatrix}, \quad \mathcal{S}(\mathbf{w}, \partial_x \mathbf{w}) = \begin{pmatrix} 0 \\ \mathbf{s} \\ \mathbf{0} \\ \vdots \\ \mathbf{0} \end{pmatrix}, \quad \mathcal{G}(\mathbf{w}, \partial_x \mathbf{w}) = \begin{pmatrix} 0 \\ \mathcal{G}^q \\ \mathcal{G}^{r,1} \\ \vdots \\ \mathcal{G}^{r,M} \end{pmatrix}.$$

The components of these vectors are defined in what follows. The first component of  $\mathcal{F}(\mathbf{w})$  is defined via  $\mathcal{F}^{m_\alpha} = q_\alpha$  for  $\alpha = 1, \dots, M$ ; moreover,  $\mathcal{F}^q = (\mathcal{F}^{q_1}, \dots, \mathcal{F}^{q_M})^T$ , where  $\mathcal{F}^{q_\alpha} = q_\alpha^2 / m_\alpha$  for  $\alpha = 1, \dots, M$

and

$$\mathcal{F}^{r,\alpha} := \frac{q_\alpha}{m_\alpha} \begin{pmatrix} r_{1,\alpha} \\ \vdots \\ r_{N,\alpha} \end{pmatrix}, \quad \alpha = 1, \dots, M.$$

The components of  $\mathbf{s} = (s_1, \dots, s_M)^T$  defining the vector  $\mathcal{S}$  are given by

$$s_\alpha := gm_\alpha \partial_x(z_b + h) + gh^2 \left( \left( \frac{l_\alpha}{2} + \sum_{\beta=\alpha+1}^M l_\beta \right) \partial_x \bar{\rho}_\alpha + \partial_x \left( \sum_{\beta=\alpha+1}^M l_\beta (\bar{\rho}_\beta - \bar{\rho}_\alpha) \right) \right), \quad \alpha = 1, \dots, M,$$

where  $h$  and  $\bar{\rho}_\alpha$  are computed as described in (1.5.2) and (1.5.12), respectively. Finally, the sub-vectors of  $\mathcal{G}$  are defined by  $\mathcal{G}^q = (\mathcal{G}^{q_1}, \dots, \mathcal{G}^{q_M})^T$  with

$$\mathcal{G}^{q_\alpha} = (\tilde{u}_{\alpha+1/2} G_{\alpha+1/2} - \tilde{u}_{\alpha-1/2} G_{\alpha-1/2})/l_\alpha, \quad \text{for } \alpha = 1, \dots, M,$$

and

$$\mathcal{G}^{r,\alpha} := \frac{1}{l_\alpha} \left( G_{\alpha+1/2} \tilde{\Phi}_{\alpha+1/2} - G_{\alpha-1/2} \tilde{\Phi}_{\alpha-1/2} - \begin{pmatrix} \rho_1(\tilde{f}_{1,\alpha+1/2} - \tilde{f}_{1,\alpha-1/2}) \\ \vdots \\ \rho_N(\tilde{f}_{N,\alpha+1/2} - \tilde{f}_{N,\alpha-1/2}) \end{pmatrix} \right), \quad \alpha = 1, \dots, M,$$

where  $\tilde{\Phi}_{\alpha+1/2} = (\tilde{\phi}_{1,\alpha+1/2}, \dots, \tilde{\phi}_{N,\alpha+1/2})$ .

Since we will use the flux function of the unknowns  $m_\alpha$  to compute the flux function for the unknown  $\bar{m}$ , we also consider the part of the source term related to the unknowns  $m_\alpha$ , which is defined by

$$\mathcal{G}^{m_\alpha} := (G_{\alpha+1/2} - G_{\alpha-1/2})/l_\alpha, \quad \alpha = 1, \dots, M.$$

(see (1.5.3)). At this point we introduce the following notation which will be used later. We denote

$$\mathbf{w}_\alpha = \begin{pmatrix} m_\alpha \\ q_\alpha \end{pmatrix}, \quad \mathcal{F}_\alpha := \begin{pmatrix} \mathcal{F}^{m_\alpha} \\ \mathcal{F}^{q_\alpha} \end{pmatrix}, \quad \mathcal{S}_\alpha := \begin{pmatrix} 0 \\ s_\alpha \end{pmatrix}, \quad \mathcal{G}_\alpha := \begin{pmatrix} \mathcal{G}^{m_\alpha} \\ \mathcal{G}^{q_\alpha} \end{pmatrix}, \quad \alpha = 1, \dots, M.$$

Note that using this notation, from the definition of the global system we obtain

$$\partial_t \mathbf{w}_\alpha + \partial_x \mathcal{F}_\alpha(\mathbf{w}_\alpha) = \mathcal{S}_\alpha + \mathcal{G}_\alpha, \quad \alpha = 1, \dots, M.$$

### 1.6.2 Path-conservative method

We consider an HLL-path-conservative method where we set the path as segments (PVM-1U method, see [26]). Nevertheless, in what follows we describe the definition of the method in a form that allows us to avoid the computation of the transport matrix of the system. Moreover, this formulation takes into account that the flux associated with the unknown  $\bar{m}$  can be written as the average of the fluxes associated with  $m_\alpha$ . A second or higher order extention of the method can be done following [29]. We discretize the spatial domain into cells  $\mathcal{C}_i := [x_{i-1/2}, x_{i+1/2}]$  of width  $\Delta x$  centered at  $x_i = (i - 1/2)\Delta x$ ,

$i \in \mathbb{Z}$ , and discretize time via  $t_n = n\Delta t$ ,  $n \in \mathbb{N}_0$ . We denote by  $\mathbf{w}_{\alpha,i}^n$  the approximate value of  $\mathbf{w}(x, t_n)$  for layer  $\alpha$ ; similar notation is used for other quantities.

The HLL-PVM-1U method is defined by the following two coefficients,

$$\begin{aligned}\alpha_{0,i+1/2}^n &= \frac{S_{R,i+1/2}^n |S_{L,i+1/2}^n| - S_{L,i+1/2}^n |S_{R,i+1/2}^n|}{S_{R,i+1/2}^n - S_{L,i+1/2}^n}, \\ \alpha_{1,i+1/2}^n &= \frac{|S_{R,i+1/2}^n| - |S_{L,i+1/2}^n|}{S_{R,i+1/2}^n - S_{L,i+1/2}^n}.\end{aligned}$$

Here the characteristic velocities  $S_{L,i+1/2}^n$  and  $S_{R,i+1/2}^n$  are global approximations (they are the same for each layer) of the minimum and maximum wave speed. Taking into account Theorem A.2.1 (see Appendix A.2) we set the following definition of  $S_{L,i+1/2}^n$  and  $S_{R,i+1/2}^n$ ,

$$S_{L,i+1/2}^n = \bar{u}_{i+1/2}^n - \Psi_{i+1/2}^n, \quad S_{R,i+1/2}^n = \bar{u}_{i+1/2}^n + \Psi_{i+1/2}^n, \quad (1.6.1)$$

where

$$\begin{aligned}\bar{u}_{i+1/2}^n &:= \frac{1}{M} \sum_{\beta=1}^M u_{\beta,i+1/2}^n, \\ \Psi_{i+1/2}^n &:= \frac{2M-1}{\sqrt{2M(2M-1)}} \left( 2 \sum_{\beta=1}^M (\bar{u}_{i+1/2}^n - u_{\beta,i+1/2}^n)^2 + \frac{gh_{i+1/2}^n}{\rho_0} \left( \rho_0 + \frac{1}{M} \sum_{\beta=1}^M (2\beta-1)\bar{\rho}_{\beta,i+1/2}^n \right) \right)^{1/2},\end{aligned}$$

where  $M$  is the number of layers. The HLL-PVM-1U method proposed can be written as

$$\mathbf{w}_{\alpha,i}^{n+1} = \mathbf{w}_{\alpha,i}^n - \frac{\Delta t}{\Delta x} (\tilde{\mathcal{F}}_{\alpha,i+1/2}^n - \tilde{\mathcal{F}}_{\alpha,i-1/2}^n) + \Delta t \mathcal{S}_{\alpha,i}^n + \Delta t \mathcal{G}_{\alpha,i}^n,$$

where here the numerical flux  $\tilde{\mathcal{F}}_{\alpha,i+1/2}^n = (\tilde{\mathcal{F}}_{i+1/2}^{m_\alpha,n}, \tilde{\mathcal{F}}_{i+1/2}^{q_\alpha,n})^\top$  is given by

$$\begin{aligned}\tilde{\mathcal{F}}_{\alpha,i+1/2}^n &:= \frac{1}{2} \left( \mathcal{F}_\alpha(\mathbf{w}_{\alpha,i+1}^n) + \mathcal{F}_\alpha(\mathbf{w}_{\alpha,i}^n) \right) - \frac{1}{2} \left( \alpha_{0,i+1/2}^n (\mathbf{w}_{\alpha,i+1}^n - \mathbf{w}_{\alpha,i}^n + \mathcal{C}_{\alpha,i+1/2}^n + \mathbf{S}_{\alpha,i+1/2}^n) \right. \\ &\quad \left. + \alpha_{1,i+1/2}^n (\mathcal{F}_\alpha(\mathbf{w}_{\alpha,i+1}^n) - \mathcal{F}_\alpha(\mathbf{w}_{\alpha,i}^n) + \mathbf{S}_{\alpha,i+1/2}^n) \right),\end{aligned}$$

where

$$\begin{aligned}\mathcal{C}_{\alpha,i+1/2}^n &= \begin{pmatrix} \bar{\rho}_{\alpha,i+1}^n + \bar{\rho}_{\alpha,i}^n (z_{i+1} - z_i) \\ 0 \end{pmatrix}, \quad \mathcal{S}_{\alpha,i}^n = \frac{1}{2} (\mathbf{S}_{\alpha,i+1/2}^n + \mathbf{S}_{\alpha,i-1/2}^n), \quad \mathbf{S}_{\alpha,i+1/2}^n = g \begin{pmatrix} 0 \\ s_{\alpha,i+1/2}^n \end{pmatrix}, \\ s_{\alpha,i+1/2}^n &= \frac{1}{2} \left( (m_{i+1}^n + m_i^n)(\eta_{i+1}^n - \eta_i^n) + (h_{i+1}^{2,n} + h_i^{2,n}) \left( \frac{l_\alpha}{2} + \sum_{\beta=\alpha+1}^M l_\beta \right) (\bar{\rho}_{\alpha,i+1}^n - \bar{\rho}_{\alpha,i}^n) \right. \\ &\quad \left. + (h_{i+1}^n + h_i^n) \sum_{\beta=\alpha+1}^M l_\beta ((\bar{\rho}_{\beta,i+1}^n - \bar{\rho}_{\alpha,i+1}^n) h_{i+1}^n - (\bar{\rho}_{\beta,i}^n - \bar{\rho}_{\alpha,i}^n) h_i^n) \right),\end{aligned}$$

and

$$\mathcal{G}_{\alpha,i}^n = \begin{pmatrix} \mathcal{G}_i^{m_\alpha,n} \\ \mathcal{G}_i^{q_\alpha,n} \end{pmatrix}.$$

To compute  $\mathcal{G}_i^{m_\alpha, n}$  and  $\mathcal{G}_i^{q_\alpha, n}$  we approximate the transfer term  $G_{\alpha+1/2}$  by setting

$$G_{\alpha+1/2, i}^n := \frac{1}{2} (G_{\alpha+1/2, i+1/2}^n + G_{\alpha+1/2, i-1/2}^n),$$

where  $G_{\alpha+1/2, i+1/2}^n$  is an approximation at  $x = x_{i+1/2}$ . By using the recursivity equality (1.5.7), we approximate the transfer term by

$$\begin{aligned} \rho_0 \frac{\hat{\rho}_{\alpha+1}^n + \hat{\rho}_\alpha^n}{\hat{\rho}_{\alpha+1}^n \hat{\rho}_\alpha^n} G_{\alpha+1/2, i+1/2}^n &= \rho_0 \frac{\hat{\rho}_\alpha^n + \hat{\rho}_{\alpha-1}^n}{\hat{\rho}_\alpha^n \hat{\rho}_{\alpha-1}^n} G_{\alpha-1/2, i+1/2}^n + \frac{l_\alpha}{\Delta x} (R_{\alpha, i+1}^n - \bar{R}_{i+1}^n - R_{\alpha, i}^n + \bar{R}_i^n) \\ &\quad + \sum_{j=1}^N (\hat{f}_{j, \alpha+1/2, i+1/2}^n - \hat{f}_{j, \alpha-1/2, i+1/2}^n) (\rho_j - \rho_0), \end{aligned}$$

with

$$\begin{aligned} \hat{\rho}_\alpha^n &:= \frac{1}{2} (\bar{\rho}_{\alpha, i+1}^n + \bar{\rho}_{\alpha, i}^n), \quad \alpha = 1, \dots, M; \\ \hat{f}_{j, \alpha+1/2, i+1/2}^n &:= \frac{1}{2} (f_{j, \alpha+1/2, i+1}^n + f_{j, \alpha+1/2, i}^n), \quad \alpha = 1, \dots, M, \quad j = 1, \dots, N, \end{aligned}$$

where  $f_{j, \alpha+1/2, i}^n$  is the numerical approximation of the vertical flux  $\tilde{f}_{j, \alpha+1/2}$  given by

$$\begin{aligned} f_{j, \alpha+1/2}^n &= \frac{1}{2} (\phi_{j, \alpha} v_j^{\text{MLB}}(\Phi_\alpha) + \phi_{j, \alpha+1} v_j^{\text{MLB}}(\Phi_{\alpha+1})) - \frac{E_{\alpha+1}}{2} (\phi_{j, \alpha+1} - \phi_{j, \alpha}) \\ &\quad - \frac{\phi_{j, \alpha}}{2} |v_j^{\text{MLB}}(\Phi_{\alpha+1}) - v_j^{\text{MLB}}(\Phi_\alpha)| \operatorname{sgn}(\phi_{j, \alpha+1} - \phi_{j, \alpha}), \end{aligned}$$

based on [21, Scheme 8] and where  $\Phi_\alpha := (\phi_{1, \alpha}, \dots, \phi_{N, \alpha})^T$  and  $E_\alpha := \max_{j=1, \dots, N} |v_j^{\text{MLB}}(\Phi_\alpha)|$ , where  $v_j^{\text{MLB}}$  is the hindered settling velocity given by (1.2.15). Then we have

$$\begin{aligned} \mathcal{G}_i^{m_\alpha, n} &= (G_{\alpha+1/2, i}^n - G_{\alpha-1/2, i}^n) / l_\alpha, \\ \mathcal{G}_i^{q_\alpha, n} &= (\bar{u}_{\alpha+1/2, i}^n G_{\alpha+1/2, i}^n - \bar{u}_{\alpha-1/2, i}^n G_{\alpha-1/2, i}^n) / l_\alpha, \\ \bar{u}_{\alpha+1/2, i}^n &= \frac{1}{2} \left( \frac{u_{\alpha+1, i+1}^n + u_{\alpha, i+1}^n}{2} + \frac{u_{\alpha+1, i}^n + u_{\alpha, i}^n}{2} \right). \end{aligned}$$

Moreover, since the solid concentrations are passive scalars in the system, i.e.  $\mathcal{F}^{r_{j, \alpha}} = (r_{j, \alpha} / m_\alpha) \mathcal{F}^{m_\alpha}$ , we use the following upwinding formula to compute the numerical flux relative to  $r_{j, \alpha}^n$ :

$$\tilde{\mathcal{F}}_{i+1/2}^{r_{j, \alpha}, n} = \begin{cases} (r_{j, \alpha, i}^n / m_{\alpha, i}^n) \tilde{\mathcal{F}}_{i+1/2}^{m_\alpha, n} & \text{if } \tilde{\mathcal{F}}_{i+1/2}^{m_\alpha, n} > 0, \\ (r_{j, \alpha, i+1}^n / m_{\alpha, i+1}^n) \tilde{\mathcal{F}}_{i+1/2}^{m_\alpha, n} & \text{otherwise,} \end{cases} \quad j = 1, \dots, N.$$

Finally, the numerical scheme to approximate the unknowns of the problem is defined as follows:

$$\begin{aligned} \bar{m}_i^{n+1} &= \bar{m}_i^n - \frac{\Delta t}{\Delta x} \sum_{\beta=1}^M l_\beta \tilde{\mathcal{F}}_{i+1/2}^{m_\beta, n}, \\ q_{\alpha, i}^{n+1} &= q_{\alpha, i}^n - \frac{\Delta t}{\Delta x} (\tilde{\mathcal{F}}_{i+1/2}^{q_\alpha, n} - \tilde{\mathcal{F}}_{i-1/2}^{q_\alpha, n}) + \frac{\Delta t}{2} (s_{\alpha, i+1/2}^n + s_{\alpha, i-1/2}^n) + \Delta t \mathcal{G}_i^{q_\alpha, n}, \\ r_{j, \alpha, i}^{n+1} &= r_{j, \alpha, i}^n - \frac{\Delta t}{\Delta x} (\tilde{\mathcal{F}}_{i+1/2}^{r_{j, \alpha}, n} - \tilde{\mathcal{F}}_{i-1/2}^{r_{j, \alpha}, n}) + \Delta t \mathcal{G}_i^{r_{j, \alpha}, n}, \end{aligned}$$

with

$$\begin{aligned}\mathcal{G}_i^{r_{j,\alpha},n} &= \frac{1}{l_\alpha} (\bar{\phi}_{j,\alpha+1/2,i}^n G_{\alpha+1/2,i}^n - \bar{\phi}_{j,\alpha-1/2,i}^n G_{\alpha-1/2,i}^n) - \frac{\rho_j}{l_\alpha} (\hat{f}_{j,\alpha+1/2,i+1/2}^n - \hat{f}_{j,\alpha-1/2,i+1/2}^n), \\ \bar{\phi}_{j,\alpha+1/2,i}^n &= \frac{1}{2} \left( \frac{1}{2} \left( \frac{r_{j,\alpha+1,i+1}^n}{m_{\alpha+1,i+1}^n} + \frac{r_{j,\alpha,i+1}^n}{m_{\alpha,i+1}^n} \right) + \frac{1}{2} \left( \frac{r_{j,\alpha+1,i}^n}{m_{\alpha+1,i}^n} + \frac{r_{j,\alpha,i}^n}{m_{\alpha,i}^n} \right) \right).\end{aligned}$$

## 1.7 Numerical tests

### 1.7.1 Preliminaries

In all tests we use the global constants  $g = 9.8 \text{ m/s}^2$  (acceleration of gravity),  $\phi_{\max} = 0.68$  ((nominal) maximal total solids concentration, a dimensionless volume fraction), and employ the Richardson-Zaki hindered settling factor (1.2.12) with  $n_{RZ} = 4.7$ . The viscosity and density of the pure fluid are  $\mu_0 = 0.02416 \text{ Pas}$  and  $\rho_0 = 1208 \text{ kg/m}^3$ , respectively. In all tests the particles are assumed to have the same density  $\rho_1 = \dots = \rho_N = 2790 \text{ kg/m}^3$ . These parameters correspond to an experiment by Schneider et al. [59].

We limit the computation of numerical solutions to four tests. Firstly, one case of zero horizontal but one vertical direction (Test 1.1), and two cases of one horizontal and one vertical direction (Test 1.2 and 1.3). In the latter tree cases, the (horizontal)  $x$ -interval  $[0, L]$  is subdivided into  $C$  subintervals  $[x_{i-1/2}, x_{i+1/2}] = [(i-1)\Delta x, i\Delta x]$  of length  $\Delta x = L/C$ , centered at  $x_i = (i-1/2)\Delta x$ ,  $i = 1, \dots, C$ . In what follows, we use the following CFL condition to determine  $\Delta t$  in each iteration:

$$\frac{\Delta t}{\Delta x} \max_{1 \leq i \leq C} \max\{|S_{R,i+1/2}|, |S_{L,i+1/2}|\} = \text{CFL},$$

where  $S_{R,i+1/2}$  and  $S_{L,i+1/2}$  are the bounds of the eigenvalues defined in (1.6.1) and  $\text{CFL} = 0.5$ . Furthermore, for Test 1.3 we compute an approximate  $L^1$  error at a fixed end time  $t = t_{\text{end}}$  of a scalar component  $g_i$  of the numerical solution by means of a reference solution based on a number of  $C_{\text{ref}}$  cells. Precisely, let us denote by  $\{g_i(t_{\text{end}})\}_{i=1}^C$  and  $\{\tilde{g}_i^{\text{ref}}(t_{\text{end}})\}_{i=1}^{C_{\text{ref}}}$  the numerical solution at time  $t_{\text{end}}$  calculated with  $C$  and  $C_{\text{ref}}$  cells, respectively, where we assume that  $\nu := C_{\text{ref}}/C \in \mathbb{N}$ . Then we compute the projected reference solution  $\{\tilde{g}_i^{\text{ref}}(t_{\text{end}})\}_{i=1}^C$  using

$$\tilde{g}_i^{\text{ref}}(t_{\text{end}}) = \frac{1}{\nu} \sum_{k=1}^{\nu} g_{\nu(i-1)+k}^{\text{ref}}(t_{\text{end}}), \quad i = 1, \dots, C.$$

Then, we define the approximate  $L^1$  error of the numerical solution  $\{g_i(t_{\text{end}})\}_{i=1}^C$  at time  $t = t_{\text{end}}$  as

$$e_{C,C_{\text{ref}}}(t_{\text{end}}) := \frac{1}{C} \sum_{j=1}^C |\tilde{g}_i^{\text{ref}}(t_{\text{end}}) - g_i(t_{\text{end}})|. \quad (1.7.1)$$

Finally, a 3D simulation (Test 1.4) is presented. With the purpose of brevity we do not give the details in this chapter for the model and the numerical method. For the implementation of the numerical method we consider a rectangular grid in the horizontal 2D domain and the usual application of a 1D finite volume method at each edge of the cell.

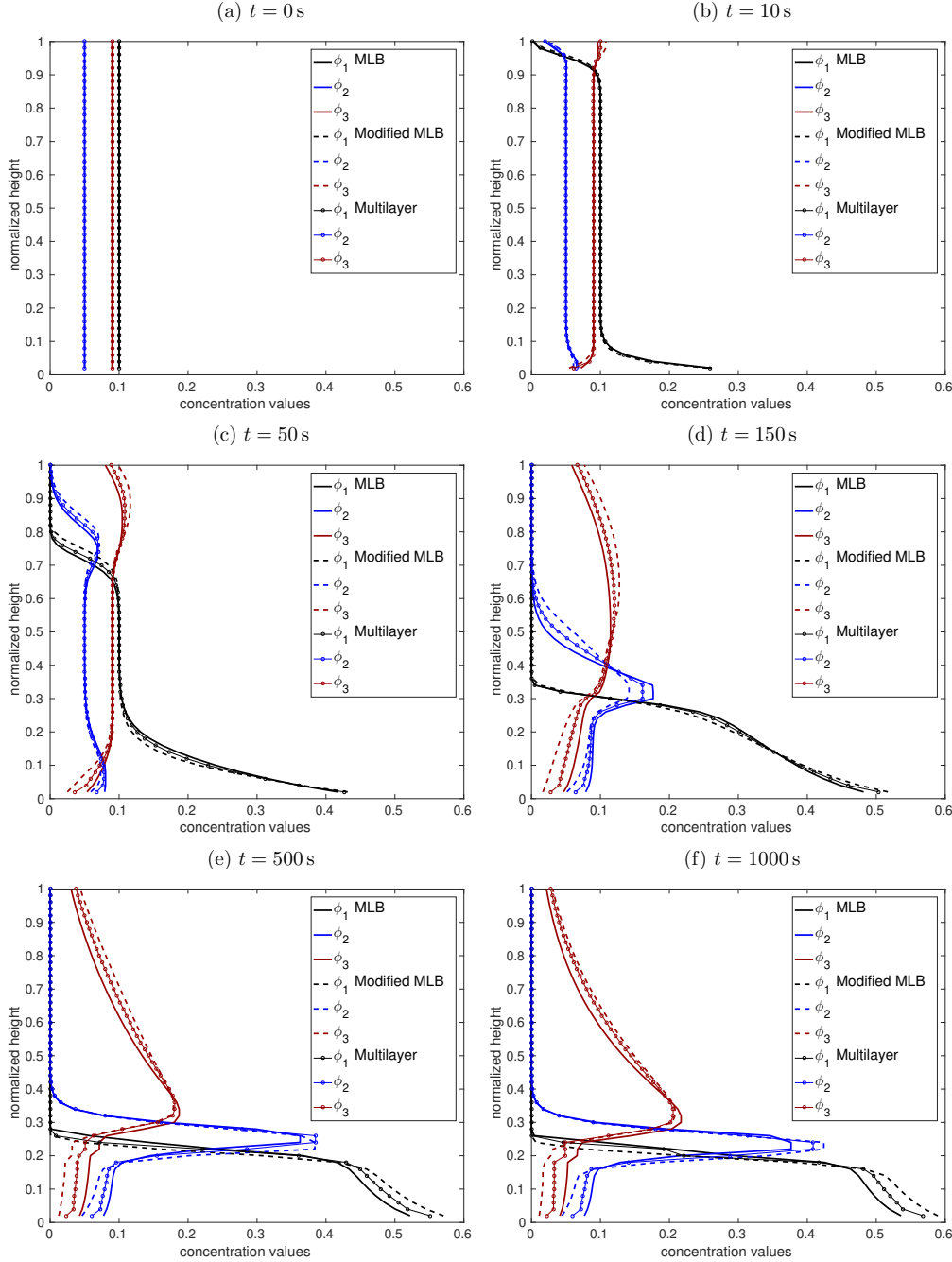


Figure 1.3: Test 1.1: Concentrations of the solid species with respect the normalized height at times  $t = 0, 10, 50, 150, 500$ , and  $1000\text{ s}$ .

### 1.7.2 Test 1.1: one-dimensional vertical sedimentation

In the first numerical test we consider  $N = 3$  solid species dispersed in a viscous fluid. The solid particle diameters are  $d_1 = 4.96 \times 10^{-4}\text{ m}$ ,  $d_2 = 3.25 \times 10^{-4}\text{ m}$  and  $d_3 = 1.0 \times 10^{-4}\text{ m}$ .

We consider a vertical domain of height  $h = 0.3\text{ m}$  discretized into  $M = 50$  layers ( $z_i$  nodes), with

initial solid concentrations  $\phi_1(t = 0) = 0.1$ ,  $\phi_2(t = 0) = 0.05$  and  $\phi_3(t = 0) = 0.09$  constant in all the domain. Figure 1.3 displays simulated concentration profiles at different times. Comparing the simulated behaviour of the modified MLB model (defined by (1.2.15)) with that of the original MLB model (that is recovered if we set  $\lambda_1 = \dots = \lambda_N = 1$  in (1.2.15)), we can see that the modified MLB velocities predict that the solid particles settle slightly more slowly than when the classical MLB velocities are used. That said, we remark that the 1D vertical modified MLB model coincides with the proposed multilayer approximation only if the transfer term  $G_{\alpha+1/2}$  is set to zero. In other words, if we block the transfer of mass term across the interface in the multilayer approach, we recover the classical one-dimensional numerical method for polydisperse sedimentation [21] but with the new MLB velocity.

The 1D vertical model corresponds to solving the following system of ODEs that represent a semi-discretization of the spatio-temporal model:

$$\partial_t \phi_{j,\alpha} = -\frac{1}{hl_\alpha} (f_{j,\alpha+1/2} - f_{j,\alpha-1/2}), \quad j = 1, \dots, N, \quad \alpha = 1, \dots, M,$$

where  $f_{j,\alpha+1/2}$  is the numerical approximation of the vertical flux function  $f_j = \phi_j v_j^{\text{MLB}}$ .

The mass transfer is not equal to zero in this new multilayer model even though the horizontal velocities are equal zero. In this case, from the definition (A.1.5) of  $G_{\alpha+1/2}$  we deduce the transfer term

$$G_{\alpha+1/2} = \rho_0 \sum_{j=0}^N \tilde{f}_{j,\alpha+1/2}.$$

Since within the classical MLB model, the average velocity does not take into account the densities of the particles, it can be deduced that

$$\sum_{j=0}^N \tilde{f}_{j,\alpha+1/2} = 0.$$

Then  $G_{\alpha+1/2} = 0$ . With the proposed modification of MLB model,  $G_{\alpha+1/2} \neq 0$  because this term takes into account the exact mass conservation, which implies that

$$\sum_{j=0}^N \rho_j \tilde{f}_{j,\alpha+1/2} = 0.$$

As a consequence, the proposed model is able to reproduce a vertical velocity of the fluid generated by the vertical movement of the solid particles. However, the three models predict fairly similar sedimentation behaviour of the three models. The larger species settle faster than those with smaller size, and the smaller particles float (that is, move upward) when the biggest particles settle. This behavior is expected. At  $t = 500$  s the solution is almost stationary. In Figure 1.3 a very small variation in the concentration of the smallest particles can be observed if we compare the figures corresponding to  $t = 500$  and  $t = 1000$  s.

### 1.7.3 Test 1.2: sedimentation with imposed velocity

In this numerical test we simulate bidisperse sedimentation in a horizontal channel, with an inclined bottom, of length  $L = 1$  m. Here and in Test 1.3 we use  $C = 150$  subintervals and  $M = 10$  layers in

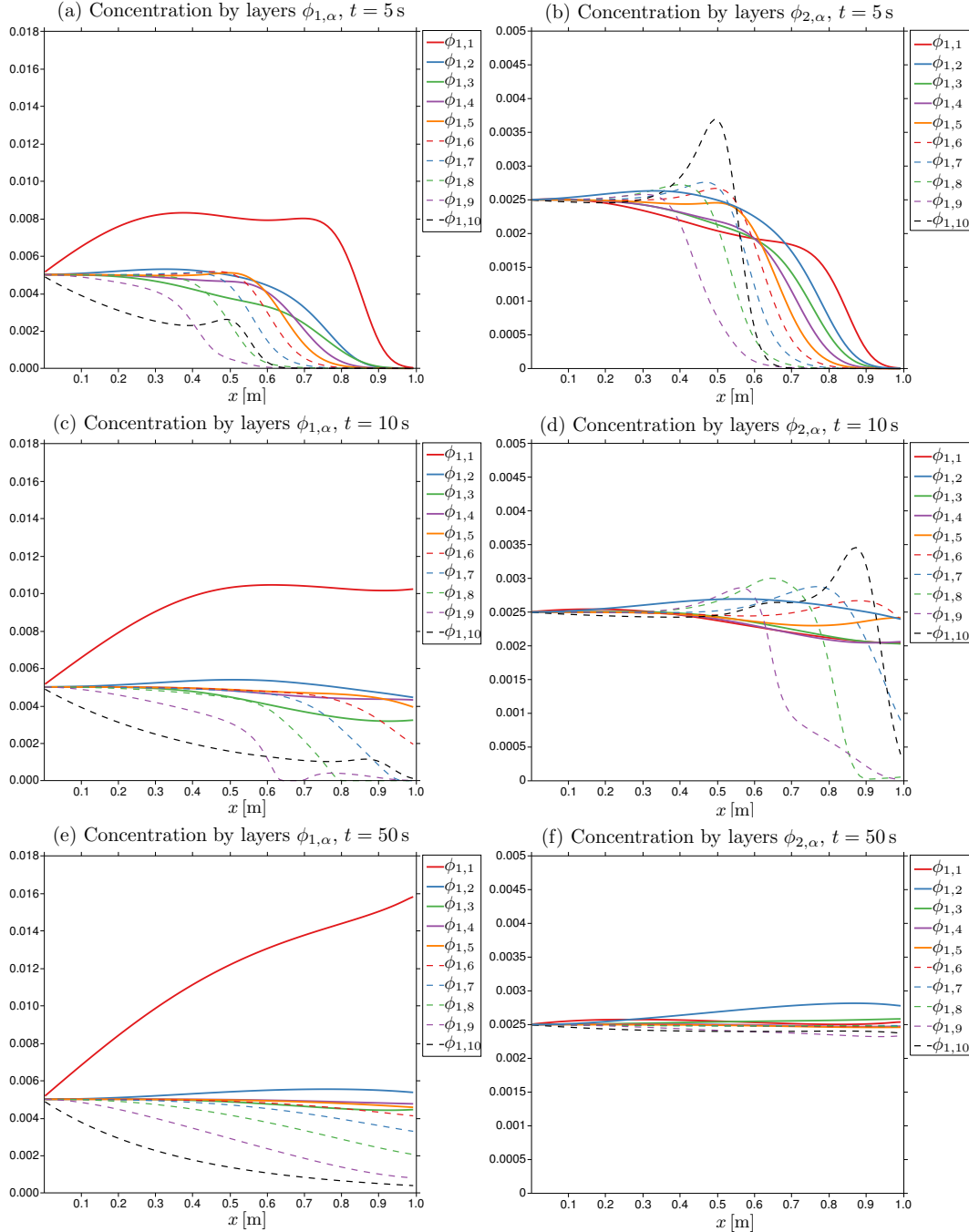


Figure 1.4: Test 1.2: Concentration of solid species  $\phi_1$ ,  $\phi_2$  by layer.

the horizontal and vertical discretization, respectively, and in both tests we use  $N = 2$  solids species of diameters  $d_1 = 4.96 \times 10^{-4}$  m and  $d_2 = 1.25 \times 10^{-4}$  m, respectively (these are the original particle sizes used in [59]). The bottom elevation is given by  $z_B(x) = -0.1x + 0.1$  m for  $x \in [0, L]$ . We here assume the initial condition

$$\phi_{1,\alpha}(0, x) = 0, \quad \phi_{2,\alpha}(0, x) = 0 \quad u_\alpha(0, x) = 0 \quad \text{for all } \alpha = 1, \dots, M, \text{ for all } x \in [0, L],$$

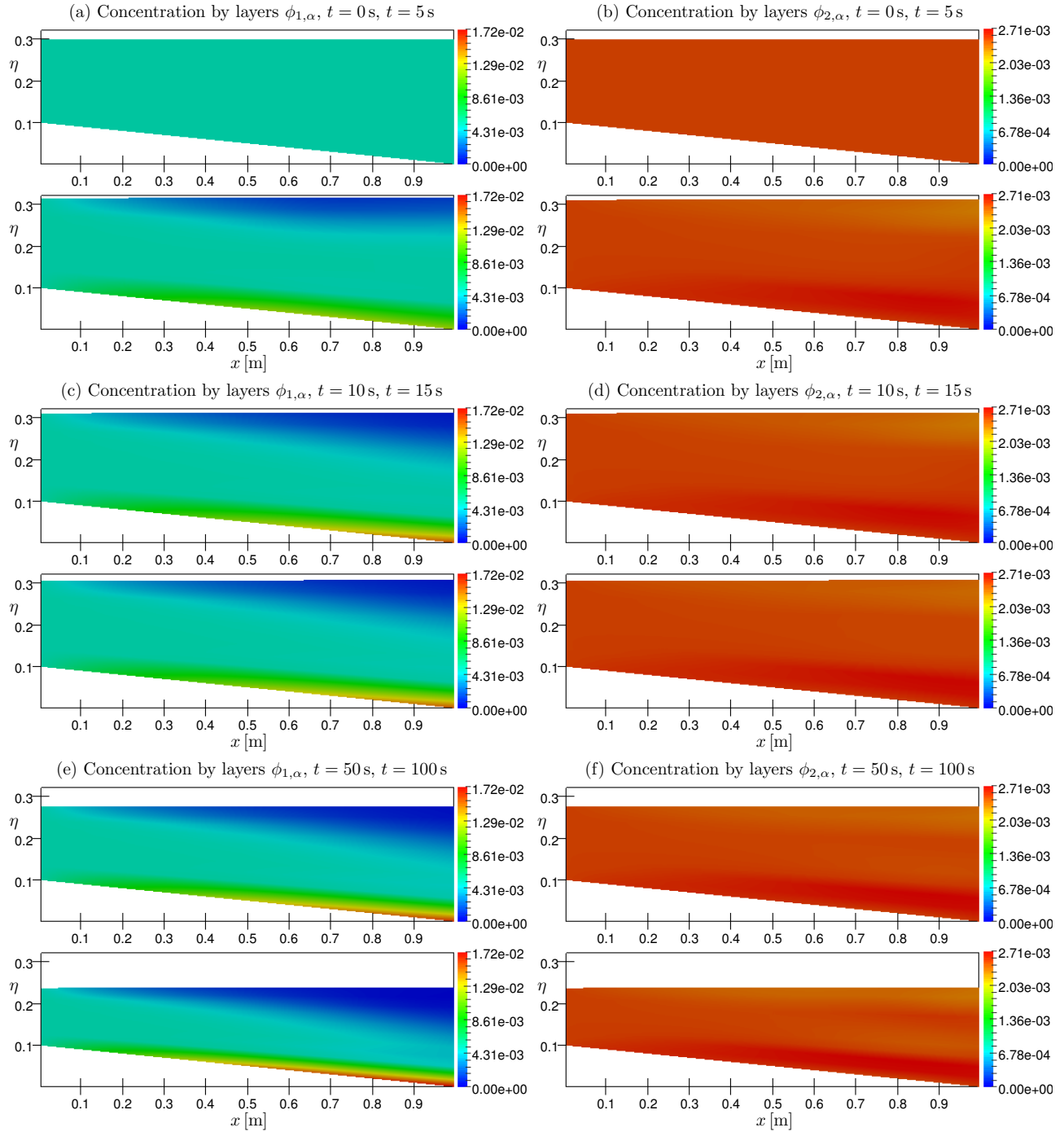


Figure 1.5: Test 1.2: Concentration of solid species  $\phi_1, \phi_2$  by colors,  $\eta(x) = z_B(x) + h(x)$  m.

and for the height  $h(t = 0) = 0.3 - z_B$ . Furthermore, as boundary condition we impose at  $x = 0$  a linear horizontal velocity  $u(z)|_{x=0} = 0.133z + 0.128$  m/s, whose average value is 0.15 m/s. A uniform

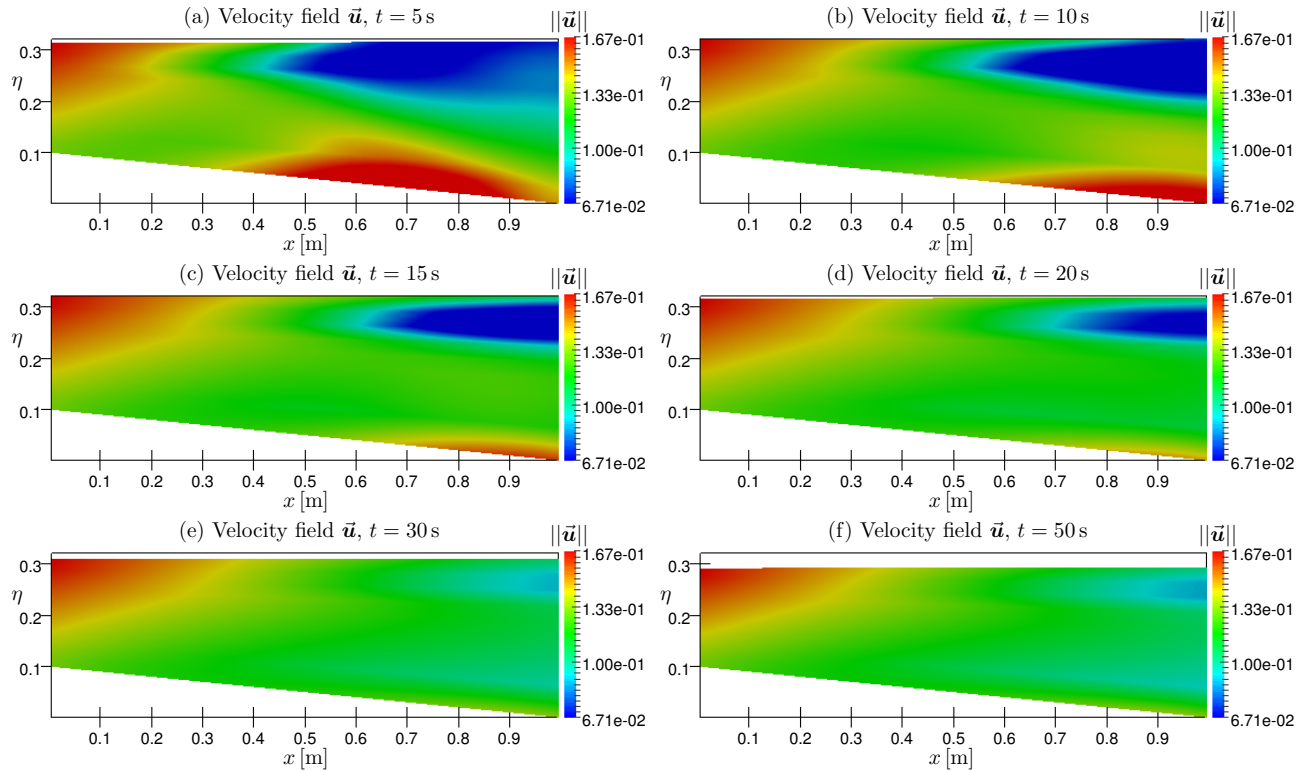


Figure 1.6: Test 1.2: Magnitude of the velocity field  $\vec{u}$  and free surface,  $\eta(x) = z_B(x) + h(x)$  m.

distribution of the sediment concentrations is set at the left boundary, i.e.,

$$\phi_{1,\alpha|x=0} = \frac{1}{M} \sum_{\beta=1}^M \phi_{1,\beta|x=0}, \quad \phi_{2,\alpha|x=0} = \frac{1}{M} \sum_{\beta=1}^M \phi_{2,\beta|x=0} \quad \text{for all } \alpha = 1, \dots, M$$

with  $\sum_{\beta=1}^M \phi_{1,\beta|x=0} = 0.05$  and  $\sum_{\beta=1}^M \phi_{2,\beta|x=0} = 0.025$ . At the right boundary a homogeneous Neumann condition is imposed.

Here, we are interested in seeing how the particles, besides settling due to the force of gravity, are transported horizontally when horizontal velocities are imposed on the left boundary. In Test 1.1 we have seen that some particles, depending on their size, move downward or upward, and the bigger particles settle faster than smaller particles (in the same environment). The difference here is that we impose linear horizontal velocities by layers and fixed concentrations over the left boundary and we want to see the behavior of the particles (horizontal movement, sedimentation and suspension of some particles). In Figures 1.4 and 1.5 for the first species we can see both phenomena, namely settling and horizontal transport of the particles due to the imposed horizontal velocity at the fluid.

We see for example in Figures 1.5 (a) and (c) and more clearly in Figure 1.5 (e) and correspondingly Figures 1.4 (a), (c) and (e) that the particles of bigger size are deposited rapidly over the bottom, furthermore we see how the concentration goes from initial condition ( $\phi_{1,\alpha} = 0$ ) to high concentration in the first layer, decreasing from the bottom to the free surface. In all the domain the concentration in the first layer always is greater than in the upper layers, due to the size of species 1. Furthermore this behavior is present at all times from  $t = 0$  to  $t = 100$  s.

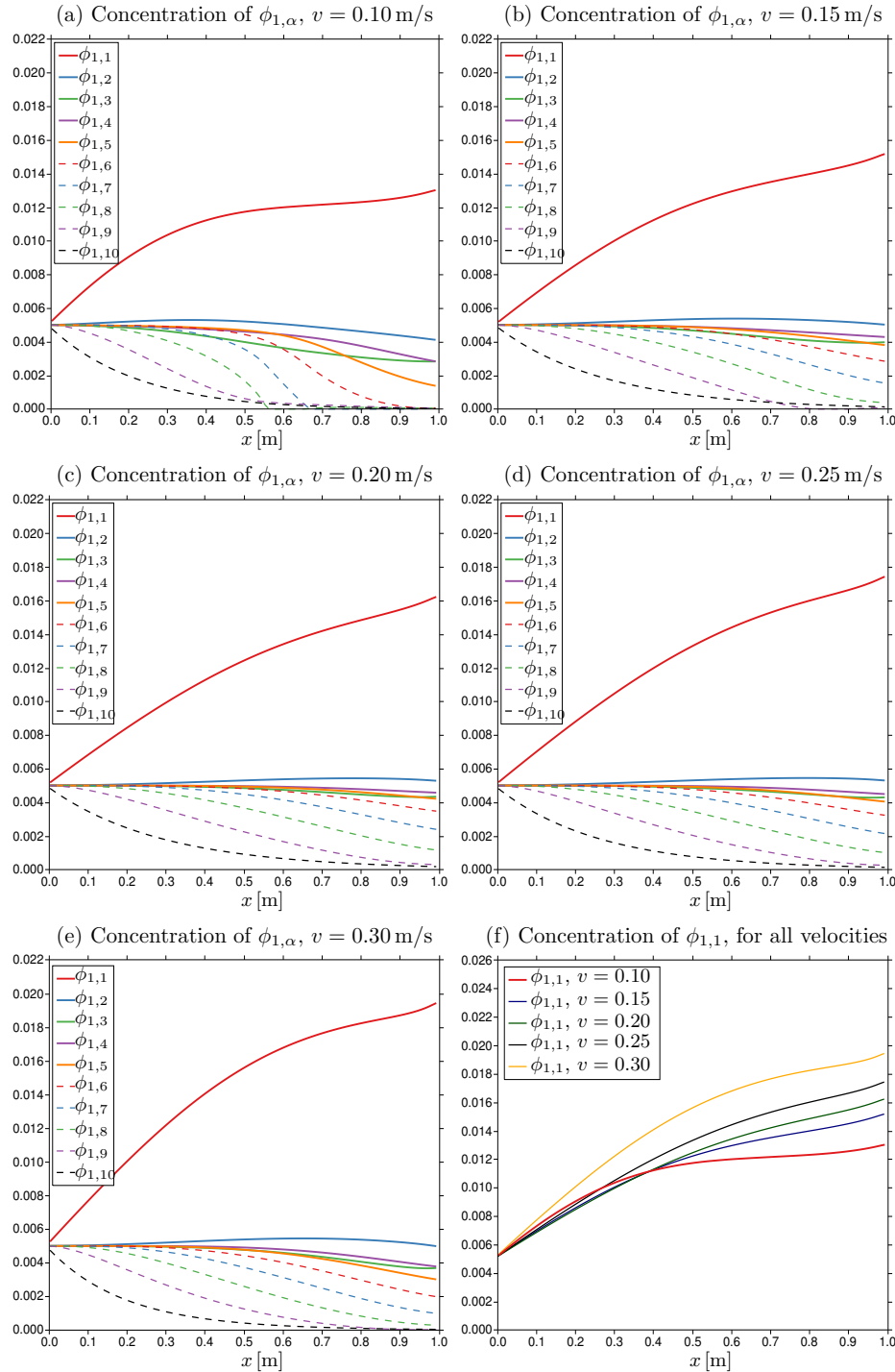


Figure 1.7: Test 1.2: Concentration for different constant velocities imposed in the left boundary in  $t = 100 \text{ s}$ .

If we make reference to the applications (water recovery for example), we can say that in the free surface close to the right boundary we obtain fluid free of particles of species 1 but yet with particles of species 2 at smaller concentration, as we see in Figures 1.4 and 1.5 in lines of concentration by layers

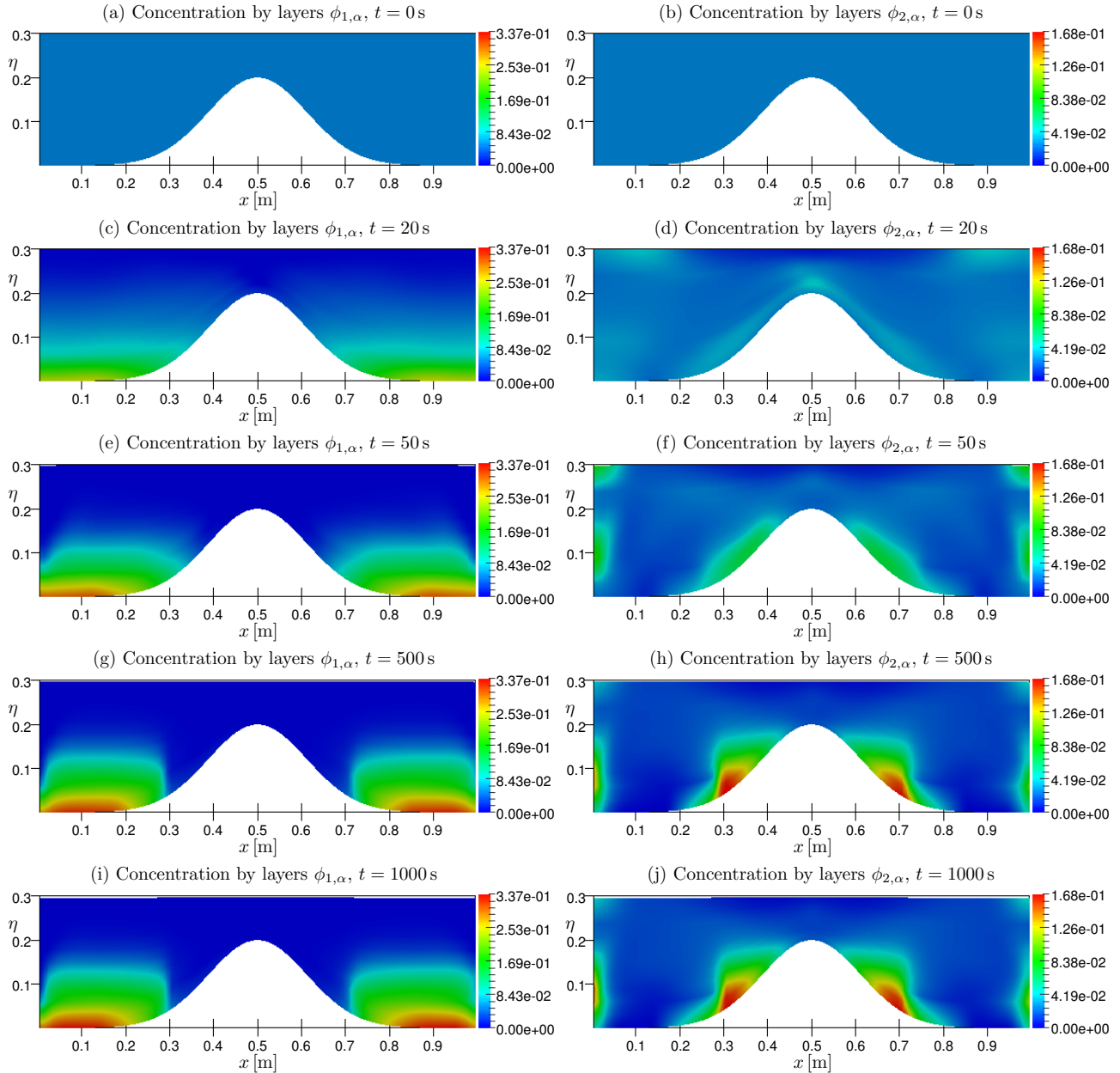


Figure 1.8: Test 1.3: Concentration of  $\phi_1$  and  $\phi_2$  by color in a domain with a bump,  $\eta(x) = z_B(x) + h(x)$  m.

and concentration by color, respectively. On the other hand, we can observe the horizontal movement of both solid species from the left to the right boundary, see Figures 1.4 and 1.5. Clearly, the concentration of each solid species  $\phi_{1,\alpha}$  and  $\phi_{2,\alpha}$  increases from zero to positive values in all layers. The behaviour of the smaller particles is more difficult to predict due to the suspension phenomena that appear when the bigger particles settle faster. For this reason, we can see how the concentration of these particles decreases more slowly than that of species 1. The particles of species 2 are in suspension for more time, in other words the sedimentation process for this species is slower. We can see in Figures 1.5 (b) and (d) for times  $t = 0, 5, 10, 15$  s that the concentration of the upper layers begins to

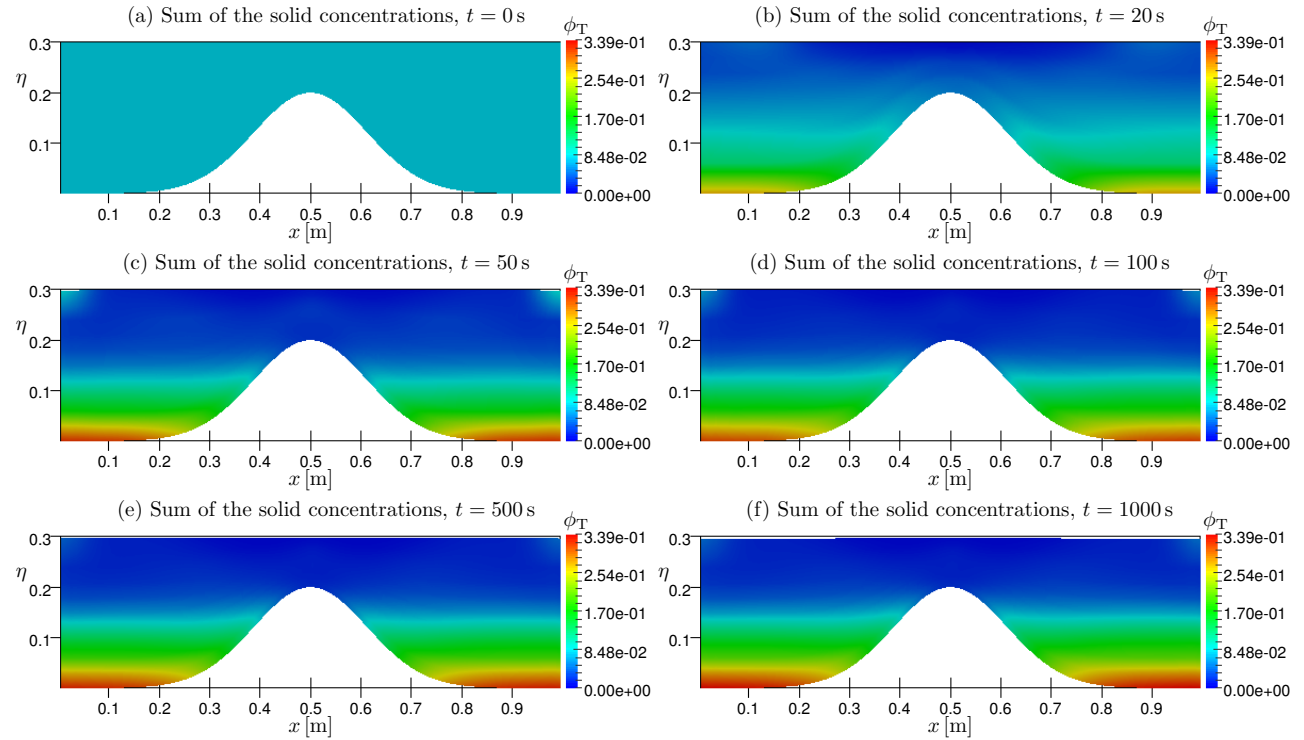


Figure 1.9: Test 1.3: Concentration by color by  $\phi_T = \phi_1 + \phi_2$ ,  $\eta(x) = z_B(x) + h(x)$  m.

increase in the middle of the domain, this means that in this place the particles of species 2 are clearly in suspension near to the free surface. In the following times, in Figures 1.5 (e) and (f) we see that some particles begin to settle and the concentration in the second layer increases. We note here that the concentrations in the first layer for species 2 is small because the larger particles have occupied the space, as we have also seen in Figures 1.3 (e) and (f) in Test 1.1. In Figure 1.6 the evolution of the velocity of the fluid is presented, where we have colored the magnitude of the velocity field.

Finally, to see the influence of the velocity magnitude imposed as boundary conditions we have considered the following values:  $v = 0.10, 0.15, 0.20, 0.25, 0.30$  m/s respectively, constant in all layers as boundary condition in the left and we have kept the same initial condition and we have simulated the sedimentation process with the same diameters and solid densities for the particles. In Figure 1.7, for simplicity we only show concentrations for species 1 at time  $t = 100$  s for the different horizontal velocities. We can see how for a bigger velocity the concentration of species 1 increases in the first layer due to a higher velocity, greater flow and therefore there is a higher influx of particles, which accumulate rapidly at the bottom of the domain. In Figure 1.7 (f) we see the difference in the concentration of species 1 in the first layer for different horizontal velocities.

#### 1.7.4 Test 1.3: sedimentation in a domain with a bump

In this numerical test we simulate bidisperse sedimentation process over a horizontal channel with a bump of length  $L = 1$  m. We use  $N = 2$  solids species dispersed in a viscous fluid; the particle sizes and densities are the same as in Test 1.2. The bottom elevation is given by  $z_B(x) = 0.2 \exp(-40(x-0.5)^2)$  m

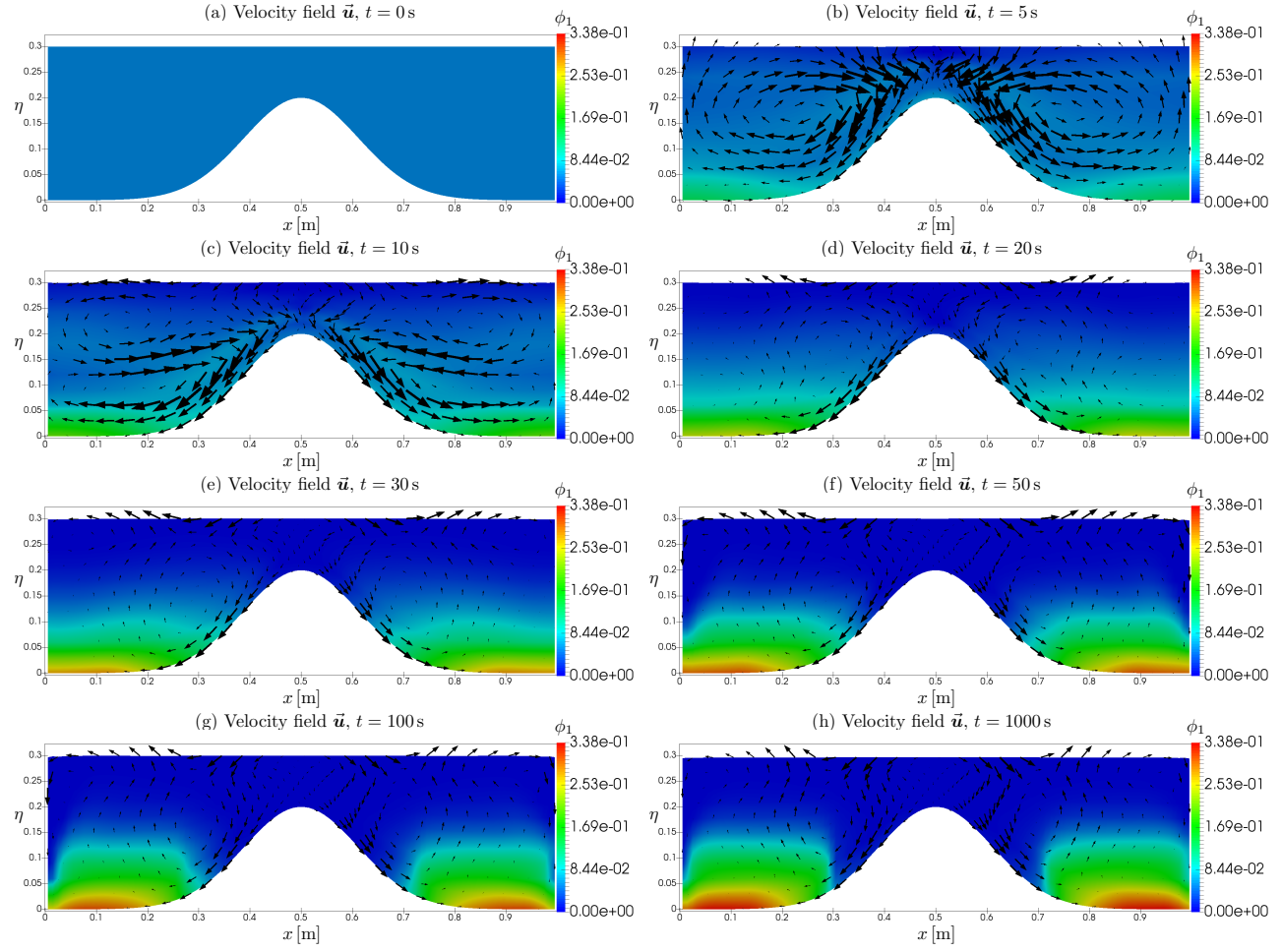


Figure 1.10: Test 1.3: Velocity field  $\vec{u}$  over concentration  $\phi_1$ ,  $\eta(x) = z_B(x) + h(x)$ .

for  $x \in [0, L]$ . The initial condition for the height is  $h(t = 0) = 0.3 - z_B$ . For  $\alpha = 1, \dots, M$ , the initial condition for the concentration of each species

$$\phi_{1,\alpha} = \frac{1}{M} \sum_{\beta=1}^M \phi_{1,\beta}(0, x), \quad \phi_{2,\alpha} = \frac{1}{M} \sum_{\beta=1}^M \phi_{2,\beta}(0, x), \quad u_\alpha(0, x) = 0, \quad x \in [0, L],$$

with  $\sum_{\beta=1}^M \phi_{1,\beta}(0, x) = 0.05$ ,  $\sum_{\beta=1}^M \phi_{2,\beta}(0, x) = 0.025$ . The sediment concentrations are vertically uniformly distributed at each point  $x$ . As boundary condition we impose a closed basin.

In Figure 1.8 we present the simulated concentrations of species 1 ( $\phi_1$ ) to the right and species 2 ( $\phi_2$ ) to the left. We can see the behavior of the particles of the different species when there is a bump in the domain. The bigger particles are deposited rapidly over the bottom, in this case to both sides of the bump, where we can find high concentration of species 1, as we can see in Figures 1.8 (a), (c), (e), (g) and (i). The smaller particles initially remain in suspension, but at larger simulated times these particles begin to settle and occupy where the concentration of species 1 is small (see Figures 1.8 (f), (h) and (j)). To see the global behavior of all particles dispersed in the fluid we display in Figure 1.9 the sum of the concentrations of the all species and we can see how these are deposited in the bottom

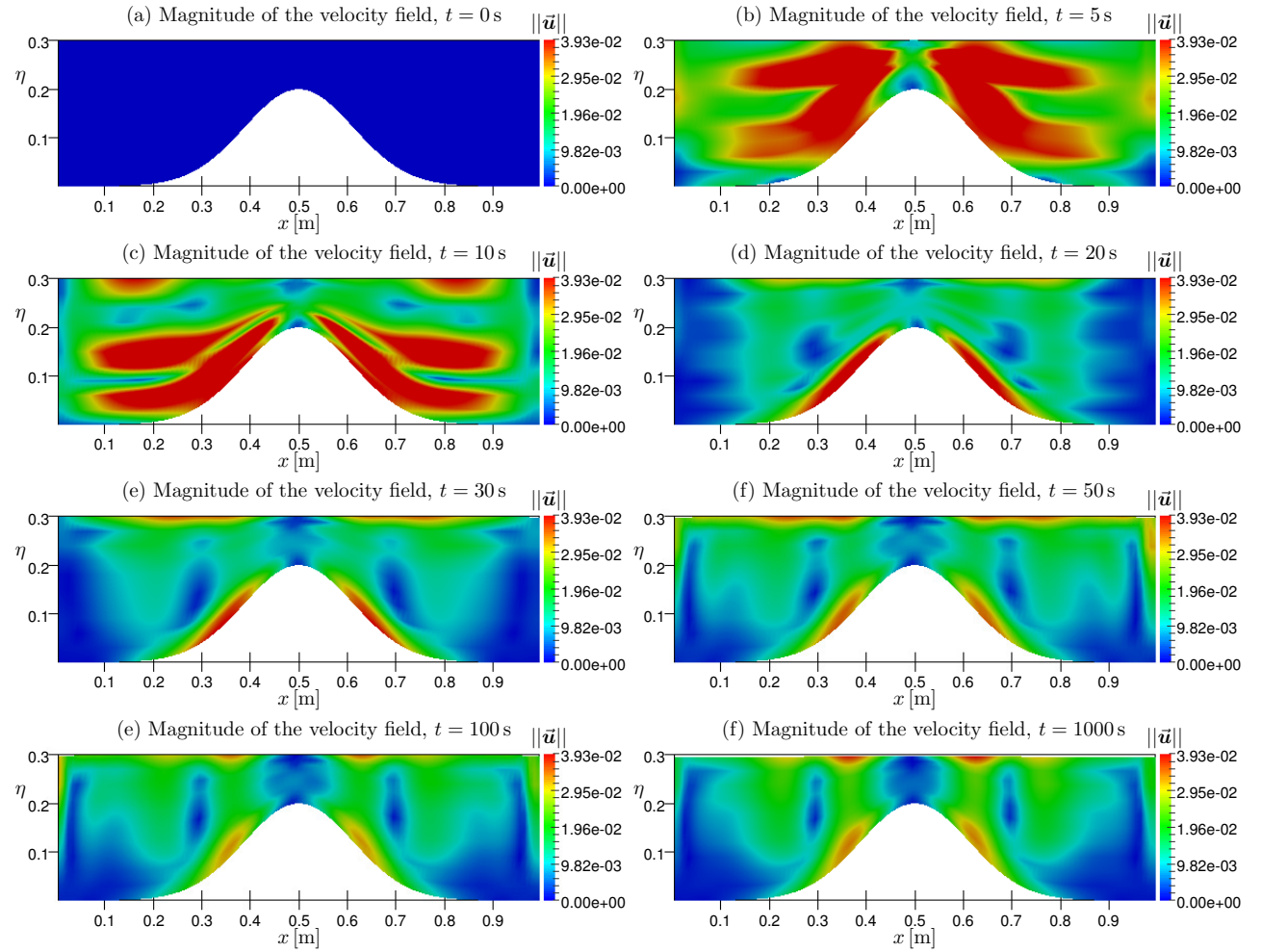


Figure 1.11: Test 1.3: Magnitude of the velocity field  $\vec{u}$ ,  $\eta(x) = z_B(x) + h(x)$ .

on both side of the bump and also as some particles of species 2 are kept in suspension. In Figure 1.10 and Figure 1.11 we show the velocity field of the fluid and its magnitude respectively, which is a consequence of the particles movement, and we can see how recirculations appear to both sides of the bump. In the first times high velocities appear avoiding that some particles settle rapidly. We see in Figures 1.8 (c) and 1.10 (c) how some particles are in suspension because they are inside of an eddy. At larger times the velocity decreases and the particles settle. A similar test with  $N = 3$  species can be found in [23].

Finally in Table 1.1 we show the numerical error computed with (1.7.1) at time  $t = 1\text{s}$  using a reference solution with  $C_{\text{ref}} = 5120$ . Only the error of some numerical solution are presented due to the big quantities of them. CPU times are also presented in Table 1.1, corresponding to a Laptop with Intel Core I5 (2.20 Ghz  $\times$  4) and 8GB of RAM.

$C$	$L^1$ error $r_{1,2}$	$L^1$ error $r_{1,4}$	$L^1$ error $r_{1,6}$	$L^1$ error $r_{1,8}$	$L^1$ error $r_{1,10}$	
40	7.33e-04	8.93e-05	1.18e-04	7.71e-05	6.76e-05	
80	5.45e-04	6.13e-05	8.50e-05	6.56e-05	4.99e-05	
160	3.89e-04	4.24e-05	5.87e-05	5.37e-05	3.51e-05	
320	2.44e-04	2.73e-05	3.87e-05	3.92e-05	2.35e-05	

$C$	$L^1$ error $r_{2,2}$	$L^1$ error $r_{2,4}$	$L^1$ error $r_{2,6}$	$L^1$ error $r_{2,8}$	$L^1$ error $r_{2,10}$	
40	3.73e-04	4.53e-05	5.94e-05	5.01e-05	3.79e-05	
80	2.78e-04	3.12e-05	4.26e-05	3.98e-05	3.03e-05	
160	1.98e-04	2.16e-05	2.94e-05	3.15e-05	2.22e-05	
320	1.24e-04	1.39e-05	1.94e-05	2.25e-05	1.53e-05	

$C$	$L^1$ error $\bar{m}$	$L^1$ error $q_2$	$L^1$ error $q_4$	$L^1$ error $q_6$	$L^1$ error $q_8$	$L^1$ error $q_{10}$	CPU t. [s]
40	1.27e-04	8.90e-04	3.86e-04	4.80e-04	6.18e-04	3.73e-04	0.168821
80	3.72e-05	7.42e-04	2.76e-04	3.55e-04	4.65e-04	2.46e-04	0.577368
160	1.34e-05	5.47e-04	1.81e-04	2.42e-04	3.18e-04	1.47e-04	2.143434
320	6.92e-06	3.44e-04	1.10e-04	1.51e-04	2.00e-04	8.02e-05	8.825133

Table 1.1: Test 1.3: approximate  $L^1$  errors for (top)  $r_{1,\alpha}$ , (middle)  $r_{2,\alpha}$  and (bottom)  $\bar{m}$  and  $q_\alpha$ , in each case for  $\alpha = 2, 4, 6, 8, 10$  at time  $t = 1$  s.

### 1.7.5 Test 1.4: sedimentation in a 3D domain

The last numerical test simulates a cylindrical dam break involving bidisperse sedimentation over a 3D paraboloid bottom given by

$$z(x, y) = \begin{cases} 0.71((x - 0.5)^2 + (y - 0.5)^2) & \text{for } (x - 0.5)^2 + (y - 0.5)^2 \leq 0.21, \\ 0.15 & \text{otherwise,} \end{cases} \quad (x, y) \in [0, 1]^2.$$

The diameters of the solid particles are as in Test 1.2. Here we use a rectangular grid of  $100 \times 100$  cells in the horizontal directions and  $M = 10$  layers in the vertical direction. For all  $\alpha = 1, \dots, M$  the initial condition is given by

$$\phi_{1,\alpha}(0, \mathbf{x}) = \begin{cases} 0.05 & \text{for } (x - 0.2)^2 + (y - 0.5)^2 \leq 0.1, \\ 0 & \text{otherwise,} \end{cases} \quad \mathbf{u}_\alpha(0, \mathbf{x}) = 0,$$

$$\phi_{2,\alpha}(0, \mathbf{x}) = \begin{cases} 0.025 & \text{for } (x - 0.2)^2 + (y - 0.5)^2 \leq 0.1, \\ 0 & \text{otherwise,} \end{cases}$$

along with the height  $h(t = 0) = 0.3 - z_B$ . Figures 1.12 and 1.13 show the concentrations  $\phi_1$  of the big particles and  $\phi_2$  of the small particles, respectively, inside the fluid domain and as a vertical cut in the middle of the domain, all seen from below. We show the solution at times  $t = 0, 7, 15, 30$  s because at these times the movement of the mixture exhibits interesting features. At short times we can see how both species of particles oscillate from right to left and back until the particles lose velocity and

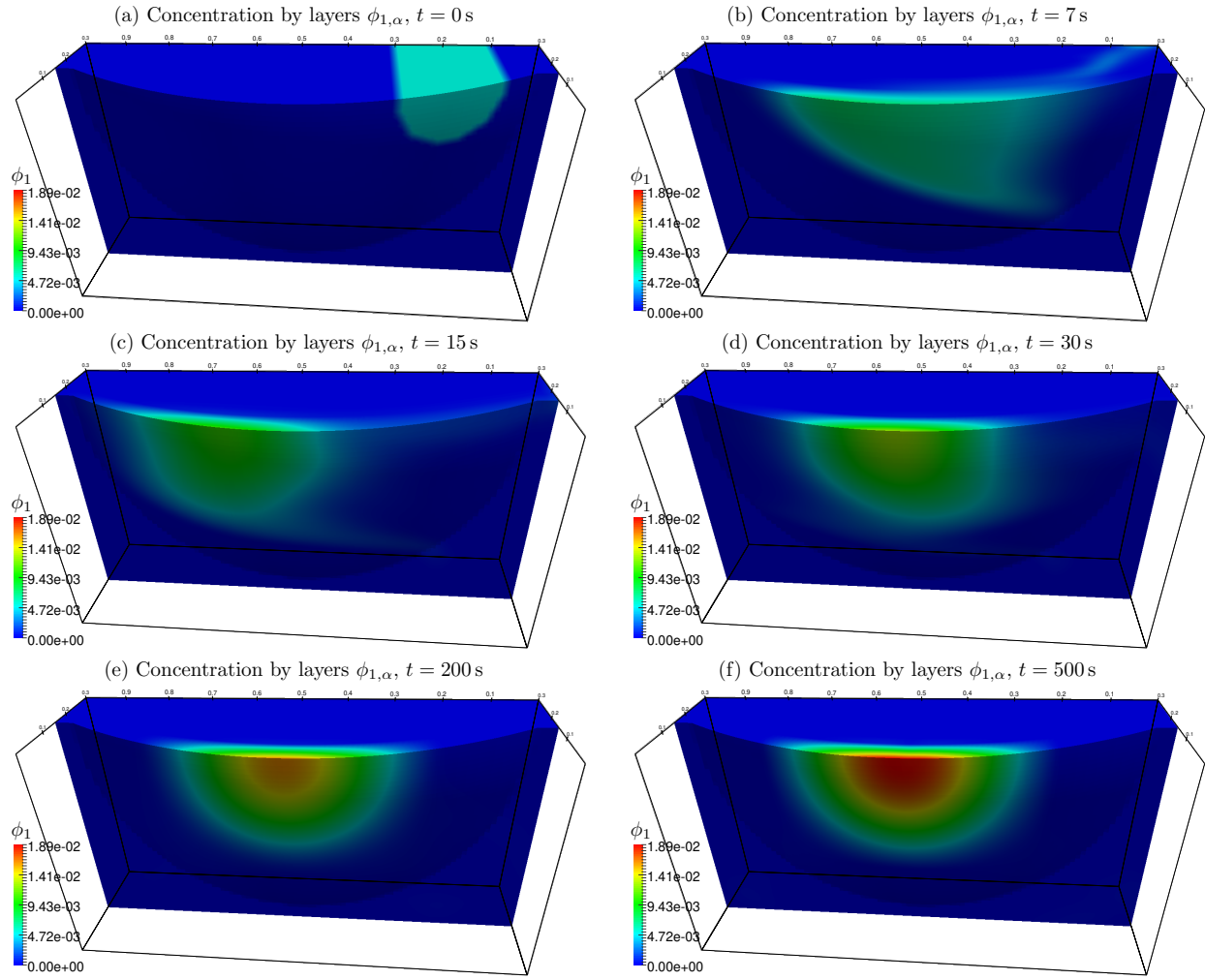


Figure 1.12: Test 1.4: Concentration of  $\phi_1$  by color in a 3D domain,  $\eta(\mathbf{x}) = z_B(\mathbf{x}) + h(\mathbf{x})$  m.

settle. In Figure 1.12 we see that the bigger particles move faster than the small ones and Figures 1.13 and 1.15 illustrate how the small particles are carried to the right wall (from this point of view of the solution) due to the recirculation of the mixture produced. Due to the small size of the particles of species 2 ( $\phi_2$ ), the movement of the mixture moves these particles to point of the domain where the concentration of the big particles is small. (This phenomenon can be seen in Test 1.3.) At large times all particles settle and we observe a stratification of the sediment as illustrated in Test 1.1. In Figure 1.14 we show the total concentration  $\phi_T = \phi_1 + \phi_2$ . Figure 1.15 displays the evolution of the velocity of the mixture. In Figure 1.15 (a) (for  $t = 1$ s) two circulations can be observed, one at each side of the dam break. At the next instant we see how the velocity changes its direction in an oscillating manner. Finally, we remark that the velocity decreases in time; in Figure 1.15 (f) (corresponding to  $t = 50$ s) it is already small. The computational time to compute the solution for  $t = 500$ s was four days and six hours. However, these times do not worry because this code can easily be parallelized to attain shorter CPU times.

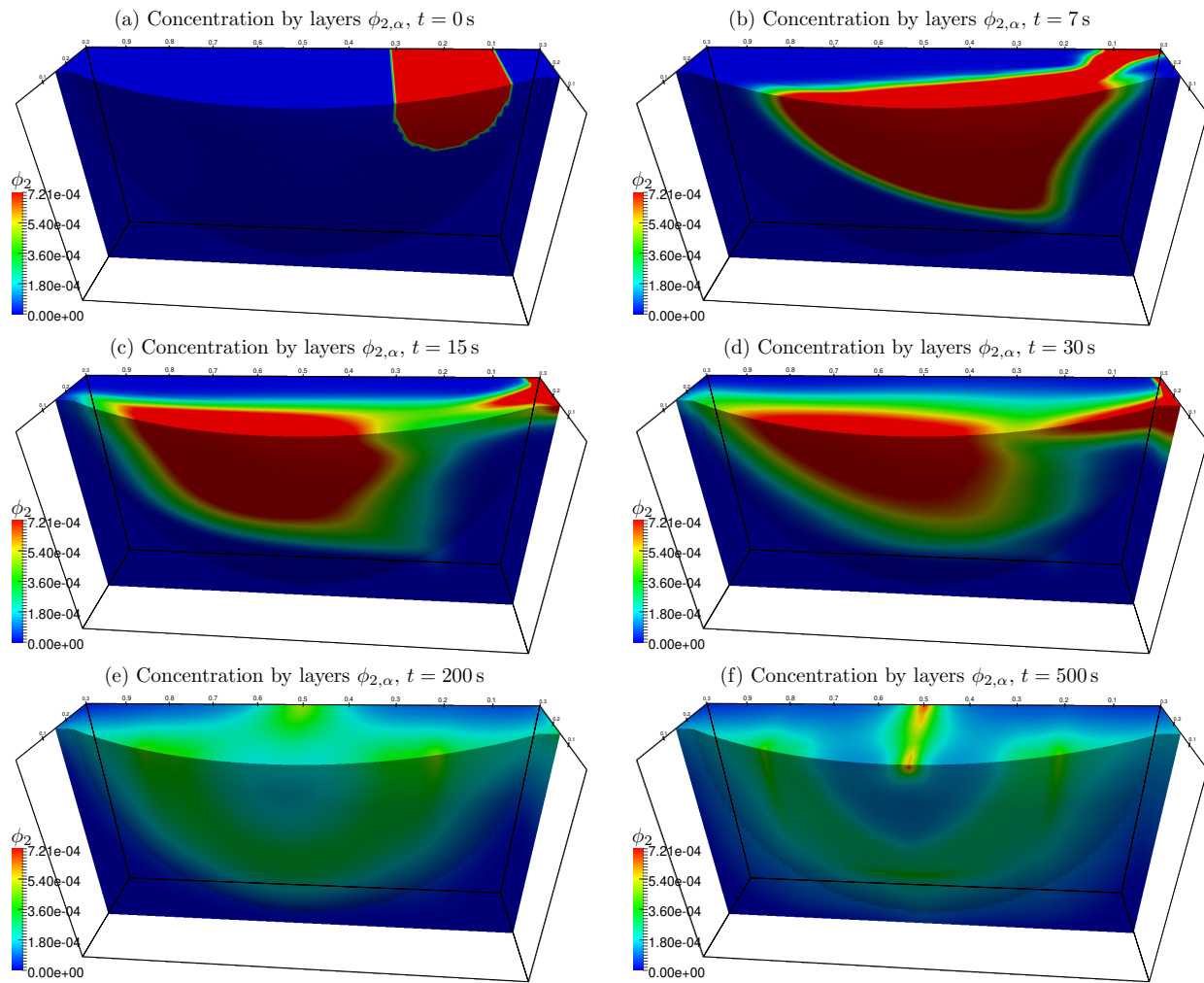


Figure 1.13: Test 1.4: Concentration of  $\phi_2$  by color in a 3D domain,  $\eta(\mathbf{x}) = z_B(\mathbf{x}) + h(\mathbf{x})$  m.

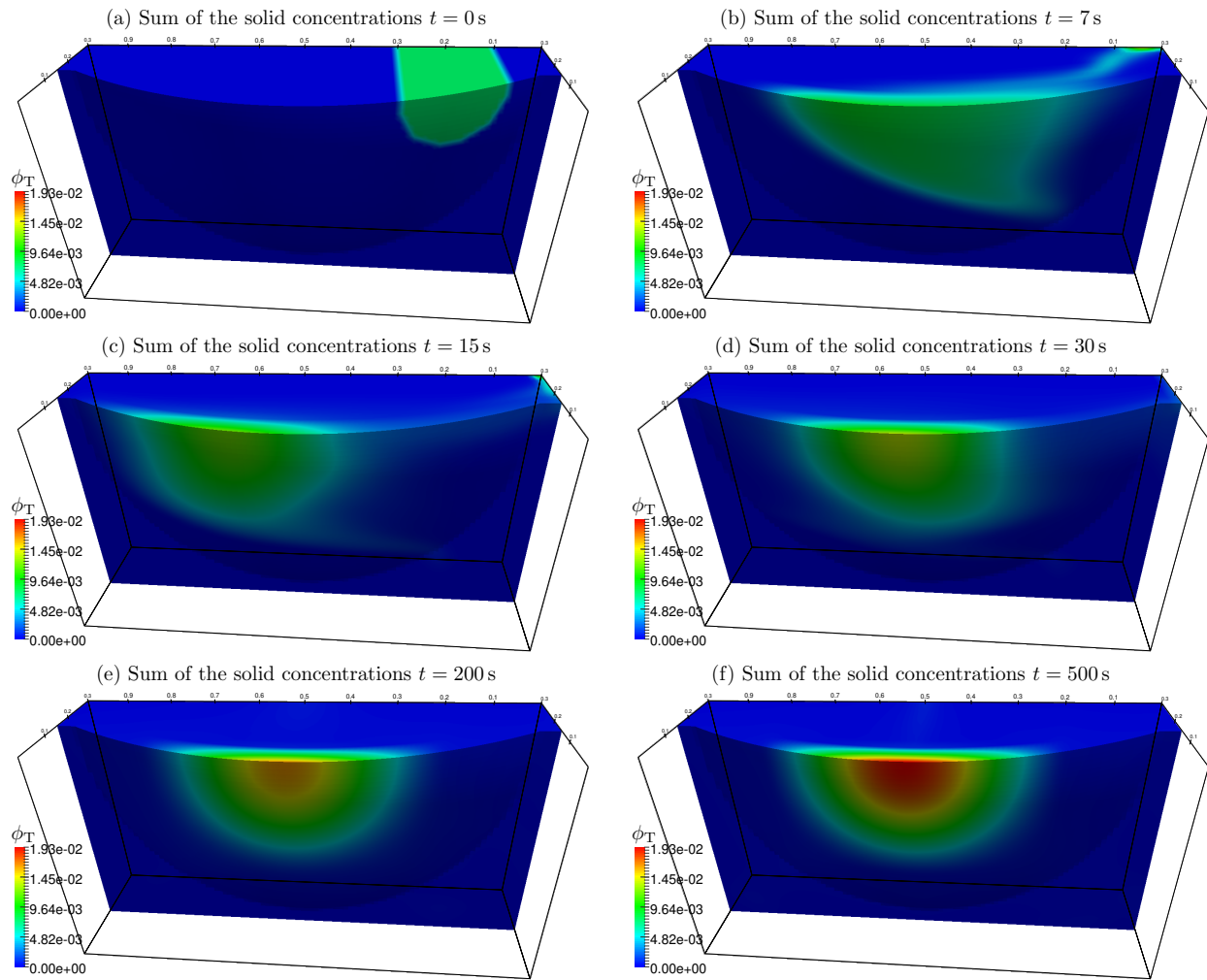


Figure 1.14: Test 1.4: Concentration by color by  $\phi_T = \phi_1 + \phi_2$ ,  $\eta(\mathbf{x}) = z_B(\mathbf{x}) + h(\mathbf{x})$  m.

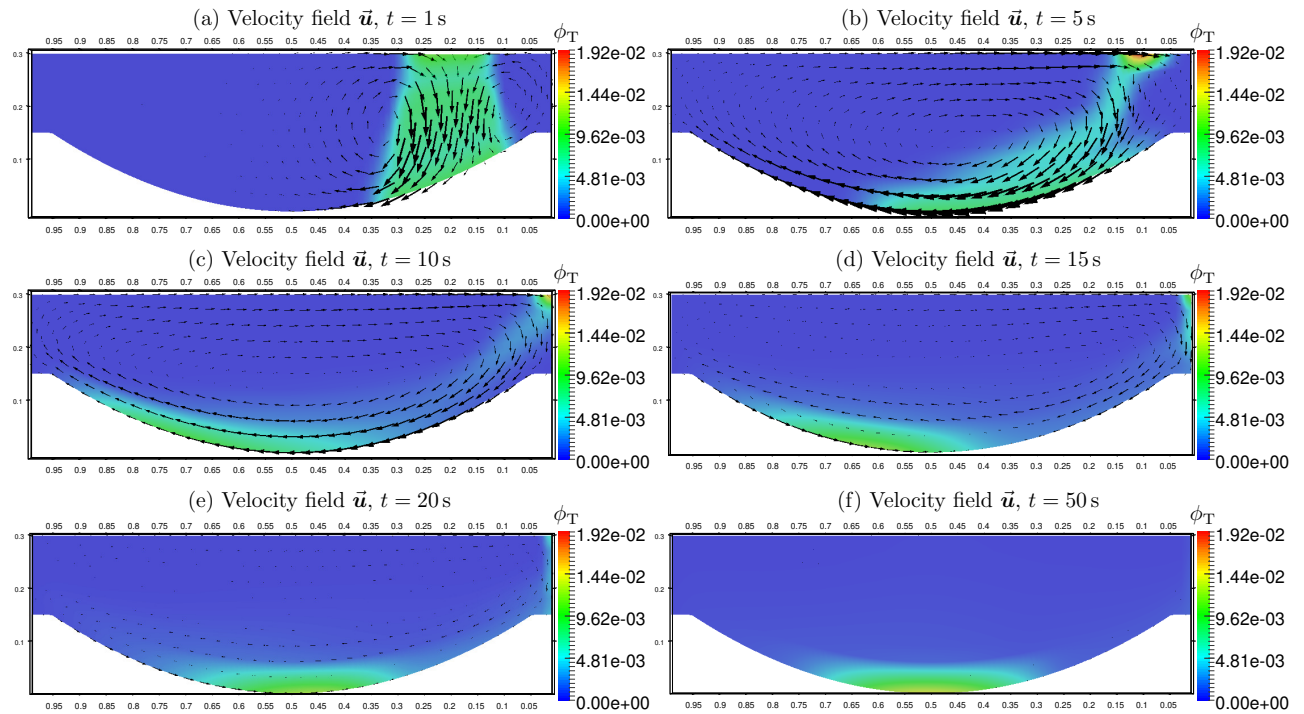


Figure 1.15: Test 1.4: Concentration by color by  $\phi_T = \phi_1 + \phi_2$ ,  $\eta(\mathbf{x}) = z_B(\mathbf{x}) + h(\mathbf{x})$  m.

# CHAPTER 2

---

## A multilayer shallow water model for polydisperse sedimentation with sediment compressibility and mixture viscosity

---

### 2.1 Introduction

The purpose of **Chapter 2** is to present a three-dimensional shallow water model to study polydisperse sedimentation and sediment transport in a viscous fluid, considering sediment compressibility and mixture viscosity effects. The fluid, as in **Chapter 1** is assumed to be loaded with finely dispersed solid particles that belong to a finite number of species ( $N$ ) that differ in density and size. The  $j$  densities  $\rho_j$  present in the model are constant in space and time, but the total density of the mixture is space-time dependent, so the polydisperse sedimentation process is modeled as a compressible mixture.

The formulation of the model allows one to recover the global mass and linear momentum balance laws of the mixture and incorporates sediment compressibility and mixture viscosity phenomena through the effective solid stress tensor  $\sigma_e(\phi)$  and the viscous stress tensor  $\mathbf{T}^E(\mathbf{v})$  respectively. Some definition for the effective solid stress tensor and some parameters in this definition for real materials can be found in the literature. The effective solid stress tensor must satisfy (2.2.5), in other words this is activated when the total concentration  $\phi$  is greater than of a fix gel point  $\phi_c$ , it is when  $\phi > \phi_c$ .

To solve some difficulties that arise after considering sediment compressibility and mixture viscosity here we make a dimensional analysis applied to the global mass conservation and linear momentum balance equations, and using the shallow domain hypothesis we can conclude that the horizontal components of the compression term and the horizontal terms of the viscous stress tensor can be neglected. This results in a final model that is vertically consistent with the classical one-dimensional vertical model.

As in **Chapter 1**, in this Chapter we develop a multilayer shallow water model for three-dimensional polydisperse sedimentation process, and in contrast to previous **Chapter 1**, sediment compressibility and mixture viscosity are taken into account satisfying global mass and linear momentum balance laws of the mixture, which means that the mixture description is consistent with a single-phase flow model.

The multilayer model can be stated as a system of balance laws of the type

$$\mathcal{C}(\partial_t \hat{\mathbf{W}} + \nabla_{\mathbf{x}} \cdot \mathbf{F}(\hat{\mathbf{W}}) + \mathcal{P}(\hat{\mathbf{W}})) = \mathcal{C}(\mathcal{G}^+(\hat{\mathbf{W}}) - \mathcal{G}^-(\hat{\mathbf{W}})), \quad (2.1.1)$$

where  $t$  is time,  $\mathbf{x}$  are the horizontal space coordinates,  $\mathcal{C} \in \mathcal{M}_{(M(N+2)+1) \times M(N+3)}$  is a matrix,  $\hat{\mathbf{W}} = \hat{\mathbf{W}}(t, \mathbf{x})$  is the unknown vector of  $(N+3)M$  scalar unknown functions that represent the total mass of the mixture, the horizontal velocities component in each of the  $M$  layers, and the  $N$  solids concentrations in each of the  $M$  layers.  $\mathbf{F}(\hat{\mathbf{W}})$  is the flux vector function,  $\mathcal{P}(\hat{\mathbf{W}})$  contains pressure terms, and  $\mathcal{G}^\pm(\hat{\mathbf{W}})$  contains mass transfer terms at the interfaces. These functions are specified in Section 2.6 of this Chapter.

To design numerical scheme to solve the system (2.1.1), we use a rotational invariance property of the equations. Later, we show some numerical simulations to illustrate the coupled solids volume fraction and flow fields in various scenarios and the mixture behavior with sediment compressibility and mixture viscosity are activated.

## 2.2 Governing equations

### 2.2.1 Continuity equations and linear momentum balances

Let us consider  $N \in \mathbb{N}$  species of spherical solid particles dispersed in a viscous fluid. For each solid species  $j$ ,  $j = 1, \dots, N$ , we denote by  $\phi_j$ ,  $\rho_j$ , and  $d_j$  its volumetric concentration, density, and particle diameter, respectively. Furthermore, we denote by  $\mathbf{v}_j = (u_j, v_j, w_j)^T \in \mathbb{R}^3$  its phase velocity with the horizontal component  $(u_j, v_j) \in \mathbb{R}^2$  and vertical component  $w_j \in \mathbb{R}$ . The same notation is used for the fluid indexed by  $j = 0$ . The model is based on the continuity and linear momentum balance equations for the  $N$  solid species and the fluid. As in **Chapter 1**, for  $j = 0, \dots, N$  the continuity and linear momentum equations are given by

$$\begin{aligned}\partial_t(\rho_j \phi_j) + \nabla \cdot (\rho_j \phi_j \mathbf{v}_j) &= 0, \\ \partial_t(\rho_j \phi_j \mathbf{v}_j) + \nabla \cdot (\rho_j \phi_j \mathbf{v}_j \otimes \mathbf{v}_j) &= \nabla \cdot \mathbf{T}_j + \rho_j \phi_j \mathbf{b} + \mathbf{m}_j^f + \mathbf{m}_j^s, \quad j = 0, \dots, N,\end{aligned}\tag{2.2.1}$$

where  $\mathbf{T}_j$  denotes the stress tensor of particle species  $j$ ,  $j = 1, \dots, N$ ,  $\mathbf{T}_0$  that of the fluid,  $\mathbf{b}$  is the body force,  $\mathbf{m}_j^f$  and  $\mathbf{m}_{ji}^s$  are the interaction forces per unit volume between solid species  $j$  and the fluid and between the solid species  $j$  and  $i$ , respectively, and  $\mathbf{m}_j^s = \mathbf{m}_{j1}^s + \dots + \mathbf{m}_{jN}^s$  is the particle-particle interaction terms of species  $j$ . For the fluid we obtain  $\mathbf{m}_0^f = -\mathbf{m}_1^f - \dots - \mathbf{m}_N^f$  and  $\mathbf{m}_0^s = 0$ . For very low Reynolds numbers there is considerable experimental and theoretical justification [9] for neglecting the quantities  $\mathbf{m}_{ji}^s$ . Let  $\Phi := (\phi_0, \dots, \phi_N)^T$ . We define the density  $\rho = \rho(\Phi)$  of the mixture and its mass-average velocity  $\mathbf{v}$  by

$$\begin{aligned}\rho &:= \rho(\Phi) := \rho_0 \phi_0 + \rho_1 \phi_1 + \dots + \rho_N \phi_N, \\ \mathbf{v} &:= (u, v, w)^T := \frac{1}{\rho} \sum_{m=0}^N \rho_m \phi_m \mathbf{v}_m = \frac{1}{\rho} \left[ \left( \rho - \sum_{j=1}^N \rho_j \phi_j \right) \mathbf{v}_0 + \sum_{k=1}^N \rho_k \phi_k \mathbf{v}_k \right],\end{aligned}\tag{2.2.2}$$

The importance of defining the average velocity  $\mathbf{v}$  precisely as is done in (2.2.2) is that this formulation allows us to recover the global mass and linear momentum balance laws for the mixture. In fact, summing from  $j = 0$  to  $j = N$  the continuity and linear momentum balance equations (2.2.1) yields

$$\partial_t \rho + \nabla \cdot (\rho \mathbf{v}) = 0, \quad \partial_t(\rho \mathbf{v}) + \nabla \cdot (\rho \mathbf{v} \otimes \mathbf{v}) = \nabla \cdot \Sigma + \rho \mathbf{b},\tag{2.2.3}$$

where  $\rho$  and  $\mathbf{v}$  are given by (2.2.2) and setting  $\mathbf{T} := \mathbf{T}_0 + \mathbf{T}_1 + \dots + \mathbf{T}_N$  and defining the diffusion velocities  $\mathbf{u}_j^d := \mathbf{v}_j - \mathbf{v}$ , the stress tensor of the mixture

$$\boldsymbol{\Sigma} := \mathbf{T} - \sum_{j=0}^N \rho_j \phi_j \mathbf{u}_j^d \otimes \mathbf{u}_j^d$$

is obtained. The stress tensor of each solid phase can be written as

$$\mathbf{T}_j = -p_j \mathbf{I} + \mathbf{T}_j^E \quad \text{with} \quad p_j = (\phi_j/\phi)(\phi p + \sigma_e(\phi)), \quad j = 0, \dots, N, \quad (2.2.4)$$

where  $p_j$  is the pressure of phase  $j$ . For the stress tensor of the fluid we get  $p_0 = (1 - \phi)p$ . The total concentration of particles is  $\phi = \phi_1 + \dots + \phi_N$  and  $\mathbf{T}_0^E$  and  $\mathbf{T}_j^E$  are viscous stress tensors of the fluid and solid phases, respectively. The effective solid stress  $\sigma_e(\phi)$  can be defined by

$$\sigma_e(\phi) = \begin{cases} 0 & \text{for } \phi \leq \phi_c, \\ \sigma_0 ((\phi/\phi_c)^k - 1) & \text{for } \phi > \phi_c, \end{cases} \quad \sigma'_e(\phi) = \begin{cases} 0 & \text{for } \phi \leq \phi_c, \\ (\sigma_0/\phi_c^k) k \phi^{k-1} & \text{for } \phi > \phi_c \end{cases} \quad (2.2.5)$$

with parameters  $\sigma_0 > 0$  and  $k \geq 1$ , and where  $\phi_c$  denotes the so-called critical concentration or gel point. Values for real materials for these parameters can be found in the literature. The solid-fluid interaction force per unit volume is given by

$$\mathbf{m}_j^f = \alpha_j(\Phi) \mathbf{u}_j + p \nabla \phi_j, \quad j = 0, \dots, N, \quad (2.2.6)$$

where  $\alpha_j$  is the resistance coefficient for the transfer of momentum between the fluid and solid phase species  $j$  [9]. Finally here we assume that gravity is the only body force, i.e.,  $\mathbf{b} = g\mathbf{k}$ , where  $\mathbf{k}$  is the downward-pointing unit vector.

Defining the slip velocities  $\mathbf{u}_j := \mathbf{v}_j - \mathbf{v}_0$  (including  $\mathbf{u}_0 = \mathbf{0}$ ) and  $\lambda_j := \rho_j \phi_j / \rho$  for  $j = 1, \dots, N$ , we can derive for each solid species

$$\rho_j \phi_j \mathbf{v}_j = \rho_j \phi_j (\mathbf{u}_j + \mathbf{v} - (\lambda_1 \mathbf{u}_1 + \dots + \lambda_N \mathbf{u}_N)), \quad j = 0, \dots, N; \quad (2.2.7)$$

hence as in **Chapter 1** the mass and linear momentum equations for all phases are given by

$$\begin{aligned} \partial_t(\rho_j \phi_j) + \nabla \cdot (\rho_j \phi_j (\mathbf{u}_j + \mathbf{v} - (\lambda_1 \mathbf{u}_1 + \dots + \lambda_N \mathbf{u}_N))) &= 0, \quad j = 0, \dots, N, \\ \rho_j \phi_j D_t \mathbf{v}_j &= \nabla \cdot \mathbf{T}_j^E - \phi_j \nabla p - \rho_j \phi_j g \mathbf{k} + \alpha_j \mathbf{u}_j - \nabla \left( \frac{\phi_j}{\phi} \sigma_e(\phi) \right), \quad j = 1, \dots, N, \\ \rho_0 (1 - \phi) D_t \mathbf{v}_0 &= -(1 - \phi) \nabla p + \nabla \cdot \mathbf{T}_0^E + \rho_0 (1 - \phi) g \mathbf{k} - (\alpha_1 \mathbf{u}_1 + \dots + \alpha_N \mathbf{u}_N), \end{aligned} \quad (2.2.8)$$

where we have used the standard notation  $D_t \mathbf{v} = \partial_t \mathbf{v} + (\mathbf{v} \cdot \nabla) \mathbf{v}$ . The systems of equations (2.2.1) and (2.2.8) are equivalent and therefore both allow us to recover (2.2.3).

## 2.2.2 Explicit formula for the slip velocities with effective solid stress

The system (2.2.8) is closed by an explicit expression for the slip velocities  $\mathbf{u}_j$ . In [9] the explicit formula

$$\mathbf{u}_j = g \frac{\phi_j}{\alpha_j(\Phi)} \left( (\bar{\rho}_j - \bar{\rho}^T \Phi) \mathbf{k} + \frac{\sigma_e(\phi)}{g \phi_j} \nabla \left( \frac{\phi_j}{\phi} \right) + \frac{1 - \phi}{g \phi} \nabla \sigma_e(\phi) \right), \quad j = 1, \dots, N. \quad (2.2.9)$$

for these relative velocities was derived, where  $\bar{\rho}_j := \rho_j - \rho_0$  for  $j = 1, \dots, N$  are reduced densities and  $\bar{\boldsymbol{\rho}} := (\bar{\rho}_1, \dots, \bar{\rho}_N)^T$ . In **Chapter 1** we only considered the case when  $\sigma_e \equiv 0$ , that is, sediment compressibility was not taken into account. In other words, the slip velocities used in **Chapter 1** are the simplest possible, namely

$$\mathbf{u}_j = g \frac{\phi_j}{\alpha_j(\Phi)} (\bar{\rho}_j - \bar{\boldsymbol{\rho}}^T \Phi) \mathbf{k}, \quad j = 1, \dots, N.$$

Following [9, 20, 46, 48] we choose  $\phi_j/\alpha_j(\Phi) = -d_j^2 V(\phi)/18\mu_0$ , where  $\mu_0$  is the viscosity of the pure fluid, and  $V(\phi)$  is a hindrance factor that is assumed to satisfy  $V(\phi) > 0$  and  $V'(\phi) < 0$  for  $0 < \phi < \phi_{\max}$ . This factor can be chosen as the Richardson-Zaki [56] function

$$V(\phi) = \begin{cases} (1 - \phi)^{n_{RZ}-2} & \text{for } \phi \leq \phi_{\max}, \\ 0 & \text{for } \phi > \phi_{\max}, \end{cases} \quad n_{RZ} > 2. \quad (2.2.10)$$

Setting  $\mu := -gd_1^2/(18\mu_0)$  and  $\delta_j := d_j^2/d_1^2$ ,  $j = 1, \dots, N$ , we obtain the final form of the slip velocities

$$\mathbf{u}_j = \mu \delta_j V(\phi) \left( (\bar{\rho}_j - \bar{\boldsymbol{\rho}}^T \Phi) \mathbf{k} + \frac{\sigma_e(\phi)}{g \phi_j} \nabla \left( \frac{\phi_j}{\phi} \right) + \frac{1 - \phi}{g \phi} \nabla \sigma_e(\phi) \right), \quad j = 1, \dots, N. \quad (2.2.11)$$

Inserting (2.2.11) into (2.2.7) and denoting  $\Phi := (\phi_1, \dots, \phi_N)^T$  and let  $\boldsymbol{\delta} := (\delta_1, \dots, \delta_N)^T$ ,  $\boldsymbol{\lambda} := (\lambda_1, \dots, \lambda_N)^T$  we get that for each solid species

$$\rho_j \phi_j \mathbf{v}_j = \rho_j f_j^M(\Phi) \mathbf{k} + \rho_j \phi_j \mathbf{v} - \mathbf{a}_j(\Phi, \nabla \Phi), \quad (2.2.12)$$

where we define for  $j = 1, \dots, N$

$$\begin{aligned} f_j^M(\Phi) &:= \phi_j v_j^{\text{MLB}} = \phi_j \mu V(\phi) \left( \delta_j (\bar{\rho}_j - \bar{\boldsymbol{\rho}}^T \Phi) - \sum_{k=1}^N \lambda_k \delta_k (\bar{\rho}_k - \bar{\boldsymbol{\rho}}^T \Phi) \right), \\ \mathbf{a}_j(\Phi, \nabla \Phi) &:= -\frac{\mu}{g} \rho_j V(\phi) \left\{ \frac{(1 - \phi) \phi_j}{\phi} (\delta_j - \boldsymbol{\delta}^T \boldsymbol{\lambda}) \nabla \sigma_e(\phi) + \sigma_e(\phi) \left[ \delta_j \nabla \left( \frac{\phi_j}{\phi} \right) - \phi_j \sum_{i=1}^N \frac{\lambda_i \delta_i}{\phi_i} \nabla \left( \frac{\phi_i}{\phi} \right) \right] \right\}. \end{aligned}$$

Consistently with the global mass conservation (2.2.1), we define  $f_0^M := -(\rho_1 f_1^M + \dots + \rho_N f_N^M)/\rho_0$  and  $\mathbf{a}_0 := -(\mathbf{a}_1 + \dots + \mathbf{a}_N)$ .

Note that the velocity of each phase is much more complicated than in the framework of **Chapter 1**. This new approach poses extreme difficulties for the attempt to solve (2.2.1). Without going into detail, we do no longer have the property that the horizontal velocity of each species equals that of the mixture. This difficulty will be handled in Section 2.3.

**Remark 2.2.1.** *If  $\phi \leq \phi_c$ , then the horizontal velocity of each species equals that of the mixture and only the vertical velocity of each species differs from that of the mixture, as can be inferred from*

$$\rho_j \phi_j w_j = \rho_j \phi_j w + \rho_j f_j^M(\Phi).$$

### 2.2.3 Final form of the model equations

The final model is given by the mass and linear momentum balance equations for each species plus the fluid after substituting (2.2.9) into (2.2.8). It can be written as

$$\begin{aligned}\partial_t(\rho_j\phi_j) + \nabla \cdot (\rho_j\phi_j\mathbf{v} + \rho_jf_j^M(\Phi)\mathbf{k}) &= \nabla \cdot \mathbf{a}_j(\Phi, \nabla\Phi), \quad j = 0, \dots, N, \\ \rho_j\phi_j D_t \mathbf{v}_j &= \nabla \cdot \mathbf{T}_j^E - \phi_j \nabla p - \phi_j \rho g \mathbf{k} - \phi_j \nabla \sigma_e(\phi), \quad j = 0, \dots, N.\end{aligned}\quad (2.2.13)$$

Summing up from  $j = 0$  to  $j = N$  the linear momentum balance equations (2.2.8) yields

$$\partial_t \left( \sum_{j=0}^N \rho_j \phi_j \mathbf{v}_j \right) + \nabla \cdot \left( \sum_{j=0}^N \rho_j \phi_j \mathbf{v}_j \otimes \mathbf{v}_j \right) = \nabla \cdot \mathbf{T} - \rho g \mathbf{k}, \quad (2.2.14)$$

where  $\mathbf{T} = \sum_{j=0}^N \mathbf{T}_j = -(p + \sigma_e(\phi))\mathbf{I} + \mathbf{T}^E$ , where  $p$  is pressure and the extra stress tensor  $\mathbf{T}^E$  is given by  $\mathbf{T}^E = \frac{\eta}{2}\mathbf{D}(\mathbf{v}) + \lambda \nabla \cdot (\mathbf{v})\mathbf{I}$ , where  $\eta, \lambda \geq 0$  are viscosity terms. The strain rate  $\mathbf{D}(\mathbf{v})$  tensor is given by  $\mathbf{D}(\mathbf{v}) = \nabla \mathbf{v} + (\nabla \mathbf{v})^T$ .

## 2.3 Dimensional analysis

By a dimensional analysis we now show that only terms in the vertical direction of the extra stress tensor are important. Others terms will be discarded under the assumptions of a shallow domain, that is, the characteristic height ( $H$ ) will be assumed smaller than the characteristic length ( $L$ ). In other words, we assume that  $\varepsilon := H/L$  is small.

We define the following dimensionless variables:  $(x, y, z) = (L\tilde{x}, L\tilde{y}, H\tilde{z})$  for spatial position and  $t = (L/U)\tilde{t}$  for the characteristic time. The relation between the spatial gradient  $\nabla$  and the dimensionless gradient  $\tilde{\nabla}$  is defined by  $\nabla = (1/L)\mathbf{I}_\varepsilon \tilde{\nabla}$ , where  $\mathbf{I}_\varepsilon := \text{diag}(1, 1, 1/\varepsilon)$ . The dimensionless time derivative is  $\partial/\partial t = (U/L)\partial/\partial \tilde{t}$ . We use in some cases the following definitions for the velocity vector to simplify notation:  $\mathbf{v}_\varepsilon := (\tilde{u}, \tilde{v}, \varepsilon \tilde{w})$ ,  $\mathbf{v}_{\varepsilon,j} := (\tilde{u}_j, \tilde{v}_j, \varepsilon \tilde{w}_j)$ ,  $\tilde{\mathbf{v}} := (\tilde{u}, \tilde{v}, \tilde{w})$ , and  $\tilde{\mathbf{v}}_j = (\tilde{u}_j, \tilde{v}_j, \tilde{w}_j)$ . Furthermore, for height, densities, pressure, and viscosities we have  $h = H\tilde{h}$ ,  $\rho_j = \bar{\rho}_0 \tilde{\rho}_j$ ,  $P = \bar{\rho}_0 U^2 \tilde{P}$ ,  $\sigma_e = \bar{\rho}_0 U^2 \tilde{\sigma}_e$ ,  $\eta = \bar{\rho}_0 U H \tilde{\eta}$ ,  $\lambda = \bar{\rho}_0 U H \tilde{\lambda}$ ,  $\mu_0 = \bar{\rho}_0 U H \tilde{\mu}_0$ ,  $d_1 = H\tilde{d}_1$ , and  $\mu/g = H\tilde{d}_1/(18\bar{\rho}_0 U \tilde{\mu}_0)$ . From here so on dimensionless variables will be denoted with the tilde symbol ( $\tilde{\cdot}$ ). In light of  $\mathbf{v}_j = (u_j, v_j, w_j) = U\mathbf{v}_{\varepsilon,j}$ , the mass average velocity  $\mathbf{v}$  of the mixture satisfies

$$\mathbf{v} = \sum_{j=0}^N \frac{\rho_j \phi_j}{\rho} (u_j, v_j, w_j) = U \sum_{j=0}^N \frac{\tilde{\rho}_j \phi_j}{\tilde{\rho}} (\tilde{u}_j, \tilde{v}_j, \varepsilon \tilde{w}_j) = U \sum_{j=0}^N \frac{\tilde{\rho}_j \phi_j}{\tilde{\rho}} \mathbf{v}_{\varepsilon,j} = U \mathbf{v}_\varepsilon,$$

Furthermore, the equalities  $\rho_j \phi_j \mathbf{v}_j = \bar{\rho}_0 U \tilde{\rho}_j \phi_j \mathbf{v}_{\varepsilon,j}$  and

$$\rho_j f_j^M(\Phi) \mathbf{k} + \rho_j \phi_j \mathbf{v} - \mathbf{a}_j(\Phi, \nabla\Phi) = \bar{\rho}_0 U (\tilde{\rho}_j \tilde{f}_j^M(\Phi) \mathbf{k} + \tilde{\rho}_j \phi_j \mathbf{v}_\varepsilon - \varepsilon \mathbf{I}_\varepsilon \tilde{\mathbf{a}}_j(\Phi, \nabla\Phi))$$

imply that

$$\bar{\rho}_0 U \tilde{\rho}_j \phi_j \mathbf{v}_{\varepsilon,j} = \bar{\rho}_0 U (\tilde{\rho}_j \tilde{f}_j^M(\Phi) \mathbf{k} + \tilde{\rho}_j \phi_j \mathbf{v}_\varepsilon - \varepsilon \mathbf{I}_\varepsilon \tilde{\mathbf{a}}_j(\Phi, \nabla\Phi)). \quad (2.3.1)$$

In light of the previous equalities, the mass balance of each solid species (2.2.13) can be written as

$$\frac{\bar{\rho}_0 U}{L} \partial_{\tilde{t}} (\tilde{\rho}_j \phi_j) + \frac{\bar{\rho}_0 U}{L} \tilde{\nabla} \cdot (\mathbf{I}_\varepsilon (\tilde{\rho}_j \phi_j \mathbf{v}_\varepsilon + \tilde{\rho}_j \tilde{f}_j^M(\Phi) \mathbf{k})) = \frac{\bar{\rho}_0 U}{L} \tilde{\nabla} \cdot (\varepsilon \mathbf{I}_\varepsilon^2 \tilde{\mathbf{a}}_j), \quad (2.3.2)$$

then we get the dimensionless partial differential equation for the mass balance of each species

$$\partial_{\tilde{t}} (\tilde{\rho}_j \phi_j) + \tilde{\nabla} \cdot \left( \tilde{\rho}_j \phi_j \tilde{\mathbf{v}} + \frac{1}{\varepsilon} \tilde{\rho}_j \tilde{f}_j^M(\Phi) \mathbf{k} \right) = \tilde{\nabla} \cdot (\varepsilon \mathbf{I}_\varepsilon^2 \tilde{\mathbf{a}}_j), \quad (2.3.3)$$

or equivalently, applying the matrix  $\mathbf{I}_\varepsilon$  to equality (2.3.1),

$$\partial_{\tilde{t}} (\tilde{\rho}_j \phi_j) + \tilde{\nabla} \cdot (\tilde{\rho}_j \phi_j \tilde{\mathbf{v}}_j) = 0. \quad (2.3.4)$$

Furthermore, we define the dimensionless horizontal component of the strain-rate

$$\mathbf{D}_{\varepsilon,h}(\tilde{\mathbf{v}}) := \tilde{\nabla}_{\tilde{\mathbf{x}}} \tilde{\mathbf{v}}_h + (\tilde{\nabla}_{\tilde{\mathbf{x}}} \tilde{\mathbf{v}}_h)^T,$$

notice that  $\rho_j \phi_j \mathbf{v}_j \otimes \mathbf{v}_j = \bar{\rho}_0 U^2 \tilde{\rho}_j \phi_j \mathbf{v}_{\varepsilon,j} \otimes \mathbf{v}_{\varepsilon,j}$ , and rewrite the total pressure  $p_{\text{tot}} := p + \sigma_e(\phi)$  as  $p_{\text{tot}} = \bar{\rho}_0 U^2 (\tilde{p} + \tilde{\sigma}_e(\phi)) =: \bar{\rho}_0 U^2 \tilde{p}_{\text{tot}}$  and  $\rho g \mathbf{k} = \bar{\rho}_0 U^2 \tilde{\rho}/(\varepsilon \text{Fr}^2 L) \mathbf{k}$ , where the Froude number is given by  $\text{Fr} = U/\sqrt{gH}$ , so we get

$$\begin{aligned} & \frac{\bar{\rho}_0 U^2}{L} \partial_{\tilde{t}} \left( \sum_{j=0}^N \tilde{\rho}_j \phi_j \mathbf{v}_{\varepsilon,j} \right) + \frac{\bar{\rho}_0 U^2}{L} \tilde{\nabla} \cdot \left( \sum_{j=0}^N \tilde{\rho}_j \phi_j \mathbf{v}_{\varepsilon,j} \otimes (\mathbf{I}_\varepsilon \mathbf{v}_{\varepsilon,j}) \right) \\ &= \frac{\bar{\rho}_0 U^2}{L} \tilde{\nabla} \cdot (\tilde{p}_{\text{tot}} \mathbf{I} + \tilde{\mathbf{T}}_\varepsilon^E(\tilde{\mathbf{v}})) \mathbf{I}_\varepsilon - \frac{\bar{\rho}_0 U^2 \tilde{\rho}}{L \text{Fr}^2 \varepsilon} \mathbf{k}, \end{aligned} \quad (2.3.5)$$

where  $\tilde{\mathbf{T}}_\varepsilon^E$  is a dimensionless viscous stress tensor. Finally setting  $\tilde{\mathbf{I}} = \varepsilon \mathbf{I}_\varepsilon$ , we may rewrite the dimensionless linear momentum balance equation (2.3.5) as

$$\partial_{\tilde{t}} \left( \sum_{j=0}^N \tilde{\rho}_j \phi_j \mathbf{v}_{\varepsilon,j} \right) + \tilde{\nabla} \cdot \left( \sum_{j=0}^N \tilde{\rho}_j \phi_j \mathbf{v}_{\varepsilon,j} \otimes \mathbf{v}_j \right) = \frac{1}{\varepsilon} \tilde{\nabla} \cdot (\Sigma \tilde{\mathbf{I}}) - \frac{1}{\varepsilon} \frac{\tilde{\rho}}{\text{Fr}^2} \mathbf{k}, \quad (2.3.6)$$

where the dimensionless stress tensor is  $\Sigma := \tilde{p}_{\text{tot}} \mathbf{I} + \tilde{\mathbf{T}}_\varepsilon^E(\tilde{\mathbf{v}})$  with the dimensionless viscous stress tensor

$$\tilde{\mathbf{T}}_\varepsilon^E(\tilde{\mathbf{v}}) = \frac{\tilde{\eta}}{2} \mathbf{D}_\varepsilon(\tilde{\mathbf{v}}) + 2\varepsilon \tilde{\lambda} (\tilde{\nabla} \cdot \tilde{\mathbf{v}}) \mathbf{I},$$

where

$$\mathbf{D}_\varepsilon(\tilde{\mathbf{v}}) := \begin{bmatrix} \varepsilon \mathbf{D}_{\varepsilon,h}(\tilde{\mathbf{v}}) & \partial_{\tilde{z}} \tilde{\mathbf{v}}_h + \varepsilon^2 (\tilde{\nabla}_x \tilde{w})^T \\ (\partial_{\tilde{z}} \tilde{\mathbf{v}}_h)^T + \varepsilon^2 \tilde{\nabla}_x \tilde{w} & 2\varepsilon \partial_{\tilde{z}} \tilde{w} \end{bmatrix}. \quad (2.3.7)$$

Note that (2.3.2) and (2.3.5) allow us to easily change to the original variables. To finish this section, from here so on, the symbol tilde ( $\tilde{\cdot}$ ) will be neglected to simplify notation. Thus, the final model in dimensionless variables is given by the dimensionless mass balance equations (2.3.4) of each solid species and by the dimensionless momentum balance equation of the mixture (2.3.6)

$$\partial_t (\rho_j \phi_j) + \nabla \cdot (\rho_j \phi_j \mathbf{v}_j) = 0, \quad j = 0, \dots, N, \quad (2.3.8)$$

where

$$\rho_j \phi_j \mathbf{v}_j = \rho_j \phi_j \mathbf{v} + \frac{1}{\varepsilon} \rho_j f_j^M(\Phi) \mathbf{k} - \varepsilon \mathbf{I}_\varepsilon^2 \mathbf{a}_j, \quad (2.3.9)$$

and dimensionless momentum balance equation of the mixture

$$\partial_t \left( \sum_{j=0}^N \rho_j \phi_j \mathbf{v}_{\varepsilon,j} \right) + \nabla \cdot \left( \sum_{j=0}^N \rho_j \phi_j \mathbf{v}_{\varepsilon,j} \otimes \mathbf{v}_j \right) = \frac{1}{\varepsilon} \nabla \cdot (\Sigma \tilde{\mathbf{I}}) - \frac{1}{\varepsilon} \frac{\rho}{\text{Fr}^2} \mathbf{k}. \quad (2.3.10)$$

## 2.4 A multilayer approach

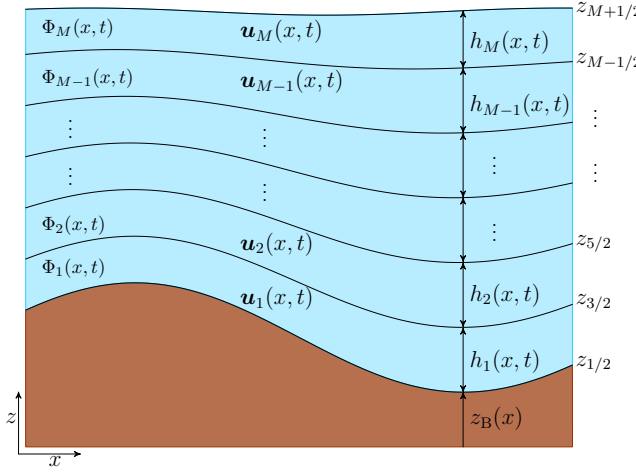


Figure 2.1: Sketch of the multilayer approach

### 2.4.1 Weak solution with discontinuities

Let us recall the conditions to be satisfied by a piecewise smooth weak solution  $(\mathbf{v}_0, \dots, \mathbf{v}_N, \phi_0, \dots, \phi_N, p_{\text{tot}})$  of (2.3.8)–(2.3.10), where  $\mathbf{v}_j$  is defined by (2.3.9).

**Definition 2.4.1.** Assume that the velocities  $\mathbf{v}_0, \dots, \mathbf{v}_N$ , the pressure  $p_{\text{tot}}$  and the volume fractions  $\phi_0, \dots, \phi_N$  are smooth in each  $\Omega_\alpha(t)$ , but possibly discontinuous across the predetermined hypersurfaces  $\Gamma_{\alpha+1/2}(t)$  for  $\alpha = 1, \dots, M - 1$ . Then

$$\mathbf{y} := (\mathbf{v}_0, \dots, \mathbf{v}_N, \phi_0, \dots, \phi_N, p_{\text{tot}}) : \Omega_T \ni (t, \mathbf{x}, z) \mapsto \mathbf{y}(t, \mathbf{x}, z) \in \mathbb{R}^{3(N+1)} \times \mathbb{R}^{N+1} \times \mathbb{R}$$

is a weak solution of (2.3.8)–(2.3.10) if the following conditions hold:

- (i) The function  $\mathbf{y}$  is a standard weak solution of (2.3.8)–(2.3.10) in each layer  $\Omega_\alpha(t)$ ,  $\alpha = 1, \dots, M$ .
- (ii) For each  $\alpha = 1, \dots, M - 1$  and  $t \in (0, T]$ , the following normal flux jump conditions across the interface  $\Gamma_{\alpha+1/2}(t)$  are satisfied: for the conservation of mass equations,

$$[(\rho_j \phi_j; \rho_j \phi_j \mathbf{v}_j)]_{t, \alpha+1/2} \cdot \boldsymbol{\eta}_{t, \alpha+1/2} = 0 \quad \text{for all } j = 1, \dots, N, \quad (2.4.1)$$

and for the momentum conservation law corresponding to equation (2.3.10),

$$\left[ \left( \sum_{j=0}^N \rho_j \phi_j \mathbf{v}_{\varepsilon, j}; \sum_{j=0}^N \rho_j \phi_j \mathbf{v}_{\varepsilon, j} \otimes \mathbf{v}_j - \frac{1}{\varepsilon} \boldsymbol{\Sigma} \tilde{\mathbf{I}} \right) \right]_{t, \alpha+1/2} \boldsymbol{\eta}_{t, \alpha+1/2} = 0, \quad (2.4.2)$$

where

$$\boldsymbol{\Sigma} = -p_{\text{tot}} \mathbf{I} + \mathbf{T}_\varepsilon^E \quad (2.4.3)$$

is the stress tensor of the mixture and  $\mathbf{v}_{\varepsilon, j} = \mathbf{I}_\varepsilon^{-1} \mathbf{v}_j$ .

There are some different ways to introduce a multilayer model. In [39] for example, the authors integrate the mass and linear momentum equations inside each layer to define the multilayer model, while in **Chapter 1** the multilayer approach is deduced as a particular weak solution of a variational formulation. For  $\alpha = 1, \dots, M$  and  $j = 0, \dots, N$  we set  $\mathbf{v}_j|_{\Omega_\alpha(t)} := \mathbf{v}_{j,\alpha} := (\mathbf{u}_{j,\alpha}, w_{j,\alpha})^T$  where  $\mathbf{u}_{j,\alpha}$ ,  $w_{j,\alpha}$  are horizontal and vertical velocities respectively,  $\phi_{j,\alpha} := \phi_j|_{\Omega_\alpha(t)}$ , volumetric concentration of the species  $j$  on layer  $\alpha$ . For  $\alpha = 1, \dots, M$ , the pressure  $p_{\text{tot},\alpha} := p_{\text{tot}}|_{\Omega_\alpha(t)}$  and the mixture velocity of each layer by

$$\mathbf{v}_\alpha = \frac{1}{\rho} \sum_{j=0}^N \rho_j \phi_{j,\alpha} \mathbf{v}_{j,\alpha} = (\mathbf{u}_\alpha, w_\alpha), \quad \alpha = 1, \dots, M.$$

In both cases we need to assume that the layer thicknesses are small enough to neglect the dependence of the horizontal velocities and the concentration of each species on the vertical variable inside each layer. This means that

$$\partial_z \mathbf{u}_{j,\alpha} = 0, \quad \partial_z \phi_{j,\alpha} = 0. \quad (2.4.4)$$

Under this assumption the vertical velocity and the (hydrostatic) pressure are piecewise linear in  $z$ , i.e.,

$$\partial_z w_{j,\alpha} = d_{j,\alpha}(t, \mathbf{x}), \quad \partial_z p_{\text{tot},\alpha}(t, \mathbf{x}) = g_\alpha(t, \mathbf{x}) \quad (2.4.5)$$

for some smooth functions  $d_{j,\alpha}(t, \mathbf{x})$ , and  $g_\alpha(t, \mathbf{x})$ . In the following section we will also use the notation  $\Phi_\alpha := (\phi_{0,\alpha}, \phi_{1,\alpha}, \dots, \phi_{N,\alpha})^T$  and  $\bar{\rho}_\alpha := \rho_0 \phi_{0,\alpha} + \rho_1 \phi_{1,\alpha} + \dots + \rho_N \phi_{N,\alpha}$ .

## 2.4.2 Mass and momentum conservation jump conditions

In what follows we analyze the jump conditions (2.4.1) and (2.4.2), where (2.4.4) implies

$$\mathbf{u}_{j,\alpha-1/2}^+(t, \mathbf{x}) = \mathbf{u}_{j,\alpha+1/2}^-(t, \mathbf{x}) = \mathbf{u}_{j,\alpha}(t, \mathbf{x}) \quad \text{and} \quad \phi_{j,\alpha-1/2}^+(t, \mathbf{x}) = \phi_{j,\alpha+1/2}^-(t, \mathbf{x}) = \phi_{j,\alpha}(t, \mathbf{x}). \quad (2.4.6)$$

We define for the lateral limits of the normal mass flux for species  $j$  at the interface  $\Gamma_{\alpha+1/2}(t)$  by

$$\begin{aligned} G_{j,\alpha+1/2}^+ &:= \rho_j \phi_{j,\alpha+1} (\partial_t z_{\alpha+1/2} + \mathbf{u}_{j,\alpha+1/2}^+ \cdot \nabla_{\mathbf{x}} z_{\alpha+1/2} - w_{j,\alpha+1/2}^+), \\ G_{j,\alpha+1/2}^- &:= \rho_j \phi_{j,\alpha} (\partial_t z_{\alpha+1/2} + \mathbf{u}_{j,\alpha+1/2}^- \cdot \nabla_{\mathbf{x}} z_{\alpha+1/2} - w_{j,\alpha+1/2}^-), \quad j = 0, 1, \dots, N. \end{aligned} \quad (2.4.7)$$

The mass conservation jump conditions (2.4.1) are then satisfied provided that

$$G_{j,\alpha+1/2} := G_{j,\alpha+1/2}^- = G_{j,\alpha+1/2}^+, \quad j = 0, 1, \dots, N, \quad (2.4.8)$$

where  $G_{j,\alpha+1/2}$  represents the normal mass flux for species  $j$  at  $\Gamma_{\alpha+1/2}(t)$ . Taking into account (2.4.6), we obtain the structure of the horizontal and vertical velocities

$$\mathbf{u}_{j,\alpha+1/2}^+ = \mathbf{u}_{\alpha+1} - \varepsilon \frac{\mathbf{a}_{\text{h},j,\alpha+1/2}^+}{\rho_j \phi_{j,\alpha+1}}, \quad \mathbf{u}_{j,\alpha+1/2}^- = \mathbf{u}_\alpha - \varepsilon \frac{\mathbf{a}_{\text{h},j,\alpha+1/2}^-}{\rho_j \phi_{j,\alpha}}, \quad (2.4.9)$$

$$w_{j,\alpha+1/2}^\pm = w_{\alpha+1/2}^\pm + \frac{\rho_j f_{j,\alpha+1/2}^\pm - a_{3,j,\alpha+1/2}^\pm}{\varepsilon \rho_j \phi_{j,\alpha+1/2}^\pm}, \quad (2.4.10)$$

where  $f_{j,\alpha+1/2}^\pm$  and  $\varepsilon \mathbf{I}_\varepsilon^2 \mathbf{a}_{j,\alpha+1/2}^\pm$  must satisfy the respective condition

$$\sum_{j=0}^N \rho_j f_{j,\alpha+1/2}^\pm = 0, \quad \sum_{j=0}^N \varepsilon \mathbf{I}_\varepsilon^2 \mathbf{a}_{j,\alpha+1/2}^\pm = \mathbf{0}.$$

We can then compute the total normal mass flux across  $\Gamma_{\alpha+1/2}(t)$  as  $G_{\alpha+1/2} := \sum_{j=0}^N G_{j,\alpha+1/2}$ , and by (2.4.7) and (2.4.8) we get the jump condition

$$G_{\alpha+1/2} = G_{\alpha+1/2}^- = G_{\alpha+1/2}^+, \quad (2.4.11)$$

for the first equation from (2.2.3), where

$$\begin{aligned} G_{\alpha+1/2}^+ &:= \bar{\rho}_{\alpha+1} (\partial_t z_{\alpha+1/2} + \mathbf{u}_{\alpha+1} \cdot \nabla_{\mathbf{x}} z_{\alpha+1/2} - w_{\alpha+1/2}^+), \\ G_{\alpha+1/2}^- &:= \bar{\rho}_\alpha (\partial_t z_{\alpha+1/2} + \mathbf{u}_\alpha \cdot \nabla_{\mathbf{x}} z_{\alpha+1/2} - w_{\alpha+1/2}^-). \end{aligned} \quad (2.4.12)$$

Then, after substituting the limits of the horizontal and vertical velocities (2.4.9) and (2.4.10) into (2.4.7) and using the definition of limits of total normal mass flux (2.4.12) and the jump condition (2.4.11), we get

$$\begin{aligned} G_{j,\alpha+1/2}^+ &= \frac{\rho_j \phi_{j,\alpha+1}}{\bar{\rho}_{\alpha+1}} G_{\alpha+1/2} - \frac{1}{\varepsilon} \rho_j f_{j,\alpha+1/2}^+ - \varepsilon \mathbf{I}_\varepsilon^2 \mathbf{a}_{j,\alpha+1/2}^+ \cdot \boldsymbol{\eta}_{\alpha+1/2} \sqrt{1 + |\nabla_{\mathbf{x}} z_{\alpha+1/2}|^2}, \\ G_{j,\alpha+1/2}^- &= \frac{\rho_j \phi_{j,\alpha}}{\bar{\rho}_\alpha} G_{\alpha+1/2} - \frac{1}{\varepsilon} \rho_j f_{j,\alpha+1/2}^- - \varepsilon \mathbf{I}_\varepsilon^2 \mathbf{a}_{j,\alpha+1/2}^- \cdot \boldsymbol{\eta}_{\alpha+1/2} \sqrt{1 + |\nabla_{\mathbf{x}} z_{\alpha+1/2}|^2}. \end{aligned} \quad (2.4.13)$$

The relationship between normal mass flux of species  $j$  and the total normal mass flux across  $\Gamma_{\alpha+1/2}(t)$  is computed using the  $j$ -th mass jump condition (2.4.8) and summing for each  $j = 0, \dots, N$  the equations from (2.4.13). This yields

$$G_{j,\alpha+1/2} = \tilde{\phi}_{j,\alpha+1/2} G_{\alpha+1/2} - \frac{1}{\varepsilon} \rho_j \tilde{f}_{j,\alpha+1/2} - \varepsilon \mathbf{I}_\varepsilon^2 \tilde{\mathbf{a}}_{j,\alpha+1/2} \cdot \boldsymbol{\eta}_{\alpha+1/2} \sqrt{1 + |\nabla_{\mathbf{x}} z_{\alpha+1/2}|^2}, \quad (2.4.14)$$

where for each  $j = 0, \dots, N$  the averages  $\tilde{\phi}_{j,\alpha+1/2}$ ,  $\tilde{f}_{j,\alpha+1/2}$  and  $\tilde{\mathbf{a}}_{j,\alpha+1/2}$  are given by

$$\begin{aligned} \tilde{\phi}_{j,\alpha+1/2} &:= \frac{1}{2} \left( \frac{\rho_j \phi_{j,\alpha+1}}{\bar{\rho}_{\alpha+1}} + \frac{\rho_j \phi_{j,\alpha}}{\bar{\rho}_\alpha} \right), \quad \tilde{f}_{j,\alpha+1/2} := \frac{1}{2} (f_{j,\alpha+1/2}^+ + f_{j,\alpha+1/2}^-), \\ \tilde{\mathbf{a}}_{j,\alpha+1/2} &:= \frac{1}{2} (\mathbf{a}_{j,\alpha+1/2}^+ + \mathbf{a}_{j,\alpha+1/2}^-). \end{aligned} \quad (2.4.15)$$

On the other hand, setting  $\mathbf{M} = \varepsilon \tilde{\mathbf{I}}^{-1}$  and writing the jump condition of species  $j$  as

$$\begin{aligned} &\llbracket (\rho_j \phi_j \mathbf{v}_{\varepsilon,j}; \rho_j \phi_j \mathbf{v}_{\varepsilon,j} \otimes \mathbf{v}_j) \rrbracket_{t,\alpha+1/2} (\partial_t z_{\alpha+1/2}, \nabla_{\mathbf{x}} z_{\alpha+1/2}, -1)^T \\ &= G_{j,\alpha+1/2} \mathbf{M} \llbracket \mathbf{v}_j \rrbracket_{t,\alpha+1/2}, \quad j = 0, 1, \dots, N, \end{aligned}$$

where  $\llbracket (\dots; \dots) \rrbracket$  is a matricial  $3 \times 4$  jump, we may rewrite the momentum jump condition (2.4.2) as

$$\frac{1}{\varepsilon} \llbracket \Sigma \tilde{\mathbf{I}} \rrbracket_{t,\alpha+1/2} \boldsymbol{\eta}_{\alpha+1/2} = \frac{1}{\sqrt{1 + |\nabla_{\mathbf{x}} z_{\alpha+1/2}|^2}} \sum_{j=0}^N G_{j,\alpha+1/2} \mathbf{M} \llbracket \mathbf{v}_j \rrbracket_{t,\alpha+1/2}. \quad (2.4.16)$$

Now, from the left-hand side of (2.4.16) it is clear that we need to define an approximation of the stress tensor at each interface  $\Gamma_{\alpha+1/2}$ . Then, for  $\alpha = 1, \dots, M - 1$ , the stress tensor from (2.4.3) is decomposed as

$$\boldsymbol{\Sigma}_{\alpha+1/2}^{\pm} = -p_{\text{tot},\alpha+1/2} \mathbf{I} + \mathbf{T}_{\varepsilon,\alpha+1/2}^{E,\pm},$$

where  $p_{\text{tot},\alpha+1/2}$  is the pressure and  $\mathbf{T}_{\varepsilon,\alpha+1/2}^{E,\pm}$  are the limit approximations of the viscous stress tensor  $\mathbf{T}_\varepsilon^E$  at  $\Gamma_{\alpha+1/2}$ . From (2.4.16) we deduce that

$$\frac{1}{\varepsilon} (\mathbf{T}_{\varepsilon,\alpha+1/2}^{E,+} - \mathbf{T}_{\varepsilon,\alpha+1/2}^{E,-}) \tilde{\mathbf{I}} \boldsymbol{\eta}_{\alpha+1/2} = \frac{1}{\sqrt{1 + |\nabla_{\mathbf{x}} z_{\alpha+1/2}|^2}} \sum_{j=0}^N G_{j,\alpha+1/2} \mathbf{M} [\mathbf{v}_j]_{t,\alpha+1/2}, \quad (2.4.17)$$

where  $\mathbf{T}_{\varepsilon,\alpha+1/2}^{E,\pm}$  should be defined such that

$$\tilde{\mathbf{T}}_{\alpha+1/2}^E := \frac{1}{2} (\mathbf{T}_{\varepsilon,\alpha+1/2}^{E,+} + \mathbf{T}_{\varepsilon,\alpha+1/2}^{E,-})$$

is an approximation of the viscous stress tensor  $\mathbf{T}_\varepsilon^E|_{\Gamma_{\alpha+1/2}}$ . Then, as in [20] we define

$$\tilde{\mathbf{T}}_{\alpha+1/2}^E = \frac{\eta}{2} \tilde{\mathbf{D}}_{\varepsilon,\alpha+1/2} + 2\varepsilon\lambda(\tilde{\nabla} \cdot \tilde{\mathbf{v}})_{\alpha+1/2} \mathbf{I} \quad (2.4.18)$$

with

$$\begin{aligned} \tilde{\mathbf{D}}_{\varepsilon,\alpha+1/2} &= \begin{bmatrix} \varepsilon \mathbf{D}_{\varepsilon,h}(\tilde{\mathbf{u}}_{h,\alpha+1/2}) & \varepsilon^2 (\nabla_{\mathbf{x}} \tilde{w}_{\alpha+1/2})^T + \mathbf{Q}_{h,\alpha+1/2} \\ \varepsilon^2 \nabla_{\mathbf{x}} \tilde{w}_{\alpha+1/2} + (\mathbf{Q}_{h,\alpha+1/2})^T & 2\varepsilon Q_{v,\alpha+1/2} \end{bmatrix}, \\ (\tilde{\nabla} \cdot \tilde{\mathbf{v}})_{\alpha+1/2} &= \nabla_{\mathbf{x}} \cdot \tilde{\mathbf{u}}_{h,\alpha+1/2} + Q_{v,\alpha+1/2}, \end{aligned} \quad (2.4.19)$$

where  $\mathbf{Q}_{\alpha+1/2} = \mathbf{Q}(\mathbf{v})|_{\Gamma_{\alpha+1/2}}$  and  $\mathbf{Q} = (Q_h, Q_v)^T$  satisfies the equation  $\mathbf{Q} - \partial_z \mathbf{v} = \mathbf{0}$ . To approximate  $\mathbf{Q}$ , the solution of this equation, we approximate  $\mathbf{v}$  by a linear interpolation in  $z$ , named as  $\tilde{\mathbf{v}}$ , such that

$$\tilde{\mathbf{v}}|_{z=\frac{1}{2}(z_{\alpha-1/2}+z_{\alpha+1/2})} = \mathbf{v}_\alpha.$$

Finally, introducing  $\tilde{\mathbf{T}}_{\alpha+1/2}^E$  in the equality (2.4.17) we get

$$\mathbf{T}_{\varepsilon,\alpha+1/2}^{E,\pm} \tilde{\mathbf{I}} \boldsymbol{\eta}_{\alpha+1/2} = \tilde{\mathbf{T}}_{\alpha+1/2}^E \tilde{\mathbf{I}} \boldsymbol{\eta}_{\alpha+1/2} \pm \frac{1}{2} \frac{\varepsilon}{\sqrt{1 + |\nabla_{\mathbf{x}} z_{\alpha+1/2}|^2}} \sum_{j=0}^N G_{j,\alpha+1/2} \mathbf{M} [\mathbf{v}_j]_{t,\alpha+1/2},$$

which satisfies the jump condition (2.4.16).

### 2.4.3 Vertical velocity of the mixture

It is well known that in the multilayer approach under hydrostatic pressure the vertical velocity disappears from the third equation of the momentum equations so we need to recover this velocity by post-processing data. In **Chapter 1** we compute vertical velocities of each species and vertical velocity of the mixture, but the former are only computed to get the vertical velocity of the mixture. In other words, it is not possible to use the vertical velocities of each species to determine the velocity of the

each species, since these velocities are not well defined for all  $t \in [0, T]$ . On the other hand, these particular velocities are important and they allow us to compute the vertical velocity of the mixture for all  $t \in [0, T]$ .

So, to compute the vertical velocities of each species we set  $\alpha \in \{1, \dots, M\}$  and integrate vertically the mass balance equations (2.3.8) over a layer  $\alpha$ , this is over  $(z_{\alpha-1/2}, z)$  for  $z \in (z_{\alpha-1/2}, z_{\alpha+1/2})$  and then we use the assumption (2.4.4) to get for  $j = 0, \dots, N$

$$\partial_t(\rho_j \phi_{j,\alpha})(z - z_{\alpha-1/2}) + \nabla_{\mathbf{x}} \cdot (\rho_j \phi_{j,a} \mathbf{u}_{j,\alpha})(z - z_{\alpha-1/2}) + \rho_j \phi_{j,\alpha} (w_{j,\alpha}(t, \mathbf{x}, z) - w_{j,\alpha-1/2}^+) = 0, \quad (2.4.20)$$

where it is clear from (2.4.20) that it is not possible to recover the vertical velocity of species  $j$  when  $\phi_{j,\alpha} = 0$ . On the other hand, if we sum all equations in (2.4.20) from  $j = 0$  to  $j = N$  we get an expression for the vertical velocity of the mixture

$$w_{\alpha}(t, \mathbf{x}, z) = w_{\alpha-1/2}^+ - \frac{1}{\bar{\rho}_{\alpha}} (\partial_t \bar{\rho}_{\alpha} + \nabla_{\mathbf{x}} \cdot (\bar{\rho}_{\alpha} \mathbf{u}_{\alpha})) (z - z_{\alpha-1/2}), \quad (2.4.21)$$

where  $w_{\alpha-1/2}^+$  is defined by using the mass jump condition (2.4.11), so this vertical velocity is given by

$$w_{\alpha-1/2}^+ = \frac{1}{\bar{\rho}_{\alpha}} ((\bar{\rho}_{\alpha} - \bar{\rho}_{\alpha-1}) \partial_t z_{\alpha-1/2} + (\bar{\rho}_{\alpha} \mathbf{u}_{\alpha} - \bar{\rho}_{\alpha-1} \mathbf{u}_{\alpha-1}) \cdot \nabla_{\mathbf{x}} z_{\alpha-1/2} + \bar{\rho}_{\alpha-1} w_{\alpha-1/2}^-),$$

and the corresponding limit of the vertical velocity  $w_{\alpha-1/2}^-$  at the interface  $\Gamma_{\alpha-1/2}(t)$  is computed using the linear profile (2.4.21) in layer  $\alpha - 1$  evaluated at  $z_{\alpha-1/2}$ :

$$w_{\alpha-1/2}^- = w_{\alpha-3/2}^+ - \frac{h_{\alpha-1}}{\bar{\rho}_{\alpha-1}} (\partial_t(\bar{\rho}_{\alpha-1}) + \nabla_{\mathbf{x}} \cdot (\bar{\rho}_{\alpha-1} \mathbf{u}_{\alpha-1})).$$

Finally, the vertical velocities of the mixture in each layer are computed recursively as follows. First, the vertical velocity  $w_{1/2}^+$  is computed using mass transference condition (2.4.12) at the bottom by

$$w_{1/2}^+ = \partial_t z_B + \mathbf{u}_1 \cdot \nabla_{\mathbf{x}} z_B - \frac{G_{1/2}}{\rho_1}.$$

Then, for  $\alpha = 1, \dots, N$  and  $z \in (z_{\alpha-1/2}, z_{\alpha+1/2})$  we obtain the vertical velocities of the mixture in each layer successively as

$$\begin{aligned} w_{\alpha}(t, \mathbf{x}, z) &= w_{\alpha-1/2}^+ - \frac{1}{\bar{\rho}_{\alpha}} (\partial_t \bar{\rho}_{\alpha} + \nabla_{\mathbf{x}} \cdot (\bar{\rho}_{\alpha} \mathbf{u}_{\alpha})) (z - z_{\alpha-1/2}), \\ w_{\alpha+1/2}^- &= w_{\alpha-1/2}^+ - \frac{h_{\alpha}}{\bar{\rho}_{\alpha}} (\partial_t \bar{\rho}_{\alpha} + \nabla_{\mathbf{x}} \cdot (\bar{\rho}_{\alpha} \mathbf{u}_{\alpha})), \\ w_{\alpha+1/2}^+ &= \frac{1}{\bar{\rho}_{\alpha+1}} ((\bar{\rho}_{\alpha+1} - \bar{\rho}_{\alpha}) \partial_t z_{\alpha+1/2} + (\bar{\rho}_{\alpha+1} \mathbf{u}_{\alpha+1} - \bar{\rho}_{\alpha} \mathbf{u}_{\alpha}) \cdot \nabla_{\mathbf{x}} z_{\alpha+1/2} + \bar{\rho}_{\alpha} w_{\alpha+1/2}^-). \end{aligned}$$

## 2.5 Closure of multilayer approach

Following [20, 38], we now derive the multilayer model using the final form of the dimensionless model (2.3.8), (2.3.9), (2.3.10). We first need to introduce the multilayer version of the hydrostatic pressure.

### 2.5.1 Multilayer version of hydrostatic pressure

Using the last equality of the linear momentum equation of the mixture (2.3.10) we get

$$\partial_z p_{\text{tot}} = -\frac{\rho}{\text{Fr}^2} + \varepsilon \left( \nabla_x \cdot \left( \frac{\eta}{2} \partial_z \mathbf{v}_h \right) + \partial_z (\eta \partial_z w) + \partial_z (2\lambda \nabla \cdot \mathbf{v}) \right) + \mathcal{O}(\varepsilon^2).$$

To recover the hydrostatic framework (assumption (2.4.5)) we neglect in this equation up to  $\mathcal{O}(\varepsilon)$  terms, which yields  $\partial_z p_{\text{tot}} = -\rho/\text{Fr}^2$ . Then the multilayer version of the pressure is given by

$$p_{\text{tot},\alpha} = p_{\alpha+1/2} + \bar{\rho}_\alpha \frac{z_{\alpha+1/2} - z}{\text{Fr}^2}, \quad p_{\alpha+1/2} = p_s + \sum_{\beta=\alpha+1}^M \frac{\bar{\rho}_\beta h_\beta}{\text{Fr}^2},$$

where the component  $p_{\alpha+1/2}$  is the pressure at interface  $\Gamma_{\alpha+1/2}(t)$ ,  $p_s$  denotes the pressure at the free surface and  $\text{Fr}$  is the Froude number. This assumption on pressure ensures that the pressure is not an unknown of the problem.

### 2.5.2 Weak formulation

The multilayer approach arises from a variational formulation of the system (2.3.8)–(2.3.10). We notice that the multilayer model is a particular weak solution of these variational identities. The weak formulation in  $\Omega_\alpha(t)$  for  $\alpha = 1, \dots, N$  is as follows (cf. **Chapter 1**). Assume that  $\mathbf{v}_{j,\alpha} \in L^2(0, T; H^1(\Omega_\alpha(t))^3)$ ,  $\partial_t \mathbf{v}_{j,\alpha} \in L^2(0, T; L^2(\Omega_\alpha(t))^3)$ ,  $\phi_{j,\alpha} \in L^2(0, T; H^1(\Omega_\alpha(t)))$ ,  $\partial_t \phi_{j,\alpha} \in L^2(0, T; L^2(\Omega_\alpha(t)))$  and  $p_{\text{tot},\alpha} \in L^2(0, T; H^1(\Omega_\alpha(t)))$ . Then a weak solution  $(\mathbf{v}_{j,\alpha}, \phi_{j,\alpha}, p_{\text{tot},\alpha})$  in  $\Omega_\alpha(t)$  should satisfy for all  $\varphi \in L^2(\Omega_\alpha(t))$  and for all  $\boldsymbol{\vartheta} \in H^1(\Omega_\alpha(t))^3$  with  $\boldsymbol{\vartheta}|_{\partial I_F} = 0$  the identities

$$\begin{aligned} & \int_{\Omega_\alpha(t)} (\partial_t (\rho_j \phi_{j,\alpha}) + \nabla \cdot (\rho_j \phi_{j,\alpha} \mathbf{v}_{j,\alpha})) \varphi \, d\Omega = 0, \\ & \int_{\Omega_\alpha(t)} \left( \sum_{j=0}^N \rho_j \partial_t (\phi_{j,\alpha} \mathbf{v}_{\varepsilon,j,\alpha}) \right) \cdot \boldsymbol{\vartheta} \, d\Omega + \int_{\Omega_\alpha(t)} \left( \sum_{j=0}^N \rho_j \nabla \cdot (\phi_{j,\alpha} \mathbf{v}_{\varepsilon,j,\alpha} \otimes \mathbf{v}_{j,\alpha}) \right) \cdot \boldsymbol{\vartheta} \, d\Omega \\ & + \frac{1}{\varepsilon} \int_{\Omega_\alpha(t)} (\mathbf{T}_{\varepsilon,\alpha}^E \tilde{\mathbf{I}}) : \nabla \boldsymbol{\vartheta} \, d\Omega - \frac{1}{\varepsilon} \int_{\Omega_\alpha(t)} (p_{\text{tot},\alpha} \tilde{\mathbf{I}}) : \nabla \boldsymbol{\vartheta} \, d\Omega + \frac{1}{\varepsilon} \int_{\Gamma_{\alpha+1/2}(t)} (\boldsymbol{\Sigma}_{\alpha+1/2}^- \tilde{\mathbf{I}}) \boldsymbol{\eta}_{\alpha+1/2} \cdot \boldsymbol{\vartheta} \, d\Gamma \\ & - \frac{1}{\varepsilon} \int_{\Gamma_{\alpha-1/2}(t)} (\boldsymbol{\Sigma}_{\alpha-1/2}^+ \tilde{\mathbf{I}}) \boldsymbol{\eta}_{\alpha-1/2} \cdot \boldsymbol{\vartheta} \, d\Gamma = -\frac{1}{\varepsilon} \int_{\Omega_\alpha(t)} \frac{g}{\text{Fr}^2} \bar{\rho}_\alpha \mathbf{k} \cdot \boldsymbol{\vartheta} \, d\Omega, \end{aligned}$$

for particular test functions  $\varphi$  and  $\boldsymbol{\vartheta}$  that satisfy  $\partial_z \varphi = 0$  and

$$\boldsymbol{\vartheta}(t, \mathbf{x}, z) = (\boldsymbol{\vartheta}_h(t, \mathbf{x}), (z - z_B) \mathcal{V}(t, \mathbf{x}))^\top,$$

where  $\boldsymbol{\vartheta}_h$  and  $\mathcal{V}$  are smooth functions that do not depend on  $z$ . We use the structure given by (2.4.4), (2.4.5) and apply straightforward calculations analogous to those of [20, Appendix C] (details are

omitted here). Then we arrive at the following multilayer version of (2.3.8)–(2.3.10):

For  $\alpha = 0, \dots, M$ :

$$\begin{aligned} \partial_t(\rho_j \phi_{j,\alpha} h_\alpha) + \nabla_{\mathbf{x}} \cdot (\rho_j \phi_{j,\alpha} h_\alpha \mathbf{u}_{j,\alpha}) &= G_{j,\alpha+1/2} - G_{j,\alpha-1/2}, \quad j = 0, 1, \dots, N, \\ \sum_{j=0}^N &\left( \rho_j h_\alpha \partial_t(\phi_{j,\alpha} \mathbf{u}_{j,\alpha}) + \rho_j h_\alpha \nabla_{\mathbf{x}} \cdot (\phi_{j,\alpha} \mathbf{u}_{j,\alpha} \otimes \mathbf{u}_{j,\alpha}) + \rho_j \phi_{j,\alpha} (w_{j,\alpha+1/2}^- - w_{j,\alpha-1/2}^+) \mathbf{u}_{j,\alpha} \right) \\ &+ \int_{z_{\alpha-1/2}}^{z_{\alpha+1/2}} \nabla_{\mathbf{x}} p_{\text{tot},\alpha} dz - \nabla_{\mathbf{x}} \cdot (h_\alpha \mathbf{T}_{h,\alpha}^E) + \tilde{\mathbf{T}}_{h,\alpha+1/2}^E (\nabla_{\mathbf{x}} z_{\alpha+1/2})^T - \frac{1}{\varepsilon} \tilde{\mathbf{T}}_{xz,\alpha+1/2}^E \\ &- \tilde{\mathbf{T}}_{h,\alpha-1/2}^E (\nabla_{\mathbf{x}} z_{\alpha-1/2})^T + \frac{1}{\varepsilon} \tilde{\mathbf{T}}_{xz,\alpha-1/2}^E \\ &= \frac{1}{2} \sum_{j=0}^N G_{j,\alpha+1/2} (\mathbf{u}_{j,\alpha+1} - \mathbf{u}_{j,\alpha}) + \frac{1}{2} \sum_{j=0}^N G_{j,\alpha-1/2} (\mathbf{u}_{j,\alpha} - \mathbf{u}_{j,\alpha-1}), \end{aligned} \tag{2.5.1}$$

where the mass transfer terms  $G_{j,\alpha+1/2}$  are given by (2.4.14), the horizontal and vertical velocities  $\mathbf{u}_{j,\alpha}$  and  $w_{\alpha+1/2}^\pm$  are given by (2.4.9) and (2.4.10), respectively, where we keep in mind the equalities (2.4.6), and the viscous stress terms are given by (2.4.18)–(2.4.19), and the integral term of (2.5.1) by

$$\int_{z_{\alpha-1/2}}^{z_{\alpha+1/2}} \nabla_{\mathbf{x}} p_{\text{tot},\alpha} dz = h_\alpha \left( \nabla_{\mathbf{x}} \bar{p}_\alpha + \frac{\bar{\rho}_\alpha}{\text{Fr}^2} \nabla_{\mathbf{x}} \bar{z}_\alpha \right),$$

where  $\bar{p}_\alpha$  and  $\bar{z}_\alpha$  are defined as

$$\bar{p}_\alpha := p_S + \sum_{\beta=\alpha+1}^M \bar{\rho}_\beta h_\beta / \text{Fr}^2 + \bar{\rho}_\alpha \frac{h_\alpha}{2\text{Fr}^2}, \quad \bar{z}_\alpha := z_B + \sum_{\beta=1}^{\alpha-1} h_\beta + \frac{h_\alpha}{2}. \tag{2.5.2}$$

To this point all equations were given in dimensionless variables. In Section 2.5.3 and from here so on we will return to the original variables.

### 2.5.3 Multilayer model in original variables

To obtain the final form of the model, first we multiply the mass and linear momentum balance equations (2.5.1) by  $\varepsilon := H/L$ , and discard all  $\mathcal{O}(\varepsilon^2)$  terms. Finally we use (2.3.3) and (2.3.5) to return to the original variables. Multiplying (2.4.9) and (2.4.10) by  $\varepsilon$  and neglecting small terms, we obtain  $\mathbf{u}_{j,\alpha} = \mathbf{u}_\alpha$ . Analogously for (2.4.14) we get

$$G_{j,\alpha+1/2} = \tilde{\phi}_{j,\alpha+1/2} G_{\alpha+1/2} - \rho_j \tilde{f}_{j,\alpha+1/2} + \tilde{a}_{3,j,\alpha+1/2}.$$

For the viscous stress tensor from (2.3.7) we have

$$\mathbf{T}_\varepsilon^E(\mathbf{v}) \tilde{\mathbf{I}} = \frac{\eta}{2} \begin{bmatrix} \varepsilon^2 \mathbf{D}_{\varepsilon,h}(\mathbf{v}) & \partial_z \mathbf{v}_h + \varepsilon^2 (\nabla_x w)^T \\ \varepsilon ((\partial_z \mathbf{v}_h)^T + \varepsilon^2 \nabla_x w) & 2\varepsilon \partial_z w \end{bmatrix} + 2\lambda (\nabla \cdot \mathbf{v}) \begin{bmatrix} \varepsilon^2 & 0 & 0 \\ 0 & \varepsilon^2 & 0 \\ 0 & 0 & \varepsilon \end{bmatrix},$$

along with an analogous expression for the approximation of the viscous stress tensor at each interface  $\tilde{\mathbf{T}}_{\alpha+1/2}^E(\mathbf{v})$ . So the multilayer approach in original variables is given by

For  $\alpha = 1, \dots, M$ :

$$\begin{aligned} & \partial_t(\rho_j \phi_{j,\alpha} h_\alpha) + \nabla_{\mathbf{x}} \cdot (\rho_j \phi_{j,\alpha} h_\alpha \mathbf{u}_\alpha) \\ &= \tilde{\phi}_{j,\alpha+1/2} G_{\alpha+1/2} - \tilde{\phi}_{j,\alpha-1/2} G_{\alpha-1/2} \\ &\quad - \rho_j (\tilde{f}_{j,\alpha+1/2} - \tilde{f}_{j,\alpha-1/2}) + \tilde{a}_{j,3,\alpha+1/2} - \tilde{a}_{j,3,\alpha-1/2}, \quad j = 0, \dots, N, \\ & h_\alpha \partial_t(\bar{\rho}_\alpha \mathbf{u}_\alpha) + h_\alpha \nabla_{\mathbf{x}} \cdot (\bar{\rho}_\alpha \mathbf{u}_\alpha \otimes \mathbf{u}_\alpha) + \sum_{j=0}^N \rho_j \phi_{j,\alpha} (w_{j,\alpha+1/2}^- - w_{j,\alpha-1/2}^+) \mathbf{u}_\alpha \\ &\quad + h_\alpha (\nabla_{\mathbf{x}} \bar{p}_\alpha + g \rho_\alpha \nabla_{\mathbf{x}} \bar{z}_\alpha) \\ &= \frac{1}{2} G_{\alpha+1/2} (\mathbf{u}_{\alpha+1} - \mathbf{u}_\alpha) + \frac{1}{2} G_{\alpha-1/2} (\mathbf{u}_\alpha - \mathbf{u}_{\alpha-1}) + \mathbf{K}_{\alpha+1/2} - \mathbf{K}_{\alpha-1/2}, \end{aligned} \tag{2.5.3}$$

where the mass transfer terms  $G_{\alpha+1/2}$  through each interface  $\Gamma_{\alpha+1/2}$  for  $\alpha = 0, \dots, M$  are given by (2.4.11) and (2.4.12), and  $\tilde{\phi}_{j,\alpha+1/2}$ ,  $\tilde{f}_{j,\alpha+1/2}$ , and  $\tilde{a}_{j,3,\alpha+1/2}$  are given by (2.4.15). The terms  $\mathbf{K}_{\alpha+1/2}$  are the viscous stress tensors that remain after discarding small terms. These terms are given by

$$\mathbf{K}_{\alpha+1/2} = \frac{\eta}{2} \mathbf{Q}_{h,\alpha+1/2}, \quad \alpha = 1, \dots, M. \tag{2.5.4}$$

The total mass equation of the mixture at layer  $\alpha$  can be recovered summing from  $j = 0$  to  $j = N$  the first equations of (2.5.3). This yields

$$\partial_t(\bar{\rho}_\alpha h_\alpha) + \nabla_{\mathbf{x}} \cdot (\bar{\rho}_\alpha h_\alpha \mathbf{u}_\alpha) = G_{\alpha+1/2} - G_{\alpha-1/2}, \quad \alpha = 1, \dots, M. \tag{2.5.5}$$

The third term of the linear momentum balance in (2.5.3) can be written as follows, where we use (2.4.21) evaluated at  $z_{\alpha+1/2}$ :

$$\bar{\rho}_\alpha (w_{\alpha+1/2}^- - w_{\alpha-1/2}^+) = -h_\alpha (\partial_t \bar{\rho}_\alpha + \nabla_{\mathbf{x}} \cdot (\bar{\rho}_\alpha \mathbf{u}_\alpha)), \quad \alpha = 1, \dots, M. \tag{2.5.6}$$

Finally, multiplying (2.5.6) by  $\mathbf{u}_\alpha$  and introducing the result into the momentum equation of (2.5.3) and using (2.5.5) multiplied by  $\mathbf{u}_\alpha$ , we get the final form of the multilayer model

For  $\alpha = 1, \dots, M$ :

$$\begin{aligned} & \partial_t(\rho_j \phi_{j,\alpha} h_\alpha) + \nabla_{\mathbf{x}} \cdot (\rho_j \phi_{j,\alpha} h_\alpha \mathbf{u}_\alpha) \\ &= \tilde{\phi}_{j,\alpha+1/2} G_{\alpha+1/2} - \tilde{\phi}_{j,\alpha-1/2} G_{\alpha-1/2} \\ &\quad - \rho_j (\tilde{f}_{j,\alpha+1/2} - \tilde{f}_{j,\alpha-1/2}) + \tilde{a}_{j,3,\alpha+1/2} - \tilde{a}_{j,3,\alpha-1/2}, \quad j = 0, \dots, N, \\ & \partial_t(h_\alpha \bar{\rho}_\alpha \mathbf{u}_\alpha) + \nabla_{\mathbf{x}} \cdot (h_\alpha \bar{\rho}_\alpha \mathbf{u}_\alpha \otimes \mathbf{u}_\alpha) + h_\alpha (\nabla_{\mathbf{x}} \bar{p}_\alpha + g \bar{\rho}_\alpha \nabla_{\mathbf{x}} \bar{z}_\alpha) \\ &= \frac{G_{\alpha+1/2}}{2} (\mathbf{u}_{\alpha+1} + \mathbf{u}_\alpha) - \frac{G_{\alpha-1/2}}{2} (\mathbf{u}_\alpha + \mathbf{u}_{\alpha-1}) + \mathbf{K}_{\alpha+1/2} - \mathbf{K}_{\alpha-1/2}, \end{aligned} \tag{2.5.7}$$

where  $\tilde{\phi}_{j,\alpha+1/2}$ ,  $\tilde{f}_{j,\alpha+1/2}$ , and  $\tilde{a}_{j,3,\alpha+1/2}$  are given by (2.4.15), the mass transfer terms  $G_{\alpha+1/2}$  for  $\alpha = 1, \dots, M$  are given by (2.4.11) and (2.4.12),  $\bar{p}_\alpha$ ,  $\bar{z}_\alpha$  are given by (2.5.2) (but in original variables), and  $\mathbf{K}_{\alpha+1/2}$  is specified by (2.5.4).

### 2.5.4 Closure of the model

We close the system by assuming that the thickness of each layer  $h_\alpha$  is a fixed fraction of the total height  $h$ , i.e.,  $h_\alpha = l_\alpha h$  for  $\alpha = 1, \dots, M$ , where  $l_1, \dots, l_M$  are positive constants such as  $l_1 + \dots + l_M = 1$ . Furthermore, defining  $m_\alpha := \bar{\rho}_\alpha h$ ,  $\mathbf{q}_\alpha := \bar{\rho}_\alpha h \mathbf{u}_\alpha$ , and  $r_{j,\alpha} := \rho_j \phi_{j,\alpha} h$  for  $\alpha = 1, \dots, M$  and  $j = 0, \dots, N$ , we can write the system (2.5.7) as follows:

$$\partial_t m_\alpha + \nabla_{\mathbf{x}} \cdot \mathbf{q}_\alpha = \frac{1}{l_\alpha} (G_{\alpha+1/2} - G_{\alpha-1/2}), \quad (2.5.8a)$$

$$\begin{aligned} \partial_t r_{j,\alpha} + \nabla_{\mathbf{x}} \cdot \left( \frac{r_{j,\alpha} \mathbf{q}_\alpha}{m_\alpha} \right) \\ = \frac{1}{l_\alpha} (\tilde{\phi}_{j,\alpha+1/2} G_{\alpha+1/2} - \tilde{\phi}_{j,\alpha-1/2} G_{\alpha-1/2}) - \frac{\rho_j}{l_\alpha} (\tilde{f}_{j,\alpha+1/2} - \tilde{f}_{j,\alpha-1/2}) \\ + \frac{1}{l_\alpha} (\tilde{a}_{j,3,\alpha+1/2} - \tilde{a}_{j,3,\alpha-1/2}), \quad j = 1, \dots, N, \end{aligned} \quad (2.5.8b)$$

$$\begin{aligned} \partial_t \mathbf{q}_\alpha + \nabla_{\mathbf{x}} \cdot \left( \frac{\mathbf{q}_\alpha \otimes \mathbf{q}_\alpha}{m_\alpha} \right) + h (\nabla_{\mathbf{x}} \bar{p}_\alpha + g \bar{\rho}_\alpha \nabla_{\mathbf{x}} \bar{z}_\alpha) \\ = \frac{1}{l_\alpha} (\tilde{\mathbf{u}}_{\alpha+1/2} G_{\alpha+1/2} - \tilde{\mathbf{u}}_{\alpha-1/2} G_{\alpha-1/2}) + \frac{1}{l_\alpha} (\mathbf{K}_{\alpha+1/2} - \mathbf{K}_{\alpha-1/2}), \end{aligned} \quad (2.5.8c)$$

where  $\bar{p}_\alpha$ ,  $\bar{z}_\alpha$ , and the average  $\tilde{\phi}_{j,\alpha+1/2}$  defined by (2.4.15) can be written as

$$\bar{p}_\alpha = p_S + g \sum_{\beta=\alpha+1}^M l_\beta m_\beta + \frac{g}{2} l_\alpha m_\alpha, \quad \bar{z}_\alpha = z_B + h \sum_{\beta=1}^{\alpha-1} l_\beta + \frac{l_\alpha}{2} h, \quad \tilde{\phi}_{j,\alpha+1/2} = \frac{1}{2} \left( \frac{r_{j,\alpha+1}}{m_{\alpha+1}} + \frac{r_{j,\alpha}}{m_\alpha} \right), \quad (2.5.9)$$

respectively, and for  $\alpha = 1, \dots, M$  the average  $\tilde{\mathbf{u}}_{\alpha+1/2}$  by

$$\tilde{\mathbf{u}}_{\alpha+1/2} := \frac{1}{2} \left( \frac{\mathbf{q}_{\alpha+1}}{m_{\alpha+1}} + \frac{\mathbf{q}_\alpha}{m_\alpha} \right),$$

Summing from  $j = 0$  to  $j = M$  the equations (2.5.8a) we get one equation for the total mass of the mixture, namely

$$\partial_t \bar{m} + \nabla_{\mathbf{x}} \cdot \left( \sum_{\beta=1}^M l_\beta \mathbf{q}_\beta \right) = G_{M+1/2} - G_{1/2}, \quad (2.5.10)$$

where  $\bar{m} := \sum_{\beta=1}^M l_\beta m_\beta$  and  $G_{M+1/2}$  and  $G_{1/2}$  represent the mass transfer on the bottom and at the free surface, respectively.

Finally, we need to derive an explicit formula for the total interlayer mass fluxes. To this end and following **Chapter 1**, for a fixed layer  $\alpha$  we consider the sums of equations (2.5.8a) from layer 1 to layer  $\alpha$  and from layer  $\alpha + 1$  to layer  $M$ , obtaining the respective equations

$$\sum_{\beta=1}^{\alpha} l_\beta (\partial_t m_\beta + \nabla_{\mathbf{x}} \cdot \mathbf{q}_\beta) = G_{\alpha+1/2} - G_{1/2}, \quad \sum_{\gamma=\alpha+1}^M l_\gamma (\partial_t m_\gamma + \nabla_{\mathbf{x}} \cdot \mathbf{q}_\beta) = G_{M+1/2} - G_{\alpha+1/2}, \quad (2.5.11)$$

Now, defining  $L_\alpha := l_1 + \dots + l_\alpha$  and using that  $m_\alpha = \bar{\rho}_\alpha h$  can be written as

$$m_\alpha = \sum_{j=0}^N r_{j,\alpha} = \rho_0 h + \sum_{j=1}^N \frac{\rho_j - \rho_0}{\rho_j} r_{j,\alpha},$$

we deduce from (2.5.11) the identities

$$L_\alpha \partial_t (\rho_0 h) + \sum_{\beta=1}^{\alpha} \sum_{j=1}^N l_\beta \partial_t r_{j,\beta} \frac{\rho_j - \rho_0}{\rho_j} + \sum_{\beta=1}^{\alpha} l_\beta \nabla_{\mathbf{x}} \cdot \mathbf{q}_\beta = G_{\alpha+1/2} - G_{1/2}, \quad (2.5.12)$$

$$(1 - L_\alpha) \partial_t (\rho_0 h) + \sum_{\gamma=\alpha+1}^M \sum_{j=1}^N l_\gamma \partial_t r_{j,\gamma} \frac{\rho_j - \rho_0}{\rho_j} + \sum_{\gamma=\alpha+1}^M l_\gamma \nabla_{\mathbf{x}} \cdot \mathbf{q}_\gamma = G_{M+1/2} - G_{\alpha+1/2}. \quad (2.5.13)$$

Subtracting (2.5.12) multiplied by  $(1 - L_\alpha)$  from (2.5.13) multiplied by  $L_\alpha$  we obtain an equation that does not depend on  $\partial_t h$ . Secondly, we use (2.5.8b) to neglect the dependence on  $\partial_t r_{j,\beta}$ . Then, using the following notation

$$\mathbf{R}_\beta := \mathbf{q}_\beta - \sum_{j=1}^N r_{j,\beta} \frac{\mathbf{q}_\beta}{m_\beta} \frac{\rho_j - \rho_0}{\rho_j}, \quad \bar{\mathbf{R}} := \sum_{\beta=1}^M l_\beta \mathbf{R}_\beta,$$

we deduce

$$\begin{aligned} & G_{\alpha+1/2} \left( 1 - \sum_{j=1}^N \frac{\rho_j - \rho_0}{\rho_j} \tilde{\phi}_{j,\alpha+1/2} \right) - (1 - L_\alpha) G_{1/2} \left( 1 - \sum_{j=1}^N \frac{\rho_j - \rho_0}{\rho_j} \tilde{\phi}_{j,1/2} \right) \\ & - L_\alpha G_{M+1/2} \left( 1 - \sum_{j=1}^N \frac{\rho_j - \rho_0}{\rho_j} \tilde{\phi}_{j,M+1/2} \right) \\ & = \sum_{\beta=1}^{\alpha} l_\beta \nabla_{\mathbf{x}} \cdot (\mathbf{R}_\alpha - \bar{\mathbf{R}}) - \sum_{j=1}^N (\rho_j - \rho_0) \left( \tilde{f}_{j,\alpha+1/2} - \frac{\tilde{a}_{j,3,\alpha+1/2}}{\rho_j} \right) \\ & + \sum_{j=1}^N (\rho_j - \rho_0) \left( (1 - L_\alpha) \left( \tilde{f}_{j,1/2} - \frac{\tilde{a}_{j,3,1/2}}{\rho_j} \right) + L_\alpha \left( \tilde{f}_{j,M+1/2} - \frac{\tilde{a}_{j,3,M+1/2}}{\rho_j} \right) \right). \end{aligned}$$

Taking into account the definition of  $\tilde{\phi}_{j,\alpha+1/2}$  (2.5.9), we obtain

$$1 - \sum_{j=1}^N \frac{\rho_j - \rho_0}{\rho_j} \tilde{\phi}_{j,\alpha+1/2} = \frac{\rho_0}{\tilde{\rho}_{\alpha+1/2}}, \quad \text{where } \tilde{\rho}_{\alpha+1/2} := \frac{2}{\frac{1}{\bar{\rho}_\alpha} + \frac{1}{\bar{\rho}_{\alpha+1}}}.$$

Finally, we deduce

$$G_{\alpha+1/2} = \frac{\tilde{\rho}_{\alpha+1/2}}{\rho_0} \sum_{\beta=1}^{\alpha} l_\beta \nabla_{\mathbf{x}} \cdot (\mathbf{R}_\beta - \bar{\mathbf{R}}) + G_{f-a,\alpha+1/2}, \quad (2.5.14)$$

where

$$G_{f-a,\alpha+1/2} := \frac{\tilde{\rho}_{\alpha+1/2}}{\rho_0} \left( - \sum_{j=1}^N (\rho_j - \rho_0) \left( \tilde{f}_{j,\alpha+1/2} - \frac{\tilde{a}_{j,3,\alpha+1/2}}{\rho_j} \right) + (1 - L_\alpha) C_{1/2} + L_\alpha C_{M+1/2} \right),$$

$$C_{l+1/2} := G_{l+1/2} \frac{\rho_0}{\tilde{\rho}_{l+1/2}} + \sum_{j=1}^N (\rho_j - \rho_0) \left( \tilde{f}_{j,l+1/2} - \frac{\tilde{a}_{j,3,l+1/2}}{\rho_j} \right) \quad \text{for } l = 0 \text{ and } l = M.$$

## 2.6 Numerical scheme

We now devise a numerical method to discretize the final system, defined by equations (2.5.8b), (2.5.8c), and (2.5.10) with the explicit definition of mass transfer (2.5.14). We consider an implicit discretization of the terms  $\mathbf{K}_{\alpha+1/2} - \mathbf{K}_{\alpha-1/2}$ , corresponding to a vertical diffusion, so these terms will not be considered in what follows in this section. If we define  $\mathbf{W}_\alpha := (m_\alpha, \mathbf{q}_\alpha, r_{1,\alpha}, \dots, r_{N,\alpha})^T$ , then the vector of unknowns of the system defined by (2.5.8b), (2.5.8c), and (2.5.10) is

$$\mathbf{W} = \mathcal{C}\hat{\mathbf{W}} \quad (2.6.1)$$

where the matrix  $\mathcal{C} \in \mathbb{R}^{(M(N+2)+1) \times M(N+3)}$  is defined as follows. We define  $\mathbf{e}_{i,N}$  to be the  $i$ -th  $N$ -dimensional unit vector ( $i = 1, \dots, N$ ) for general  $N$ ,  $\mathbf{I}_d$  to be the  $d \times d$  identity matrix,  $\mathbf{0}_d$  to be the zero vector of size  $d$ , and  $\mathbf{0}$  (without index) to be a zero matrix of unspecified size. Then we define the  $(N+2) \times (N+3)$  block  $\mathcal{C} := [\mathbf{0}_{N+2} \ \mathbf{I}_{N+2}]$ ,

$$\mathcal{C} = \begin{bmatrix} l_1 \mathbf{e}_{1,N+3}^T & l_2 \mathbf{e}_{1,N+3}^T & \cdots & l_M \mathbf{e}_{1,N+3}^T \\ \mathbf{C} & \mathbf{0} & \cdots & \mathbf{0} \\ \mathbf{0} & \mathbf{C} & \ddots & \vdots \\ \vdots & \ddots & \ddots & \mathbf{0} \\ \mathbf{0} & \cdots & \mathbf{0} & \mathbf{C} \end{bmatrix},$$

and the  $M(N+3)$  vector  $\hat{\mathbf{W}} = (\mathbf{W}_\alpha)_{1 \leq \alpha \leq M}$ , where  $\mathbf{W}_\alpha \in \mathbb{R}^{N+3}$ .

Note that relation (2.6.1) allows us to connect the full system defined by (2.5.8a)–(2.5.8c) with the compact one defined by (2.5.8b), (2.5.8c) and (2.5.10). The compact system can be written as

$$\mathcal{C}(\partial_t \hat{\mathbf{W}} + \nabla_{\mathbf{x}} \cdot \mathbf{F}(\hat{\mathbf{W}}) + \mathcal{P}(\hat{\mathbf{W}})) = \mathcal{C}(\mathcal{G}^+(\hat{\mathbf{W}}) - \mathcal{G}^-(\hat{\mathbf{W}})), \quad (2.6.2)$$

where analogously to  $\hat{\mathbf{W}}$ , each one of terms defining this system can be written by layers. That is, we define the vectors  $\mathcal{P} = (\mathcal{P}_\alpha)_{1 \leq \alpha \leq M}$  and  $\mathcal{G}^\pm = (\mathcal{G}_\alpha^\pm)_{1 \leq \alpha \leq M}$ , where  $\mathcal{P}_\alpha, \mathcal{G}_\alpha^\pm \in \mathbb{R}^{N+3}$  and

$$\mathcal{G}_\alpha^\pm = \frac{1}{l_\alpha} (\mathbf{U}_{\alpha \pm 1/2} G_{\alpha \pm 1/2} + \mathcal{G}_{f-a,\alpha}^\pm),$$

where we define

$$\begin{aligned} \mathcal{P}_\alpha &:= \left( \begin{array}{c} 0 \\ gm_\alpha \nabla_{\mathbf{x}}(z_B + h) + gh^2 \left( \frac{l_\alpha}{2} + \sum_{\beta=\alpha+1}^M l_\beta \right) \nabla_{\mathbf{x}} \bar{\rho}_\alpha + gh \nabla_{\mathbf{x}} \left( h \sum_{\beta=\alpha+1}^M l_\beta (\bar{\rho}_\beta - \bar{\rho}_\alpha) \right) \\ \mathbf{0}_N \end{array} \right), \\ \mathbf{U}_{\alpha \pm 1/2}(\hat{\mathbf{W}}) &:= \begin{pmatrix} 1 \\ \tilde{\mathbf{u}}_{\alpha \pm 1/2} \\ \tilde{\phi}_{1,\alpha \pm 1/2} \\ \vdots \\ \tilde{\phi}_{N,\alpha \pm 1/2} \end{pmatrix}, \quad \mathcal{G}_{f-a,\alpha}^\pm := \begin{pmatrix} \mathbf{0}_3 \\ -\rho_1 \tilde{f}_{1,\alpha \pm 1/2} + \tilde{a}_{1,3,\alpha \pm 1/2} \\ \vdots \\ -\rho_N \tilde{f}_{j,\alpha \pm 1/2} + \tilde{a}_{N,3,\alpha \pm 1/2} \end{pmatrix}. \end{aligned} \quad (2.6.3)$$

On the other hand,  $\mathbf{F} \in \mathbb{R}^{M(N+3) \times 2}$  is a matrix that can be partitioned as

$$\mathbf{F} = \begin{bmatrix} \mathbf{F}_1 \\ \mathbf{F}_2 \\ \vdots \\ \mathbf{F}_M \end{bmatrix}, \quad \text{where } \mathbf{F}_\alpha = \begin{bmatrix} \mathbf{q}_\alpha^T \\ (1/m_\alpha)\mathbf{q}_\alpha \otimes \mathbf{q}_\alpha \\ (r_{1,\alpha}/m_\alpha)\mathbf{q}_\alpha^T \\ \vdots \\ (r_{N,\alpha}/m_\alpha)\mathbf{q}_\alpha^T \end{bmatrix} \in \mathbb{R}^{(N+3) \times 2}, \quad \alpha = 1, \dots, M.$$

Then, to propose a discretization of (2.6.2) in two horizontal space dimensions, we first study the properties of the system corresponding to one layer, that is, we fix  $\alpha \in \{1, \dots, M\}$  and consider

$$\partial_t \mathbf{W}_\alpha + \nabla_{\mathbf{x}} \cdot \mathbf{F}_\alpha(\mathbf{W}_\alpha) + \mathcal{P}_\alpha(\hat{\mathbf{W}}) = \mathcal{G}_\alpha^+(\hat{\mathbf{W}}) - \mathcal{G}_\alpha^-(\hat{\mathbf{W}}). \quad (2.6.4)$$

For a vector  $\boldsymbol{\eta} = (\eta_1, \eta_2)^T \in \mathbb{R}^2$  with  $\|\boldsymbol{\eta}\|_2 = 1$  we define the matrices

$$\mathbf{T}_{\boldsymbol{\eta}} := \begin{bmatrix} 1 & 0 & 0 & \mathbf{0}_N^T \\ 0 & \eta_1 & \eta_2 & \mathbf{0}_N^T \\ 0 & -\eta_2 & \eta_1 & \mathbf{0}_N^T \\ \mathbf{0}_N & \mathbf{0}_N & \mathbf{0}_N & \mathbf{I}_N \end{bmatrix} \in \mathbb{R}^{(N+3) \times (N+3)}, \quad \hat{\mathbf{T}}_{\boldsymbol{\eta}} := \mathbf{I}_M \otimes \mathbf{T}_{\boldsymbol{\eta}} \in \mathbb{R}^{M(N+3) \times M(N+3)}. \quad (2.6.5)$$

**Proposition 2.6.1.** *The flux functions  $\mathbf{F}_\alpha$  from system (2.5.8a)-(2.5.8c), satisfy the following rotational invariance property*

$$\mathbf{F}_\alpha(\mathbf{W}_\alpha)\boldsymbol{\eta} = \mathbf{T}_{\boldsymbol{\eta}}^{-1}[\mathbf{F}_\alpha]_1(\mathbf{T}_{\boldsymbol{\eta}}\mathbf{W}_\alpha), \quad (2.6.6)$$

for  $\boldsymbol{\eta} := (\eta_1, \eta_2) \in \mathbb{R}^2$  and  $\mathbf{T}_{\boldsymbol{\eta}} \in \mathcal{M}_{N+3, N+3}$  given by (2.6.5).

**Proof.** of Prop. 2.6.1 First we calculate  $\mathbf{T}_{\boldsymbol{\eta}}\mathbf{W}_\alpha$ , getting

$$\mathbf{T}_{\boldsymbol{\eta}}\mathbf{W}_\alpha = (m_\alpha, q_{\boldsymbol{\eta}}, q_{\boldsymbol{\eta}^\perp}, \{r_{j,\alpha}\}_{j=1}^N)^T, \quad (2.6.7)$$

with  $q_{\boldsymbol{\eta}} = \eta_1 q_{\alpha,1} + \eta_2 q_{\alpha,2}$  and  $q_{\boldsymbol{\eta}^\perp} = -\eta_2 q_{\alpha,1} + \eta_1 q_{\alpha,2}$ . Now, noticing that

$$\mathbf{F}_\alpha(\mathbf{W}_\alpha)\boldsymbol{\eta} = \begin{pmatrix} q_{\boldsymbol{\eta}} \\ \eta_1 \frac{q_{\alpha,1}^2}{m_\alpha} + \eta_2 \frac{q_{\alpha,1}q_{\alpha,2}}{m_\alpha} \\ \eta_1 \frac{q_{\alpha,1}q_{\alpha,2}}{m_\alpha} + \eta_2 \frac{q_{\alpha,2}^2}{m_\alpha} \\ \{\frac{r_{j,\alpha}}{m_\alpha} q_{\boldsymbol{\eta}}\}_{j=1}^N \end{pmatrix},$$

then, multiplying the above equation by  $\mathbf{T}_{\boldsymbol{\eta}}$  we compute

$$\mathbf{T}_{\boldsymbol{\eta}}\mathbf{F}_\alpha(\mathbf{W}_\alpha)\boldsymbol{\eta} = \begin{pmatrix} q_{\boldsymbol{\eta}} \\ \eta_1^2 \frac{q_{\alpha,1}^2}{m_\alpha} + 2\eta_1\eta_2 \frac{q_{\alpha,1}q_{\alpha,2}}{m_\alpha} + \eta_2^2 \frac{q_{\alpha,2}^2}{m_\alpha} \\ -\eta_1\eta_2 \frac{q_{\alpha,1}^2}{m_\alpha} - \eta_2^2 \frac{q_{\alpha,1}q_{\alpha,2}}{m_\alpha} + \eta_1^2 \frac{q_{\alpha,1}q_{\alpha,2}}{m_\alpha} + \eta_1\eta_2 \frac{q_{\alpha,2}^2}{m_\alpha} \\ \{\frac{r_{j,\alpha}}{m_\alpha} q_{\boldsymbol{\eta}}\}_{j=1}^N \end{pmatrix},$$

where

$$\eta_1^2 \frac{q_{\alpha,1}^2}{m_\alpha} + 2\eta_1\eta_2 \frac{q_{\alpha,1}q_{\alpha,2}}{m_\alpha} + \eta_2^2 \frac{q_{\alpha,2}^2}{m_\alpha} = \frac{1}{m_\alpha}(\eta_1 q_{\alpha,1} + \eta_2 q_{\alpha,2})^2 = \frac{q_{\boldsymbol{\eta}}^2}{m_\alpha},$$

$$-\eta_1\eta_2 \frac{q_{\alpha,1}^2}{m_\alpha} - \eta_2^2 \frac{q_{\alpha,1}q_{\alpha,2}}{m_\alpha} + \eta_1^2 \frac{q_{\alpha,1}q_{\alpha,2}}{m_\alpha} + \eta_1\eta_2 \frac{q_{\alpha,2}^2}{m_\alpha} = \frac{1}{m_\alpha}(\eta_1 q_{\alpha,1} + \eta_2 q_{\alpha,2})(-\eta_2 q_{\alpha,1} + \eta_1 q_{\alpha,2}) = \frac{q_{\boldsymbol{\eta}} q_{\boldsymbol{\eta}^\perp}}{m_\alpha},$$

summarizing, we have that

$$\mathbf{T}_{\boldsymbol{\eta}} \mathbf{F}_\alpha(\mathbf{W}_\alpha) \boldsymbol{\eta} = \left( q_{\boldsymbol{\eta}}, \frac{q_{\boldsymbol{\eta}}^2}{m_\alpha}, \frac{q_{\boldsymbol{\eta}} q_{\boldsymbol{\eta}^\perp}}{m_\alpha}, \left\{ \frac{r_{j,\alpha}}{m_\alpha} q_{\boldsymbol{\eta}} \right\}_{j=1}^N \right)^T,$$

finally, only we have note that after to evaluate  $\mathbf{F}_\alpha$  in (2.6.7) get

$$[\mathbf{F}_\alpha]_1(\mathbf{T}_{\boldsymbol{\eta}} \mathbf{W}_\alpha) = \left( q_{\boldsymbol{\eta}}, \frac{q_{\boldsymbol{\eta}}^2}{m_\alpha}, \frac{q_{\boldsymbol{\eta}} q_{\boldsymbol{\eta}^\perp}}{m_\alpha}, \left\{ \frac{r_{j,\alpha}}{m_\alpha} q_{\boldsymbol{\eta}} \right\}_{j=1}^N \right)^T,$$

to conclude (2.6.6)

$$\mathbf{F}_\alpha(\mathbf{W}_\alpha) \boldsymbol{\eta} = \mathbf{T}_{\boldsymbol{\eta}}^{-1} [\mathbf{F}_\alpha]_1(\mathbf{T}_{\boldsymbol{\eta}} \mathbf{W}_\alpha),$$

where  $[\mathbf{F}_\alpha]_1 = \mathbf{F}_\alpha \mathbf{e}_{1,2}$  is the first column of  $[\mathbf{F}_\alpha]$ . ■

For  $\boldsymbol{\eta}^\perp = (-\eta_2, \eta_1)^T$  and  $\mathbf{f} : \mathbb{R}^2 \rightarrow \mathbb{R}^2$  we have  $\nabla_{\mathbf{x}} \cdot \mathbf{f} = \partial_{\boldsymbol{\eta}}(\mathbf{f} \cdot \boldsymbol{\eta}) + \partial_{\boldsymbol{\eta}^\perp}(\mathbf{f} \cdot \boldsymbol{\eta}^\perp)$ . Moreover, the quantities  $\mathbf{U}_{\alpha \pm 1/2}(\hat{\mathbf{W}})$  defined in (2.6.3) satisfy  $\mathbf{T}_{\boldsymbol{\eta}} \mathbf{U}_{\alpha \pm 1/2}(\hat{\mathbf{W}}) = \mathbf{U}_{\alpha \pm 1/2}(\hat{\mathbf{T}}_{\boldsymbol{\eta}} \hat{\mathbf{W}})$ , and  $\mathcal{P}_\alpha$  and  $\mathcal{G}_\alpha^\pm(\hat{\mathbf{W}})$  satisfy

$$\mathbf{T}_{\boldsymbol{\eta}} \mathcal{P}_\alpha(\hat{\mathbf{W}}) = \mathcal{P}_{\boldsymbol{\eta},\alpha}(\hat{\mathbf{W}}) + \mathcal{P}_{\boldsymbol{\eta}^\perp,\alpha}(\hat{\mathbf{W}})$$

with

$$\begin{aligned} \mathcal{P}_{\boldsymbol{\eta},\alpha} &= \left( g m_\alpha \partial_{\boldsymbol{\eta}}(z_B + h) + g h^2 \left( \frac{l_\alpha}{2} + \sum_{\beta=\alpha+1}^M l_\beta \right) \partial_{\boldsymbol{\eta}} \bar{\rho}_\alpha + g h \partial_{\boldsymbol{\eta}} \left( h \sum_{\beta=\alpha+1}^M l_\beta (\bar{\rho}_\beta - \bar{\rho}_\alpha) \right) \right) \mathbf{e}_{2,N+3}, \\ \mathcal{P}_{\boldsymbol{\eta}^\perp,\alpha} &= \left( g m_\alpha \partial_{\boldsymbol{\eta}^\perp}(z_B + h) + g h^2 \left( \frac{l_\alpha}{2} + \sum_{\beta=\alpha+1}^M l_\beta \right) \partial_{\boldsymbol{\eta}^\perp} \bar{\rho}_\alpha + g h \partial_{\boldsymbol{\eta}^\perp} \left( h \sum_{\beta=\alpha+1}^M l_\beta (\bar{\rho}_\beta - \bar{\rho}_\alpha) \right) \right) \mathbf{e}_{3,N+3}. \end{aligned}$$

and

$$\begin{aligned} \mathbf{T}_{\boldsymbol{\eta}} \mathcal{G}_\alpha^\pm(\hat{\mathbf{W}}) &= \mathbf{U}_{\alpha \pm 1/2}(\hat{\mathbf{T}}_{\boldsymbol{\eta}} \hat{\mathbf{W}}) G_{\boldsymbol{\eta},\alpha \pm 1/2} + \frac{1}{2} \mathcal{G}_{f-a,\alpha}^\pm(\hat{\mathbf{T}}_{\boldsymbol{\eta}} \hat{\mathbf{W}}) \partial_{\boldsymbol{\eta}}((\mathbf{x} - \bar{\mathbf{x}})^T \boldsymbol{\eta}) \\ &\quad + \mathbf{U}_{\alpha \pm 1/2}(\hat{\mathbf{T}}_{\boldsymbol{\eta}} \hat{\mathbf{W}}) G_{\boldsymbol{\eta}^\perp,\alpha \pm 1/2} + \frac{1}{2} \mathcal{G}_{f-a,\alpha}^\pm(\hat{\mathbf{T}}_{\boldsymbol{\eta}} \hat{\mathbf{W}}) \partial_{\boldsymbol{\eta}^\perp}((\mathbf{x} - \bar{\mathbf{x}})^T \boldsymbol{\eta}^\perp) \\ &=: \mathcal{G}_{\boldsymbol{\eta},\alpha}^\pm(\hat{\mathbf{W}}) + \mathcal{G}_{\boldsymbol{\eta}^\perp,\alpha}^\pm(\hat{\mathbf{W}}), \end{aligned}$$

where  $\mathbf{T}_{\boldsymbol{\eta}} \mathcal{G}_{f-a,\alpha}^\pm(\hat{\mathbf{W}}) = \mathcal{G}_{f-a,\alpha}^\pm(\hat{\mathbf{T}}_{\boldsymbol{\eta}} \hat{\mathbf{W}})$  and we have used that  $G_{\alpha+1/2} = G_{\boldsymbol{\eta},\alpha+1/2} + G_{\boldsymbol{\eta}^\perp,\alpha+1/2}$  with

$$G_{\boldsymbol{\eta},\alpha+1/2} = \frac{\tilde{\rho}_{\alpha+1/2}}{\rho_0} \sum_{\beta=1}^\alpha l_\beta (\partial_{\boldsymbol{\eta}}(\mathbf{R}_\alpha - \bar{\mathbf{R}}))^T \boldsymbol{\eta} + \frac{G_{f-a,\alpha+1/2}}{2} \partial_{\boldsymbol{\eta}}((\mathbf{x} - \bar{\mathbf{x}})^T \boldsymbol{\eta}),$$

$$G_{\boldsymbol{\eta}^\perp,\alpha+1/2} = \frac{\tilde{\rho}_{\alpha+1/2}}{\rho_0} \sum_{\beta=1}^\alpha l_\beta (\partial_{\boldsymbol{\eta}^\perp}(\mathbf{R}_\alpha - \bar{\mathbf{R}}))^T \boldsymbol{\eta}^\perp + \frac{G_{f-a,\alpha+1/2}}{2} \partial_{\boldsymbol{\eta}^\perp}((\mathbf{x} - \bar{\mathbf{x}})^T \boldsymbol{\eta}^\perp).$$

The system (2.6.4) can now be written as

$$\begin{aligned} \partial_t \mathbf{W}_\alpha + \partial_{\boldsymbol{\eta}} (\mathbf{F}_\alpha(\mathbf{W}_\alpha) \boldsymbol{\eta}) + \partial_{\boldsymbol{\eta}^\perp} (\mathbf{F}_\alpha(\mathbf{W}_\alpha) \boldsymbol{\eta}^\perp) &+ \mathbf{T}_{\boldsymbol{\eta}}^{-1} \mathcal{P}_{\boldsymbol{\eta},\alpha}(\hat{\mathbf{W}}) + \mathbf{T}_{\boldsymbol{\eta}}^{-1} \mathcal{P}_{\boldsymbol{\eta}^\perp,\alpha}(\hat{\mathbf{W}}) \\ &= \mathbf{T}_{\boldsymbol{\eta}}^{-1} \mathcal{G}_{\boldsymbol{\eta},\alpha}^+(\hat{\mathbf{W}}) + \mathbf{T}_{\boldsymbol{\eta}}^{-1} \mathcal{G}_{\boldsymbol{\eta}^\perp,\alpha}^+(\hat{\mathbf{W}}) - \mathbf{T}_{\boldsymbol{\eta}}^{-1} \mathcal{G}_{\boldsymbol{\eta},\alpha}^-(\hat{\mathbf{W}}) - \mathbf{T}_{\boldsymbol{\eta}}^{-1} \mathcal{G}_{\boldsymbol{\eta}^\perp,\alpha}^-(\hat{\mathbf{W}}), \end{aligned} \quad (2.6.8)$$

then, multiplying system (2.6.8) by  $\mathbf{T}_{\boldsymbol{\eta}}$  and using Prop. 2.6.1, we obtain

$$\partial_t (\mathbf{T}_{\boldsymbol{\eta}} \mathbf{W}_\alpha) + \partial_{\boldsymbol{\eta}} [\mathbf{F}_\alpha]_1 (\mathbf{T}_{\boldsymbol{\eta}} \mathbf{W}_\alpha) + \mathcal{P}_{\boldsymbol{\eta},\alpha}(\hat{\mathbf{W}}) = \mathcal{G}_{\boldsymbol{\eta},\alpha}^+(\hat{\mathbf{W}}) - \mathcal{G}_{\boldsymbol{\eta},\alpha}^-(\hat{\mathbf{W}}) + S_{\boldsymbol{\eta}^\perp}, \quad (2.6.9)$$

where

$$\begin{aligned} S_{\boldsymbol{\eta}^\perp} = \mathbf{T}_{\boldsymbol{\eta}} \Big( &- \partial_{\boldsymbol{\eta}^\perp} (\mathbf{F}_\alpha(\mathbf{W}_\alpha) \boldsymbol{\eta}^\perp) - \mathbf{T}_{\boldsymbol{\eta}}^{-1} \mathcal{P}_{\boldsymbol{\eta}^\perp,\alpha}(\hat{\mathbf{W}}) \\ &+ \mathbf{T}_{\boldsymbol{\eta}}^{-1} \left( \mathbf{U}_{\alpha+1/2}(\hat{\mathbf{W}}) G_{\boldsymbol{\eta}^\perp,\alpha+1/2} + \frac{1}{2} \mathcal{G}_{f-a,\alpha}^+(\hat{\mathbf{W}}) \partial_{\boldsymbol{\eta}^\perp} ((\mathbf{x} - \bar{\mathbf{x}})^\top \boldsymbol{\eta}^\perp) \right) \\ &- \mathbf{T}_{\boldsymbol{\eta}}^{-1} \left( \mathbf{U}_{\alpha-1/2}(\hat{\mathbf{W}}) G_{\boldsymbol{\eta}^\perp,\alpha-1/2} - \frac{1}{2} \mathcal{G}_{f-a,\alpha}^-(\hat{\mathbf{W}}) \partial_{\boldsymbol{\eta}^\perp} ((\mathbf{x} - \bar{\mathbf{x}})^\top \boldsymbol{\eta}^\perp) \right) \Big). \end{aligned}$$

The numerical scheme is designed by defining a numerical approximation of the rotated system (2.6.9) at each edge of the control volumes grid, by neglecting tangential variations in each edge of the control volume, that is, neglecting the term  $S_{\boldsymbol{\eta}^\perp}$ , where  $\boldsymbol{\eta}$  is the normal vector at each edge. Let us denote by  $\{V_i\}_{i=1}^{N_c}$  control volumes that define a partition of the domain, by  $E_{i,j}$  the interface between two adjacent control volume  $V_i$  and  $V_j$ , being  $\boldsymbol{\eta}_{i,j}$  the unitary normal vector from  $V_i$  to  $V_j$ . For each control volume  $V_i$  we define the set of neighboring control volumes by  $K_i$  and by  $|V_i|$  and  $|E_{i,j}|$  the area and the length of each edge  $E_{i,j}$  respectively. The center of mass of the control volume  $V_i$  will be denoted by  $\mathbf{x}_i$  and the center of the edge  $E_{i,j}$  by  $\mathbf{x}_{i,j}$ .

The design of the numerical method is done by taking into account that the original system (2.6.2), multiplied by  $\hat{\mathbf{T}}_{\boldsymbol{\eta}_{i,j}}$ , is rewritten as (2.6.9). Then we denote by  $\mathbf{W}_i^n$  the average values of the unknowns over the control volume  $V_i$  at time  $t^n$ . We propose the following 2D finite volume method to approximate the system (2.6.2):

$$\mathbf{W}_i^{n+1} = \mathbf{W}_i^n - \frac{\Delta t}{|V_i|} \sum_{j \in K_i} |E_{i,j}| \mathcal{C} \hat{\mathbf{T}}_{\boldsymbol{\eta}_{i,j}}^{-1} (\hat{\mathcal{F}}_{i,j} + \hat{\mathcal{P}}_{i,j} - \hat{\mathcal{G}}_{i,j}^+ + \hat{\mathcal{G}}_{i,j}^-),$$

where

$$\hat{\mathcal{F}}_{i,j} = (\mathcal{F}_{i,j,\alpha})_{1 \leq \alpha \leq M}, \quad \hat{\mathcal{P}}_{i,j} = (\mathcal{P}_{i,j,\alpha})_{1 \leq \alpha \leq M}, \quad \hat{\mathcal{G}}_{i,j}^\pm = (\mathcal{G}_{i,j,\alpha}^\pm)_{1 \leq \alpha \leq M}.$$

We define  $\mathcal{F}_{i,j,\alpha}$  for  $\alpha = 1, \dots, M$  by an HLL-PVM-1U method [26] to define the first and second component. This approach relies on left and right bounds of the eigenvalues,  $S_L$  and  $S_R$ , of the transport matrix of the full system. That implies to consider a HLL method of the full system and not a local independent method for each layer. For the other components we use that  $\mathcal{F}_{i,j,\alpha}$  is an approximation  $[\mathbf{F}_\alpha]_1(\mathbf{T}_{\boldsymbol{\eta}} \mathbf{W}_\alpha)$  on edge  $E_{i,j}$ . Then, from the third component the flux components correspond to passive transport equations. Then we define for  $k = 1, 2$

$$\begin{aligned} [\mathcal{F}_{i,j,\alpha}]_k = &\left[ \frac{1}{2} ([\mathbf{F}_\alpha]_1(T_{\boldsymbol{\eta}_{i,j}} \mathbf{W}_{i,\alpha}) + [\mathbf{F}_\alpha]_1(T_{\boldsymbol{\eta}_{i,j}} \mathbf{W}_{j,\alpha})) - \frac{1}{2} (a_{0,i,j}(T_{\boldsymbol{\eta}_{i,j}}(\mathbf{W}_{j,\alpha} - \mathbf{W}_{i,\alpha}) + \mathbf{b}_{i,j,\alpha}) \right. \\ &\left. + a_{1,i,j}([\mathbf{F}_\alpha]_1(T_{\boldsymbol{\eta}_{i,j}} \mathbf{W}_{j,\alpha}) - [\mathbf{F}_\alpha]_1(T_{\boldsymbol{\eta}_{i,j}} \mathbf{W}_{i,\alpha}) + \mathcal{P}_{i,j,\alpha})) \right]_k \end{aligned}$$

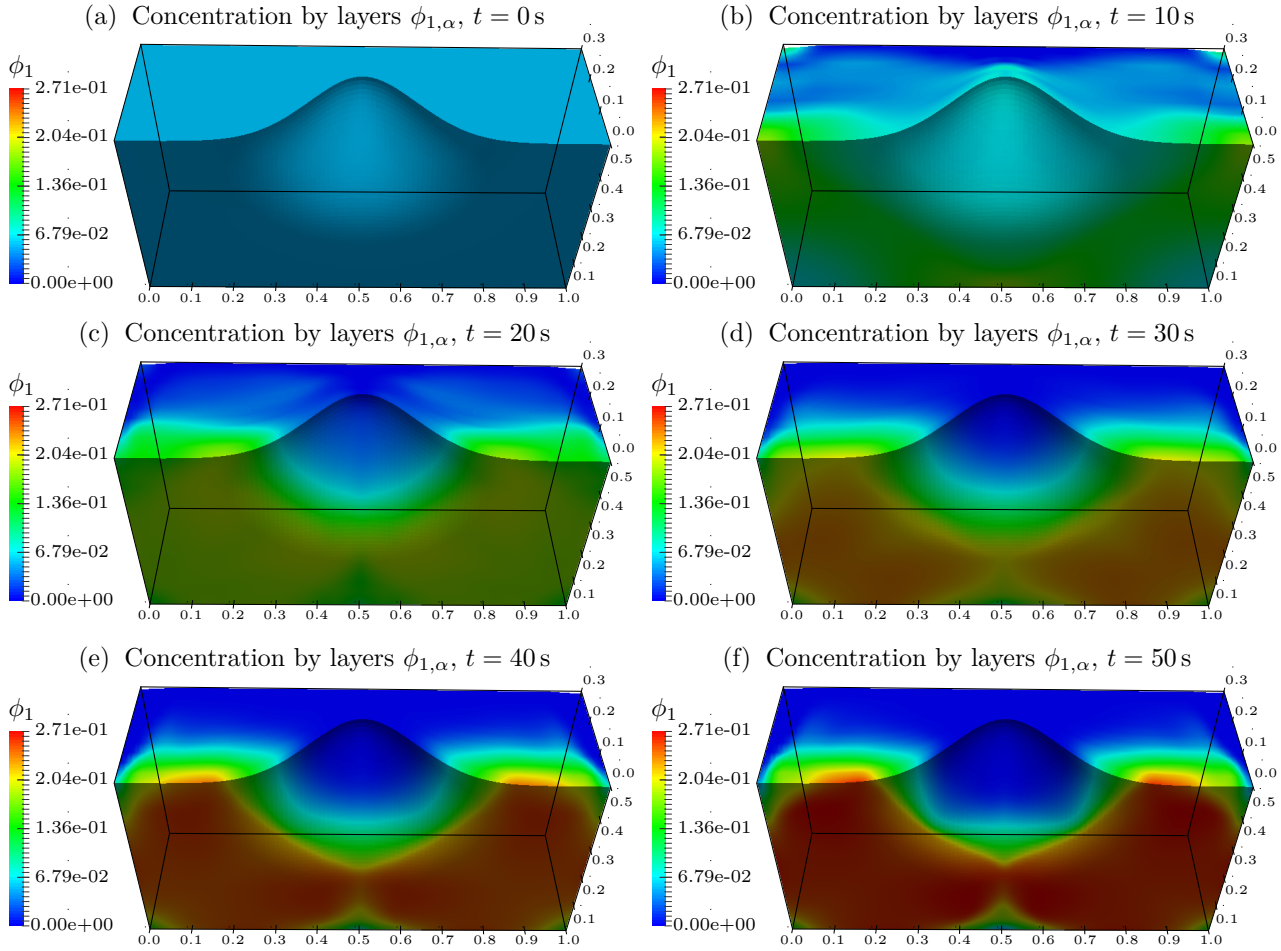


Figure 2.2: Test 2.1: Concentration of species 1 ( $\phi_1$ ) by color in a domain with a bump.

and for  $k = 3, \dots, N + 3$

$$[\mathcal{F}_{i,j,\alpha}]_k = [\mathcal{F}_{i,j,\alpha}]_1 \left( \frac{[T_{\eta_{i,j}} \mathbf{W}_{i,\alpha}]_k}{[T_{\eta_{i,j}} \mathbf{W}_{i,\alpha}]_1} \frac{1 + \text{sgn}([\mathcal{F}_{i,j,\alpha}]_1)}{2} + \frac{[T_{\eta_{i,j}} \mathbf{W}_{j,\alpha}]_k}{[T_{\eta_{i,j}} \mathbf{W}_{j,\alpha}]_1} \frac{1 - \text{sgn}([\mathcal{F}_{i,j,\alpha}]_1)}{2} \right).$$

The HLL-PVM-1U method is defined by the coefficients

$$a_{0,i,j} = \frac{S_{R,i,j}^n |S_{L,i,j}^n| - S_{L,i,j}^n |S_{R,i,j}^n|}{S_{R,i,j}^n - S_{L,i,j}^n}, \quad a_{1,i,j} = \frac{|S_{R,i,j}^n| - |S_{L,i,j}^n|}{S_{R,i,j}^n - S_{L,i,j}^n}.$$

The characteristic velocities  $S_{L,i,j}^n$  and  $S_{R,i,j}^n$  are global approximations of the minimum and maximum wave speed of the rotated system (2.6.9) obtained by neglecting the tangential terms, that is, by setting  $S_{\eta_{i,j}}^\perp = 0$ . In this case we obtain a 1D system evaluated at  $T_{\eta_{i,j}} \hat{\mathbf{W}}$  with an extra passive scalar corresponding to the tangential velocity. This extra field does not modify the maximum and minimum wave speeds of the 1D system. Then, taking into account the bound of the eigenvalues deduced in **Chapter 1** for the 1D system we define  $S_{L,i,j}$  and  $S_{R,i,j}$  as follows:

$$S_{L,i,j} := \bar{u}_{i,j}^n - \Psi_{i,j}^n, \quad S_{R,i,j} := \bar{u}_{i,j}^n + \Psi_{i,j}^n,$$

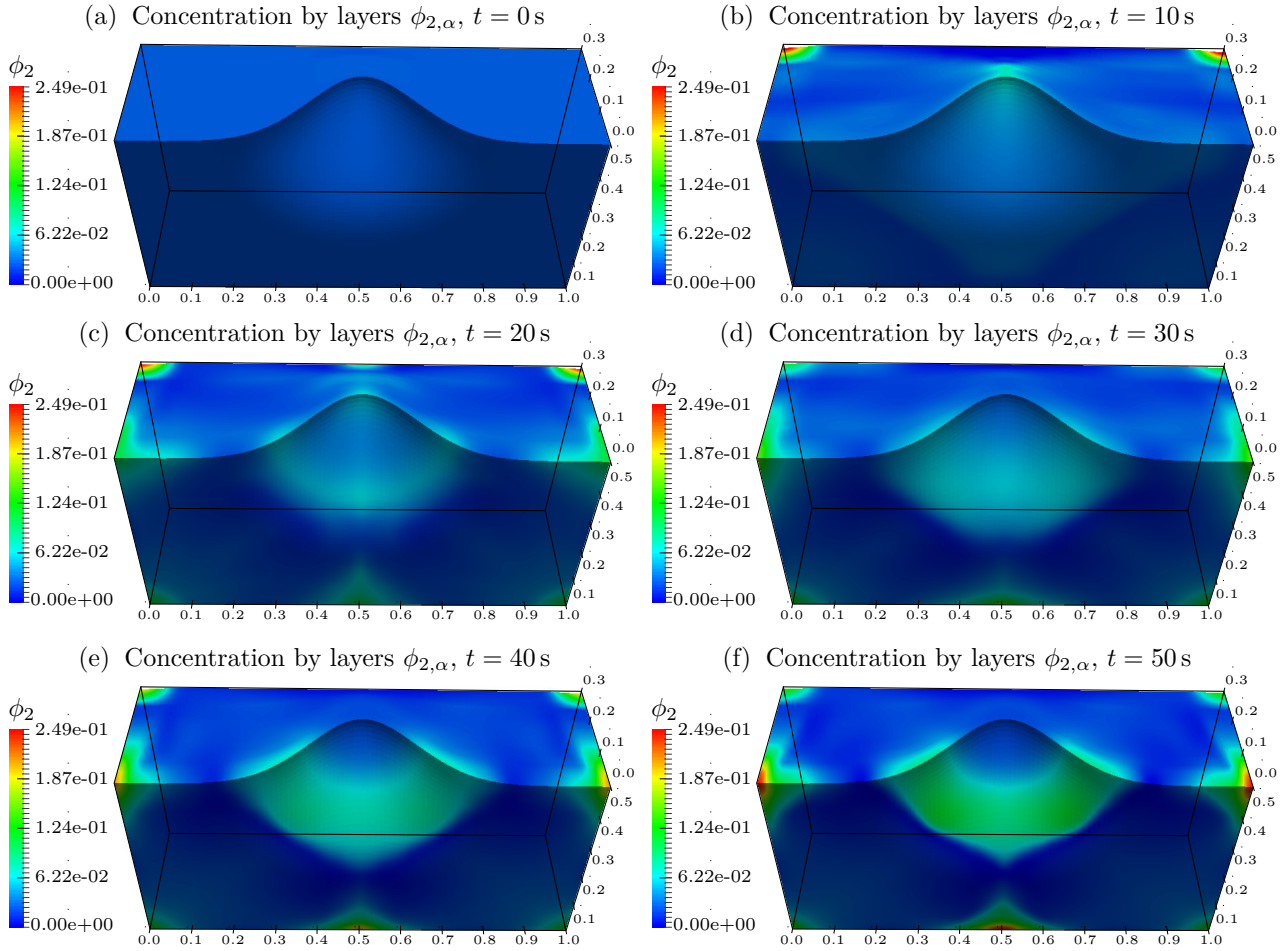


Figure 2.3: Test 2.1: Concentration of species 2 ( $\phi_2$ ) by color in a domain with a bump.

where

$$\bar{u}_{i,j}^n := \frac{1}{M} \sum_{\beta=1}^M \frac{1}{2} (\mathbf{u}_{\beta,i}^n + \mathbf{u}_{\beta,j}^n)^T \boldsymbol{\eta}_{i,j},$$

$$\Psi_{i,j}^n := \frac{2M-1}{\sqrt{2M(2M-1)}} \left( 2 \sum_{\beta=1}^M (\bar{u}_{i,j}^n - u_{\beta,i,j}^n)^2 + \frac{g(h_i^n + h_j^n)}{2\rho_0} \left( \rho_0 + \frac{1}{M} \sum_{\beta=1}^M (2\beta-1) \frac{\bar{\rho}_{\beta,i}^n + \bar{\rho}_{\beta,j}^n}{2} \right) \right)^{1/2}.$$

We define  $\mathcal{P}_{i,j,\alpha}$  to be zero for all components except for the second one. Specifically, we set

$$\mathcal{P}_{i,j,\alpha} = \left( g \frac{m_{i,\alpha}^n + m_{j,\alpha}^n}{2} (z_{B,j} + h_j^n - z_{B,i} - h_i^n) + g \frac{(h_i^n)^2 + (h_j^n)^2}{2} \left( \frac{l_\alpha}{2} + \sum_{\beta=\alpha+1}^M l_\beta \right) (\bar{\rho}_{\alpha,j}^n - \bar{\rho}_{\alpha,i}^n) \right.$$

$$\left. + g \frac{h_i^n + h_j^n}{2} \sum_{\beta=\alpha+1}^M l_\beta (m_{j,\beta}^n - m_{j,\alpha}^n + m_{i,\beta}^n - m_{i,\alpha}^n) \right) \mathbf{e}_{2,N+3},$$

$$\mathcal{G}_{i,j,\alpha}^\pm = \mathbf{U}_{i,j,\alpha\pm 1/2} G_{i,j,\alpha\pm 1/2} + \frac{1}{2} \mathcal{G}_{i,f-a,\alpha}^\pm (\mathbf{x}_{i,j} - \mathbf{x}_i)^T \boldsymbol{\eta}_{i,j},$$

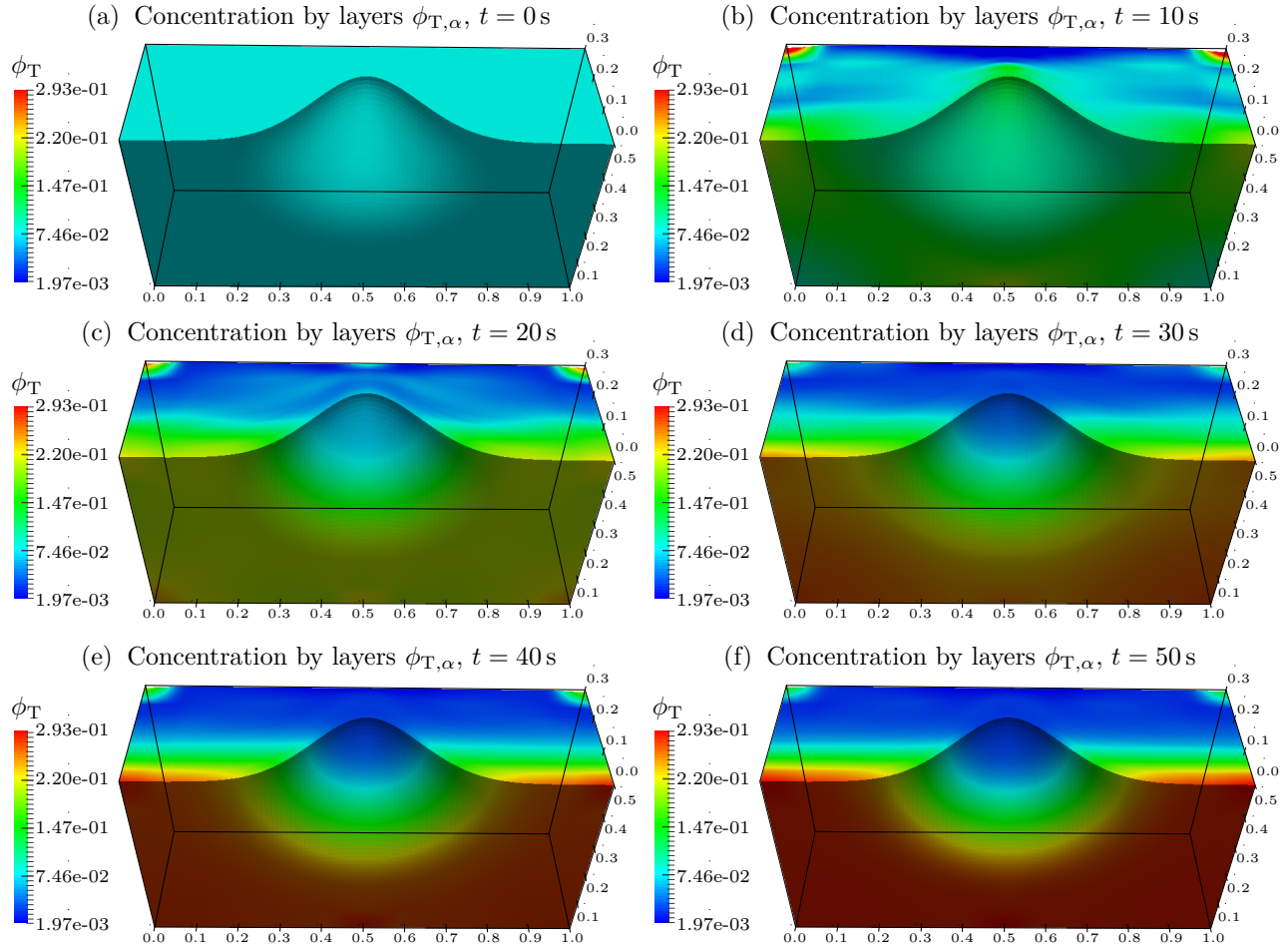


Figure 2.4: Test 2.1: Total concentration of solid particles,  $\phi_T = \phi_1 + \phi_2$  by color in a domain with a bump.

where

$$\begin{aligned} \mathbf{U}_{i,j,\alpha \pm 1/2} &= \frac{1}{4} (\mathbf{U}(\mathbf{T}_{\eta_{i,j}} \mathbf{W}_{i,\alpha}) + \mathbf{U}(\mathbf{T}_{\eta_{i,j}} \mathbf{W}_{j,\alpha}) + \mathbf{U}(\mathbf{T}_{\eta_{i,j}} \mathbf{W}_{i,\alpha+1}) + \mathbf{U}(\mathbf{T}_{\eta_{i,j}} \mathbf{W}_{j,\alpha+1})), \\ G_{i,j,\alpha+1/2} &= \frac{\tilde{\rho}_{i,j,\alpha+1/2}}{\rho_0} \sum_{\beta=1}^{\alpha} l_{\beta} \left( (\mathbf{R}_{j,\alpha} - \bar{\mathbf{R}}_j) - (\mathbf{R}_{i,\alpha} - \bar{\mathbf{R}}_i) \right) + \frac{G_{i,f-a,\alpha+1/2}}{2} (\mathbf{x}_{i,j} - \mathbf{x}_i)^T \boldsymbol{\eta}_{i,j}. \end{aligned}$$

By  $\mathcal{G}_{i,f-a,\alpha}^{\pm}$  and  $G_{i,f-a,\alpha+1/2}$  we denote any second-order approximation of  $\mathcal{G}_{f-a,\alpha}^{\pm}$  and  $G_{f-a,\alpha+1/2}$  at  $\mathbf{x}_i$ , respectively. Finally, in order to obtain a well-balanced finite volume solver we utilize the following definition of  $\mathbf{b}_{i,j,\alpha}$ ,

$$\mathbf{b}_{i,j,\alpha} = \left( \frac{\bar{\rho}_{i,\alpha}^n + \bar{\rho}_{j,\alpha}^n}{2} (z_{B,j} - z_{B,i}) \right) \mathbf{e}_{1,N+3}.$$

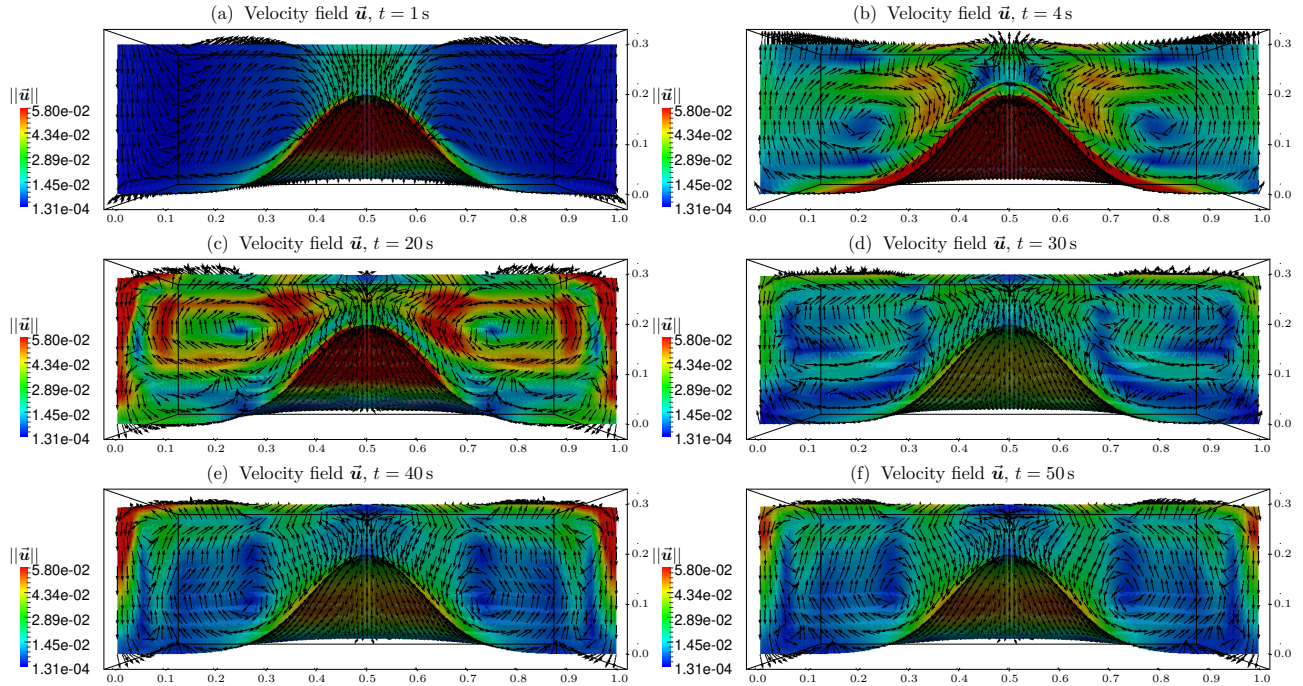


Figure 2.5: Test 2.1: Velocity field of the mixture over magnitude of the velocity.

## 2.7 Numerical tests

In the following numerical simulations we use the global acceleration of gravity constants  $g = 9.8 \text{ m/s}^2$ ,  $\phi_{\max} = 0.68$  (the (nominal) maximal total solids volume fraction), and employ the Richardson-Zaki hindered settling factor (2.2.10) with  $n_{\text{RZ}} = 4.7$ . The viscosity and density of the pure fluid are  $\mu_0 = 0.02416 \text{ Pa s}$  and  $\rho_0 = 1208 \text{ kg/m}^3$ , respectively,  $\eta = \eta(\phi)$  is the concentration-dependent viscosity defined by  $\eta(\phi) := \mu_0(1.0 - \phi/0.95)^{-\beta}$ ,  $\beta = 2.5$ . Other parameters in (2.2.5) are set  $\sigma_0 = 0.22 \text{ Pa}$ ,  $\alpha = 5$  and the gel point  $\phi_c = 0.1$ . In all tests the particles are assumed to have the same density  $\rho_1 = \dots = \rho_N = 2790 \text{ kg/m}^3$ .

### 2.7.1 Test 2.1: bidisperse sedimentation in a domain with a bump

In Test 2.1 we are interested in studying the behavior of a mixture with  $N = 2$  different solid species dispersed in a viscous fluid with a viscosity  $\mu_0$ . In this first test we consider  $\mathbf{T}^E = \sigma_e = 0$  (without viscous stress tensor and without compression). The solid particle diameters are  $d_1 = 4.96 \times 10^{-4} \text{ m}$  and  $d_2 = 3.25 \times 10^{-4} \text{ m}$  respectively. The discretization of the domain is given by  $100 \times 100$  cells and  $M = 10$  layers in the horizontal and vertical directions, respectively. The bottom elevation is given by

$$z_B(x, y) = \exp(-40((x - 0.5)^2 + (y - 0.5)^2)) \text{ m}$$

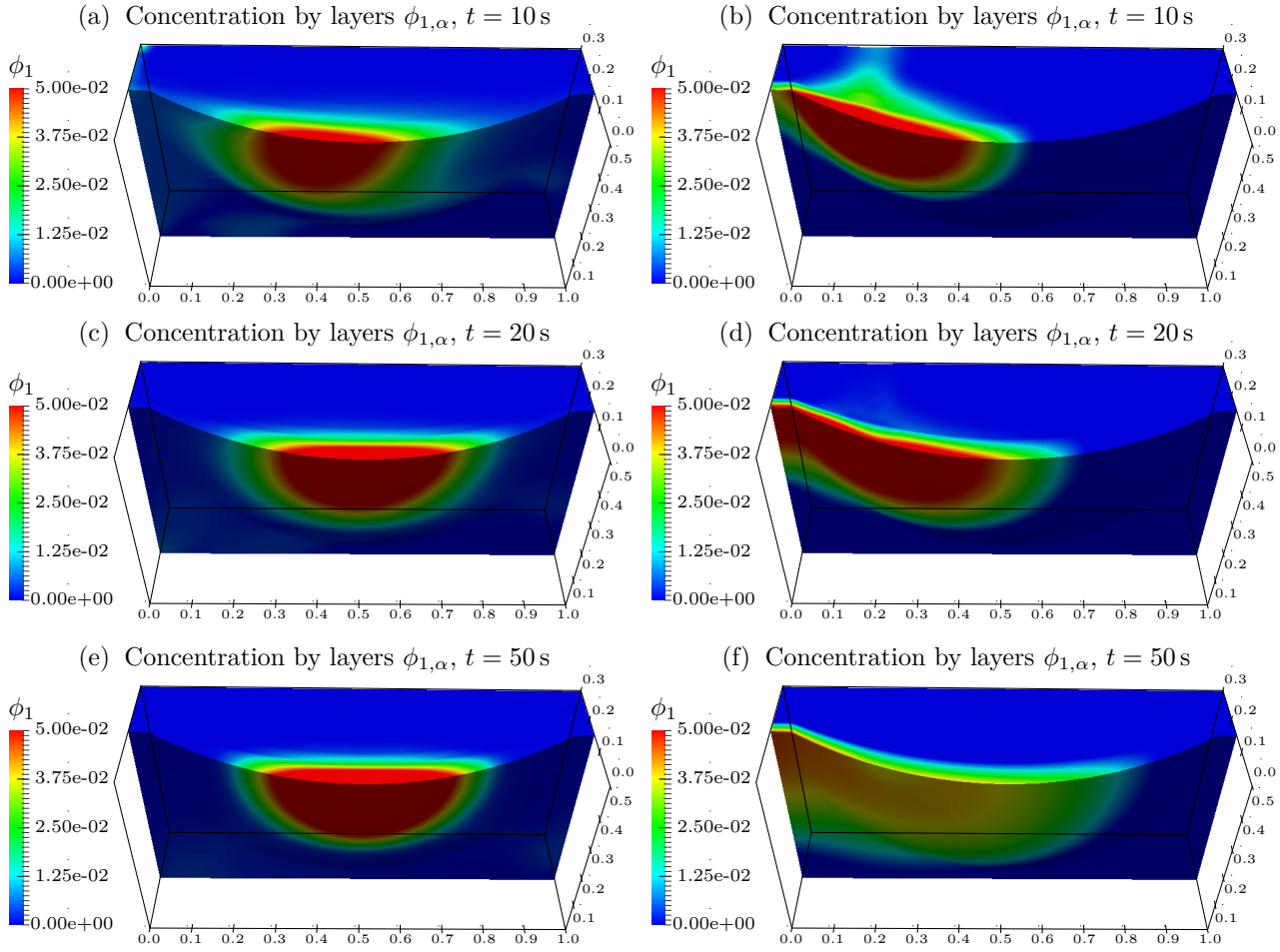


Figure 2.6: Test 2.2: Concentration of species 1 ( $\phi_1$ ) by color in a 3D domain with compression and viscous stress tensor deactivated (left) versus concentration of species 1 with stress tensor and compression terms activated (right).

for  $(x, y) \in [0, 1] \times [0, 1]$ . For  $\alpha = 1, \dots, M$ , the initial condition for the concentrations and the horizontal velocities are given by

$$\phi_{1,\alpha}(0, x, y) = 0.05, \quad \phi_{2,\alpha}(0, x, y) = 0.025, \quad u_\alpha(0, x, y) = 0, \quad (x, y) \in [0, 1] \times [0, 1].$$

The initial height is  $h(0, x, y) = 0.3 - z_B(x, y)$ . Furthermore, as boundary condition we impose a closed basin.

In Figures 2.2, 2.3 and 2.4 we present the numerical results of the concentrations each species,  $\phi_1$  and  $\phi_2$ , and the total concentration, respectively. This simulation is a three-dimensional version of [20, Test 1.2]. In Figure 2.2 high concentrations of species 1 can be observed since the bigger particles are deposited rapidly over the bottom around the bump. In Figure 2.3 we see how some fine particles remain in suspension close to the wall. At larger simulated times the smaller particles begin to settle and occupy zones where the concentration of species 1 is small, as can be seen in Figure 2.2 (f) and Figure 2.3 (f) at time  $t = 50$  s. The joint behavior of all particles dispersed in the fluid is displayed

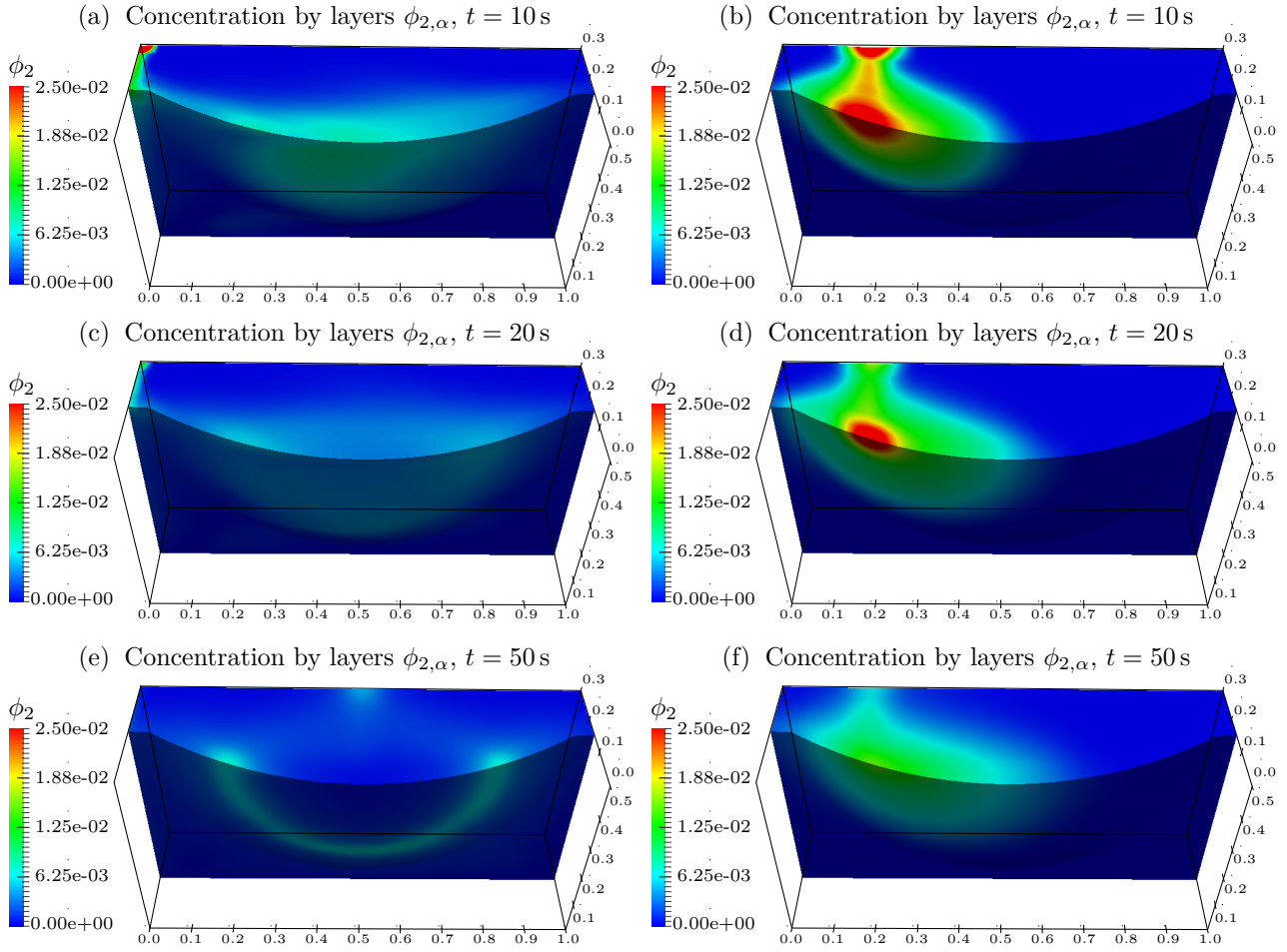


Figure 2.7: Test 2.2: Concentration of species 2 ( $\phi_2$ ) by color in a 3D domain with compression and viscous stress tensor deactivated (left) versus concentration of species 2 with stress tensor and compression terms activated (right).

in Figure 2.4. Here the global sedimentation process can be seen and we can see as the particles are deposited on the bottom around the bump but some fine particles (species 2) are kept in suspension at short times.

The velocity field of the mixture and its magnitude is presented in Figure 2.5 at different times. The movement of the mixture is a natural consequence of the movement of the particles. Some important recirculations can be seen around the bump. At larger times the velocity decreases and the particles settle more easily.

### 2.7.2 Test 2.2: cylindrical dam break

In this second numerical simulation we compare the behavior of the bidisperse sedimentation process with compression and mixture viscosity with the same mixture without compression and mixture viscosity in a paraboloid domain. To this we simulate a dam break problem over a paraboloid bottom

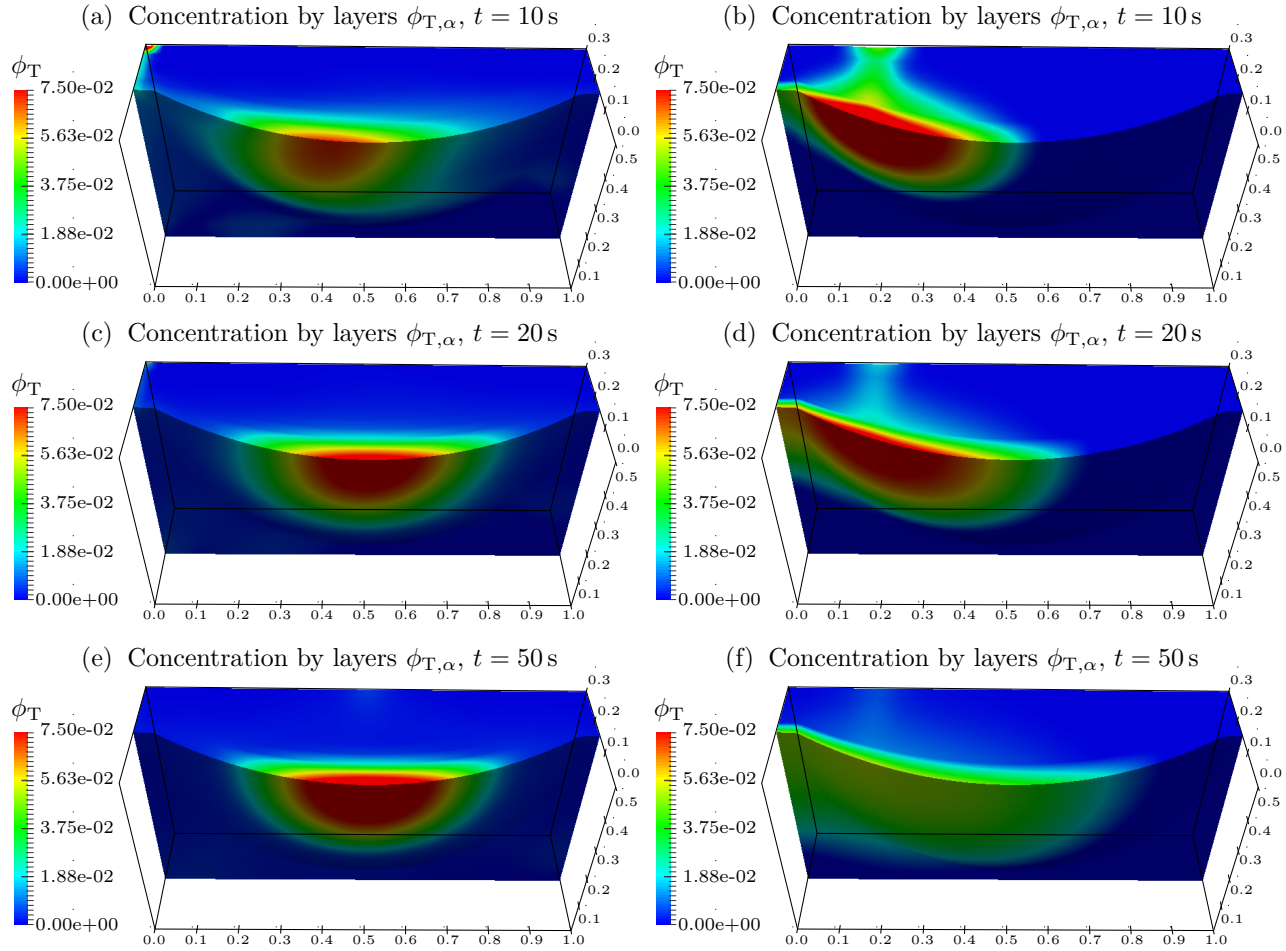


Figure 2.8: Test 2.2: Total concentration of solid particles  $\phi_T = \phi_1 + \phi_2$  by color in a 3D domain with compression and viscous stress tensor deactivated (left) versus total concentration of solid particles with stress tensor and compression terms activated (right).

given by

$$z_B(x, y) = \begin{cases} 0.71((x - 0.5)^2 + (y - 0.5)^2) & \text{for } (x - 0.5)^2 + (y - 0.5)^2 \leq 0.21, \\ 0.15 & \text{otherwise,} \end{cases} \quad (x, y) \in [0, 1] \times [0, 1].$$

The diameters of the solid particles are as in Test 2.1. Here we use a rectangular grid of  $100 \times 100$  cells in the horizontal directions and  $M = 10$  layers in the vertical direction. For all  $\alpha = 1, \dots, M$  the initial condition is given by

$$\phi_{1,\alpha}(0, \mathbf{x}) = \begin{cases} 0.05 & \text{for } (x - 0.2)^2 + (y - 0.5)^2 \leq 0.1, \\ 0 & \text{otherwise,} \end{cases} \quad \mathbf{u}_\alpha(0, \mathbf{x}) = 0,$$

$$\phi_{2,\alpha}(0, \mathbf{x}) = \begin{cases} 0.025 & \text{for } (x - 0.2)^2 + (y - 0.5)^2 \leq 0.1, \\ 0 & \text{otherwise,} \end{cases}$$

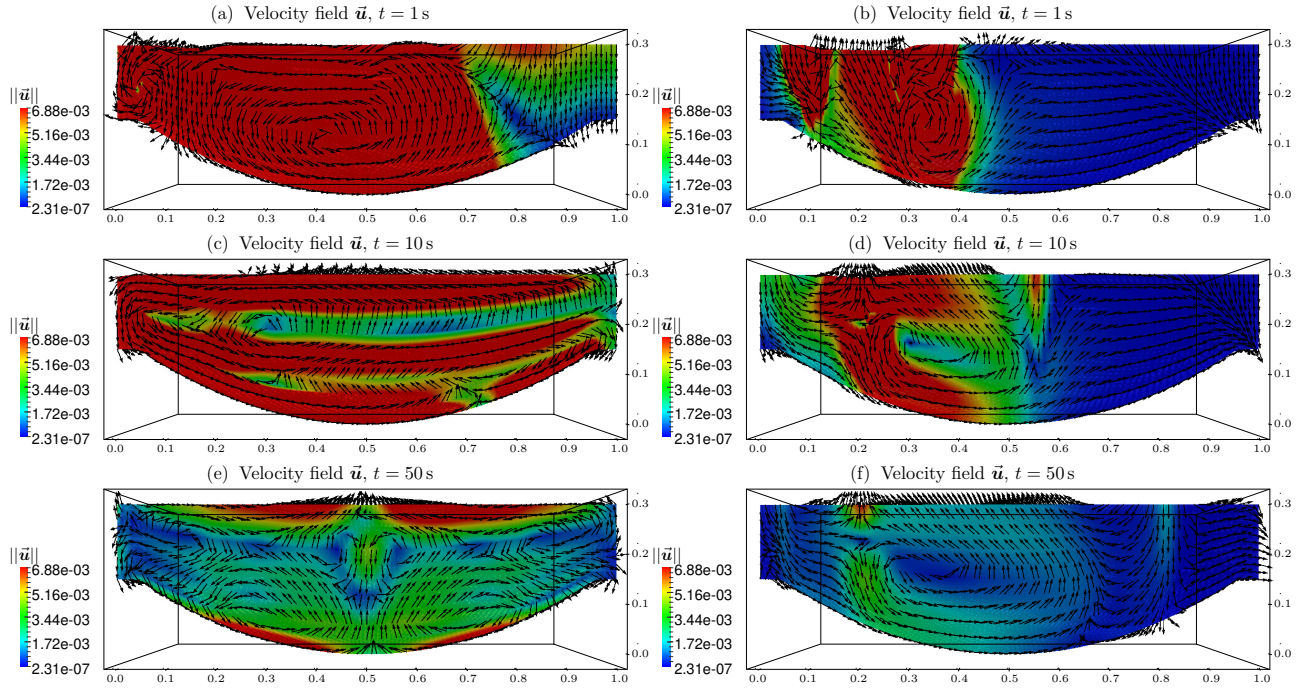


Figure 2.9: Test 2.2: Velocity field of mixture over her magnitud by color. Comparison between a mixture with compression and viscous stress tensor deactivated (left) versus a mixture with stress tensor and compression terms activated (right).

and for the height  $h(0, x, y) = 0.3 - z_B(x, y)$ . Figures 2.6, 2.7, 2.8 and 2.9 show the comparison between a simulation without compression and mixture viscosity Case 1 (left) and with them Case 2 (right) for bigger particles  $\phi_1$  (species 1), fine particles  $\phi_2$  (species 2), for the total concentration  $\phi_T$  and for the velocity field of the mixture. The first that we can see is that in both cases the bigger particles go down faster than of the small particles, furthermore the small particles go to zones of the domain where the concentration of the bigger particles is small (Figure 2.6 (a), (c), (e) and Figure 2.7 (b), (d), (f), respectively). As we can see in Case 1 (left) in Figures 2.6, 2.7 and 2.8 (plots (a), (c) and (e) in each case), the movement of the solid particles in the mixture is oscillating for short times and from  $t = 50$  s the solid particles almost stop and from this time on the velocity field begins to be nearly symmetrical (see Figure 2.9 (a), (c), (e)). In Case 1 the solid particles move freely in the mixture. Instead, if we activate the compression and mixture viscosity terms (viscous stress) we can see from Figures 2.6, 2.7 and 2.8 (plots (b), (d) and (f) in each case) how the movement of the each solid species is slower than the Case 1, the reason is because for  $\phi$  bigger than the gel point  $\phi_c$  the particles begin to compress and on the other hand when the concentration increases the viscosity of the mixture also increases, then the movement of the solid particles begins to be more dense than of the first case. In this Case 2 (right) the solid particles do not move oscillatorily as we can see in Figures 2.6, 2.7 and 2.8 (plots (b), (d) and (f) in each case). Finally, we comment that the velocity field is still not symmetrical at time  $t = 50$  s (see Figure 2.9 (b), (d), (f)). The mixture of Case 2 (right) moves with more difficulties than the mixture of Case 1.

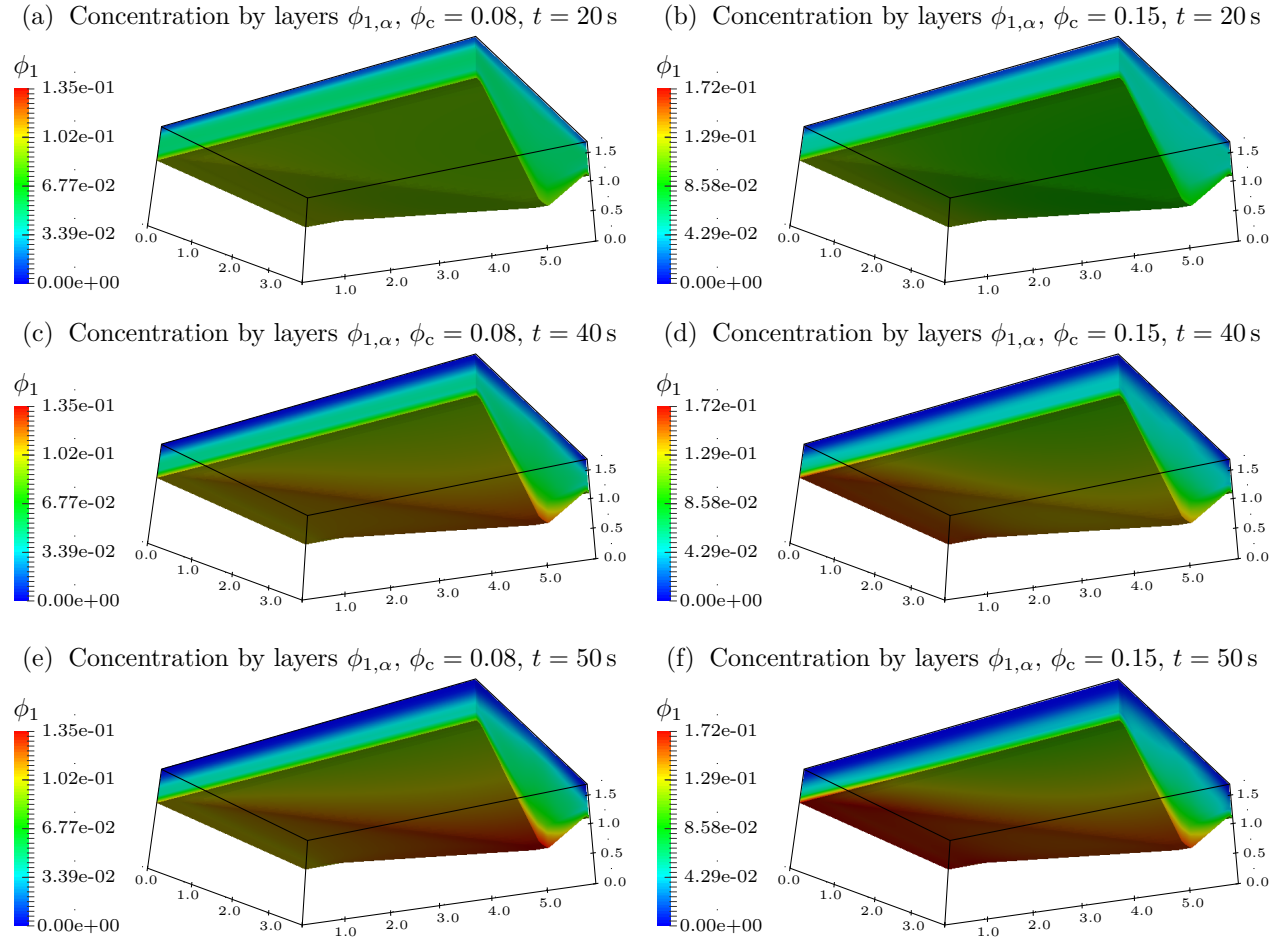


Figure 2.10: Test 2.4: Concentration of species 1 ( $\phi_1$ ) by color with gel point  $\phi_c = 0.08$  (left) versus concentration of species 1 with gel point  $\phi_c = 0.15$  (right).

### 2.7.3 Test 2.3: bidisperse sedimentation process in real bathymetry for different gel point.

In the following numerical simulation we examine the behavior of the mixture when the gel point  $\phi$  is varied. To this we simulate a bi-bidisperse sedimentation process in a real configuration with compression and viscosity mixture terms activated. The bathymetry for this numerical simulation is given by

$$z_B(x, y) = \begin{cases} 1.1 & \text{for } 0 \leq x < 0.4, 0 \leq y \leq 4, \\ 1.1 & \text{for } 0.4 \leq x \leq 5.8 - a, 0 \leq y < a, \\ -\frac{1.1}{1.875-a}(y - a) + 1.1 & \text{for } 0.4 \leq x \leq 5.8 - a, a \leq y < \mathcal{L}_1, \\ -\frac{1.1}{5.3}(x - 0.4) + 1.1 & \text{for } 0.4 \leq x \leq 5.8 - a, \mathcal{L}_1 \leq y \leq \mathcal{L}_2, \\ -\frac{1.1}{(2.125-(4-a))}(y - (4 - a)) + 1.1 & \text{for } 0.4 \leq x \leq 5.8 - a, \mathcal{L}_2 < y \leq 4 - a, \\ 1.1 & \text{for } 0.4 \leq x \leq 5.8 - a, 4 - a < y \leq 4, \\ z_B(5.8 - a, y) & \text{for } 5.8 - a < x \leq 5.8, 0 \leq y \leq 4, \end{cases} \quad (2.7.1)$$

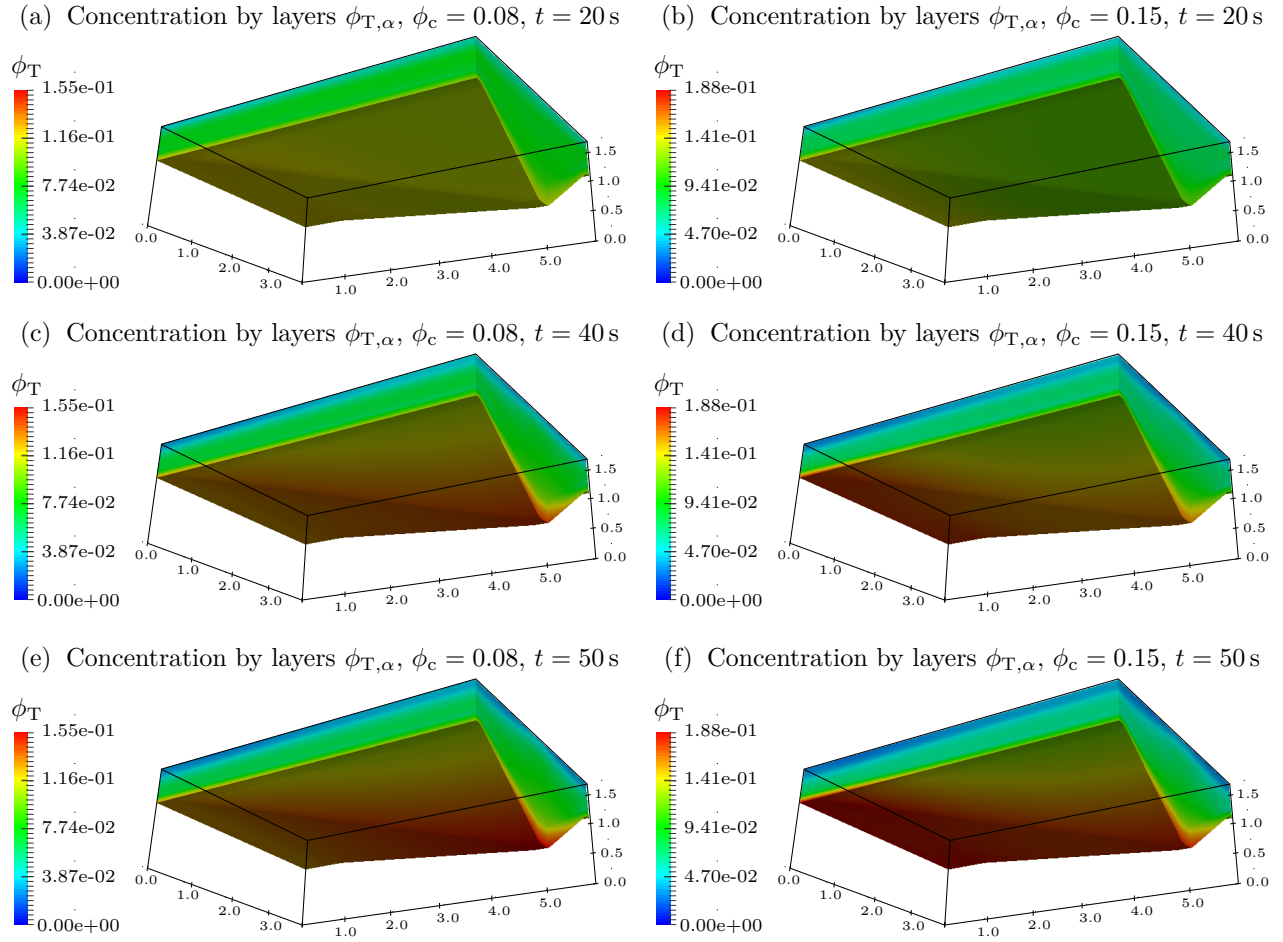


Figure 2.11: Test 2.4: Total concentration of solid species  $\phi_T$  with gel point  $\phi_c = 0.08$  (left) versus total concentration of solid species with gel point  $\phi_c = 0.15$  (right).

where the lines are given by  $\mathcal{L}_1 : y = \frac{1.875-a}{5.3}(x - 0.4) + a$ ,  $\mathcal{L}_2 : y = \frac{2.125-(4-a)}{5.3}(x - 0.4) + 4 - a$  and the parameter  $a = 0.116$ . For  $\alpha = 1, \dots, M$ , the initial condition is the same that we have used in numerical Test 2.1,

$$\phi_{1,\alpha}(0, x, y) = 0.05, \quad \phi_{2,\alpha}(0, x, y) = 0.025, \quad u_\alpha(0, x, y) = 0, \quad (x, y) \in [0, 5.8] \times [0, 4].$$

For the height  $h(0, x, y) = 1.7 - z_B(x, y)$  m. In this numerical simulation we only analyze the total concentration of the mixture Figure 2.11 and the concentration of the bigger particles in the mixture Figure 2.10 since it is for difficult to see differences in the behavior of the small particles dispersed in the mixture. In Figures 2.10 and 2.11 we can see the behavior of each species for different gel points,  $\phi_c = 0.08$  (left) and  $\phi_c = 0.15$  (right). Note that for small times when the compression is deactivated (before  $\phi_c = 0.08$ ) there is no difference in the concentrations. We will show only times when  $\phi_c \geq 0.08$ . In this figure we can see that when the gel point is small, the particles begin to compress before they settle, and the movement of these particles is slow and they move with difficulties in the horizontal direction. This means that when we activate the gel point  $\phi_c = 0.08$  the particles essentially settle and with difficulties move horizontally. They begin to compress anticipatedly (see Figure 2.10 (left), 2.11).

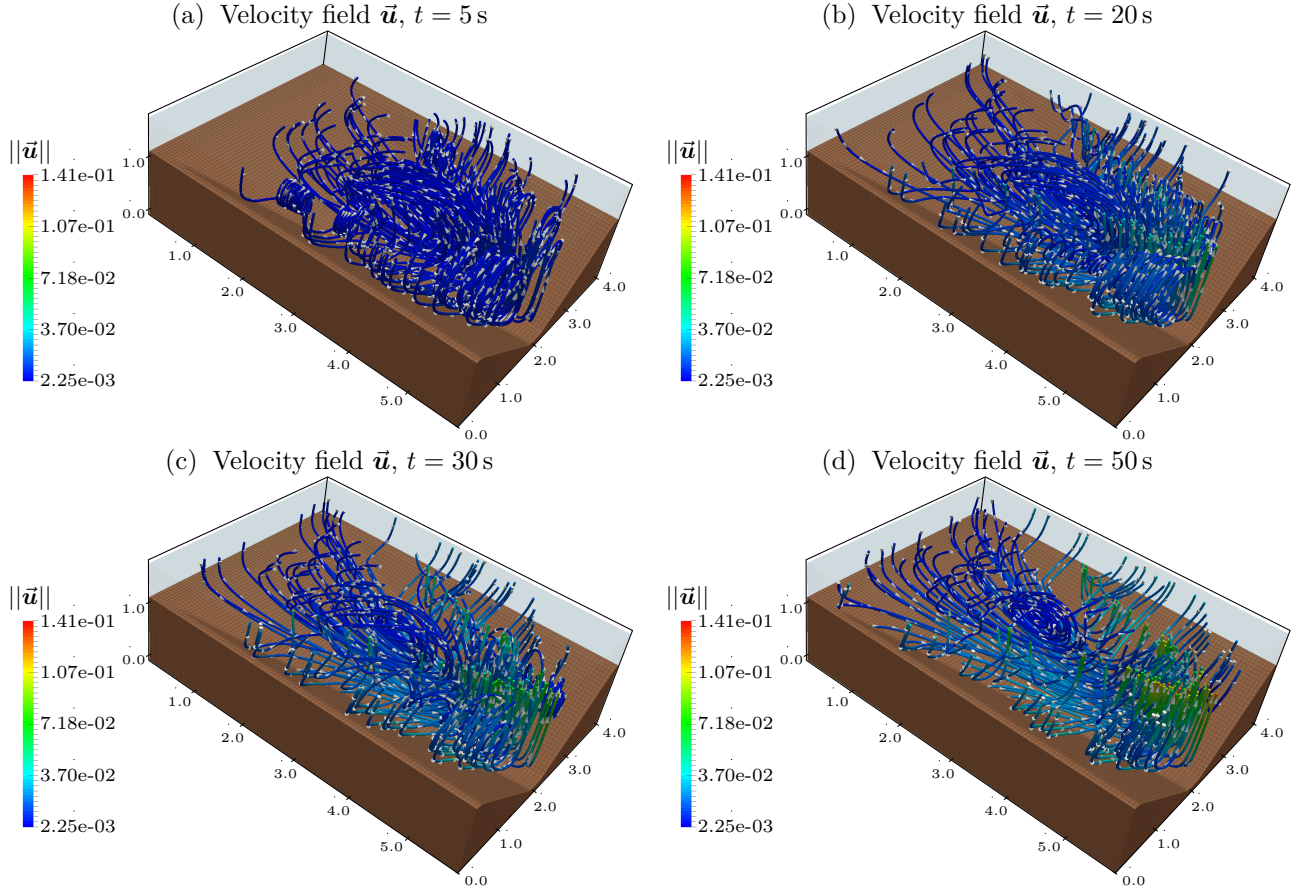


Figure 2.12: Test 2.4: Velocity field of the mixture with gel point  $\phi_c = 0.15$ .

On the other hand, when we active the gel point later  $\phi_c = 0.15$ , first the particles settle faster than in the case before (see Figure 2.10 (b), (d) and (e)), and after the particles have settled they begin to compress and the movement of the particles begins to be more slow. We need to be careful with this comparison because if we see the equalities (2.2.5) keeping constant  $\sigma_0$  we can observe two effects when  $\phi_c$  increases, first the compression starts later and the capacity of compression is smaller than when the  $\phi_c$  is small. Finally, Figure 2.12 shows the velocity field of the mixture only for gel point  $\phi_c = 0.15$  at some times, here we can see several recirculations at least one for each slope on the bottom.

#### 2.7.4 Test 2.4: bidisperse sedimentation process in real bathymetry with different $\sigma_0$

The last numerical simulation shows a bidisperse sedimentation of the same mixture before (same diameters, densities, species), and initial and boundary conditions are as in Test 2.3. The bottom is given by (2.7.1). Here we keep constant the gel point  $\phi_c = 0.1$  and study the behavior of the mixture when the parameter  $\sigma_0$  in (2.2.5) is varied. This term represent the force or capacity of compression, it is clear from (2.2.5) that when  $\sigma_0$  is increased,  $\sigma_e$  increases as well (keeping constant the gel point). When the compression term is deactivated all species settle faster than when the compression term is

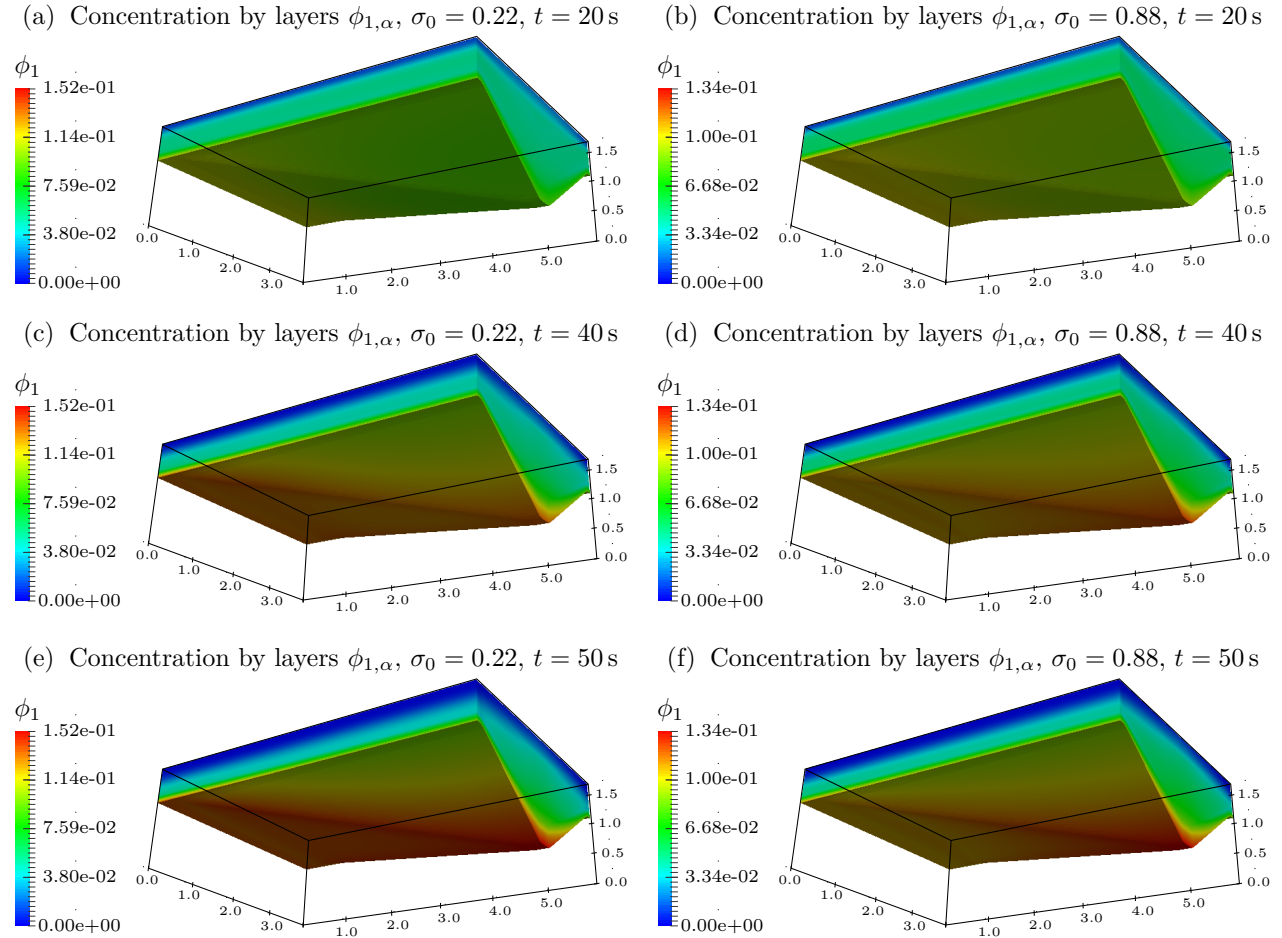


Figure 2.13: Test 2.4: Concentration of species 1 ( $\phi_1$ ) by color with  $\sigma_0 = 0.22$  (left) versus  $\sigma_0 = 0.88$  (right) with a fixed gel point  $\phi_c = 0.1$ .

activated and they move to the deepest zone. On the other hand, as we can see in Figures 2.13 and 2.14 with  $\sigma_0 = 0.22$  (left) and  $\sigma_0 = 0.88$  (right) if we active the compression term the particles begin to move with more difficulty to the deepest zone. In Figures 2.13 and 2.14 (b), (d), (f) for  $\sigma_0 = 0.88$  we can see that the maximum of the concentration is smaller than of the maximum concentration for  $\sigma_0 = 0.22$ .

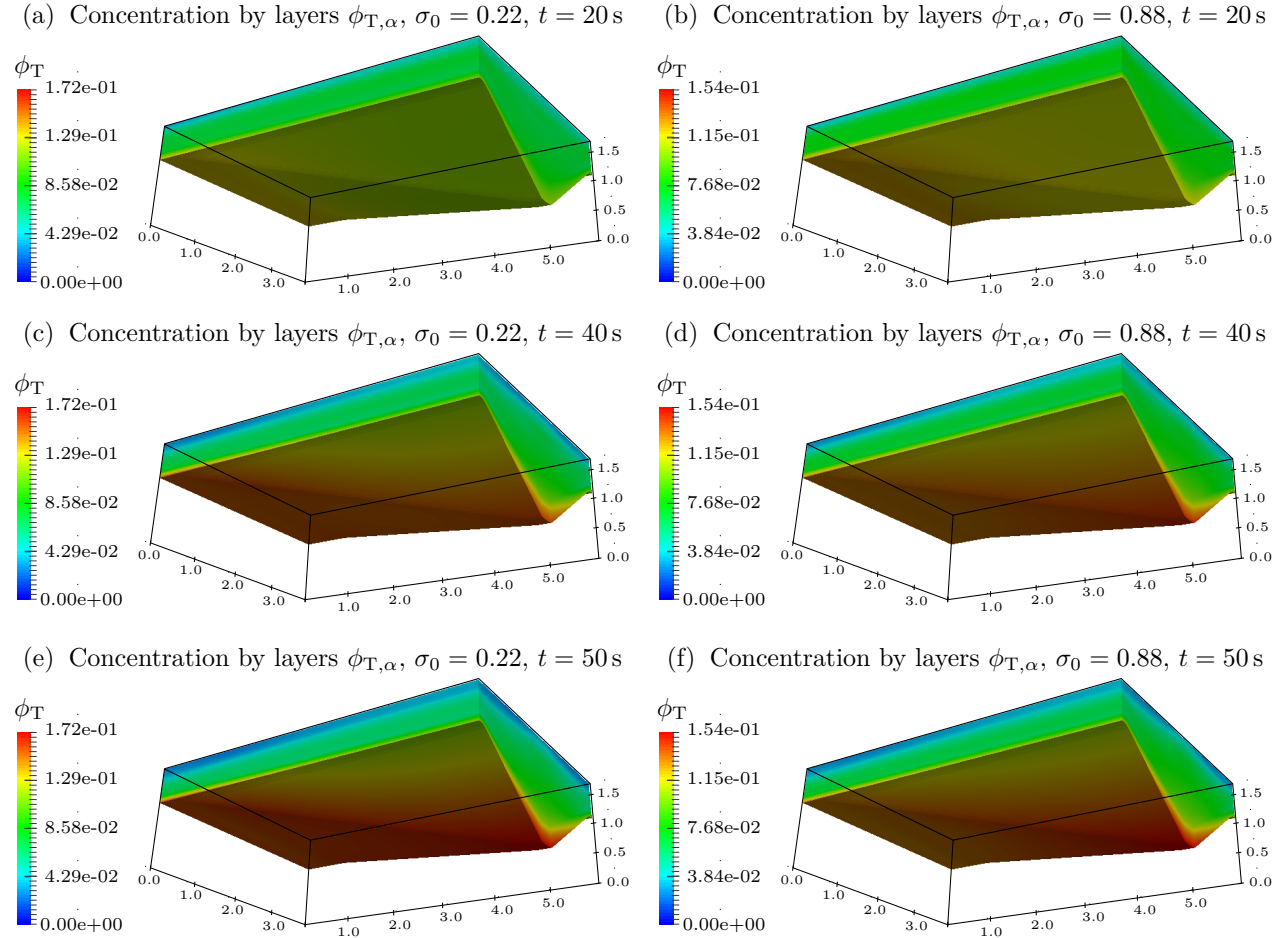


Figure 2.14: Test 2.4: Total concentration of solid species  $\phi_T = \phi_1 + \phi_2$  by color with  $\sigma_0 = 0.22$  (left) versus  $\sigma_0 = 0.88$  (right) with a fixed gel point  $\phi_c = 0.1$ .

# CHAPTER 3

---

## Multilayer shallow water model for polydisperse sedimentation with non-hydrostatic pressure

---

### 3.1 Introduction

This chapter is devoted to show ongoing work on a natural extension of the model presented in Chapter 1 to non-hydrostatic effects. To this end, as in previous chapters, we assume that the fluid contains finely dispersed solid particles that belong to a finite number of species ( $N$ ) differing in size and density. Here, we will not consider sediment compressibility and mixture viscosity. We extend the multilayer model for polydisperse sedimentation deduced in Chapter 1 to non-hydrostatic pressure.

We introduce the non-hydrostatic pressure as a deviation of the hydrostatic pressure as follows:

$$p_T(x, z, t) = p_0(x, t) + \int_z^{z_{M+1/2}} g \rho(s) ds + \Pi(x, z, t),$$

where  $p_0$  and  $\Pi$  are the pressure at free surface and the non-hydrostatic part of the pressure, respectively. This total pressure is inserted in the linear momentum equation of the mixture (see [13, 42, 43]). The multilayer model presented in this chapter has been deduced following some ideas introduced in [41] to approximate the Euler equations. In contrast, in this chapter we deduce the multilayer version of the coupled multilayer shallow water system with polydisperse sedimentation model.

The final multilayer model with non-hydrostatic pressure is given by  $M(4+N)$  equations for the mass of the mixture, velocity field, and concentrations of all solid species in each layer, plus  $M$  equations by vertical velocity at the center of each layer. These last  $M$  equations allow us to close the multilayer system. The unknowns of the model are the mass of the mixture  $m_\alpha$  and the velocity field  $\mathbf{u}_\alpha$ ,  $\bar{w}_\alpha$  in each layer, the concentrations of the solid species in each layer  $\phi_{j,\alpha}$ , and the non-hydrostatic pressure at each interface  $\Pi_{\alpha+1/2}$ . The model derived in this chapter has the form of a system of conservation laws with non-conservative products suitable to design numerical method to solve numerically. Finally, we comment that the design of numerical schemes for this model is an ongoing work.

## 3.2 Mathematical model

### 3.2.1 Mass and linear balance equations

The mathematical model arises following the theory of mixtures developed by Truesdell and Toupin (1957), which we allow us to consider the mixture as a superposition of continuous media, so the  $N \in \mathbb{N}$  species of spherical solid particles dispersed in a viscous fluid satisfies the mass and linear momentum balance equations. From **Chapter 2**, equations (2.2.1) we have

$$\begin{aligned}\partial_t(\rho_j \phi_j) + \nabla \cdot (\rho_j \phi_j \mathbf{v}_j) &= 0, \\ \partial_t(\rho_j \phi_j \mathbf{v}_j) + \nabla \cdot (\rho_j \phi_j \mathbf{v}_j \otimes \mathbf{v}_j) &= \nabla \cdot \mathbf{T}_j - \rho_j \phi_j g \mathbf{k} + \mathbf{m}_j^f + \mathbf{m}_j^s,\end{aligned}\quad j = 0, \dots, N,$$

where for each solid species  $j$ ,  $j = 1, \dots, N$ , we denote by  $\phi_j$ ,  $\rho_j$ ,  $\mathbf{v}_j = (u_j, v_j, w_j)^T \in \mathbb{R}^3$  its volumetric concentration, density and the phase velocity, respectively. The horizontal and vertical component of the velocity field are  $(u_j, v_j) \in \mathbb{R}^2$  and  $w_j \in \mathbb{R}$ , respectively. The stress tensor of particle species  $j$  is denoted by  $\mathbf{T}_j$ ,  $\mathbf{m}_j^f$  is the interaction forces per unit volume between solid species  $j$  and the fluid,  $\mathbf{m}_j^s = \mathbf{m}_{j1}^s + \dots + \mathbf{m}_{jN}^s$  and  $\mathbf{m}_{ji}^s$  are the particle-particle interaction terms of species  $j$  and the interaction forces per unit volume between the solid species  $j$  and  $i$ , respectively. For the fluid, indexed by  $j = 0$  we have  $\mathbf{m}_0^f = -\mathbf{m}_1^f - \dots - \mathbf{m}_N^f$  and  $\mathbf{m}_0^s = 0$ . Using the definitions (2.2.4) for  $\mathbf{T}_j$  and (2.2.6) for  $\mathbf{m}_j^f$  and the same considerations made on  $\mathbf{m}_j^s$  in **Chapter 1** and **Chapter 2** after to discard the effective stress tensor  $\sigma_e$  and the viscous stress tensor  $\mathbf{T}_j^E$  that model the sediment compressibility and mixture viscosity, respectively. Then, we obtain the following mathematical model

$$\begin{aligned}\partial_t(\rho_j \phi_j) + \nabla \cdot (\rho_j \phi_j \mathbf{v}_j) &= 0, \\ \partial_t(\rho_j \phi_j \mathbf{v}_j) + \nabla \cdot (\rho_j \phi_j \mathbf{v}_j \otimes \mathbf{v}_j) &= -\phi_j \nabla p - \rho_j \phi_j g \mathbf{k} + \alpha_j \mathbf{u}_j,\end{aligned}\quad j = 0, \dots, N, \quad (3.2.1)$$

where  $\mathbf{u}_j := \mathbf{v}_j - \mathbf{v}_0$  is the solid-fluid relative velocity and following [9, 46, 48] the resistance coefficient for the transfer of momentum between the fluid and solid phase species  $j$  satisfies  $\phi_j/\alpha_j(\Phi) = -d_j^2 V(\phi)/18\mu_0$ , where  $\mu_0$  is the viscosity of the pure fluid,  $d_j$  is the diameter of solid particle  $j$  and  $V(\phi)$  is the hindered settling factor given by (1.2.12)

$$V(\phi) = \begin{cases} (1 - \phi)^{n_{RZ}-2} & \text{for } \phi \leq 1, \\ 0 & \text{for } \phi > 1, \end{cases} \quad n_{RZ} > 2,$$

that satisfies  $V(\phi) > 0$  and  $V'(\phi) < 0$  for  $0 < \phi < \phi_{\max}$ . This expression is known as Richardson-Zaki function (see [56]). Of course, as in **Chapter 1** and **Chapter 2**, the system (3.2.1) allows us to recover the global mass and linear momentum balance equations of the mixture, namely

$$\partial_t \rho + \nabla \cdot (\rho \mathbf{v}) = 0, \quad \partial_t(\rho \mathbf{v}) + \nabla \cdot (\rho \mathbf{v} \otimes \mathbf{v}) = \nabla \cdot \Sigma + \rho \mathbf{b}, \quad (3.2.2)$$

where, using the diffusion velocities  $\mathbf{u}_j^d := \mathbf{v}_j - \mathbf{v}$ , the stres tensor of equations (3.2.2) is given by

$$\Sigma := -p \mathbf{I} - \sum_{j=0}^N \rho_j \phi_j \mathbf{u}_j^d \otimes \mathbf{u}_j^d.$$

Defining the total density  $\rho$  of the mixture and the mass-average velocity field  $\mathbf{v}$  of the mixture as in previous chapters by

$$\begin{aligned}\rho &:= \rho(\Phi) := \rho_0\phi_0 + \rho_1\phi_1 + \cdots + \rho_N\phi_N, \\ \mathbf{v} &:= (u, v, w)^T := \frac{1}{\rho} \sum_{m=0}^N \rho_m \phi_m \mathbf{v}_m = \frac{1}{\rho} \left[ \left( \rho - \sum_{j=1}^N \rho_j \phi_j \right) \mathbf{v}_0 + \sum_{k=1}^N \rho_k \phi_k \mathbf{v}_k \right],\end{aligned}\quad (3.2.3)$$

and the slip velocity  $\mathbf{u}_j$  without compression terms as in (1.2.13) by

$$\mathbf{u}_j = \mu \delta_j V(\phi) (\bar{\rho}_j - \bar{\rho}^T \Phi) \mathbf{k}, \quad j = 1, \dots, N, \quad (3.2.4)$$

and noticing that from equality (1.2.4) of **Chapter 1**

$$\rho_j \phi_j \mathbf{v}_j = \rho_j \phi_j (\mathbf{u}_j + \mathbf{v} - (\lambda_1 \mathbf{u}_1 + \cdots + \lambda_N \mathbf{u}_N)), \quad j = 1, \dots, N, \quad (3.2.5)$$

we can get the final form of the mathematical model of the system (3.2.1). This derivation is summarized in the following section.

### 3.2.2 Final form of the model

To obtain the mathematical model, from system (3.2.1) simply we need to introduce the equality (3.2.5) in the mass equations of system (3.2.1) and use the definition (3.2.4) for the slip velocities. Summarizing, the final model is given by the mass balance equations of the solid particles and the linear momentum balance equation of the mixture. The model is given by

$$\partial_t (\rho_j \phi_j) + \nabla \cdot (\rho_j \phi_j \mathbf{v} + \rho_j f_j^M(\Phi) \mathbf{k}) = 0, \quad j = 0, \dots, N, \quad (3.2.6)$$

and summing from  $j = 0$  to  $j = N$  the linear momentum balance equations from (3.2.1), we get

$$\partial_t \left( \sum_{j=0}^N \rho_j \phi_j \mathbf{v}_j \right) + \nabla \cdot \left( \sum_{j=0}^N \rho_j \phi_j \mathbf{v}_j \otimes \mathbf{v}_j \right) = -\nabla p - \rho g \mathbf{k}, \quad (3.2.7)$$

$\rho$  and  $\mathbf{v}$  are given by equalities (3.2.3), the vertical fluxes of with modified MLB model of (3.2.6) are

$$f_j^M(\Phi) := \phi_j v_j^{\text{MLB}} = \phi_j \mu V(\phi) \left( \delta_j (\bar{\rho}_j - \bar{\rho}^T \Phi) - \sum_{k=1}^N \lambda_k \delta_k (\bar{\rho}_k - \bar{\rho}^T \Phi) \right), \quad j = 1, \dots, N,$$

with  $\lambda_k = \rho_k \phi_k / \rho$ ,  $\bar{\rho}_k = \rho_k - \rho_0$  for  $k = 1, \dots, N$  and the vector  $\bar{\rho} := (\bar{\rho}_1, \dots, \bar{\rho}_N)^T$ . From here so on we will denote the pressure of equation (3.2.7) by  $p_T$ , furthermore

$$p_T(x, z, t) = p_0(x, t) + \int_z^{z_{M+1/2}} g \rho(s) ds + \Pi(x, z, t), \quad (3.2.8)$$

where we denote by  $\Pi(x, z, t)$  the deviation of the pressure from the hydrostatic counterpart and  $p_0$  the pressure at free surface.

### 3.3 Multilayer model with non-hydrostatic pressure

In this section we present some ingredients following the **Chapter 1**, to get the multilayer version of the system of partial differential equations integrated with the equations (3.2.6), (3.2.7) and with the non-hydrostatic pressure (3.2.8). To this, we will need to use the Definition 1.3.1 from **Chapter 1** which give us the framework to compute the mass and linear momentum jump conditions through the interfaces  $\Gamma_{\alpha+1/2}$  (see **Preliminaries** for notation). While we have considered that the viscous stress tensor it has been discarded, we comment here that the viscous stress tensor must be considered to get the correct multilayer model, the reason is for that there is a close relationship between the jump condition of this tensor with the jump condition of the velocity field as we can see in **Chapter 1** equality (1.3.16). So, in this section we will consider the viscous stress tensor temporally, i.e., the stress tensor  $\mathbf{T}$  will be considered as

$$\mathbf{T} = -p_T \mathbf{I} + \mathbf{T}^E,$$

then, the linear momentum balance equation of the mixture (3.2.7) can be written as

$$\partial_t \left( \sum_{j=0}^N \rho_j \phi_j \mathbf{v}_j \right) + \nabla \cdot \left( \sum_{j=0}^N \rho_j \phi_j \mathbf{v}_j \otimes \mathbf{v}_j \right) = \nabla \cdot \mathbf{T} - \rho g \mathbf{k}. \quad (3.3.1)$$

#### 3.3.1 Mass and linear momentum jump conditions

As in the previous chapters, in this section we summarize the mass and linear momentum jump conditions through the interfaces (0.1.1). First, as we have commented previously in this chapter, if we leave out sediment compressibility (from **Chapter 1** equality (1.2.14) or **Chapter 2**) equality (2.2.12) we get that the horizontal velocities of each species are equal to the horizontal velocities of the mixture, i.e,  $\mathbf{u}_{j,\alpha} = \mathbf{u}_\alpha$ . As in previous chapters we have the following assumption,

**Assumption 3.3.1.** *We assume that the layer thicknesses are small enough to neglect the dependence of the horizontal velocities and the concentration of each species on the vertical variable inside each layer, i.e.,*

$$\partial_z \mathbf{u}_\alpha = 0, \quad \partial_z \phi_{j,\alpha} = 0.$$

*Then, the vertical velocity is piecewise linear in  $z$ . This means that  $\partial_z w_{j,\alpha} = d_{j,\alpha}(t, \mathbf{x})$  for smooth functions  $d_{j,\alpha}(t, \mathbf{x})$ .*

In light of Assumption 3.3.1, the limits for the horizontal velocities of the mixture and of the concentrations are given by

$$\mathbf{u}_{\alpha-1/2}^+(t, \mathbf{x}) = \mathbf{u}_{\alpha+1/2}^-(t, \mathbf{x}) = \mathbf{u}_\alpha(t, \mathbf{x}) \quad \text{and} \quad \phi_{j,\alpha-1/2}^+(t, \mathbf{x}) = \phi_{j,\alpha+1/2}^-(t, \mathbf{x}) = \phi_{j,\alpha}(t, \mathbf{x}). \quad (3.3.2)$$

Then the mass jump condition (1.3.6) implies that the limits of the normal mass flux for species  $j$  at  $\Gamma_{\alpha+1/2}(t)$  satisfy

$$G_{j,\alpha+1/2} := G_{j,\alpha+1/2}^- = G_{j,\alpha+1/2}^+, \quad j = 0, 1, \dots, N, \quad (3.3.3)$$

where

$$\begin{aligned} G_{j,\alpha+1/2}^+ &:= \rho_j \phi_{j,\alpha+1} (\partial_t z_{\alpha+1/2} + \mathbf{u}_{\alpha+1} \cdot \nabla_{\mathbf{x}} z_{\alpha+1/2} - w_{j,\alpha+1/2}^+), \\ G_{j,\alpha+1/2}^- &:= \rho_j \phi_{j,\alpha} (\partial_t z_{\alpha+1/2} + \mathbf{u}_\alpha \cdot \nabla_{\mathbf{x}} z_{\alpha+1/2} - w_{j,\alpha+1/2}^-), \end{aligned} \quad (3.3.4)$$

The mass jump condition of the mixture can be deduced from equalities (3.3.3) and (3.3.4). This yields

$$G_{\alpha+1/2} = G_{\alpha+1/2}^- = G_{\alpha+1/2}^+, \quad (3.3.5)$$

where the limits  $G_{\alpha+1/2}^-$ ,  $G_{\alpha+1/2}^+$  from (3.3.5) are given by

$$\begin{aligned} G_{\alpha+1/2}^+ &:= \bar{\rho}_{\alpha+1} (\partial_t z_{\alpha+1/2} + \mathbf{u}_{\alpha+1} \cdot \nabla_{\mathbf{x}} z_{\alpha+1/2} - w_{\alpha+1/2}^+), \\ G_{\alpha+1/2}^- &:= \bar{\rho}_\alpha (\partial_t z_{\alpha+1/2} + \mathbf{u}_\alpha \cdot \nabla_{\mathbf{x}} z_{\alpha+1/2} - w_{\alpha+1/2}^-). \end{aligned} \quad (3.3.6)$$

For  $j = 0, \dots, N$ , the relationship between  $G_{j,\alpha+1/2}$  and  $G_{\alpha+1/2}$  is given as in **Chapter 1**, equation (1.3.10)

$$G_{j,\alpha+1/2} = \tilde{\phi}_{j,\alpha+1/2} G_{\alpha+1/2} - \rho_j \tilde{f}_{j,\alpha+1/2}, \quad (3.3.7)$$

where we define the averages

$$\tilde{\phi}_{j,\alpha+1/2} := \frac{1}{2} \left( \frac{\rho_j \phi_{j,\alpha+1}}{\bar{\rho}_{\alpha+1}} + \frac{\rho_j \phi_{j,\alpha}}{\bar{\rho}_\alpha} \right), \quad \tilde{f}_{j,\alpha+1/2} = \frac{1}{2} (f_{j,\alpha+1/2}^+ + f_{j,\alpha+1/2}^-). \quad (3.3.8)$$

Using the mass jump condition (3.3.3), we can get the following jump condition through each interface  $\Gamma_{\alpha+1/2}(t)$ , for  $j = 0, \dots, N$

$$[(\rho_j \phi_j \mathbf{v}_j; \rho_j \phi_j \mathbf{v}_j \otimes \mathbf{v}_j)]_{t,\alpha+1/2} \cdot (\partial_t z_{\alpha+1/2}, \nabla_{\mathbf{x}} z_{\alpha+1/2}, -1)^T = G_{j,\alpha+1/2} [\mathbf{v}_j]_{t,\alpha+1/2}.$$

Then, the linear momentum jump condition (1.3.2) can be written as

$$[\mathbf{T}]_{t,\alpha+1/2} \cdot \boldsymbol{\eta}_{\alpha+1/2} = \frac{1}{\sqrt{1 + |\nabla_{\mathbf{x}} z_{\alpha+1/2}|^2}} \sum_{j=0}^N G_{j,\alpha+1/2} [\mathbf{v}_j]_{t,\alpha+1/2},$$

which allows us to achieve that the jump condition is satisfied by the viscous stress tensor at each interface  $\Gamma_{\alpha+1/2}(t)$ . For  $\alpha = 1, \dots, M-1$  the jump condition for the viscous stress tensor is given by

$$\mathbf{T}_{\alpha+1/2}^{E,\pm} \boldsymbol{\eta}_{\alpha+1/2} = \tilde{\mathbf{T}}_{\alpha+1/2}^E \boldsymbol{\eta}_{\alpha+1/2} \pm \frac{1}{2} \frac{1}{\sqrt{1 + |\nabla_{\mathbf{x}} z_{\alpha+1/2}|^2}} \sum_{j=0}^N G_{j,\alpha+1/2} [\mathbf{v}_j]_{t,\alpha+1/2}, \quad (3.3.9)$$

where  $\mathbf{T}_{\alpha+1/2}^{E,\pm}$  is given by

$$\tilde{\mathbf{T}}_{\alpha+1/2}^E = \frac{1}{2} (\mathbf{T}_{\alpha+1/2}^{E,+} + \mathbf{T}_{\alpha+1/2}^{E,-}).$$

This quantity represents an approximation of the viscous stress tensor  $\mathbf{T}^E$  at each interface  $\Gamma_{\alpha+1/2}(t)$ , that satisfies the jump condition (1.3.2) (see for some details Section 1.3.3 and Section 2.4.2 from **Chapter 1** and **Chapter 2**, respectively). Equation (3.3.9) gives a very important relation between the viscous stress tensor and the velocity field and as we have said before, an essential property to get correct multilayer model.

### 3.3.2 Integration of the mass balance equation

To get the multilayer version of the mass balance equation (3.2.6), we follow Section 1.4 of **Chapter 1**, so the integral form of the mass balance equations (see for details Section 1.4) from (1.4.1) is given, for all  $\alpha = 0, \dots, M$  and  $j = 0, 1, \dots, N$  by

$$\begin{aligned} 0 &= \int_{\Omega_\alpha(t)} (\partial_t(\rho_j \phi_j) + \nabla_{\mathbf{x}} \cdot (\rho_j \phi_j \mathbf{v}_j)) \varphi \, d\Omega \\ &= \int_{I_F(t)} \varphi(t, \mathbf{x}) \left( \partial_t \left( \int_{z_{\alpha-1/2}}^{z_{\alpha+1/2}} \rho_j \phi_j \, dz \right) + \nabla_{\mathbf{x}} \cdot \left( \int_{z_{\alpha-1/2}}^{z_{\alpha+1/2}} (\rho_j \phi_j \mathbf{u}) \, dz \right) - \rho_j \phi_{j,\alpha} \partial_t z_{\alpha+1/2} \right. \\ &\quad \left. - \rho_j \phi_{j,\alpha} \mathbf{u}_{\alpha+1/2}^- \cdot \nabla_{\mathbf{x}} z_{\alpha+1/2} + \rho_j \phi_{j,\alpha} w_{j,\alpha+1/2}^- + \rho_j \phi_{j,\alpha} \partial_t z_{\alpha-1/2} \right. \\ &\quad \left. + \rho_j \phi_{j,\alpha} \mathbf{u}_{\alpha-1/2}^+ \cdot \nabla_{\mathbf{x}} z_{\alpha-1/2} - \rho_j \phi_{j,\alpha} w_{j,\alpha-1/2}^+ \right) \, d\mathbf{x} \end{aligned}$$

for all  $\varphi(t, \cdot) \in L^2(I_F(t))$ . Using Assumption 3.3.1 along with equalities (3.3.2) we get

$$\begin{aligned} 0 &= \int_{I_F(t)} \varphi(t, \mathbf{x}) \left( \partial_t(\rho_j \phi_{j,\alpha} h_\alpha) + \nabla_{\mathbf{x}} \cdot (\rho_j \phi_{j,\alpha} h_\alpha \mathbf{u}_\alpha) - \rho_j \phi_{j,\alpha} \partial_t z_{\alpha+1/2} - \rho_j \phi_{j,\alpha} \mathbf{u}_\alpha \cdot \nabla_{\mathbf{x}} z_{\alpha+1/2} \right. \\ &\quad \left. + \rho_j \phi_{j,\alpha} w_{j,\alpha+1/2}^- + \rho_j \phi_{j,\alpha} \partial_t z_{\alpha-1/2} + \rho_j \phi_{j,\alpha} \mathbf{u}_\alpha \cdot \nabla_{\mathbf{x}} z_{\alpha-1/2} - \rho_j \phi_{j,\alpha} w_{j,\alpha-1/2}^+ \right) \, d\mathbf{x}, \end{aligned} \quad (3.3.10)$$

then, according to definitions (3.3.4), the multilayer version of the mass balance equations (3.2.6) arises as a particular solution of the integral form (3.3.10). This is

$$\partial_t(\rho_j \phi_{j,\alpha} h_\alpha) + \nabla_{\mathbf{x}} \cdot (\rho_j \phi_{j,\alpha} h_\alpha \mathbf{u}_\alpha) = G_{j,\alpha+1/2} - G_{j,\alpha-1/2}, \quad (3.3.11)$$

where  $G_{j,\alpha+1/2}$  represents the mass transfer of species  $j$  through the interface  $\Gamma_{\alpha+1/2}(t)$ . Furthermore, as in previous chapters using (3.3.7) with the averages (3.3.8), the mass equation of each solid species (3.3.11) can be written as

$$\begin{aligned} \partial_t(\rho_j \phi_{j,\alpha} h_\alpha) + \nabla_{\mathbf{x}} \cdot (\rho_j \phi_{j,\alpha} h_\alpha \mathbf{u}_\alpha) &= \tilde{\phi}_{j,\alpha+1/2} G_{\alpha+1/2} - \tilde{\phi}_{j,\alpha-1/2} G_{\alpha-1/2} \\ &\quad - \rho_j (\tilde{f}_{j,\alpha+1/2} - \tilde{f}_{j,\alpha-1/2}). \end{aligned} \quad (3.3.12)$$

for  $j = 0, \dots, N$ . The multilayer model will consider the solid mass conservation equations (3.3.12) (i.e.,  $j = 1, \dots, N$ ) plus the sum of all of them.

### 3.3.3 Integration of the momentum conservation equation

To get the multilayer version of the momentum balance equation (3.3.1), we follow Section 1.4 from **Chapter 1**, but here, we extend Assumption 1.4.1 to non-hydrostatic pressure. Unlike the previous assumption on (1.4.2), here we consider test functions  $\boldsymbol{\vartheta} = (\boldsymbol{\vartheta}_h, \vartheta_z)^T$  with  $\boldsymbol{\vartheta}_h = \boldsymbol{\vartheta}_h(t, \mathbf{x})$ ,  $\vartheta_z = \vartheta_z(t, \mathbf{x})$  both independent of  $z$  and  $\boldsymbol{\vartheta}|_{\partial I_F} = 0$ . In previous chapters, under hydrostatic pressure Assumption 1.4.1, the vertical component of the momentum equation of the mixture is reduced to hydrostatic property  $\partial_z p = \rho g$ . In contrast, here we get an equation for the vertical velocity of the

mixture. For  $\alpha = 1, \dots, M$ , from equations (1.4.1) we have that

$$\begin{aligned} & \int_{\Omega_\alpha(t)} \left( \sum_{j=0}^N \rho_j \partial_t (\phi_{j,\alpha} \mathbf{v}_{j,\alpha}) \cdot \boldsymbol{\vartheta} \right) d\Omega + \int_{\Omega_\alpha(t)} \left( \sum_{j=0}^N \rho_j \nabla \cdot (\phi_{j,\alpha} \mathbf{v}_{j,\alpha} \otimes \mathbf{v}_{j,\alpha}) \cdot \boldsymbol{\vartheta} \right) d\Omega \\ &= \int_{\Omega_\alpha(t)} p_{T,\alpha} \nabla \cdot \boldsymbol{\vartheta} d\Omega - \int_{\Omega_\alpha(t)} \mathbf{T}_\alpha^E : \nabla \boldsymbol{\vartheta} d\Omega + \int_{\Gamma_{\alpha-1/2}(t)} (\mathbf{T}_{\alpha-1/2}^+ \boldsymbol{\vartheta}^T) \cdot \boldsymbol{\eta}_{\alpha-1/2} d\Gamma \\ &\quad - \int_{\Gamma_{\alpha+1/2}(t)} (\mathbf{T}_{\alpha+1/2}^- \boldsymbol{\vartheta}^T) \cdot \boldsymbol{\eta}_{\alpha+1/2} d\Gamma - \int_{\Omega_\alpha(t)} g \rho_\alpha \mathbf{k} \cdot \boldsymbol{\vartheta} d\Omega, \end{aligned} \quad (3.3.13)$$

where, from equation (3.2.8),  $p_{T,\alpha} = p_\alpha + \Pi_\alpha$ , where  $p_\alpha$  and  $\Pi_\alpha$  are the multilayer versions of the hydrostatic and non-hydrostatic counterpart of the pressure, respectively. In light of Assumption 3.3.1, the hydrostatic pressure is given as in Assumption 1.4.1 by

$$p_\alpha(t, \mathbf{x}, z) = p_0 + g \sum_{\beta=\alpha+1}^M \rho_\beta h_\beta + \rho_\alpha g(z_{\alpha+1/2} - z).$$

Taking into account definition (0.1.2) for  $\Omega_\alpha(t)$  from **Preliminaries**, Assumption 3.3.1, the independence of  $z$  of  $\boldsymbol{\vartheta}$  and writing (3.3.13) as  $\mathcal{I}_1 + \mathcal{I}_2 = \mathcal{I}_3 + \mathcal{I}_4 + \mathcal{I}_5 + \mathcal{I}_6 + \mathcal{I}_7$ , where  $\mathcal{I}_1, \dots, \mathcal{I}_7$  stand for each of the signed integrals of (3.3.13), we obtain

$$\mathcal{I}_1 = \int_{I_F} \left( h_\alpha \partial_t (\rho_\alpha \mathbf{u}_\alpha) \cdot \boldsymbol{\vartheta}_h + \int_{z_{\alpha-1/2}}^{z_{\alpha+1/2}} \partial_t (\rho_\alpha w_\alpha) \vartheta_z dz \right) d\mathbf{x},$$

and using Leibniz's rule for differentiation under the integral, we get that

$$\int_{z_{\alpha-1/2}}^{z_{\alpha+1/2}} \partial_t (\rho_\alpha w_\alpha) \vartheta_z dz = \left( \partial_t \left( \rho_\alpha \int_{z_{\alpha-1/2}}^{z_{\alpha+1/2}} w_\alpha dz \right) - \rho_\alpha (w_{\alpha+1/2}^- \partial_t z_{\alpha+1/2} - w_{\alpha-1/2}^+ \partial_t z_{\alpha-1/2}) \right) \vartheta_z,$$

moreover, under Assumption 3.3.1 we have a linear profile for  $w_\alpha$  inside each layer, such that

$$\int_{z_{\alpha-1/2}}^{z_{\alpha+1/2}} w_\alpha dz = h_\alpha \bar{w}_\alpha.$$

Therefore,  $\mathcal{I}_1$  can be written as follows:

$$\mathcal{I}_1 = \int_{I_F} \left( h_\alpha \partial_t (\rho_\alpha \mathbf{u}_\alpha) \cdot \boldsymbol{\vartheta}_h + \partial_t (\rho_\alpha h_\alpha \bar{w}_\alpha) - \rho_\alpha (w_{\alpha+1/2}^- \partial_t z_{\alpha+1/2} - w_{\alpha-1/2}^+ \partial_t z_{\alpha-1/2}) \right) \vartheta_z d\mathbf{x}. \quad (3.3.14)$$

**Remark 3.3.1.** From equation (1.2.14) or (2.2.12) without sediment compressibility we can conclude that the horizontal velocities of the each solid species coincide with the horizontal velocities of the mixture at each layer. Furthermore, keeping this in mind we can get

$$\mathbf{v}_{j,\alpha} \otimes \mathbf{v}_{j,\alpha} = \begin{bmatrix} \mathbf{u}_\alpha \otimes \mathbf{u}_\alpha & w_{j,\alpha} \mathbf{u}_\alpha \\ w_{j,\alpha} \mathbf{u}_\alpha^T & w_{j,\alpha}^2 \end{bmatrix}.$$

Considering Remark 3.3.1,  $\mathcal{I}_2$  can be written as

$$\begin{aligned}
\mathcal{I}_2 &= \int_{\Omega_\alpha(t)} \nabla \cdot \left( \sum_{j=0}^N \rho_j \phi_j \begin{bmatrix} \mathbf{u}_\alpha \otimes \mathbf{u}_\alpha & w_{j,\alpha} \mathbf{u}_\alpha \\ w_{j,\alpha} \mathbf{u}_\alpha^\top & w_{j,\alpha}^2 \end{bmatrix} \right) \boldsymbol{\vartheta} \, dz \, d\mathbf{x} \\
&= \int_{\Omega_\alpha(t)} \nabla \cdot \left( \begin{bmatrix} \rho_\alpha \mathbf{u}_\alpha \otimes \mathbf{u}_\alpha & \rho_\alpha w_\alpha \mathbf{u}_\alpha \\ \rho_\alpha w_\alpha \mathbf{u}_\alpha^\top & \sum_{j=1}^N \rho_j \phi_j w_{j,\alpha}^2 \end{bmatrix} \right) \boldsymbol{\vartheta} \, dz \, d\mathbf{x} \\
&= \int_{I_F} \left( h_\alpha \nabla_{\mathbf{x}} \cdot (\rho_\alpha \mathbf{u}_\alpha \otimes \mathbf{u}_\alpha) \cdot \boldsymbol{\vartheta}_h + \int_{z_{\alpha-1/2}}^{z_{\alpha+1/2}} \partial_z (\rho_\alpha w_\alpha \mathbf{u}_\alpha) \cdot \boldsymbol{\vartheta}_h \, dz \right. \\
&\quad \left. + \int_{z_{\alpha-1/2}}^{z_{\alpha+1/2}} \nabla_{\mathbf{x}} \cdot (\rho_\alpha w_\alpha \mathbf{u}_\alpha^\top) \vartheta_z \, dz + \int_{z_{\alpha-1/2}}^{z_{\alpha+1/2}} \partial_z \left( \sum_{j=0}^N \rho_j \phi_j w_{j,\alpha}^2 \right) \vartheta_z \, dz \right) \, d\mathbf{x},
\end{aligned} \tag{3.3.15}$$

and using Leibniz's rule for the right hand side terms of equation (3.3.15), we have

$$\begin{aligned}
\int_{z_{\alpha-1/2}}^{z_{\alpha+1/2}} \partial_z (\rho_\alpha w_\alpha \mathbf{u}_\alpha) \cdot \boldsymbol{\vartheta}_h \, dz &= \rho_\alpha \mathbf{u}_\alpha (w_{\alpha+1/2}^- - w_{\alpha-1/2}^+) \cdot \boldsymbol{\vartheta}_h, \\
\int_{z_{\alpha-1/2}}^{z_{\alpha+1/2}} \nabla_{\mathbf{x}} \cdot (\rho_\alpha w_\alpha \mathbf{u}_\alpha^\top) \vartheta_z \, dz &= \left( \nabla_{\mathbf{x}} \cdot (\rho_\alpha \mathbf{u}_\alpha^\top h_\alpha \bar{w}_\alpha) \right. \\
&\quad \left. - \rho_\alpha \mathbf{u}_\alpha^\top \cdot (w_{\alpha+1/2}^- \nabla_{\mathbf{x}} z_{\alpha+1/2} - w_{\alpha-1/2}^+ \nabla_{\mathbf{x}} z_{\alpha-1/2}) \right) \vartheta_z, \\
\int_{z_{\alpha-1/2}}^{z_{\alpha+1/2}} \partial_z \left( \sum_{j=1}^N \rho_j \phi_j w_{j,\alpha}^2 \right) \vartheta_z \, dz &= \sum_{j=0}^N \rho_j \phi_j ((w_{j,\alpha+1/2}^2)^- - (w_{j,\alpha-1/2}^2)^+) \vartheta_z,
\end{aligned} \tag{3.3.16}$$

respectively. Inserting equalities (3.3.16) in (3.3.15),  $\mathcal{I}_2$  can be written as

$$\begin{aligned}
\mathcal{I}_2 &= \int_{I_F} \left[ \begin{array}{l} h_\alpha \nabla_{\mathbf{x}} \cdot (\rho_\alpha \mathbf{u}_\alpha \otimes \mathbf{u}_\alpha) + \rho_\alpha \mathbf{u}_\alpha (w_{\alpha+1/2}^- - w_{\alpha-1/2}^+) \\ \nabla_{\mathbf{x}} \cdot (\rho_\alpha \mathbf{u}_\alpha h_\alpha \bar{w}_\alpha) - \rho_\alpha \mathbf{u}_\alpha (w_{\alpha+1/2}^- \nabla_{\mathbf{x}} \cdot z_{\alpha+1/2} - w_{\alpha-1/2}^+ \nabla_{\mathbf{x}} \cdot z_{\alpha-1/2}) \\ \quad + \sum_{j=0}^N \rho_j \phi_j ((w_{j,\alpha+1/2}^2)^- - (w_{j,\alpha-1/2}^2)^+) \end{array} \right] \cdot \boldsymbol{\vartheta} \, d\mathbf{x}.
\end{aligned} \tag{3.3.17}$$

For the pressure terms  $\mathcal{I}_3$ , we have that they satisfy

$$\begin{aligned}
\mathcal{I}_3 &= - \int_{I_F} \left( \int_{z_{\alpha-1/2}}^{z_{\alpha+1/2}} \nabla p_{T,\alpha} \, dz \right) \cdot \boldsymbol{\vartheta} \, d\mathbf{x} + \int_{I_F} p_{T,\alpha-1/2} \boldsymbol{\vartheta} \cdot \boldsymbol{\eta}_{\alpha-1/2} \sqrt{1 + |\nabla_{\mathbf{x}} z_{\alpha-1/2}|^2} \, d\mathbf{x} \\
&\quad - \int_{I_F} p_{T,\alpha+1/2} \boldsymbol{\vartheta} \cdot \boldsymbol{\eta}_{\alpha+1/2} \sqrt{1 + |\nabla_{\mathbf{x}} z_{\alpha+1/2}|^2} \, d\mathbf{x} := \mathcal{I}_{3a} + \mathcal{I}_{3b} + \mathcal{I}_{3c}.
\end{aligned}$$

Using the symmetry of the stress tensor and terms  $\mathcal{I}_5$ ,  $\mathcal{I}_6$  we obtain

$$\begin{aligned}
\mathcal{I}_{3b} + \mathcal{I}_5 &= \int_{I_F} \mathbf{T}_{\alpha-1/2}^{E,+} (\nabla_{\mathbf{x}} z_{\alpha-1/2}, -1)^\top \cdot \boldsymbol{\vartheta} \, d\mathbf{x}, \\
\mathcal{I}_{3c} + \mathcal{I}_6 &= - \int_{I_F} \mathbf{T}_{\alpha+1/2}^{E,-} (\nabla_{\mathbf{x}} z_{\alpha+1/2}, -1)^\top \cdot \boldsymbol{\vartheta} \, d\mathbf{x}.
\end{aligned}$$

while  $\mathcal{I}_7$  is given by

$$\mathcal{I}_7 = - \int_{I_F} g h_\alpha \rho_\alpha \mathbf{k} \cdot \boldsymbol{\vartheta} \, d\mathbf{x}. \tag{3.3.18}$$

Finally, using (3.3.14), (3.3.17), (3.3.18) and the jump condition (3.3.9), we can get the multilayer version of the momentum equation (3.3.1), which is given by

$$\begin{aligned}
& h_\alpha \partial_t (\rho_\alpha \mathbf{u}_\alpha) + h_\alpha \nabla_{\mathbf{x}} \cdot (\rho_\alpha \mathbf{u}_\alpha \otimes \mathbf{u}_\alpha) + \rho_\alpha \mathbf{u}_\alpha (w_{\alpha+1/2}^- - w_{\alpha-1/2}^+) = - \int_{z_{\alpha-1/2}}^{z_{\alpha+1/2}} \nabla_{\mathbf{x}} p_{T,\alpha} dz \\
& + h_\alpha \nabla \cdot \mathbf{T}_{H,\alpha}^E - \tilde{\mathbf{T}}_{H,\alpha+1/2}^E (\nabla_{\mathbf{x}} z_{\alpha+1/2}, -1) + \tilde{\mathbf{T}}_{H,\alpha-1/2}^E (\nabla_{\mathbf{x}} z_{\alpha-1/2}, -1) \\
& + \frac{1}{2} G_{\alpha+1/2} (\mathbf{u}_{\alpha+1} - \mathbf{u}_\alpha) + \frac{1}{2} G_{\alpha-1/2} (\mathbf{u}_\alpha - \mathbf{u}_{\alpha-1}), \\
& \partial_t (\rho_\alpha h_\alpha \bar{w}_\alpha) - \rho_\alpha (w_{\alpha+1/2}^- \partial_t z_{\alpha+1/2} - w_{\alpha-1/2}^+ \partial_t z_{\alpha-1/2}) + \nabla_{\mathbf{x}} \cdot (\rho_\alpha h_\alpha \mathbf{u}_\alpha^T \bar{w}_\alpha) \\
& - \rho_\alpha \mathbf{u}_\alpha^T \cdot (w_{\alpha+1/2}^- \nabla_{\mathbf{x}} z_{\alpha+1/2} - w_{\alpha-1/2}^+ \nabla_{\mathbf{x}} z_{\alpha-1/2}) + \sum_{j=0}^N \rho_j \phi_j ((w_{j,\alpha+1/2}^2)^- - (w_{j,\alpha-1/2}^2)^+) \\
& = - \int_{z_{\alpha-1/2}}^{z_{\alpha+1/2}} \partial_z p_{T,\alpha} dz + h_\alpha \nabla \cdot \mathbf{T}_{z,\alpha}^E - \tilde{\mathbf{T}}_{z,\alpha+1/2}^E (\nabla_{\mathbf{x}} z_{\alpha+1/2}, -1) + \tilde{\mathbf{T}}_{z,\alpha-1/2}^E (\nabla_{\mathbf{x}} z_{\alpha-1/2}, -1) \\
& + \frac{1}{2} \sum_{j=0}^N G_{j,\alpha+1/2} (w_{j,\alpha+1/2}^+ - w_{j,\alpha+1/2}^-) + \frac{1}{2} \sum_{j=0}^N G_{j,\alpha-1/2} (w_{j,\alpha-1/2}^+ - w_{j,\alpha-1/2}^-) - g h_\alpha \rho_\alpha.
\end{aligned} \tag{3.3.19}$$

### Horizontal components of momentum equation of mixture

Using, as in previous chapters the total mass of the mixture of layer  $\alpha$ , (1.3.19) at  $z = z_{\alpha+1/2}$  multiplied by horizontal velocities  $\mathbf{u}_\alpha$ ,

$$\rho_\alpha (w_{\alpha+1/2}^- - w_{\alpha-1/2}^+) \mathbf{u}_\alpha = -h_\alpha \mathbf{u}_\alpha (\partial_t \rho_\alpha + \nabla_{\mathbf{x}} (\rho_\alpha \mathbf{u}_\alpha)),$$

and summing from 0 to  $N$  all equations (3.3.11) multiplied by  $\mathbf{u}_\alpha$

$$\mathbf{u}_\alpha \partial_t (\rho_\alpha h_\alpha) + \mathbf{u}_\alpha \nabla_{\mathbf{x}} \cdot (\rho_\alpha h_\alpha \mathbf{u}_\alpha) = (G_{\alpha+1/2} - G_{\alpha-1/2}) \mathbf{u}_\alpha,$$

from equalities (3.3.19) we can write the horizontal components of the momentum equation as

$$\begin{aligned}
\partial_t (\rho_\alpha h_\alpha \mathbf{u}_\alpha) + \nabla_{\mathbf{x}} \cdot (\rho_\alpha h_\alpha \mathbf{u}_\alpha \otimes \mathbf{u}_\alpha) + \int_{z_{\alpha-1/2}}^{z_{\alpha+1/2}} \nabla_{\mathbf{x}} p_{T,\alpha} dz &= \frac{G_{\alpha+1/2}}{2} (\mathbf{u}_{\alpha+1} + \mathbf{u}_\alpha) - \frac{G_{\alpha-1/2}}{2} (\mathbf{u}_\alpha + \mathbf{u}_{\alpha-1}),
\end{aligned} \tag{3.3.20}$$

and the horizontal components of pressure terms that appear in (3.3.20) are given by

$$\begin{aligned}
\int_{z_{\alpha-1/2}}^{z_{\alpha+1/2}} \nabla_{\mathbf{x}} p_{T,\alpha} dz &= h_\alpha (\nabla_{\mathbf{x}} \bar{p}_\alpha + \rho_\alpha g \nabla_{\mathbf{x}} \bar{z}_\alpha) + \nabla_{\mathbf{x}} (h_\alpha \bar{\Pi}_\alpha) \\
&\quad - \Pi_{\alpha+1/2} \nabla_{\mathbf{x}} z_{\alpha+1/2} + \Pi_{\alpha-1/2} \nabla_{\mathbf{x}} z_{\alpha-1/2},
\end{aligned} \tag{3.3.21}$$

where

$$\bar{p}_\alpha = p_0 + g \sum_{\beta=\alpha+1}^M \rho_\beta h_\beta + g \rho_\alpha \frac{h_\alpha}{2}, \quad \bar{z}_\alpha = z_B + \sum_{\beta=1}^{\alpha-1} h_\beta + \frac{h_\alpha}{2},$$

and

$$\bar{\Pi}_\alpha = \frac{1}{h_\alpha} \int_{z_{\alpha-1/2}}^{z_{\alpha+1/2}} \Pi dz,$$

respectively. Then, using equality (3.3.21) in (3.3.20) we may rewrite the horizontal components of the momentum equation as

$$\begin{aligned} \partial_t(\rho_\alpha h_\alpha \mathbf{u}_\alpha) + \nabla_{\mathbf{x}} \cdot (\rho_\alpha h_\alpha \mathbf{u}_\alpha \otimes \mathbf{u}_\alpha) + h_\alpha (\nabla_{\mathbf{x}} \bar{p}_\alpha + \rho_\alpha g \nabla_{\mathbf{x}} \bar{z}_\alpha) + \nabla_{\mathbf{x}} (h_\alpha \bar{\Pi}_\alpha) \\ - \Pi_{\alpha+1/2} \nabla_{\mathbf{x}} z_{\alpha+1/2} + \Pi_{\alpha-1/2} \nabla_{\mathbf{x}} z_{\alpha-1/2} = \frac{G_{\alpha+1/2}}{2} (\mathbf{u}_{\alpha+1} + \mathbf{u}_\alpha) - \frac{G_{\alpha-1/2}}{2} (\mathbf{u}_\alpha + \mathbf{u}_{\alpha-1}). \end{aligned} \quad (3.3.22)$$

### Vertical component of the momentum equation of mixture

The vertical component of the momentum equation of the mixture is given from (3.3.19) by

$$\begin{aligned} \partial_t(\rho_\alpha h_\alpha \bar{w}_\alpha) - \rho_\alpha (w_{\alpha+1/2}^- \partial_t z_{\alpha+1/2} - w_{\alpha-1/2}^+ \partial_t z_{\alpha-1/2}) \\ + \nabla_{\mathbf{x}} \cdot (\rho_\alpha h_\alpha \mathbf{u}_\alpha^T \bar{w}_\alpha) - \rho_\alpha \mathbf{u}_\alpha^T \cdot (w_{\alpha+1/2}^- \nabla_{\mathbf{x}} z_{\alpha+1/2} - w_{\alpha-1/2}^+ \nabla_{\mathbf{x}} z_{\alpha-1/2}) \\ + \sum_{j=0}^N \rho_j \phi_j ((w_{j,\alpha+1/2}^2)^- - (w_{j,\alpha-1/2}^2)^+) = - \int_{z_{\alpha-1/2}}^{z_{\alpha+1/2}} \partial_z p_{T,\alpha} dz - gh_\alpha \rho_\alpha \\ + \frac{1}{2} \sum_{j=0}^N G_{j,\alpha+1/2} (w_{j,\alpha+1/2}^+ - w_{j,\alpha+1/2}^-) + \frac{1}{2} \sum_{j=0}^N G_{j,\alpha-1/2} (w_{j,\alpha-1/2}^+ - w_{j,\alpha-1/2}^-). \end{aligned} \quad (3.3.23)$$

If the structure of the total pressure (3.2.8) is taken into account, the integral term of (3.3.23) can be solved as

$$\begin{aligned} - \int_{z_{\alpha-1/2}}^{z_{\alpha+1/2}} \partial_z p_{T,\alpha} dz &= - \int_{z_{\alpha-1/2}}^{z_{\alpha+1/2}} (-g\rho_\alpha + \partial_z \Pi_\alpha) dz \\ &= gh_\alpha \rho_\alpha - (\Pi_{\alpha+1/2} - \Pi_{\alpha-1/2}). \end{aligned} \quad (3.3.24)$$

On the other hand, we can recover the mass transfer terms as

$$\begin{aligned} - \sum_{j=0}^N w_{j,\alpha+1/2}^- G_{j,\alpha+1/2} &= - \rho_\alpha w_{\alpha+1/2}^- \partial_t z_{\alpha+1/2} - \rho_\alpha \mathbf{u}_\alpha^T \cdot w_{\alpha+1/2}^- \nabla_{\mathbf{x}} z_{\alpha+1/2} \\ &\quad + \sum_{j=0}^N \rho_j \phi_j (w_{j,\alpha+1/2}^2)^-, \\ \sum_{j=0}^N w_{j,\alpha-1/2}^+ G_{j,\alpha-1/2} &= \rho_\alpha w_{\alpha-1/2}^+ \partial_t z_{\alpha-1/2} + \rho_\alpha \mathbf{u}_\alpha^T \cdot w_{\alpha-1/2}^+ \nabla_{\mathbf{x}} z_{\alpha-1/2} \\ &\quad - \sum_{j=0}^N \rho_j \phi_j (w_{j,\alpha-1/2}^2)^+, \end{aligned} \quad (3.3.25)$$

Finally, using equalities (3.3.24) and (3.3.25) in equation (3.3.23) we get

$$\begin{aligned} \partial_t(\rho_\alpha h_\alpha \bar{w}_\alpha) + \nabla_{\mathbf{x}} \cdot (\rho_\alpha h_\alpha \mathbf{u}_\alpha^T \bar{w}_\alpha) + (\Pi_{\alpha+1/2} - \Pi_{\alpha-1/2}) \\ = \frac{1}{2} \sum_{j=0}^N G_{j,\alpha+1/2} (w_{j,\alpha+1/2}^+ + w_{j,\alpha+1/2}^-) - \frac{1}{2} \sum_{j=0}^N G_{j,\alpha-1/2} (w_{j,\alpha-1/2}^+ + w_{j,\alpha-1/2}^-). \end{aligned} \quad (3.3.26)$$

Summarizing, the horizontal and vertical components of the balance equation (3.3.19) are given by equations (3.3.22) and (3.3.26)

$$\begin{aligned} \partial_t(\rho_\alpha h_\alpha \mathbf{u}_\alpha) + \nabla_{\mathbf{x}} \cdot (\rho_\alpha h_\alpha \mathbf{u}_\alpha \otimes \mathbf{u}_\alpha) + h_\alpha (\nabla_{\mathbf{x}} \bar{p}_\alpha + \rho_\alpha g \nabla_{\mathbf{x}} \bar{z}_\alpha) + \nabla_{\mathbf{x}} (h_\alpha \bar{\Pi}_\alpha) \\ - \Pi_{\alpha+1/2} \nabla_{\mathbf{x}} z_{\alpha+1/2} + \Pi_{\alpha-1/2} \nabla_{\mathbf{x}} z_{\alpha-1/2} = \frac{G_{\alpha+1/2}}{2} (\mathbf{u}_{\alpha+1} + \mathbf{u}_\alpha) - \frac{G_{\alpha-1/2}}{2} (\mathbf{u}_\alpha + \mathbf{u}_{\alpha-1}), \\ \partial_t(\rho_\alpha h_\alpha \bar{w}_\alpha) + \nabla_{\mathbf{x}} \cdot (\rho_\alpha h_\alpha \mathbf{u}_\alpha^T \bar{w}_\alpha) + (\Pi_{\alpha+1/2} - \Pi_{\alpha-1/2}) \\ = \frac{1}{2} \sum_{j=0}^N G_{j,\alpha+1/2} (w_{j,\alpha+1/2}^+ + w_{j,\alpha+1/2}^-) - \frac{1}{2} \sum_{j=0}^N G_{j,\alpha-1/2} (w_{j,\alpha-1/2}^+ + w_{j,\alpha-1/2}^-). \end{aligned} \quad (3.3.27)$$

To get a solvable multilayer model we need to know how approximate  $\bar{w}_\alpha$ ,  $\bar{\Pi}_\alpha$  and the vertical velocities  $w_{j,\alpha+1/2}^\pm$  from equation (3.3.27).

## 3.4 Closure of the multilayer model

### 3.4.1 Mass conservation inside each layer

In order to close the momentum equations (3.3.27), we need to have the following additional equation. Integrating from  $z_{\alpha-1/2}$  to  $z_\alpha$  (middle of the layer  $\alpha$ ) the sum of all mass equations of the solid species we get

$$\bar{w}_\alpha = w_{\alpha-1/2}^+ - \frac{1}{\rho_\alpha} (\partial_t \rho_\alpha + \nabla_{\mathbf{x}} \cdot (\rho_\alpha \mathbf{u}_\alpha)) \frac{h_\alpha}{2}, \quad (3.4.1)$$

and using the definition (3.3.6) for the total mass transfer term  $G_{\alpha-1/2}$ , we can get an expression for the vertical velocity  $w_{\alpha-1/2}^+$  at each interface, given by

$$\rho_\alpha w_{\alpha-1/2}^+ = G_{\alpha-1/2} - \rho_\alpha \partial_t z_{\alpha-1/2} - \rho_\alpha \mathbf{u}_\alpha \cdot \nabla_{\mathbf{x}} z_{\alpha-1/2}, \quad (3.4.2)$$

then, introducing equality (3.4.2) in (3.4.1) we get

$$\begin{aligned} \rho_\alpha \bar{w}_\alpha &= \tilde{\rho}_{\alpha-1/2} \sum_{\beta=1}^{\alpha-1} l_\beta \nabla_{\mathbf{x}} \cdot (h(\mathbf{u}_\beta - \bar{\mathbf{u}})) + G_{f-a,\alpha-1/2} - \rho_\alpha \partial_t z_{\alpha-1/2} - \rho_\alpha \mathbf{u}_\alpha \cdot \nabla_{\mathbf{x}} z_{\alpha-1/2} \\ &\quad - \frac{h_\alpha}{2} \partial_t \rho_\alpha - \frac{h_\alpha}{2} \nabla_{\mathbf{x}} \cdot (\rho_\alpha \mathbf{u}_\alpha), \end{aligned} \quad (3.4.3)$$

where we have used an extension of equality (A.1.5) for the definition of  $G_{\alpha-1/2}$ , given by

$$G_{\alpha+1/2} = \frac{\tilde{\rho}_{\alpha+1/2}}{\rho_0} \sum_{\beta=1}^{\alpha} l_\beta \nabla_{\mathbf{x}} \cdot (\mathbf{R}_\beta - \bar{\mathbf{R}}) + G_{f-a,\alpha+1/2}, \quad (3.4.4)$$

with

$$\mathbf{R}_\beta := \mathbf{q}_\beta - \sum_{j=1}^N r_{j,\beta} \frac{\mathbf{q}_\beta}{m_\beta} \frac{\rho_j - \rho_0}{\rho_j}, \quad \bar{\mathbf{R}} := \sum_{\beta=1}^M l_\beta \mathbf{R}_\beta.$$

$G_{f-a,\alpha-1/2}$  is given by

$$G_{f-a,\alpha-1/2} = \frac{\tilde{\rho}_{\alpha-1/2}}{\rho_0} \left( - \sum_{j=1}^M (\rho_j - \rho_0) \tilde{f}_{j,\alpha-1/2} + (1 - L_\alpha) C_{1/2} + L_\alpha C_{M+1/2} \right),$$

with

$$C_{l+1/2} = G_{l+1/2} \frac{\rho_0}{\tilde{\rho}_{l+1/2}} + \sum_{j=1}^M (\rho_j - \rho_0) \tilde{f}_{j,l+1/2} \quad \text{for } l = 0 \text{ and } l = M.$$

Note that by using the definition of  $\mathbf{R}_\beta$  we can also rewrite equality (3.4.4) as

$$G_{\alpha+1/2} = \tilde{\rho}_{\alpha+1/2} \sum_{\beta=1}^{\alpha} l_\beta \nabla_{\mathbf{x}} \cdot (h(\mathbf{u}_\beta - \bar{\mathbf{u}})) + G_{f-a,\alpha+1/2},$$

where the average  $\tilde{\rho}_{\alpha+1/2}$  and  $h$  are given by

$$\tilde{\rho}_{\alpha+1/2} := \frac{2}{\frac{1}{\bar{\rho}_\alpha} + \frac{1}{\bar{\rho}_{\alpha+1}}} \quad \text{and} \quad h = \frac{1}{\rho_0} \left( m_\alpha - \sum_{j=1}^N \frac{\rho_j - \rho_0}{\rho_j} r_{j,\alpha} \right),$$

respectively. Furthermore, since  $z_{\alpha-1/2} = z_B + h \sum_{\beta=1}^{\alpha-1} l_\beta$ , (3.4.3) can be written as

$$\begin{aligned} \rho_\alpha \bar{w}_\alpha &= -\rho_\alpha \partial_t z_B + G_{f-a,\alpha-1/2} + \tilde{\rho}_{\alpha-1/2} \sum_{\beta=1}^{\alpha-1} l_\beta \nabla_{\mathbf{x}} \cdot (h(\mathbf{u}_\beta - \bar{\mathbf{u}})) \\ &\quad - \rho_\alpha \mathbf{u}_\alpha \cdot \nabla_{\mathbf{x}} z_{\alpha-1/2} - \frac{h_\alpha}{2} \nabla_{\mathbf{x}} \cdot (\rho_\alpha \mathbf{u}_\alpha) \\ &\quad - \left( \frac{l_\alpha}{2} + \frac{\rho_\alpha}{\rho_0} \left( L_{\alpha-1} - \frac{l_\alpha}{2} \right) \right) \partial_t m_\alpha + \frac{\rho_\alpha}{\rho_0} \left( L_{\alpha-1} - \frac{l_\alpha}{2} \right) \sum_{j=1}^N \frac{\rho_j - \rho_0}{\rho_j} \partial_t r_{j,\alpha}. \end{aligned} \quad (3.4.5)$$

### 3.4.2 Closure of the multilayer model with non-hydrostatic pressure

Assumption 3.3.1 allows to get the multilayer system given by equation (3.3.12), (3.3.27) and (3.4.5). Then, an expression for the pressure term  $\bar{\Pi}$  of the horizontal component of the momentum equation (3.3.22) need to be obtained.

**Proposition 3.4.1.** *If  $w_{j,\alpha}$  is linear in  $z$  (Assumption 3.3.1), then  $\Pi$  is quadratic in  $z$ .*

**Proof.** of Prop. 3.4.1. Noticing that from equation (3.2.8) we get

$$\partial_z p_T = \rho g + \partial_z \Pi,$$

then inserting the previous equality into the vertical component of the momentum equation (3.2.7) restricted to  $\Omega_\alpha$ , we conclude that  $\Pi$  is quadratic in  $z$ , directly.  $\blacksquare$

**Assumption 3.4.1.** For  $j = 1, \dots, N$  and  $\alpha = 1, \dots, M$ , where  $N$  and  $M$  are number of solid species and number of layers, respectively, we assume that the vertical velocities  $w_{j,\alpha}$  are constant only in vertical momentum equation.

Assumption 3.4.1 allows us to conclude that  $\Pi$  is linear in  $z$ . Then we can rewrite  $\bar{\Pi}_\alpha$  as follows

$$\bar{\Pi}_\alpha = \frac{\Pi_{\alpha+1/2} + \Pi_{\alpha-1/2}}{2}, \quad (3.4.6)$$

furthermore, the vertical component of the momentum equations (3.3.27) can be written as

$$\begin{aligned} & \partial_t(\rho_\alpha h_\alpha \bar{w}_\alpha) + \nabla_{\mathbf{x}} \cdot (\rho_\alpha h_\alpha \mathbf{u}_\alpha^T \bar{w}_\alpha) + (\Pi_{\alpha+1/2} - \Pi_{\alpha-1/2}) \\ &= \frac{1}{2} \sum_{j=0}^N G_{j,\alpha+1/2} (w_{j,\alpha+1} + w_{j,\alpha}) - \frac{1}{2} \sum_{j=0}^N G_{j,\alpha-1/2} (w_{j,\alpha} + w_{j,\alpha-1}). \end{aligned} \quad (3.4.7)$$

Now, following the structure of the vertical velocity from the **Chapter 1** given by (1.2.17), we have that

$$w_{j,\alpha} = w_\alpha + \phi_{j,\alpha}^{-1} f_{j,\alpha}^M(\Phi), \quad \alpha = 1, \dots, M, \quad (3.4.8)$$

then, using the equality (3.4.8) in (3.4.7) and Assumption 1.5.1, we get the vertical momentum equation

$$\begin{aligned} & \partial_t(\rho_\alpha h \bar{w}_\alpha) + \nabla_{\mathbf{x}} \cdot (\rho_\alpha h \mathbf{u}_\alpha^T \bar{w}_\alpha) + \frac{1}{l_\alpha} (\Pi_{\alpha+1/2} - \Pi_{\alpha-1/2}) \\ &= \frac{G_{\alpha+1/2}}{2l_\alpha} (\bar{w}_{\alpha+1} + \bar{w}_\alpha) - \frac{G_{\alpha-1/2}}{2l_\alpha} (\bar{w}_\alpha + \bar{w}_{\alpha-1}) \\ &+ \frac{1}{2l_\alpha} \sum_{j=0}^N G_{j,\alpha+1/2} \left( \frac{f_{j,\alpha+1}^M}{\phi_{j,\alpha+1}} + \frac{f_{j,\alpha}^M}{\phi_{j,\alpha}} \right) - \frac{1}{2l_\alpha} \sum_{j=0}^N G_{j,\alpha-1/2} \left( \frac{f_{j,\alpha}^M}{\phi_{j,\alpha}} + \frac{f_{j,\alpha-1}^M}{\phi_{j,\alpha-1}} \right). \end{aligned} \quad (3.4.9)$$

Finally, introducing (3.4.6) in the horizontal component of the momentum equation (3.3.27) and using Assumption 1.5.1, we can write the horizontal momentum equation as

$$\begin{aligned} & \partial_t(\rho_\alpha h \mathbf{u}_\alpha) + \nabla_{\mathbf{x}} \cdot (\rho_\alpha h \mathbf{u}_\alpha \otimes \mathbf{u}_\alpha) + h(\nabla_{\mathbf{x}} \bar{p}_\alpha + \rho_\alpha g \nabla_{\mathbf{x}} \bar{z}_\alpha) + \nabla_{\mathbf{x}} (h \frac{\Pi_{\alpha+1/2} + \Pi_{\alpha-1/2}}{2}) \\ & - \frac{\Pi_{\alpha+1/2}}{l_\alpha} \nabla_{\mathbf{x}} z_{\alpha+1/2} + \frac{\Pi_{\alpha-1/2}}{l_\alpha} \nabla_{\mathbf{x}} z_{\alpha-1/2} = \frac{G_{\alpha+1/2}}{2l_\alpha} (\mathbf{u}_{\alpha+1} + \mathbf{u}_\alpha) - \frac{G_{\alpha-1/2}}{2l_\alpha} (\mathbf{u}_\alpha + \mathbf{u}_{\alpha-1}). \end{aligned} \quad (3.4.10)$$

### 3.4.3 Final form of the multilayer system with non-hydrostatic pressure

In this section we summarize the multilayer model obtained in previous sections. The model with non-hydrostatic pressure is composed by equation (3.3.12), (3.4.10), (3.4.9) and the closure equation (3.4.5). For  $\alpha = 1, \dots, M$ , using the following notation:

$$m_\alpha := \bar{\rho}_\alpha h, \quad \mathbf{q}_\alpha := \bar{\rho}_\alpha h \mathbf{u}_\alpha, \quad \mathcal{Q}_\alpha = m_\alpha \bar{w}_\alpha, \quad \text{and} \quad r_{j,\alpha} := \rho_j \phi_{j,\alpha} h, \quad \text{for } j = 0, \dots, N,$$

the multilayer system for polydisperse sedimentation with non-hydrostatic pressure can be written as

$$\begin{aligned}
\partial_t m_\alpha + \nabla_{\mathbf{x}} \cdot \mathbf{q}_\alpha &= \frac{1}{l_\alpha} (G_{\alpha+1/2} - G_{\alpha-1/2}), \\
\partial_t \mathbf{q}_\alpha + \nabla_{\mathbf{x}} \cdot \left( \frac{\mathbf{q}_\alpha \otimes \mathbf{q}_\alpha}{m_\alpha} \right) + h(\nabla_{\mathbf{x}} \bar{p}_\alpha + \rho_\alpha g \nabla_{\mathbf{x}} \bar{z}_\alpha) + \nabla_{\mathbf{x}} \left( h \frac{\Pi_{\alpha-1/2} + \Pi_{\alpha+1/2}}{2} \right) \\
&\quad - \frac{1}{l_\alpha} (\Pi_{\alpha+1/2} \nabla_{\mathbf{x}} z_{\alpha+1/2} - \Pi_{\alpha-1/2} \nabla_{\mathbf{x}} z_{\alpha-1/2}) = \frac{G_{\alpha+1/2}}{2l_\alpha} \left( \frac{\mathbf{q}_{\alpha+1}}{m_{\alpha+1}} + \frac{\mathbf{q}_\alpha}{m_\alpha} \right) - \frac{G_{\alpha-1/2}}{2l_\alpha} \left( \frac{\mathbf{q}_\alpha}{m_\alpha} + \frac{\mathbf{q}_{\alpha-1}}{m_{\alpha-1}} \right), \\
\partial_t \mathcal{Q}_\alpha + \nabla_{\mathbf{x}} \cdot \left( \mathbf{q}_\alpha \frac{\mathcal{Q}_\alpha}{m_\alpha} \right) + \frac{1}{l_\alpha} (\Pi_{\alpha+1/2} - \Pi_{\alpha-1/2}) &= \frac{G_{\alpha+1/2}}{2l_\alpha} \left( \frac{\mathcal{Q}_{\alpha+1}}{m_{\alpha+1}} + \frac{\mathcal{Q}_\alpha}{m_\alpha} \right) - \frac{G_{\alpha-1/2}}{2l_\alpha} \left( \frac{\mathcal{Q}_\alpha}{m_\alpha} + \frac{\mathcal{Q}_{\alpha-1}}{m_{\alpha-1}} \right) \\
&\quad + \frac{1}{2l_\alpha} \sum_{j=0}^N G_{j,\alpha+1/2} \left( \frac{f_{j,\alpha+1}^M}{\phi_{j,\alpha+1}} + \frac{f_{j,\alpha}^M}{\phi_{j,\alpha}} \right) - \frac{1}{2l_\alpha} \sum_{j=0}^N G_{j,\alpha-1/2} \left( \frac{f_{j,\alpha}^M}{\phi_{j,\alpha}} + \frac{f_{j,\alpha-1}^M}{\phi_{j,\alpha-1}} \right), \\
\partial_t (r_{j,\alpha}) + \nabla_{\mathbf{x}} \cdot (r_{j,\alpha} \frac{\mathbf{q}_\alpha}{m_\alpha}) &= \frac{1}{l_\alpha} (\tilde{\phi}_{j,\alpha+1/2} G_{\alpha+1/2} - \tilde{\phi}_{j,\alpha-1/2} G_{\alpha-1/2}) \quad \text{for } j = 1, \dots, N, \\
&\quad - \frac{\rho_j}{l_\alpha} (\tilde{f}_{j,\alpha+1/2} - \tilde{f}_{j,\alpha-1/2}), \\
\mathcal{Q}_\alpha &= -m_\alpha \partial_t z_B + h G_{f-a,\alpha-1/2} + \tilde{m}_{\alpha-1/2} \sum_{\beta=1}^{\alpha-1} l_\beta \nabla_{\mathbf{x}} \cdot (h(\mathbf{u}_\beta - \bar{\mathbf{u}})) - \mathbf{q}_\alpha \cdot \nabla_{\mathbf{x}} z_{\alpha-1/2} - l_\alpha \frac{h}{2} \nabla_{\mathbf{x}} \cdot \mathbf{q}_\alpha \\
&\quad + \frac{l_\alpha}{2} \mathbf{q}_\alpha \cdot \nabla_{\mathbf{x}} h - \left( \frac{hl_\alpha}{2} + \frac{m_\alpha}{\rho_0} \left( L_{\alpha-1} - \frac{l_\alpha}{2} \right) \right) \partial_t m_\alpha + \frac{m_\alpha}{\rho_0} \left( L_{\alpha-1} - \frac{l_\alpha}{2} \right) \sum_{j=1}^N \frac{\rho_j - \rho_0}{\rho_j} \partial_t r_{j,\alpha}, 
\end{aligned} \tag{3.4.11}$$

where the averages  $\tilde{\phi}_{j,\alpha+1/2}$ ,  $\tilde{m}_{\alpha+1/2}$  and the quantities  $\bar{p}_\alpha$ ,  $\bar{z}_\alpha$ , and  $h$  are given by

$$\begin{aligned}
\tilde{m}_{\alpha+1/2} &:= \frac{2}{\frac{1}{m_\alpha} + \frac{1}{m_{\alpha+1}}}, \quad \tilde{\phi}_{j,\alpha+1/2} := \frac{1}{2} \left( \frac{r_{j,\alpha+1}}{m_{\alpha+1}} + \frac{r_{j,\alpha}}{m_\alpha} \right), \quad \bar{p}_\alpha = p_S + g \sum_{\beta=\alpha+1}^M l_\beta m_\beta + \frac{g}{2} l_\alpha m_\alpha, \\
\bar{z}_\alpha &= z_B + h \left( L_{\alpha-1} + \frac{l_\alpha}{2} \right), \quad h = \frac{1}{\rho_0} \left( m_\alpha - \sum_{j=1}^N \frac{\rho_j - \rho_0}{\rho_j} r_{j,\alpha} \right),
\end{aligned}$$

respectively. Note that equation (3.4.11) is deduced multiplying (3.4.5) by  $h$ .

---

## Conclusions and future work

---

### Conclusions

In this thesis, we have formulated a multilayer shallow water model framework for polydisperse sedimentation, in **Chapter 1** a multilayer model without sediment compressibility and mixture viscosity in one horizontal dimension has been presented, in **Chapter 2** we have added sediment compressibility and mixture viscosity phenomena and we have extended to two horizontal dimensions, and, in **Chapter 3** we have presented a multilayer model with non-hydrostatic pressure. These models can be used for simulations in industrial applications such as clarification tanks, wastewater treatment, and thickeners in the mining industry, but they are especially suitable for the description of natural geophysical processes such as sediment transport and polydisperse sedimentation in rivers and estuaries. These models provide the velocity field of the mixture, the concentrations of the each solid species, and the total mass of the mixture. We recall that the description of the movement of the mixture in terms of the mass-average velocity  $\mathbf{v}$  has the advantage that the mass and linear momentum balance of the mixture is recovered. This contrasts with earlier treatments [9, 24, 39] that are based on the volume-average velocity that is divergence free, and therefore constant in one space dimension. The latter property is an advantage especially for the description of unit operations with controllable volume flow rates, but it does not allow for a straightforward derivation of the momentum balance of the mixture.

These models are vertically consistent with the classical one dimensional vertical model when sediment compressibility and mixture viscosity are activated. Naturally, under Assumption 1.4.1 of shallow domain, the compression term is essentially vertical. If we do not have this assumption, the resultant system of **Chapter 2** given by (2.2.13)–(2.2.14) is much more complicated to solve, since the compression term would be activated in all directions.

### Future works

The results obtained in the develop of this thesis have motivated some ongoing and future work:

- Numerical scheme to multilayer model for polydisperse sedimentation with non-hydrostatic pressure.

In **Chapter 3** (ongoing work), we have obtained a multilayer model for polydisperse sedimentation with non-hydrostatic pressure, but we do not have designed numerical schemes yet. We are analyzing some strategies to design a numerical scheme and solve numerically.

- **High order methods to hyperbolic system with non-conservative products.** We are interested in develop an extension of the numerical schemes obtained to high order numerical schemes, especially when the non-hydrostatic pressure is present.
- **Mathematical model for polydisperse sedimentation with erosion.** A natural extension of the models developed in this thesis, it is to design a mathematical model suitable to simulate erosion process.

## Acknowledgments

RB is supported by Fondecyt project 1170473; CRHIAM, project CONICYT/Fondap/15130015; and CONICYT/PIA/Concurso Apoyo a Centros Científicos y Tecnológicos de Excelencia con Financiamiento Basal AFB170001. EDFN is supported by the Spanish Government and FEDER through the Research project MTM 2015-70490-C2-2-R. VO is supported by CONICYT scholarship.

---

## Conclusiones y trabajos futuros

---

### Conclusiones

En esta tesis, hemos formulado un marco de referencia para modelos multicapa en aguas poco profundas con sedimentación polidispersa, en **Capítulo 1** se ha presentado un modelo multicapa en una dimensión horizontal, donde no hemos considerado la compresibilidad de sedimentos ni la viscosidad de la mezcla. En **Capítulo 2** hemos agregado términos que modelan compresibilidad de sedimentos y viscosidad de la mezcla, además hemos extendido el modelo a dos dimensiones horizontales. En **Capítulo 3** hemos presentado un modelo multicapa donde hemos considerado presión no hidrostática. Estos modelos pueden ser utilizados para hacer simulaciones con aplicaciones industriales, tales como en tanques de clarificación y espesadores en la industria minera, así como también en procesos de tratamiento de aguas residuales, pero son especialmente adecuados para la descripción y simulación de procesos geofísicos naturales tales como el transporte de sedimentos y procesos de sedimentación polidispersa en ríos y estuarios. Estos modelos proporcionan el campo de velocidad de la mezcla, las concentraciones de cada especie sólida y la masa total de la mezcla. Recordamos que hemos descrito el movimiento de la mezcla en función de la velocidad másica promedio  $\bar{v}$  lo cual tiene la ventaja de que nos permite recuperar la ley de balance de masa y de momento lineal de la mezcla. En contraste con los planteamientos hechos anteriormente [9, 24, 39] los cuales se basan en velocidad volumétrica promedio con divergencia nula y por tanto, constante en una dimensión espacial. Esta última propiedad es una ventaja especialmente para la descripción de unidades de operación industrial con caudales controlables, pero no permiten obtener directamente la ley de balance de momento lineal de la mezcla.

Estos modelos son verticalmente consistentes con los modelos unidimensionales clásicos cuando los términos que modelan la compresibilidad del sedimento y la viscosidad de la mezcla están activados. Naturalmente, bajo la Suposición 1.4.1 sobre dominios poco profundos, el término de compresión es esencialmente vertical. Si no tuviéramos a disposición esta suposición, el sistema de EDP resultante en el **Capítulo 2** conformado por las ecuaciones (2.2.13)–(2.2.14) sería mucho mas complicado de resolver, pues el término de compresión actuaría en todas las direcciones.

### Trabajos futuros

Los resultados obtenidos en el desarrollo de esta tesis ha motivado algunos trabajos actualmente en curso y otros a desarrollar a futuro:

- Esquema numérico para modelo multicapa con sedimentación polidispersa y presión

**no hidrostática.**

En el **Capítulo 3** (trabajo en progreso), hemos obtenido un modelo multicapa para sedimentación polidispersa, en el cual hemos introducido presión no hidrostática, pero no hemos propuesto un método numérico aún. Actualmente analizamos algunas estrategias que permitan resolver y diseñar un esquema numérico para el modelo propuesto.

- **Métodos de alto orden para sistemas hiperbólicos con productos no-conservativos.** Estamos interesados en desarrollar una extensión de los esquemas numéricos propuestos, a métodos numéricos de alto orden, especialmente cuando la presión no hidrostática está presente en el modelo.
- **Modelos para sedimentación polidispersa con erosión.** Una extensión natural del trabajo desarrollado en esta tesis, es diseñar modelos matemáticos que permitan simular también el proceso de erosión.

## Acknowledgments

RB es financiado por proyecto Fondecyt 1170473; CRHIAM, proyecto CONICYT/Fondap/15130015; y CONICYT/PIA/Concurso Apoyo a Centros Científicos y Tecnológicos de Excelencia con Financiamiento Basal AFB170001. EDFN es financiado por el gobierno Español y FEDER a través del proyecto de Investigación MTM 2015-70490-C2-2-R. VO es financiado por becas de doctorado nacional de CONICYT.

# APPENDIX A

---

## Appendix

---

### A.1 Explicit formula of the total interlayer mass fluxes

For the case of a single density of all phases the definition of  $G_{\alpha+1/2}$  can be easily deduced, as is shown in [2]. On the other hand, for a multilayer model with variable density proposed in [5] the computation of  $G_{\alpha+1/2}$  is done numerically as the solution of a non-linear implicit system. In this subsection we show that although the model proposed in this paper can be seen as a multilayer model with variable density akin to that of [5], we can deduce an explicit definition of  $G_{\alpha+1/2}$  in terms of the other unknowns of the problem. To this end, for a fixed layer  $\alpha$  we consider the sums of the equations (1.5.3) from layer 1 to layer  $\alpha$  and from layer  $\alpha + 1$  to layer  $M$ , respectively. This yields the equations

$$\sum_{\beta=1}^{\alpha} l_{\beta}(\partial_t m_{\beta} + \partial_x q_{\beta}) = G_{\alpha+1/2} - G_{1/2}, \quad \sum_{\gamma=\alpha+1}^M l_{\gamma}(\partial_t m_{\gamma} + \partial_x q_{\gamma}) = G_{M+1/2} - G_{\alpha+1/2}.$$

By using (1.5.1) we can write  $m_{\alpha}$  in terms of  $h$  and  $r_{j,\alpha}$ . Then the above equations can be rewritten as

$$L_{\alpha} \partial_t(\rho_0 h) + \sum_{\beta=1}^{\alpha} \sum_{j=1}^N l_{\beta} \partial_t r_{j,\beta} \frac{\rho_j - \rho_0}{\rho_j} + \sum_{\beta=1}^{\alpha} l_{\beta} \partial_x q_{\beta} = G_{\alpha+1/2} - G_{1/2}, \quad (\text{A.1.1})$$

$$(1 - L_{\alpha}) \partial_t(\rho_0 h) + \sum_{\gamma=\alpha+1}^M \sum_{j=1}^N l_{\gamma} \partial_t r_{j,\gamma} \frac{\rho_j - \rho_0}{\rho_j} + \sum_{\gamma=\alpha+1}^M l_{\gamma} \partial_x q_{\gamma} = G_{M+1/2} - G_{\alpha+1/2}. \quad (\text{A.1.2})$$

Now we can combine previous equations to eliminate the dependence on  $\partial_t(\rho_0 h)$ . We subtract equation (A.1.1) multiplied by  $(1 - L_{\alpha})$  from equation (A.1.2) multiplied by  $L_{\alpha}$ . As a result we obtain

$$\begin{aligned} & (1 - L_{\alpha}) \sum_{\beta=1}^{\alpha} \sum_{j=1}^N l_{\beta} \partial_t r_{j,\beta} \frac{\rho_j - \rho_0}{\rho_j} - L_{\alpha} \sum_{\gamma=\alpha+1}^M \sum_{j=1}^N l_{\gamma} \partial_t r_{j,\gamma} \frac{\rho_j - \rho_0}{\rho_j} \\ &= G_{\alpha+1/2} - (1 - L_{\alpha}) \sum_{\beta=1}^{\alpha} l_{\beta} \partial_x q_{\beta} + L_{\alpha} \sum_{\gamma=\alpha+1}^M l_{\gamma} \partial_x q_{\gamma} - (1 - L_{\alpha}) G_{1/2} - L_{\alpha} G_{M+1/2}. \end{aligned}$$

Utilizing (1.5.4) to substitute  $\partial_t r_{j,\beta}$  and  $\partial_t r_{j,\gamma}$  in the previous equation we get

$$\begin{aligned} & (G_{\alpha+1/2} - (1 - L_\alpha)G_{1/2} - L_\alpha G_{M+1/2}) \left( 1 - \sum_{j=1}^N \frac{\rho_j - \rho_0}{\rho_j} \tilde{\phi}_{j,\alpha+1/2} \right) \\ & = (1 - L_\alpha) \sum_{\beta=1}^{\alpha} l_\beta \left( \partial_x q_\beta - \sum_{j=1}^N \partial_x(r_{j,\beta} u_\beta) \frac{\rho_j - \rho_0}{\rho_j} \right) - L_\alpha \sum_{\gamma=\alpha+1}^M l_\gamma \left( \partial_x q_\gamma - \sum_{j=1}^N \partial_x(r_{j,\gamma} u_\gamma) \frac{\rho_j - \rho_0}{\rho_j} \right) \\ & \quad - \sum_{j=1}^N (\tilde{f}_{j,\alpha+1/2} - (1 - L_\alpha)\tilde{f}_{j,1/2} - L_\alpha \tilde{f}_{j,M+1/2})(\rho_j - \rho_0). \end{aligned}$$

Moreover, in view the definition of  $\tilde{\phi}_{j,\alpha+1/2}$  given by (1.3.11) or (1.5.6), the number that multiplies  $G_{\alpha+1/2}$  is always positive. In fact, we obtain

$$1 - \sum_{j=1}^N \frac{\rho_j - \rho_0}{\rho_j} \tilde{\phi}_{j,\alpha+1/2} = \frac{1}{2} \left( \frac{\rho_0}{\bar{\rho}_{\alpha+1}} + \frac{\rho_0}{\bar{\rho}_\alpha} \right) = \frac{\rho_0(\bar{\rho}_{\alpha+1} + \bar{\rho}_\alpha)}{2\bar{\rho}_\alpha\bar{\rho}_{\alpha+1}}. \quad (\text{A.1.3})$$

Furthermore, we can use that

$$\sum_{j=0}^N \rho_j \tilde{f}_{j,\alpha+1/2} = 0 \Leftrightarrow \sum_{j=1}^N \rho_j \tilde{f}_{j,\alpha+1/2} = -\rho_0 \tilde{f}_{0,\alpha+1/2}. \quad (\text{A.1.4})$$

Introducing (A.1.3), (A.1.4), and the fact that  $\tilde{f}_{j,1/2} = \tilde{f}_{j,M+1/2} = 0$ , we get the equality

$$\begin{aligned} G_{\alpha+1/2} & = (1 - L_\alpha)G_{1/2} + L_\alpha G_{M+1/2} \\ & + \frac{2\bar{\rho}_\alpha\bar{\rho}_{\alpha+1}}{\rho_0(\bar{\rho}_{\alpha+1} + \bar{\rho}_\alpha)} \left( (1 - L_\alpha) \sum_{\beta=1}^{\alpha} l_\beta \left( \partial_x q_\beta - \sum_{j=1}^N \partial_x(r_{j,\beta} u_\beta) \frac{\rho_j - \rho_0}{\rho_j} \right) \right. \\ & \quad \left. - L_\alpha \sum_{\gamma=\alpha+1}^M l_\gamma \left( \partial_x q_\gamma - \sum_{j=1}^N \partial_x(r_{j,\gamma} u_\gamma) \frac{\rho_j - \rho_0}{\rho_j} \right) + \rho_0 \sum_{j=0}^N \tilde{f}_{j,\alpha+1/2} \right). \end{aligned} \quad (\text{A.1.5})$$

## A.2 A bound of the characteristic velocities

In order to find a bound of the characteristic velocities of the proposed multilayer model (1.5.3)–(1.5.5), we rewrite the model in the form  $\partial_t \tilde{\mathbf{w}} + \mathcal{A}(\tilde{\mathbf{w}}) \partial_x \tilde{\mathbf{w}} = \mathbf{b}$  with

$$\tilde{\mathbf{w}} = (m_1, \dots, m_M, q_1, \dots, q_M, r_{1,1}, \dots, r_{N,1}, \dots, r_{1,M}, \dots, r_{N,M})^T.$$

An explicit bound of the minimum and maximum eigenvalues of  $\mathcal{A}$  in dependence of the all horizontal velocities and all densities by layer is provided in the following theorem.

**Theorem A.2.1.** *If  $\lambda_k$  for  $k = 1, \dots, 2M + NM$  denote the eigenvalues of  $\mathcal{A}$  and these are real, then*

$$\bar{u} - \Psi \leq \lambda_k \leq \bar{u} + \Psi \quad \text{for all } k = 1, \dots, 2M + NM,$$

where

$$\bar{u} := \frac{1}{M} \sum_{\beta=1}^M u_\beta,$$

$M$  is the number of the layers,  $N$  is the number of solid particle species and the quantity  $\Psi$  is defined as

$$\Psi := \sqrt{\frac{2M-1}{2M}} \left( 2 \sum_{i=1}^M (\bar{u} - u_i)^2 + gh\rho_0^{-1} \left( \rho_0 + \frac{1}{M} \sum_{\beta=1}^M (2\beta-1)\bar{\rho}_\beta \right) \right)^{1/2}.$$

Since  $\sqrt{(2M-1)/(2M)} \leq 1$ , another bound can be defined by considering only the second factor of  $\psi$ . To prove Theorem A.2.1 it is sufficient to apply the result presented in [52] to the characteristic polynomial of matrix  $\mathcal{A}$ . This result states that if all the roots  $x$  of a polynomial of degree  $n$ , that is, solutions  $x$  of

$$a_n x^n + a_{n-1} x^{n-1} + \dots + a_0 = 0,$$

are real, then they lie in the range bounded by

$$-\frac{a_{n-1}}{na_n} \pm (n-1) \left( \frac{a_{n-1}^2}{n^2 a_n^2} - \frac{2a_{n-2}}{n(n-1)a_n} \right)^{1/2}.$$

### A.3 A particular weak solution with hydrostatic pressure: deduction of equations

We detail here the calculations needed to obtain the system (1.4.6), starting with the equations of mass conservation. We choose a scalar test function  $\varphi = \varphi(t, \mathbf{x})$  that is independent of  $z$ . Then, in general for a weak solution  $\mathbf{v}_j$  the mass conservation equation (1.2.19) yields for all  $\alpha = 0, \dots, M$  and  $j = 0, 1, \dots, N$ :

$$\begin{aligned} 0 &= \int_{\Omega_\alpha(t)} (\partial_t(\rho_j \phi_j) + \nabla_{\mathbf{x}} \cdot (\rho_j \phi_j \mathbf{v}_j)) \varphi \, d\Omega \\ &= \int_{I_F(t)} \varphi(t, \mathbf{x}) \left( \int_{z_{\alpha-1/2}}^{z_{\alpha+1/2}} (\partial_t(\rho_j \phi_j) + \nabla_{\mathbf{x}} \cdot (\rho_j \phi_j \mathbf{u}) + \partial_z(\rho_j \phi_j w_j)) \, dz \right) d\mathbf{x} \\ &= \int_{I_F(t)} \varphi(t, \mathbf{x}) \left( \partial_t \left( \int_{z_{\alpha-1/2}}^{z_{\alpha+1/2}} \rho_j \phi_j \, dz \right) + \nabla_{\mathbf{x}} \cdot \left( \int_{z_{\alpha-1/2}}^{z_{\alpha+1/2}} (\rho_j \phi_j \mathbf{u}) \, dz \right) - \rho_j \phi_{j,\alpha} \partial_t z_{\alpha+1/2} \right. \\ &\quad \left. - \rho_j \phi_{j,\alpha} \mathbf{u}_{\alpha+1/2}^- \cdot \nabla_{\mathbf{x}} z_{\alpha+1/2} + \rho_j \phi_{j,\alpha} w_{j,\alpha+1/2}^- + \rho_j \phi_{j,\alpha} \partial_t z_{\alpha-1/2} \right. \\ &\quad \left. + \rho_j \phi_{j,\alpha} \mathbf{u}_{\alpha-1/2}^+ \cdot \nabla_{\mathbf{x}} z_{\alpha-1/2} - \rho_j \phi_{j,\alpha} w_{j,\alpha-1/2}^+ \right) d\mathbf{x}. \end{aligned}$$

Moreover, noticing that  $\partial_t h_\alpha = \partial_t z_{\alpha+1/2} - \partial_t z_{\alpha-1/2}$ , we obtain that for all  $\varphi(t, \cdot) \in L^2(I_F(t))$ ,

$$\begin{aligned} 0 &= \int_{I_F(t)} \varphi(t, \mathbf{x}) \left( \partial_t(\rho_j \phi_{j,\alpha} h_\alpha) + \nabla_{\mathbf{x}} \cdot (\rho_j \phi_{j,\alpha} h_\alpha \mathbf{u}_\alpha) - \rho_j \phi_{j,\alpha} \partial_t z_{\alpha+1/2} - \rho_j \phi_{j,\alpha} \mathbf{u}_{\alpha+1/2}^- \cdot \nabla_{\mathbf{x}} z_{\alpha+1/2} \right. \\ &\quad \left. + \rho_j \phi_{j,\alpha} w_{j,\alpha+1/2}^- + \rho_j \phi_{j,\alpha} \partial_t z_{\alpha-1/2} + \rho_j \phi_{j,\alpha} \mathbf{u}_{\alpha-1/2}^+ \cdot \nabla_{\mathbf{x}} z_{\alpha-1/2} - \rho_j \phi_{j,\alpha} w_{j,\alpha-1/2}^+ \right) d\mathbf{x}. \end{aligned} \tag{A.3.1}$$

Introducing  $\mathbf{u}_\alpha$  with assumptions (1.3.4) in the equation (A.3.1), and taking into account (1.3.6) and (1.3.7), we obtain the mass conservation laws (1.4.3):

$$\partial_t(\rho_j \phi_{j,\alpha} h_\alpha) + \nabla_{\mathbf{x}} \cdot (\rho_j \phi_{j,\alpha} h_\alpha \mathbf{u}_\alpha) = G_{j,\alpha+1/2} - G_{j,\alpha-1/2}. \quad (\text{A.3.2})$$

As for the momentum balance equations, we consider test functions  $\boldsymbol{\vartheta} \in H^1(\Omega_\alpha)$  that satisfy (1.4.2). The weak formulation (1.4.1) follows taking into account the structure of  $\mathbf{v}$ , integrating (1.2.21) with respect to the variable  $z$  and identifying each of the two components of the vector test functions. However, due to the hydrostatic pressure framework the equations that correspond to the vertical component can be omitted. This is equivalent to identifying the weak formulation for test functions in the form  $(\boldsymbol{\vartheta}_h, 0)^T$ , with  $\boldsymbol{\vartheta}_h = \boldsymbol{\vartheta}_h(t, \mathbf{x})$  independently of  $z$ , with  $\boldsymbol{\vartheta}_h|_{\partial I_F} = 0$ . Then, from (1.4.1) and using these test functions, we obtain for the horizontal momentum conservation equation

$$\begin{aligned} & \int_{\Omega_\alpha(t)} \left( \sum_{j=0}^N \rho_j \partial_t(\phi_{j,\alpha} \mathbf{u}_\alpha) \cdot \boldsymbol{\vartheta}_h \right) d\Omega + \int_{\Omega_\alpha(t)} \left( \sum_{j=0}^N \rho_j \nabla_{\mathbf{x}} \cdot (\phi_{j,\alpha} \mathbf{u}_\alpha \otimes \mathbf{u}_\alpha) \cdot \boldsymbol{\vartheta}_h \right) d\Omega \\ & + \int_{\Omega_\alpha(t)} \left( \sum_{j=0}^N \rho_j \partial_z(\phi_{j,\alpha} w_{j,\alpha} \mathbf{u}_\alpha) \cdot \boldsymbol{\vartheta}_h \right) d\Omega + \int_{\Omega_\alpha(t)} \mathbf{T}_{h,\alpha}^E : \nabla_{\mathbf{x}} \boldsymbol{\vartheta} d\Omega - \int_{\Omega_\alpha(t)} p_\alpha \nabla_{\mathbf{x}} \cdot \boldsymbol{\vartheta}_h d\Omega \quad (\text{A.3.3}) \\ & + \int_{\Gamma_{\alpha+1/2}(t)} (\mathbf{T}_{\alpha+1/2}^-(\boldsymbol{\vartheta}_h, 0)^T) \cdot \boldsymbol{\eta}_{\alpha+1/2} d\Gamma - \int_{\Gamma_{\alpha-1/2}(t)} (\mathbf{T}_{\alpha-1/2}^+(\boldsymbol{\vartheta}_h, 0)^T) \cdot \boldsymbol{\eta}_{\alpha-1/2} d\Gamma = 0 \end{aligned}$$

for all  $\alpha = 1, \dots, M$ , where  $\mathbf{T}_{h,\alpha}^E = \mathbf{T}_h^E(\mathbf{v}_\alpha)$ . Taking into account the definition of  $\Omega_\alpha(t)$  in Section 0.1 and the assumption on the independence of  $z$  of  $\mathbf{u}_\alpha$  and  $\boldsymbol{\vartheta}_h$  and writing (A.3.3) as  $\mathcal{I}_1 + \dots + \mathcal{I}_7 = 0$ , where  $\mathcal{I}_1, \dots, \mathcal{I}_7$  stand for each of the signed integrals in the left-hand side of (A.3.3), we obtain

$$\begin{aligned} \mathcal{I}_1 &= \int_{I_F} \left( \int_{z_{\alpha-1/2}}^{z_{\alpha+1/2}} \partial_t(\rho(\Phi_\alpha) \mathbf{u}_\alpha) \cdot \boldsymbol{\vartheta}_h d\mathbf{x} \right) dz = \int_{I_F} h_\alpha \partial_t(\rho(\Phi_\alpha) \mathbf{u}_\alpha) \cdot \boldsymbol{\vartheta}_h d\mathbf{x}, \\ \mathcal{I}_2 &= \int_{I_F} h_\alpha \nabla_{\mathbf{x}} \cdot (\rho(\Phi_\alpha) \mathbf{u}_\alpha \otimes \mathbf{u}_\alpha) \cdot \boldsymbol{\vartheta}_h d\mathbf{x}, \\ \mathcal{I}_3 &= \sum_{j=0}^N \int_{I_F} \int_{z_{\alpha-1/2}}^{z_{\alpha+1/2}} \rho_j \partial_z(\phi_{j,\alpha} w_{j,\alpha} \mathbf{u}_\alpha) \cdot \boldsymbol{\vartheta}_h dz d\mathbf{x} = \sum_{j=0}^N \int_{I_F} \rho_j \phi_{j,\alpha} (w_{j,\alpha+1/2}^- - w_{j,\alpha-1/2}^+) \mathbf{u}_\alpha \cdot \boldsymbol{\vartheta}_h d\mathbf{x}, \\ \mathcal{I}_4 &= \int_{I_F} \left( \int_{z_{\alpha-1/2}}^{z_{\alpha+1/2}} \mathbf{T}_{h,\alpha}^E : \nabla_{\mathbf{x}} \boldsymbol{\vartheta}_h dz \right) d\mathbf{x} = \int_{I_F} h_\alpha \mathbf{T}_{h,\alpha}^E : \nabla_{\mathbf{x}} \boldsymbol{\vartheta}_h d\mathbf{x} = - \int_{I_F} \nabla_{\mathbf{x}} \cdot (h_\alpha \mathbf{T}_{h,\alpha}^E) \cdot \boldsymbol{\vartheta}_h d\mathbf{x}, \\ \mathcal{I}_5 &= - \int_{I_F} \left( \int_{z_{\alpha-1/2}}^{z_{\alpha+1/2}} p_\alpha dz \right) \nabla \cdot \boldsymbol{\vartheta}_h d\mathbf{x} = \int_{I_F} \boldsymbol{\vartheta}_h \cdot \nabla_{\mathbf{x}} \left( \int_{z_{\alpha-1/2}}^{z_{\alpha+1/2}} p_\alpha dz \right) d\mathbf{x} \\ &= \int_{I_F} \boldsymbol{\vartheta}_h \cdot \left( \int_{z_{\alpha-1/2}}^{z_{\alpha+1/2}} \nabla_{\mathbf{x}} p_\alpha dz + p_{\alpha+1/2} \nabla_{\mathbf{x}} z_{\alpha+1/2} - p_{\alpha-1/2} \nabla_{\mathbf{x}} z_{\alpha-1/2} \right) d\mathbf{x} \\ &= \int_{I_F} \boldsymbol{\vartheta}_h \cdot \left( \int_{z_{\alpha-1/2}}^{z_{\alpha+1/2}} \nabla_{\mathbf{x}} p_\alpha dz \right) d\mathbf{x} + \int_{I_F} p_{\alpha+1/2}(\boldsymbol{\vartheta}_h, 0)^T \cdot \boldsymbol{\eta}_{\alpha+1/2} \sqrt{1 + |\nabla_{\mathbf{x}} z_{\alpha+1/2}|^2} d\mathbf{x} \\ &\quad - \int_{I_F} p_{\alpha-1/2}(\boldsymbol{\vartheta}_h, 0)^T \cdot \boldsymbol{\eta}_{\alpha-1/2} \sqrt{1 + |\nabla_{\mathbf{x}} z_{\alpha-1/2}|^2} d\mathbf{x} =: \mathcal{I}_{5a} + \mathcal{I}_{5b} + \mathcal{I}_{5c}, \\ \mathcal{I}_6 &= \int_{I_F} (\mathbf{T}_{\alpha+1/2}^-(\boldsymbol{\vartheta}_h, 0)^T) \cdot \boldsymbol{\eta}_{\alpha+1/2} \sqrt{1 + |\nabla_{\mathbf{x}} z_{\alpha+1/2}|^2} d\mathbf{x}, \end{aligned}$$

and where  $\mathcal{I}_7$  is handled analogously to  $\mathcal{I}_6$ . Moreover, by (1.3.13), we can simplify

$$\begin{aligned}\mathcal{I}_6 + \mathcal{I}_{5b} &= \int_{I_F} (\mathbf{T}_{\alpha+1/2}^{E,-}(\boldsymbol{\vartheta}_h, 0)^T) \cdot (\nabla_{\mathbf{x}} z_{\alpha+1/2}, -1)^T d\mathbf{x} \\ &= \int_{I_F} (\mathbf{T}_{h,\alpha+1/2}^{E,-}(\nabla_{\mathbf{x}} z_{\alpha+1/2})^T - \mathbf{T}_{xz,\alpha+1/2}^{E,-}) \cdot \boldsymbol{\vartheta}_h d\mathbf{x}.\end{aligned}$$

Furthermore, since  $\mathbf{T}_{\alpha+1/2}^{E,-}$  is a symmetric matrix, we have that

$$(\mathbf{T}_{\alpha+1/2}^{E,-}(\boldsymbol{\vartheta}_h, 0)^T) \cdot (\nabla_{\mathbf{x}} z_{\alpha+1/2}, -1)^T = (\mathbf{T}_{\alpha+1/2}^{E,-}(\nabla_{\mathbf{x}} z_{\alpha+1/2}, -1)^T) \cdot (\boldsymbol{\vartheta}_h, 0)^T.$$

The sum  $\mathcal{I}_7 + \mathcal{I}_{5c}$  can be simplified in a similar way. Then the weak formulation (A.3.3), corresponding to the horizontal momentum equation for this set of test functions, can be written as follows:

$$\begin{aligned}\int_{I_F} \boldsymbol{\vartheta}_h \cdot \left( h_\alpha \partial_t (\rho(\Phi_\alpha) \mathbf{u}_\alpha) + h_\alpha \nabla_{\mathbf{x}} \cdot (\rho(\Phi_\alpha) \mathbf{u}_\alpha \otimes \mathbf{u}_\alpha) + \sum_{j=0}^N \rho_j \phi_{j,\alpha} (w_{j,\alpha+1/2}^- - w_{j,\alpha-1/2}^+) \mathbf{u}_\alpha \right. \\ \left. + \int_{z_{\alpha-1/2}}^{z_{\alpha+1/2}} \nabla_{\mathbf{x}} p_\alpha dz - \nabla_{\mathbf{x}} \cdot (h_\alpha \mathbf{T}_h^E) + (\mathbf{T}_{h,\alpha+1/2}^{E,-}(\nabla_{\mathbf{x}} z_{\alpha+1/2})^T - \mathbf{T}_{xz,\alpha+1/2}^{E,-}) \right. \\ \left. - (\mathbf{T}_{h,\alpha-1/2}^{E,+}(\nabla_{\mathbf{x}} z_{\alpha-1/2})^T - \mathbf{T}_{xz,\alpha-1/2}^{E,+}) \right) d\mathbf{x} = 0, \quad \forall \boldsymbol{\vartheta}_h.\end{aligned}$$

Taking into account (1.3.16) we deduce

$$\begin{aligned}h_\alpha \partial_t (\rho(\Phi_\alpha) \mathbf{u}_\alpha) + h_\alpha \nabla_{\mathbf{x}} \cdot (\rho(\Phi_\alpha) \mathbf{u}_\alpha \otimes \mathbf{u}_\alpha) + \sum_{j=0}^N \rho_j \phi_{j,\alpha} (w_{j,\alpha+1/2}^- - w_{j,\alpha-1/2}^+) \mathbf{u}_\alpha + \int_{z_{\alpha-1/2}}^{z_{\alpha+1/2}} \nabla_{\mathbf{x}} p_\alpha dz \\ - \nabla_{\mathbf{x}} \cdot (h_\alpha \mathbf{T}_h^E) + (\tilde{\mathbf{T}}_{h,\alpha+1/2}^E(\nabla_{\mathbf{x}} z_{\alpha+1/2})^T - \tilde{\mathbf{T}}_{xz,\alpha+1/2}^E) - (\tilde{\mathbf{T}}_{h,\alpha-1/2}^E(\nabla_{\mathbf{x}} z_{\alpha-1/2})^T - \tilde{\mathbf{T}}_{xz,\alpha-1/2}^E) \\ = \frac{G_{\alpha+1/2}}{2} (\mathbf{u}_{\alpha+1} - \mathbf{u}_\alpha) + \frac{G_{\alpha-1/2}}{2} (\mathbf{u}_\alpha - \mathbf{u}_{\alpha-1}).\end{aligned}\tag{A.3.4}$$

Using (1.3.18) evaluated at  $z = z_{\alpha+1/2}$  and multiplied by  $\mathbf{u}_\alpha$ , we may write (A.3.4) in the form

$$\begin{aligned}h_\alpha \rho(\Phi_\alpha) \partial_t \mathbf{u}_\alpha + h_\alpha \rho(\Phi_\alpha) \mathbf{u}_\alpha \cdot \nabla_{\mathbf{x}} \mathbf{u}_\alpha + \int_{z_{\alpha-1/2}}^{z_{\alpha+1/2}} \nabla_{\mathbf{x}} p_\alpha dz - \nabla_{\mathbf{x}} \cdot (h_\alpha \mathbf{T}_h^E) \\ + (\tilde{\mathbf{T}}_{h,\alpha+1/2}^E(\nabla_{\mathbf{x}} z_{\alpha+1/2})^T - \tilde{\mathbf{T}}_{xz,\alpha+1/2}^E) - (\tilde{\mathbf{T}}_{h,\alpha-1/2}^E(\nabla_{\mathbf{x}} z_{\alpha-1/2})^T - \tilde{\mathbf{T}}_{xz,\alpha-1/2}^E) \\ = \frac{G_{\alpha+1/2}}{2} (\mathbf{u}_{\alpha+1} - \mathbf{u}_\alpha) + \frac{G_{\alpha-1/2}}{2} (\mathbf{u}_\alpha - \mathbf{u}_{\alpha-1}).\end{aligned}\tag{A.3.5}$$

On the other hand, combining the equation (A.3.5) with (1.4.4) multiplied by  $\mathbf{u}_\alpha$ , we obtain the evolution equation for the momentum (1.4.5):

$$\begin{aligned}\partial_t (\rho(\Phi_\alpha) h_\alpha \mathbf{u}_\alpha) + \nabla_{\mathbf{x}} \cdot (h_\alpha \rho(\Phi_\alpha) \mathbf{u}_\alpha \otimes \mathbf{u}_\alpha) + \int_{z_{\alpha-1/2}}^{z_{\alpha+1/2}} \nabla_{\mathbf{x}} p_\alpha dz - \nabla_{\mathbf{x}} \cdot (h_\alpha \mathbf{T}_h^E) \\ + (\tilde{\mathbf{T}}_{h,\alpha+1/2}^E(\nabla_{\mathbf{x}} z_{\alpha+1/2})^T - \tilde{\mathbf{T}}_{xz,\alpha+1/2}^E) - (\tilde{\mathbf{T}}_{h,\alpha-1/2}^E(\nabla_{\mathbf{x}} z_{\alpha-1/2})^T - \tilde{\mathbf{T}}_{xz,\alpha-1/2}^E) \\ = \frac{G_{\alpha+1/2}}{2} (\mathbf{u}_{\alpha+1} + \mathbf{u}_\alpha) - \frac{G_{\alpha-1/2}}{2} (\mathbf{u}_\alpha + \mathbf{u}_{\alpha-1}),\end{aligned}\tag{A.3.6}$$

where, in light of Assumption 1.4.1, we obtain

$$\begin{aligned} \int_{z_{\alpha-1/2}}^{z_{\alpha+1/2}} \nabla_{\mathbf{x}} p_{\alpha} dz &= h_{\alpha} \left( \nabla_{\mathbf{x}} \left( p_S + g \sum_{\beta=\alpha+1}^M \rho(\Phi_{\beta}) h_{\beta} + g \rho(\Phi_{\alpha}) \frac{h_{\alpha}}{2} \right) + g \rho(\Phi_{\alpha}) \nabla_{\mathbf{x}} \left( z_b + \sum_{\beta=1}^{\alpha-1} h_{\beta} + \frac{h_{\alpha}}{2} \right) \right) \\ &= h_{\alpha} (\nabla_{\mathbf{x}} \bar{p}_{\alpha} + g \rho(\Phi_{\alpha}) \nabla_{\mathbf{x}} \bar{z}_{\alpha}). \end{aligned} \quad (\text{A.3.7})$$

Finally, introducing (A.3.7) in equation (A.3.6) and adding the equations (A.3.2) we obtain the system (1.4.6).

## A.4 Miscellaneous technical results

### A.4.1 Proof of 1.5.1

To see demonstrate that the second equality of (1.5.1) is correct, we recall that  $1 - \phi_0 = \phi = \phi_1 + \cdots + \phi_N$  (see Section 1.2.2). In other words, the total volumetric fraction satisfies  $\phi_0 + \phi_1 + \cdots + \phi_N = 1$ . Then we have

$$\begin{aligned} m_{\alpha} = \bar{\rho}_{\alpha} h &= \sum_{j=0}^N \rho_j \phi_{j,\alpha} h = \rho_0 \phi_{0,\alpha} h + \sum_{j=1}^N r_{j,\alpha} = \rho_0 h \left( 1 - \sum_{j=1}^N \phi_{j,\alpha} \right) + \sum_{j=1}^N r_{j,\alpha} \\ &= \rho_0 h - \sum_{j=1}^N \rho_0 \phi_{j,\alpha} h + \sum_{j=1}^N r_{j,\alpha} = \rho_0 h - \sum_{j=1}^N \rho_0 \frac{\rho_j}{\rho_j} \phi_{j,\alpha} h + \sum_{j=1}^N \frac{\rho_j}{\rho_j} r_{j,\alpha} \\ &= \rho_0 h - \sum_{j=1}^N \frac{\rho_0}{\rho_j} r_{j,\alpha} + \sum_{j=1}^N \frac{\rho_j}{\rho_j} r_{j,\alpha} = \rho_0 h + \sum_{j=1}^N \frac{\rho_j - \rho_0}{\rho_j} r_{j,\alpha}. \end{aligned}$$

### A.4.2 Proof of 1.3.12

The momentum jump condition (1.3.2) is given by

$$\begin{aligned} 0 &= \llbracket \left( \sum_{j=0}^N \rho_j \phi_j \mathbf{v}_j; \sum_{j=0}^N \rho_j \phi_j \mathbf{v}_j \otimes \mathbf{v}_j - \mathbf{T} \right) \rrbracket_{t,\alpha+1/2} \cdot \mathbf{n}_{t,\alpha+1/2} \\ &= \llbracket \left( \sum_{j=0}^N \rho_j \phi_j \mathbf{v}_j; \sum_{j=0}^N \rho_j \phi_j \mathbf{v}_j \otimes \mathbf{v}_j - \mathbf{T} \right) \rrbracket_{t,\alpha+1/2} \cdot (\partial_t z_{\alpha+1/2}, \nabla_{\mathbf{x}} z_{\alpha+1/2}, -1)^T \\ &= \sum_{j=0}^N \llbracket (\rho_j \phi_j \mathbf{v}_j; \rho_j \phi_j \mathbf{v}_j \otimes \mathbf{v}_j) \rrbracket_{t,\alpha+1/2} \cdot (\partial_t z_{\alpha+1/2}, \nabla_{\mathbf{x}} z_{\alpha+1/2}, -1)^T - \llbracket \mathbf{T} \rrbracket_{t,\alpha+1/2} \cdot (\nabla_{\mathbf{x}} z_{\alpha+1/2}, -1)^T. \end{aligned}$$

Finally we get

$$\llbracket \mathbf{T} \rrbracket_{t,\alpha+1/2} \cdot (\nabla_{\mathbf{x}} z_{\alpha+1/2}, -1)^T = \sum_{j=0}^N \llbracket (\rho_j \phi_j \mathbf{v}_j; \rho_j \phi_j \mathbf{v}_j \otimes \mathbf{v}_j) \rrbracket_{t,\alpha+1/2} \cdot (\partial_t z_{\alpha+1/2}, \nabla_{\mathbf{x}} z_{\alpha+1/2}, -1)^T.$$

*Remark:* The object inside of the jump operator is a matrix of order  $3 \times 4$ ,  $\rho_j \phi_j \mathbf{v}_j$  is a column of size 3 and  $\rho_j \phi_j \mathbf{v}_j \otimes \mathbf{v}_j$  is a matrix of order  $3 \times 3$ .

---

## Bibliography

---

- [1] E. AUDUSSE, *A multilayer Saint-Venant model: derivation and numerical validation*, Discrete Contin. Dyn. Syst. Ser. B, 5 (2005), pp. 189–214.
- [2] E. AUDUSSE, M. BRISTEAU, B. PERTHAME, AND J. SAINTE-MARIE, *A multilayer Saint-Venant system with mass exchanges for shallow water flows. derivation and numerical validation*, ESAIM: Math. Model. Numer. Anal., 45 (2011), pp. 169–200.
- [3] E. AUDUSSE AND M.-O. BRISTEAU, *Finite-volume solvers for a multilayer Saint-Venant system*, Int. J. Appl. Math. Comput. Sci., 17 (2007), pp. 311–319.
- [4] E. AUDUSSE, M. O. BRISTEAU, AND A. DECOENE, *Numerical simulations of 3D free surface flows by a multilayer Saint-Venant model*, Internat. J. Numer. Methods Fluids, 56 (2008), pp. 331–350.
- [5] E. AUDUSSE, M.-O. BRISTEAU, M. PELANTI, AND J. SAINTE-MARIE, *Approximation of the hydrostatic Navier–Stokes system for density stratified flows by a multilayer model: Kinetic interpretation and numerical solution*, Journal of Computational Physics, 230 (2011), pp. 3453–3478.
- [6] L. G. AUSTIN, C. H. LEE, AND F. CONCHA, *Hindered settling and classification partition curves*, Minerals & Metallurgical Process., 9 (1992), pp. 161–168.
- [7] E. BARSKY, *Critical regimes of two-phase flows with a polydisperse solid phase*, Fluid Mechanics and Its Applications, Springer, Dordrecht, 2010.
- [8] D. K. BASSON, S. BERRES, AND R. BÜRGER, *On models of polydisperse sedimentation with particle-size-specific hindered-settling factors*, Appl. Math. Model., 33 (2009), pp. 1815–1835.
- [9] S. BERRES, R. BÜRGER, K. H. KARLSEN, AND E. M. TORY, *Strongly degenerate parabolic-hyperbolic systems modeling polydisperse sedimentation with compression*, SIAM J. Appl. Math., 64 (2003), pp. 41–80.
- [10] R. T. BONNECAZE, H. E. HUPPERT, AND J. R. LISTER, *Patterns of sedimentation from poly-dispersed turbidity currents*, Proc. Roy. Soc. Lond. A, 452 (1996), pp. 2247–2261.
- [11] S. BOSCARINO, R. BÜRGER, P. MULET, G. RUSSO, AND L. M. VILLADA, *Linearly implicit IMEX Runge-Kutta methods for a class of degenerate convection-diffusion problems*, SIAM J. Sci. Comput., 37 (2015), pp. B305–B331.

- [12] S. BOSCARINO, R. BÜRGER, P. MULET, G. RUSSO, AND L. M. VILLADA, *On linearly implicit IMEX Runge-Kutta methods for degenerate convection-diffusion problems modeling polydisperse sedimentation*, Bull. Braz. Math. Soc. (N. S.), 47 (2016), pp. 171–185.
- [13] M.-O. BRISTEAU, A. MANGENEY, J. SAINTE-MARIE, AND N. SEGUIN, *An energy-consistent depth-averaged euler system: Derivation and properties*, Discrete and Continuous Dynamical Systems - Series B, 20 (2014).
- [14] R. BÜRGER, C. CHALONS, AND L. M. VILLADA, *Antidiffusive Lagrangian-remap schemes for models of polydisperse sedimentation*, Numer. Methods Partial Differential Equations, 32 (2016), pp. 1109–1136.
- [15] R. BÜRGER, S. DIEHL, S. FARÅS, I. NOPENS, AND E. TORFS, *A consistent modelling methodology for secondary settling tanks: A reliable numerical method*, Water Sci. Tech., 68 (2013), pp. 192–208.
- [16] R. BÜRGER, S. DIEHL, M. C. MARTÍ, P. MULET, I. NOPENS, E. TORFS, AND P. A. VANROLLEGHEM, *Numerical solution of a multi-class model for batch settling in water resource recovery facilities*, Appl. Math. Model., 49 (2017), pp. 415–436.
- [17] R. BÜRGER, R. DONAT, P. MULET, AND C. A. VEGA, *Hyperbolicity analysis of polydisperse sedimentation models via a secular equation for the flux Jacobian*, SIAM J. Appl. Math., 70 (2010), pp. 2186–2213.
- [18] R. BÜRGER, R. DONAT, P. MULET, AND C. A. VEGA, *On the implementation of WENO schemes for a class of polydisperse sedimentation models*, J. Comput. Phys., 230 (2011), pp. 2322–2344.
- [19] R. BÜRGER, S. EVJE, K. H. KARLSEN, AND K.-A. LIE, *Numerical methods for the simulation of the settling of flocculated suspensions*, Chem. Eng. J., 80 (2000), pp. 91–104.
- [20] R. BÜRGER, E. D. FERNÁNDEZ-NIETO, AND V. OSORES, *A dynamic multilayer shallow water model for polydisperse sedimentation*, ESAIM: Math. Model. Numer. Anal., 53 (2019), pp. 1391–1432.
- [21] R. BÜRGER, A. GARCÍA, K. H. KARLSEN, AND J. D. TOWERS, *A family of numerical schemes for kinematic flows with discontinuous flux*, J. Eng. Math., 60 (2009), pp. 387–425.
- [22] R. BÜRGER, P. MULET, AND L. M. VILLADA, *Regularized nonlinear solvers for IMEX methods applied to diffusively corrected multispecies kinematic flow models*, SIAM J. Sci. Comput., 35 (2013), pp. B751–B777.
- [23] R. BÜRGER AND V. OSORES, *Proceedings of the international conference on numerical analysis, computing and applications in science, engineering and technology*, (ICNumACA'18), Mohandas College of Engineering & Technology, Anad, Nedumangad, Thiruvananthapuram, Kerala, India, (2019), pp. 48 – 67.
- [24] R. BÜRGER, W. L. WENDLAND, AND F. CONCHA, *Model equations for gravitational sedimentation-consolidation processes*, ZAMM Z. Angew. Math. Mech., 80 (2000), pp. 79–92.

- [25] M. J. CASTRO, C. ESCALANTE, AND T. MORALES DE LUNA, *Modelling and simulation of non-hydrostatic shallow flows*, (2017), pp. 119–126.
- [26] M. J. CASTRO DÍAZ AND E. FERNÁNDEZ-NIETO, *A class of computationally fast first order finite volume solvers: PVM methods*, SIAM Journal on Scientific Computing, 34 (2012), pp. A2173–A2196.
- [27] M. J. CASTRO DÍAZ, E. D. FERNÁNDEZ-NIETO, A. M. FERREIRO, AND C. PARÉS, *Two-dimensional sediment transport models in shallow water equations. A second order finite volume approach on unstructured meshes*, Comput. Methods Appl. Mech. Engrg., 198 (2009), pp. 2520–2538.
- [28] M. J. CASTRO DÍAZ, E. D. FERNÁNDEZ-NIETO, T. MORALES DE LUNA, G. NARBONA-REINA, AND C. PARÉS, *A HLLC scheme for nonconservative hyperbolic problems. Application to turbidity currents with sediment transport*, ESAIM Math. Model. Numer. Anal., 47 (2013), pp. 1–32.
- [29] M. J. CASTRO DÍAZ, J. GALLARDO, AND C. PARÉS, *High order finite volume schemes based on reconstruction of states for solving hyperbolic systems with nonconservative products. applications to shallow-water systems*, Math. Comp. 75 (2006), 1103–1134, 75 (2006), pp. 1103–1134.
- [30] C. M. CHOUX AND T. H. DRUITT, *Analogue study of particle segregation in pyroclastic density currents, with implications for the emplacement mechanisms of large ignimbrites*, Sedimentology, 49 (2002), pp. 907–928.
- [31] G. DAL MASO, P. G. LEFLOCH, AND F. MURAT, *Definition and weak stability of nonconservative products*, J. Math. Pures Appl. (9), 74 (1995), pp. 483–548.
- [32] S. DIEHL, *Shock-wave behaviour of sedimentation in wastewater treatment: A rich problem*, in Analysis for Science, Engineering and Beyond, K. Åström, L.-E. Persson, and S. D. Silvestrov, eds., Berlin, Heidelberg, 2012, Springer Berlin Heidelberg, pp. 175–214.
- [33] R. DONAT AND P. MULET, *A secular equation for the Jacobian matrix of certain multispecies kinematic flow models*, Numer. Methods Partial Differential Equations, 26 (2010), pp. 159–175.
- [34] R. DORRELL AND A. J. HOGG, *Sedimentation of bidisperse suspensions*, Int. J. Multiphase Flow, 36 (2010), pp. 481–490.
- [35] R. DORRELL, A. J. HOGG, E. SUMNER, AND P. TALLING, *The structure of the deposit produced by sedimentation of polydisperse suspensions*, J. Geophys. Res., 116 (2011), p. F01024.
- [36] C. ESCALANTE, T. M. DE LUNA, AND M. CASTRO, *Non-hydrostatic pressure shallow flows: Gpu implementation using finite volume and finite difference scheme*, Applied Mathematics and Computation, 338 (2018), pp. 631 – 659.
- [37] E. D. FERNÁNDEZ-NIETO, *Modelling and numerical simulation of submarine sediment shallow flows: transport and avalanches*, Bol. Soc. Esp. Mat. Apl. SeMA, (2009), pp. 83–103.
- [38] E. D. FERNÁNDEZ-NIETO, E. H. KONÉ, AND T. CHACÓN REBOLLO, *A multilayer method for the hydrostatic Navier-Stokes equations: a particular weak solution*, J. Sci. Comput., 60 (2014), pp. 408–437.

- [39] E. D. FERNÁNDEZ-NIETO, E. H. KONÉ, T. MORALES DE LUNA, AND R. BÜRGER, *A multilayer shallow water system for polydisperse sedimentation*, J. Comput. Phys., 238 (2013), pp. 281–314.
- [40] E. D. FERNÁNDEZ-NIETO AND G. NARBONA-REINA, *Extension of WAF type methods to non-homogeneous shallow water equations with pollutant*, J. Sci. Comput., 36 (2008), pp. 193–217.
- [41] E. FERNÁNDEZ-NIETO, M. PARISOT, Y. PENEL, AND J. SAINTE-MARIE, *A hierarchy of dispersive layer-averaged approximations of euler equations for free surface flows*, Communications in Mathematical Sciences, 16 (2018), pp. 1169–1202.
- [42] A. E. GREEN, N. LAWS, AND P. M. NAGHDI, *On the theory of water waves*, Proceedings of the Royal Society of London. A. Mathematical and Physical Sciences, 338 (1974), pp. 43–55.
- [43] A. E. GREEN AND P. M. NAGHDI, *A derivation of equations for wave propagation in water of variable depth*, Journal of Fluid Mechanics, 78 (1976), p. 237–246.
- [44] T. C. HARRIS, A. J. HOGG, AND H. E. HUPPERT, *Polydisperse particle-driven gravity currents*, J. Fluid Mech., 472 (2002), pp. 333–371.
- [45] G. V. KOZYRAKIS, A. I. DELIS, G. ALEXANDRAKIS, AND N. A. KAMPAKIS, *Numerical modeling of sediment transport applied to coastal morphodynamics*, Appl. Numer. Math., 104 (2016), pp. 30–46.
- [46] M. J. LOCKETT AND K. S. BASSOON, *Sedimentation of binary particle mixtures*, Powder Technol., 24 (1979), pp. 1–7.
- [47] D. L. MARCHISIO AND R. O. FOX, *Computational models for polydisperse particulate and multiphase systems*, Cambridge Series in Chemical Engineering, Cambridge University Press, Cambridge, 2013.
- [48] J. H. MASLIYAH, *Hindered settling in a multiple-species particle system*, Chem. Engrg. Sci., 34 (1979), pp. 1166–1168.
- [49] E. MEIBURG AND B. KNELLER, *Turbidity Currents and Their Deposits*, Annual Review of Fluid Mechanics, 42 (2010), pp. 135–156.
- [50] T. MORALES DE LUNA, M. J. CASTRO DÍAZ, C. PARÉS MADROÑAL, AND E. D. FERNÁNDEZ NIETO, *On a shallow water model for the simulation of turbidity currents*, Commun. Comput. Phys., 6 (2009), pp. 848–882.
- [51] O. L. MÉTAYER, S. GAVRILYUK, AND S. HANK, *A numerical scheme for the green–naghdi model*, Journal of Computational Physics, 229 (2010), pp. 2034 – 2045.
- [52] R. W. D. NICKALLS, *A new bound for polynomials when all the roots are real*, The Mathematical Gazette, 95 (2011), p. 520–526.
- [53] C. PARÉS, *Numerical methods for nonconservative hyperbolic systems: a theoretical framework*, SIAM J. Numer. Anal., 44 (2006), pp. 300–321 (electronic).

- [54] C. PARÉS AND M. CASTRO, *On the well-balance property of Roe's method for nonconservative hyperbolic systems. Applications to shallow-water systems*, M2AN Math. Model. Numer. Anal., 38 (2004), pp. 821–852.
- [55] M. PÉREZ, R. FONT, AND C. PASTOR, *A mathematical model to simulate batch sedimentation with compression behavior*, Computers & Chemical Eng., 22 (1998), pp. 1531–1541.
- [56] J. F. RICHARDSON AND W. N. ZAKI, *Sedimentation and fluidisation: Part I*, Trans. Inst. Chem. Engrs. (London), 32 (1954), pp. 34–53.
- [57] A. RUSHTON, A. S. WARD, AND R. G. HOLDICH, *Solid-liquid filtration and sedimentation technology*, 2nd ed., Wiley-VCH, Weinheim, Germany, (2000).
- [58] J. SAINTE-MARIE, *Vertically averaged models for the free surface non-hydrostatic Euler system: derivation and kinetic interpretation*, Math. Models Methods Appl. Sci., 21 (2011), pp. 459–490.
- [59] W. SCHNEIDER, G. ANESTIS, AND U. SCHAFLINGER, *Sediment composition due to settling of particles of different sizes*, Int. J. Multiphase Flow, 11 (1985), pp. 419–423.
- [60] I. TOUMI, *A weak formulation of Roe's approximate Riemann solver*, J. Comput. Phys., 102 (1992), pp. 360–373.
- [61] M. UNGARISH, *An Introduction to Gravity Currents and Intrusions*, CRC Press, Boca Raton, FL, 2009.
- [62] Y. YAMAZAKI, Z. KOWALIK, AND K. F. CHEUNG, *Depth-integrated, non-hydrostatic model for wave breaking and run-up*, International Journal for Numerical Methods in Fluids, 61 (2009), pp. 473 – 497.